

THE UNIVERSITY OF CHICAGO

REPRESENTATIONS OF THE HAND IN PRIMATE SENSORIMOTOR CORTEX

A DISSERTATION SUBMITTED TO

THE FACULTY OF THE DIVISION OF THE BIOLOGICAL SCIENCES

AND THE PRITZKER SCHOOL OF MEDICINE

IN CANDIDACY FOR THE DEGREE OF

DOCTOR OF PHILOSOPHY

COMMITTEE ON COMPUTATIONAL NEUROSCIENCE

BY

JAMES GOODMAN

CHICAGO, ILLINOIS

DECEMBER 2018

Copyright © 2018 by James Goodman.

All rights reserved.

## TABLE OF CONTENTS

<b>LIST OF FIGURES .....</b>	<b>vii</b>
<b>LIST OF TABLES .....</b>	<b>xvi</b>
<b>LIST OF PUBLICATIONS .....</b>	<b>xvii</b>
<b>ABSTRACT.....</b>	<b>xviii</b>
<b>CHAPTER 1: Introduction to haptic sensation .....</b>	<b>1</b>
Preface.....	1
Introduction .....	1
The sense of touch.....	2
Cutaneous mechanoreceptors and associated nerve fibers .....	2
Skin mechanics and afferent branching.....	6
Tactile coding in the somatosensory nerve.....	9
Stimulus magnitude .....	9
Vibratory frequency .....	11
Shape.....	12
Texture .....	15
Motion.....	19
Peripheral signals during object manipulation .....	20
The touch pathways .....	23
Tactile coding in somatosensory cortex .....	26
Vibratory frequency .....	28
Shape.....	29
Motion.....	30
Texture .....	33
Parallels between vision and touch.....	35
Parallels between audition and touch .....	35
Affective touch .....	37
The sense of proprioception .....	38
Proprioceptive receptors and their associated nerve fibers .....	38
The cortical basis of proprioception .....	40
Phenomenology of proprioception .....	42
Multimodal integration and stereognosis .....	43
Conclusions .....	44
References .....	46
<b>CHAPTER 2: Introduction to shaping behavior and principles of its neural control .....</b>	<b>64</b>

Hand shaping behavior.....	64
Introduction .....	64
The gamut of hand function.....	64
Early qualitative characterizations of hand shaping .....	65
Simple quantification of hand shaping behavior .....	66
Sophisticated quantification of hand shaping behavior: Synergies .....	66
Conclusions .....	69
The cortical motor control of the arm and hand.....	70
The basis of a neural “code” for movement .....	70
Somatotopy as an organizing principle?.....	70
A more detailed code for M1: time-varying limb forces or kinematics? .....	72
Coordinate frames in motor control.....	74
The hand as potentially a special case of motor control.....	75
M1 response properties during grasp.....	76
Synergies to simplify hand control .....	78
Conclusions .....	79
References .....	80
<b>CHAPTER 3: The structure of hand shaping behavior and its population-level neuronal representation.....</b>	<b>85</b>
Introduction .....	85
Data are complex yet structured.....	85
Control of hand posture is higher-dimensional than previously thought .....	88
Neural responses occupy a high-dimensional space .....	94
Discussion & Conclusions .....	97
References .....	99
<b>CHAPTER 4: The features of the hand represented in somatosensory and primary motor cortices .....</b>	<b>100</b>
Introduction .....	100
Results .....	102
Neural encoding models predict firing rates.....	102
Neurons encode coordinated combinations of joints spanning the entire hand .....	103
Neurons encode postures of the hand rather than its movements.....	108
Encoding of passive hand movements.....	112
Discussion .....	114
Proprioceptive neurons in somatosensory cortex have large response fields.....	114
Hand neurons encode postures over movements.....	116

Response to active vs. imposed hand movements .....	117
Dependence of postural preference on analytics approach .....	118
Hand representations reflect muscle activations .....	121
Contrasting proprioceptive and motor representations of the hand.....	123
Conclusions .....	123
References .....	125
<b>CHAPTER 5: The case against synergies for hand shaping.....</b>	<b>130</b>
Introduction .....	130
Complexity of kinematics and sensorimotor cortical responses .....	130
Testing preferential encoding of individual synergies .....	131
Testing preferential encoding of mixtures of synergies with GLMs .....	133
Testing synergy encoding in the activity of neuronal ensembles.....	134
Discussion .....	136
Conclusion.....	139
References .....	140
<b>CHAPTER 6: Conclusions.....</b>	<b>141</b>
Summary of results.....	141
Avenues of future research.....	142
Sensorimotor interplay .....	142
Informing studies of proprioceptive phenomenology .....	143
The dimensionality of hand movements.....	144
The integration of touch and proprioception .....	145
Decoding hand movements .....	145
References .....	147
<b>APPENDIX: Experimental and analytical materials and methods .....</b>	<b>150</b>
Animals and surgery.....	150
Grasp task .....	151
Kinematic recordings and processing .....	151
Neural recordings .....	154
Passive movement sessions.....	156
Intracortical microstimulation.....	156
Proximal limb data .....	157

Data Analysis ..... 157  
    Dimensionality reduction ..... 157  
    Temporal alignment..... 158  
    Classification algorithm..... 158  
    Pooling data across sessions ..... 159  
    Generalized linear model..... 162  
    Lag analysis ..... 163  
    Regularization and cross-validation ..... 163  
    Interpreting encoding models ..... 164  
    Models of postural synergy encoding..... 166  
    Simulated neural activity ..... 166  
References ..... 168

## LIST OF FIGURES

**Figure 1-1.** Medial lemniscal pathway for the sense of touch (illustration by Kenzie Green). ..... 3

**Figure 1-2.** (A) Firing rate evoked in an RA fiber by 40-Hz skin vibrations of varying amplitudes. The rate increases as a piece-wise linear function of amplitude, interspersed with entrainment plateaus over which the fiber fires an integer number of spikes per stimulus cycle (Johnson, 1974). (B) Responses of a PC fiber to a 400-Hz skin vibration at three amplitudes. The spiking response is highly patterned and repeatable and conveys information about the frequency of the stimulus (Mackevicius et al., 2012). (C) Reconstruction of the spatial pattern of activation evoked in a population of SA1 (top), RA (middle) and PC (bottom) afferents when embossed letters are scanned across the skin. The spatial pattern of activation reflects the spatial configuration of the stimulus (Phillips et al., 1988). ..... 13

**Figure 1-3.** (A) Reconstruction of the response in a population of SA1 afferents evoked by embossed dot patterns scanned across the skin. The spatial configuration of the dots is reflected in the pattern of activation evoked in the afferents. (B) Response of a PC fiber to three finely textured fabrics. Left: Microscope image of the texture; middle: spiking responses to 40 repeated presentations of the textured surface; right: power spectrum of the neural response. Each texture produces a different but highly repeatable temporal spiking pattern (Weber et al., 2013)..... 18

**Figure 1-4.** Typical trial of the object lifting task. Vertical lines denote the boundaries of the task phases. The top two colored traces show the time-varying load force (upward lines in the diagram to the left) and grip force (inward arrows) during the trial. The black trace shows the vertical position of the object as it is lifted off the support surface. The bottom three traces show spike trains of RA, SA, and PC afferents, respectively. Bursts of spikes coinciding with specific task events are circled in magenta. (adapted from Johansson and Flanagan, 2009). ..... 24

**Figure 1-5.** (A) Orientation tuned neuron in area 3b (inset shows a Gaussian fit to its RF) (adapted from Bensmaia et al., 2008). (B) Curvature and orientation tuned neurons in area 2 (Yau et al., 2013). C| Orientation-tuned neuron in S2: This neuron’s receptive field spans four digits (D2-D5) and multiple pads in each. However, its preferred orientation remains consistent across its RF (approximately aligned with the long axis of the finger) (Fitzgerald et al., 2006). ..... 31

**Figure 1-6.** (A) Direction tuning of a neuron in area 1 to scanned bars (adapted from Pei et al., 2010). (B) Responses of a ‘component’ neuron to plaids scanned in 12 directions. This neuron responds maximally when one of the plaid’s component gratings is moving in its preferred direction. C| Responses of a ‘pattern’ neuron to plaids. This neuron responds to the plaid’s global direction of motion. Such neurons are only found in area 1.(Pei et al., 2011) ..... 32

**Figure 1-7.** (A) Muscle Spindle. The spindle capsule contains three types of intrafusal muscle fiber: nuclear bag 1 fibers, which are sensitive to rate of stretch; and nuclear bag 2 and nuclear chain fibers, which are sensitive to static stretch. The  $\gamma$ -dynamic fusimotor neurons selectively innervate bag 1 fibers and adjust sensitivity to the rate of stretch, whereas the  $\gamma$ -static fusimotor neurons selectively modulate the fibers that sense static stretch. Primary (Ia) spindle afferents

innervate all three intrafusal fiber types and convey dynamic stretch information. Secondary (II) spindle afferents innervate and convey information from only the intrafusal muscle fibers that sense static stretch. (B) Golgi tendon organ (GTO). The outer tendon is resected to show the GTO (Ib) afferent and the interior collagenous mesh it innervates. A single GTO is situated in series with 10-20 motor units (bundles of muscle fibers, top). GTO afferents convey active muscle force by "counting" the number of recruited motor units (illustrations by Kenzie Green)..... 39

**Figure 1-8.** Neuron in area 2 that exhibits both tactile and proprioceptive responses (courtesy of Sung Soo Kim). This neuron’s activity is modulated simply by moving the digits (left panel). However, responses are further modulated by cutaneous stimulation (right panel). The neuron’s response is a complex function of hand conformation and cutaneous input. .... 44

**Figure 2-1.** Rectified low-pass filtered EMG activity (filled gray traces, a) is estimated (black traces, a) using combinations of patterns defined along three muscle synergies (b). A low-dimensional continuum appears at first glance to be a sufficient explanation of muscle activity. Figure from d’Avella, Saltiel, & Bizzi, 2003..... 68

**Figure 2-2.** (A) Mapping the preferred digit of different locations on a patch of motor cortex (shown reconstructed on the left) gives rise to a lack of clear somatotopic separation among the digits (right, different colors represent different preferred digits). Figures from Schieber & Hibbard, 1993. (B) At a more coarsely-grained level of detail, separation of arm and hand representations in M1 appears to follow a general pattern of an arm-coding (Forelimb P) “horseshoe” surrounding a digit-coding (Forelimb D) nucleus. Figure from Park et al., 2001.... 71

**Figure 2-3.** Firing rates of two different M1 neurons (left and right) during reach-to-grasp of different objects (far left) centered on the onset of the reach, demonstrating just a small sliver of the variety of hand-related responses in M1. Figure from Umiltà, Brochier, Spinks, & Lemon, 2007..... 77

**Figure 3-1.** Different objects give rise to a variety of different kinematics and neural activity. (A) A phase plot of three joint angles (flexion\_1 being wrist flexion angle, pro\_sup\_1 being wrist supination angle, and 2mcp\_flexion\_1 being second metacarpal flexion angle) during one monkey’s grasp of two different objects. Each trace represents kinematics during a single grasp trial. Faded triangles (“play” symbols) indicate joint angles 750ms prior to maximum aperture, well before movement began. Dark squares (“stop” symbols) indicate joint angles 750ms after maximum aperture, well after object contact where the hand adopted its final posture. Shown below the phase plot is a series of still frames of the skeletal model of the hand for one presentation of each object, illustrating the progression of the hand’s conformation from a common “start” state to a fully differentiated “grasp” state. (B) Separate plots of the same joints against time, this time for all objects. Each colored trace gives the mean kinematics for a grasp of a particular object. Shaded regions indicate  $\pm 1$  S.E.M. at each sample time. (C) Peri-event time histograms (PETHs) for three select M1 and proprioceptive somatosensory cortical neurons for all objects. PETHs are constructed by aligning each trial to the time of maximum aperture, calculating the average spike count in each 10ms bin on a per-trial basis, then smoothing the average trace with a centered Gaussian kernel with 35ms width parameter. Each colored trace gives the mean firing rate during grasping of a particular object. Shaded regions indicate  $\pm 1$  S.E.M. at each sample time. .... 86

**Figure 3-2.** Sample PETHs and PC reconstructions from neurons across all areas of cortex from which we record. These show the temporal evolution of firing rates with respect to maximum aperture and the separation of firing rate patterns as a function of object identity—and presumably as a function of the corresponding grasp conformation. All PETHs are trial-averaged firing rates of neurons from Monkey 4 in response to different objects, sorted on a neuron-by-neuron basis, computed using similar trial averaging and smoothing procedures as those PETHs in Figure 3-1C. Note that the first 3 PC reconstructions preserve object-dependent variance for a few select neurons, but often fail to capture this structure for a large number of them..... 87

**Figure 3-3.** Kinematic correlation matrices. The absolute values of correlations among joint angular coordinates for (A) Monkey 1, (B) Monkey 2, (C) Monkey 3, and (D) Monkey 4. Correlations are assessed at zero lag, and the order of joints is determined for each monkey with hierarchical clustering so that large groups of highly correlated joints can better be visualized. Joint angular coordinate key: flexion—flexion or extension (“pitch”) of the wrist joint | deviation—ulnar or radial deviation (“yaw”) of the wrist joint | pro\_sup—pronation or supination (“roll”) of the wrist joint | elbow—elbow joint | 1–5—digits 1 through 5, respectively | CMC—carpometacarpal joint | mcp—metacarpophalangeal joint | ip—interphalangeal joint (digit 1 only) | pm—proximal interphalangeal joint | md—distal interphalangeal joint | \_flexion, \_flex, \_ext—flexion or extension (“pitch”) of the joint preceding the underscore | \_abd, \_abduction—abduction or adduction (“yaw”) of the joint preceding the underscore | \_supination—pronation or supination (“roll”) of the joint preceding the underscore. .... 89

**Figure 3-4.** Analysis of kinematic structure and dimensionality. (A) Cumulative scree plot from principal component analysis (PCA) of joint postures, averaged across all four monkeys. The mean CVE first crosses the 90% boundary at 6 principal components (PCs), but more conservatively, the circled point indicates the minimum number of PCs (9) for which the average CVE was significantly greater than 90% (one-tailed one-sample t-test,  $T(3) = 7.023$ ,  $p = 2.965e-03$ , significance assessed across all 30 points on the abscissa with the Holm-Bonferroni method of multiple comparisons,  $FWER < 0.05$ ). The cumulative scree plot is truncated at 12 components but a total of 30 components are present. Vertical lines at each point indicate  $\pm 1$  S.E.M. across monkeys. (B) Cross-validated (leave-one-out) accuracy of object classification (multi-class linear discriminant analysis, i.e., LDA) based on joint angular kinematics at different task epochs, averaged across monkeys. Vertical lines at each point indicate  $\pm 1$  S.E.M. across monkeys. Dotted blue lines indicate classifiers using only the first 9 PCs, compared with solid blue lines that show results of classifiers using the full dimensionality of hand kinematics. The shaded regions indicate the mean difference  $\pm 1$  S.E.M. between the two classifiers. As this difference arises from paired data (each monkey has one classifier of each type), its own standard error is indicated with the darkness of the shaded region. The darkest region indicates the mean difference minus 1 S.E.M., and the lightest region indicates +1 S.E.M. When pooling across epochs, the cross-validated full kinematic classifier more accurately determines the object presented from out-of-sample kinematics than the one using only 9 PCs (two-tailed paired-samples t-test,  $T(59) = 9.136$ ,  $p = 6.773e-13$ ). .... 90

**Figure 3-5.** Analysis of kinematic structure and dimensionality by monkey. (A) Cumulative scree plots after applying principal component analysis (PCA) to the joint angular kinematics of each monkey. These scree plots were averaged across monkeys to obtain the plot in Figure 3A. Circles

indicate the number of components at which the cumulative scree plot for each monkey exceeds 90% of kinematic variance explained. These traces are averaged to obtain the trace in Figure 3-2A (B) Accuracy of kinematic object classification (as in Figure 3B) for each monkey at different task epochs. Again, these accuracies were averaged across monkeys to obtain the mean accuracy curve in Figure 3B. Solid lines indicate full-kinematic accuracy; dashed lines, the accuracy of classifiers using only the first few dimensions to explain at least 90% of kinematic variance—the same number of components as the corresponding circle in (A). Vertical lines at each epoch indicate  $\pm 1$  S.E.M. of classification accuracy. These traces—one from each monkey, each given equal weight—are averaged to obtain the averaged time course of classification accuracy in Figure 3-2B. .... 91

**Figure 3-6.** Visualization of “Eigen-grasps” obtained from principal component analysis (PCA) applied to the joint angular data of Monkey 2. Each row depicts a different Eigen-grasp, with a progression from left to right through that Eigen-grasp’s range of correlated joint angular movements. Although qualitative interpretations of these “Eigen-grasps” could be inferred, we find that such PCs that merely explain the largest fraction of variance fail to capture reliable yet subtle inter-object differences in grasp postures. .... 92

**Figure 3-7.** Cumulative scree plots for PCA run on standardized kinematic data (A) on a monkey-by-monkey basis and (B) averaged across monkeys. Apparent dimensionality increases when assessing kinematic dimensionality using PCA on standardized data, with individual-monkey dimensionalities spanning 8-13 dimensions (A) and monkey-averaged dimensionalities spanning 10-17 components (B). Significance of the second point in (B) is assessed as in Figure 3-4A. .. 93

**Figure 3-8.** Neural correlation matrix heatmaps. Rows of heatmaps indicate the cortical area from which neurons were recorded. Columns of heatmaps indicate the monkey from which each correlation matrix was obtained. Correlation matrices are signal correlation matrices; in other words, firing rates are averaged across trials for each object after aligning to object contact, and the correlations of these firing rates extending from 500ms to 10ms prior to contact are represented as the color in each heatmap. Trial averaging was done to permit pooling of neurons across sessions. Only heatmaps with at least 5 neurons are shown. .... 95

**Figure 3-9.** Analysis of neural structure and dimensionality. (A) Cumulative scree plot from PCA of joint postures and neural data, averaged across all four monkeys and plotted in terms of the fraction of the total number of components recorded from any given monkey. We plot in terms of fraction of number of components because population sizes recorded from each area in each monkey vary to give rise to different raw apparent neural dimensionalities that nonetheless align when instead plotted in this manner. We see that only 20% of the kinematic dimensionality is needed for the mean CVE to reach 90%, whereas for the cortical data that fraction jumps up to 40%. Each trace represents the interpolated cumulative scree plot as a function of the fraction of total number of components, averaged across monkeys. Shaded regions surrounding each trace give  $\pm 1$  S.E.M. for each point of each interpolated trace. (B) Neural classification accuracy when aligned to different epochs of grasp. Spike counts are taken over a 500ms causal window, and neurons from different sessions recorded from different monkeys are pooled to obtain these classification accuracies. We note that peak cross-validated accuracy reaches roughly 50% in population sizes on the order of 100 neurons. Vertical bars give  $\pm 1$  S.E.M. (C) A population of

roughly 200 proprioceptive or motor cortical neurons is required to reach mean peak classification accuracy (roughly 60%) of kinematic classifiers, as shown in Figure 3B. Single-monkey and pooled-monkey samples from each area are shown as each point on the plot. Logistic regression is fit to these data pooled across cortical areas. .... 96

**Figure 3-10.** Standardized cumulative scree plots averaged across 4 monkeys as a function of the fraction of the number of components needed to reach variance explained thresholds. Standardization acts to make neural responses appear even higher-dimensional, with roughly 80% of dimensions being required to explain 90% of the firing rate data. .... 97

**Figure 4-1.** Generalized linear model (GLM) procedure and performance. **(A)** Flow chart depicting how GLM uses kinematics (left) to create a weighted linear sum that is passed through a soft-plus nonlinearity (middle) to estimate firing rates (right, top) such that they are maximally likely given measured patterns of spiking activity (right, bottom). **(B)** Measured (dark) and predicted (light) peri-event time histograms (PETHs) for three different objects aligned to maximum aperture for an example neuron from area 3a. The pseudo- $R^2$  of the GLM fit to this neuron is 0.49. Vertical bars at each point indicate  $\pm 1$  S.E.M. **(C)** Pseudo- $R^2$  values for each neuron with cross-validated pseudo- $R^2$  greater than or equal to 0.05. Neurons are pooled across sessions and across different monkeys. Bar heights correspond with the mean pseudo- $R^2$  among such neurons in each area. Each point represents the pseudo- $R^2$  of a different neuron. Error bars span  $\pm 1$  standard error of the mean pseudo- $R^2$  of each area. In area 2, the pseudo- $R^2$  values of 41 out of 50 total units (82.0%) are reported, with the remaining 9 units being omitted due to having pseudo- $R^2$  values lower than 0.05; in area 3a, we report 40 of 68 (58.8%); in caudal M1, 59 of 89 (66.3%); and in rostral M1, 107 of 147 (72.8%). .... 103

**Figure 4-2.** Neurons track multiple joints distributed over the entire hand. **(A)** To count joints in response fields, we calculate the contribution of each joint to the regression weight vector and count the minimum number of joints required to account for 90% of the regression weight vector's squared norm (gray shaded area). Faded points indicate the cumulative contribution of the best N joints (abscissa) to the weight vector. Overlaid on these are the average cumulative functions across neurons in each area. **(B)** The average number of joints in a neuron's response field (RF) is roughly eight. There is no difference among areas in terms of the number of joints in the average neuron's RF. Individual points are single neuronal joint counts and can only take integer values; vertical dispersion of these points is artificially inserted to enhance visibility. Error bars in both plots indicate  $\pm 1$  S.E.M. .... 105

**Figure 4-3.** Simulated neuron populations with single-joint angular coordinate RFs and properties of their GLM fits. Left. Histogram of the number of joint predictors contained in the RF inferred via GLM. Note that every simulated neuron responded to just a single joint angular coordinate by design, and that over 70% of these simulated neurons had a GLM RF that recovered this single-predictor RF in spite of inter-joint correlations in the kinematics and noise in the simulated spike counts. Right. Distribution of pseudo- $R^2$  values of GLMs fit to these toy neurons, which is similar—by design—to the distribution seen in real cortical neuronal data. .... 107

**Figure 4-4.** The number of musculotendon complexes contained in each RF is no fewer than the number of joints in those same RFs (c.f. Figure 4-2B). The same neurons are assessed for

musculotendon counts in their RFs using similar methods as described in Figure 4-2A for joint counts. Error bars indicate  $\pm 1$  S.E.M. .... 108

**Figure 4-5.** Results of generalized linear models (GLMs) testing for preferential encoding of joint postures or movements. **(A)** The distribution of cross-validated pseudo- $R^2$  values computed for GLMs using just joint angles (Postures) as predictors or using just joint angular velocities (Movements) as predictors. Each point represents a single neuron. **(B)** Same abscissa as (A), but with each point plotted against the pseudo- $R^2$  value obtained using both posture and movement predictors on the ordinate. .... 109

**Figure 4-6.** Partial pseudo- $R^2$  of posture models on the abscissa against movement models on the ordinate. Faded points indicate individual neurons with peak pseudo- $R^2$  (non-partial) of 0.05 or greater. Overlaid fully-saturated points are means over neurons for each area, with error bars indicating  $\pm 1$  S.E.M. along each principal axis of covariance. The vast majority of unique variance in the firing rates of the typical neuron from any of these sensorimotor areas is explained by hand postural information rather than hand joint angular velocity information. .... 110

**Figure 4-7.** Partial pseudo- $R^2$  of position and velocity models for GLMs fit to neural data during a center-out reaching task. Conventions are as in Figure 4-6. Note that for the proximal limb, the majority of neurons and, indeed, the mean fall above the diagonal, indicating preferential encoding of velocities over positions. This contrasts with results for hand configurational encoding, where we observe preferential encoding of postures over movements. .... 112

**Figure 4-8.** Mean firing rates of neurons recorded during passive manipulation of the hand compared against those recorded during active, volitional grasp. **(A)** Each digit was passively manipulated by the experimenter. **(B)** Firing rates are generally similar between the two tasks, with the notable exception of area 3a neurons (see text for statistics). **(C)** We simulate firing rates in response to the kinematics from one task—the label on the abscissa—using RFs fit to firing rates and kinematics recorded during the opposite task. We note that we should expect firing rates during the passive task to be higher than those during the active grasp task (see text for statistics). Vertical lines centered on the height of each bar indicate  $\pm 1$  S.E.M. Only neurons with pseudo- $R^2 > 0.05$  are considered in (C). Samples from active and passive sessions are not paired, but are rather separate samples. .... 113

**Figure 4-9.** Properties of GLMs fit to neurons during passive manipulation of the hand. **(A)** The number of joints tracked by a neuron in each area does not generally change between the active (filled bars and points, labelled “A”) and passive (empty bars and points, labelled “P”) cases (two-sample equal-variance two-tailed T-tests:  $T_{\text{Area 2}}(46) = 0.432$ ,  $p = 6.681 \text{ e-}01$ ;  $T_{\text{Area 3a}}(43) = 0.528$ ,  $p = 6.003 \text{ e-}01$ ;  $T_{\text{Caudal M1}}(61) = -1.699$ ,  $p = 9.441 \text{ e-}02$ ), except in rostral M1 where the number of joints in the typical RF increases during passive movements RF (two-sample equal-variance two-tailed T test:  $T_{\text{Rostral M1}}(114) = -2.927$ ,  $4.137 \text{ e-}03$ ). Each point gives the number of joints in a single neuron’s RF. **(B)** Pseudo- $R^2$  for posture-only models, movement-only models, and full models. In the passive case, postures are still preferentially encoded over movements of the joints. Not shown are the differences between the partial pseudo- $R^2$  values of postural against movement models, which are no different from those in the active volitional grasp task (two-sample equal-variance two-tailed T-tests:  $T_{\text{Area 2}}(46) = -0.485$ ,  $p = 6.301 \text{ e-}01$ ;  $T_{\text{Area 3a}}(43) = -2.571$ ,  $p = 1.368 \text{ e-}02$ ;  $T_{\text{Caudal}}$

$M1(61) = -0.955$ ,  $p = 3.434 \text{ e-}01$ ;  $T_{\text{Rostral } M1}(114) = -0.279$ ,  $7.806 \text{ e-}01$ ). (C) Pseudo- $R^2$  of GLMs (provided pseudo- $R^2 > 0.05$ ) fit using the kinematics as predictors, which are not significantly different from those seen during active movement (c.f. Figure 4-1C) (two-sample equal-variance two-tailed T-tests:  $T_{\text{Area } 2}(46) = 1.092$ ,  $p = 2.804 \text{ e-}01$ ;  $T_{\text{Area } 3a}(43) = 0.631$ ,  $p = 5.313 \text{ e-}01$ ;  $T_{\text{Caudal } M1}(61) = 0.829$ ,  $p = 4.103 \text{ e-}01$ ;  $T_{\text{Rostral } M1}(114) = 1.506$ ,  $p = 1.347 \text{ e-}01$ ). Vertical lines centered on the height of each bar indicate  $\pm 1$  S.E.M. Only neurons with pseudo- $R^2 > 0.05$  are considered. Samples from active and passive sessions are not paired, but are rather separate samples..... 115

**Figure 4-10.** Reconciliation of this paper’s grasping results with previous reports of grasp encoding (Saleh et al., 2010, 2012). (A) Multi-lag models offer only a very slight, albeit significant, improvement over single-lag GLMs in terms of explaining neural activity, as evidenced by most points, or neurons, falling just above the diagonal. (B) History terms offer a significant improvement to single-lag encoding models, as evidenced by most points, or neurons, falling below the diagonal. (C) However, history terms covary more strongly with postures than they do with movements—as evidenced by the majority of points, or neurons, falling above the diagonal—and therefore could preferentially sap predictive power away from postures. (D) Regardless, posture terms are preferentially encoded in terms of partial pseudo- $R^2$  in the majority of neurons—as evidenced by the majority of points falling below the diagonal—even when accounting for history terms. (E) Posture autocorrelations (left) extend farther out temporally than do movement correlations (middle) or (unsmoothed) neural spiking autocorrelations (right) to which GLMs are fit. Underlying firing rates seem to vary on timescales similar to postures, which non-physiological spike history terms extending back as far as 250ms in the past could obscure. .... 120

**Figure 4-11.** Continuation of Figure 4-10. (A) Counting the number of neurons with each predictor in its RF for multi-lag, no-history models. Joint angular coordinates are converted to the same domain as that used previously (Saleh et al., 2010, 2012) for the purposes of comparison. Postural predictors are the most frequently encoded in both caudal and rostral motor cortices. (B) Only when re-incorporating history terms on top of using multi-lag models and counting joints rather than assessing partial pseudo- $R^2$  do we see movement predictors consistently occupying higher-rank slots than posture predictors. Velocity terms appear to have nearly exclusive representation among the top 4 most-encoded joint angular predictors, with wrist posture in caudal M1 being the lone exception. .... 122

**Figure 4-12.** Optimal neural latencies. Left. We fit GLMs fit to multiple different latencies and report for each neuron the latency associated with the largest pseudo- $R^2$  value. Shown is the latency-versus-pseudo- $R^2$  plot for an example neuron from caudal M1. Kinematic autocorrelations rendered estimates of optimal lags hazardous on a neuron-by-neuron basis (see scale of the ordinate). GLMs are used to evaluate latency rather than events such as the start of movement to account for different response fields that could give rise to different apparent latencies via the latter method. Right. Estimates of optimal latency for each cortical area after averaging across all neurons with pseudo- $R^2 > 0.05$ . We find that, on average, area 2 neurons significantly lag kinematics (one-sample T-test:  $T(40) = 2.355$ ,  $p = 2.353 \text{ e-}02$ ,  $\Delta t = 34.97$  ms), both rostral M1 (one-sample T-test:  $T(106) = -5.417$ ,  $p = 3.816 \text{ e-}07$ ,  $\Delta t = -60.73$  ms) and caudal M1 (one-sample T-test:  $T(61) = -2.611$ ,  $p = 1.134 \text{ e-}02$ ,  $\Delta t = -30.97$  ms) significantly lead kinematics, and neurons in area 3a neither significantly lead nor lag kinematics on average (one-sample T-test:  $T(41) = -1.835$ ,  $p = 7.373 \text{ e-}02$ ,  $\Delta t = -29.87$  ms). Indeed, there is a significant difference among optimal

lags across areas (one-way ANOVA:  $F(3,251) = 8.111$ ,  $p = 3.567 \times 10^{-5}$ ) that can be attributed to area 2 responses lagging kinematics relative to the other cortical areas (post-hoc Tukey’s HSD: all pairwise differences n.s. except those involving area 2,  $p_{\text{area 3a}} = 2.693 \times 10^{-2}$ ,  $p_{\text{cM1}} = 1.056 \times 10^{-2}$ ,  $p_{\text{rM1}} = 5.030 \times 10^{-2}$ , all  $\Delta \Delta t > 0$ ). Significance values of multiple T-tests are assessed here with the Holm-Bonferroni method, with  $\text{FWER} < 0.05$  for this family of four comparisons. Slightly different degrees of freedom in these statistical tests relative to the rest of the text are because we compare both joint- and muscle-based models against each other in this figure, whereas we only account for joint-based models in the rest of the text—except where explicitly stated otherwise. .... 124

**Figure 5-1.** Comparison of the peak pseudo- $R^2$  of a single joint axis GLM against that of a single principal component (PC) GLM. Peak pseudo- $R^2$  are computed for each model at their own respective optimal lags. The results of GLMs shown here are computed for those neurons with a peak multi-joint pseudo- $R^2$  value of at least 0.20. We note, as has been noted previously in M1 alone for lower-dimensional recordings of individuated finger movements (Kirsch et al., 2014; Mollazadeh et al., 2014), that neurons in sensorimotor cortices with hand response fields (RFs) do not preferentially encode any one PC of hand joint angles over a particular joint angular axis. In fact, the best PC model tends, on average, to be slightly worse-fitting than the best single joint-axis model when pooling results across areas (statistics in text). ..... 132

**Figure 5-2.** Pseudo- $R^2$  of GLMs fit using multiple predictors defined in a joint coordinate frame (abscissa) plotted against those with predictors defined in a principal component (PC) coordinate frame (ordinate). We find that even when regularizing regressions and cross-validating with respect to the LASSO penalty to obtain the best out-of-sample goodness-of-fit, both models fit neural spiking activity similarly well. All models shown have a pseudo- $R^2$  of at least 0.05. .... 134

**Figure 5-3.** The number of joints in a neuron’s RF (abscissa) plotted against the number of PCs in that neuron’s RF (ordinate). We find a lack of a significant difference, on average, between the number of PCs or the number of joints needed to explain single neurons’ spiking activity (statistics in text). Moreover, we find that in multi-PC models, the majority of neurons include in their RF at least one low-variance PC generally considered to reside outside of the hand postural synergy manifold (see text). All models shown have a pseudo- $R^2$  of at least 0.05. .... 135

**Figure 5-4.** Trial-averaged “neuronal ensemble”  $R^2$  measures using single joint axes of rotation—both the angles and angular velocities about these axes of rotation—as predictors in a multiple linear regression model (ordinate) plotted against similar models using individual PCs of hand joint movements (ordinate). We note a lack of significant difference in terms of the number of individual joint axes of rotation or kinematic PCs needed to explain neural ensemble activity (statistics in text). All models shown have a maximum pseudo- $R^2$  of at least 0.05. .... 137

**Figure 5-5.** Trial-averaged single-neuronal firing rate  $R^2$  measures using the same predictors on the ordinate and abscissa as in Figure 5-4. We note that even when averaging across trials, neural activity is no better explained by individual PCs of hand kinematics than by individual joint axes of rotation—in fact, individual joint axes of rotation explain slightly more variance in single-neuronal firing rates than do individual PCs (statistics in text). All models shown have a maximum pseudo- $R^2$  of at least 0.05. .... 137

**Figure A-1.** Behavioral task and kinematic recording methods. **(A)** Set of objects varying in shape, size, and orientation to encourage different grasps. **(B)** Presentation of objects to a monkey. An object is magnetically mounted onto a robotic arm. The monkey is seated in a chair with a photosensor placed in its armrest to discourage reaching. A trial begins once an object is mounted to the robot and the monkey’s arm is appropriately positioned to cover the photosensor in its armrest. If at any point during a trial the monkey’s arm is lifted to expose the photosensor to light, the trial is aborted. **(C)** Task timeline. Once the trial starts, the robot positions itself to present the object to the monkey. Once the robot begins to move toward the monkey, the monkey performs a grasp. Each grasp is manually scored off-line for three kinematic events: the start of movement, max aperture, and object contact (i.e., grasp). Neural data from 700ms prior to the start of movement to 10ms prior to grasp comprise the epoch of interest for analysis. After grasp, the monkey then holds the object until the robot retracts. **(D)** Positioning of reflective markers (31 total) on the monkey’s hand for kinematic recording. Triangles are placed just proximal and distal to both the elbow and wrist joints, and markers on the hand are placed at the most distal portions of each metacarpal and phalanx of each digit. Cameras capture the time-varying three-dimensional positions of these markers. With the aid of a musculoskeletal model of the arm and hand, inverse kinematics can be computed to estimate joint angles. .... 152

**Figure A-2.** Array placements relative to cortical surface landmarks. **(A)** Monkey 1 was implanted with two Utah electrode arrays (UEAs, Blackrock Microsystems, Salt Lake City, UT) in area 2 and rostral M1 and four floating microelectrode arrays (FMAs, Microprobes, Gaithersburg, MD) in area 3a and caudal M1. **(B-E)** Semichronic SC-96 arrays with individually depth-adjustable electrodes in **(B)** the right hemisphere of monkey 2, **(C)** the right hemisphere of monkey 3, **(D)** the left hemisphere of monkey 3, and **(E)** the left hemisphere of monkey 4..... 155

**Figure A-3.** Classification results for two types of cross-validation for **(A)** Monkey 2 and **(B)** Monkey 4, the two monkeys from which enough sessions (6 and 9, respectively) had been recorded to permit generalization in leave-one-session-out cross-validation. Faded traces indicate classification accuracy on one session after training on the other sessions recorded from that monkey. Bold traces indicate classification accuracy when leaving one trial out and training on all other trials pooled across sessions. Leave-one-trial-out cross-validation tends to match the overall accuracy and time course of the leave-one-session-out cross-validated accuracy curves. Kinematics across different sessions are therefore similar enough to minimize the hazard of pooling neural responses across those sessions. .... 161

**Figure A-4.** Effect of averaging kinematics over repeated trials of the same object (pooled across sessions) on the apparent dimensionality of Monkey 2’s kinematic data. Roughly 8-dimensional at 90% variance explained when not trial-averaged, the kinematics appear to be roughly 4-dimensional when trial-averaged. This indicates that within-trial variability acts to increase the apparent dimensionality of the kinematics, and presumably the neural data as well. .... 161

## LIST OF TABLES

**Table 4-1.** Multiple two-sample, equal-variance T-tests for significant differences between goodness-of-fit metrics seen in our hand data versus data from a previous report in proximal limb motor cortical neurons (Aflalo & Graziano, 2007). These proximal limb cortical data were compared with our hand data due to the lack of trial-averaging of the firing rates prior to computing goodness-of-fit. Highlighted cells indicate significant differences (FWER < 0.05, Holm-Bonferroni method). Black squares indicate the lack of enough neurons from our hand dataset to make a comparison ( $N_{\text{hand}} < 5$  with  $\text{pseudo-R}^2 > 0.05$ ). No mean  $\text{pseudo-R}^2$  value from any area or monkey in our dataset was significantly smaller than the mean  $\text{pseudo-R}^2$  seen in the previously reported M1 data to which it was compared. We assume comparability of  $\text{pseudo-R}^2$  to the traditional coefficient of determination in this analysis. We also only analyze the set of  $\text{pseudo-R}^2$  or  $R^2$  values in each dataset greater than or equal to 0.05, although this comprised the majority of our hand data (c.f. Figure 4-1) and similarly comprised roughly 65% of the previously reported M1 data. .... 104

**Table A-1.** Joints and joint angular coordinates reconstructed during inverse kinematics. \* Joint not reconstructed for Monkey 1 kinematics. \*\* Joint angular coordinate not reconstructed for Monkey 1 kinematics. .... 154

## LIST OF PUBLICATIONS

Chapter 1 has been published, in an altered form, as:

Goodman, J. M., & Bensmaia, S. J. (2018). The neural basis of haptic perception. In J. T. Wixted & J. T. Serences (Eds.), *The stevens handbook of experimental psychology and cognitive neuroscience. Volume II: Sensation, perception, and attention*. (4th ed.). New York, NY.

Chapters 3-5 are currently being submitted for publication.

A side project not part of this dissertation, but related to the broader topic of somatosensory information processing in the nervous system, has been published as:

Goodman, J. M., & Bensmaia, S. J. (2017). A Variation Code Accounts for the Perceived Roughness of Coarsely Textured Surfaces. *Scientific Reports*, 7(1), 46699.

## ABSTRACT

Despite the remarkable complexity of our hands, we effortlessly use them to grasp and manipulate objects. To achieve dexterous object manipulation requires not only a sophisticated motor system to move the hand but also a sensory system to provide sensory feedback — proprioceptive and tactile — about the consequences of those movements. While some progress has been made to understand the neural basis of touch in somatosensory cortex, much less is known about the neural basis of hand proprioception. To fill this gap, we simultaneously record time-varying joint kinematics of the hand — measured using a camera-based motion tracking system — and neural activity from somatosensory and motor cortices of rhesus macaques — using chronically implanted electrode arrays — as they perform natural grasping movements and are subjected to passive hand movements. We find that somatosensory representations of kinematics are very similar to their motor counterparts, with spiking activity preferentially encoding the postures (not the velocities) of multiple joints spanning the entire hand. Preferential encoding of hand posture stands in stark contrast to models of kinematic encoding of the shoulder and elbow, where velocities are preferentially encoded. Moreover, we observe similar response properties in somatosensory and motor cortices during both active and passive movements of the wrist and digits. We conclude that hand shaping via movements of the digits and wrist relies on different neural mechanisms than does hand transport via movements of the arm.

## **CHAPTER 1:**

### **Introduction to haptic sensation**

#### **Preface**

The goal of this dissertation, broadly speaking, is to determine the nature of how hand postures and movements are represented in somatosensory cortex. We discuss in this chapter the nature of the sense of touch and the computations performed by the nervous system as one ascends the neuraxis. We also discuss the more mysterious sense of proprioception—the modality through which hand postures and movements are sensed—and how its neural code compares and contrasts with the comparatively more well-studied neural code for touch. This chapter on haptic sensation has been published as a book chapter (Goodman & Bensmaia, 2018).

#### **Introduction**

When we interact with an object, neural signals from the skin, joints, and muscles convey information about the shape, size, weight, and texture of the object. If the object is moving across the hand, information about its direction and speed is also available. The senses of touch and proprioception play a key role in our sense of embodiment, the sense that our bodies are a part of us. Somatosensation is also very important for affective communication: We touch the people we love. Finally, haptic feedback is critical to our ability to dexterously manipulate objects. Without it, we would struggle to perform the most basic activities of daily living, like buttoning a shirt or turning a door knob. Indeed, while vision is critical to identify objects and locate them in space, only somatosensory signals provide the information about contact with objects that allows us to interact with them effectively.

## **The sense of touch**

### **Cutaneous mechanoreceptors and associated nerve fibers**

The skin contains a variety of different types of receptors that respond to different types of stimulation. Thermoreceptors respond to non-painful changes in skin temperature, nociceptors (pain receptors) respond to strong mechanical, thermal, or chemical stimulation of the skin that is liable to damage it, and low-threshold cutaneous mechanoreceptors respond to small (non-painful) skin deformations. The palmar surface of the hand contains four types of mechanoreceptors, each of which responds to different aspects of skin deformations: Merkel cells, Meissner corpuscles, Pacinian corpuscles, and Ruffini endings (Figure 1-1). These receptors convert the mechanical deformations of the skin into neural signals, which are carried to the brain by large diameter A $\beta$  nerve fibers. Afferent signals convey information about objects grasped in the hand and are interpreted by downstream structures in the brain.

*Merkel cells* are approximately 10  $\mu\text{m}$  in diameter and located in the basal epidermal layer, generally grouped in complexes of 30 x 250  $\mu\text{m}$ , most often at the base of sweat ducts (Nolano et al., 2003). They are innervated by slowly adapting type 1 (SA1) afferents, which have small receptive fields (RFs) and produce sustained response to sustained indentations of the skin (Knibestol, 1975). That is, SA1 afferents only respond to stimulation of a small patch of skin, and when that patch is indented, the response of the afferent will persist for tens of seconds or minutes. SA1 afferents are also sensitive to low-frequency skin vibrations (< 30 Hz) delivered through a small punctate probe centered on their RF (Freeman and Johnson, 1982, Muniak et al., 2007). Electrical stimulation of a single individual SA1 afferent elicits a sensation of pressure that is localized to a small patch of skin whose location coincides with that of the receptive field (Ochoa and Torebjork, 1983).

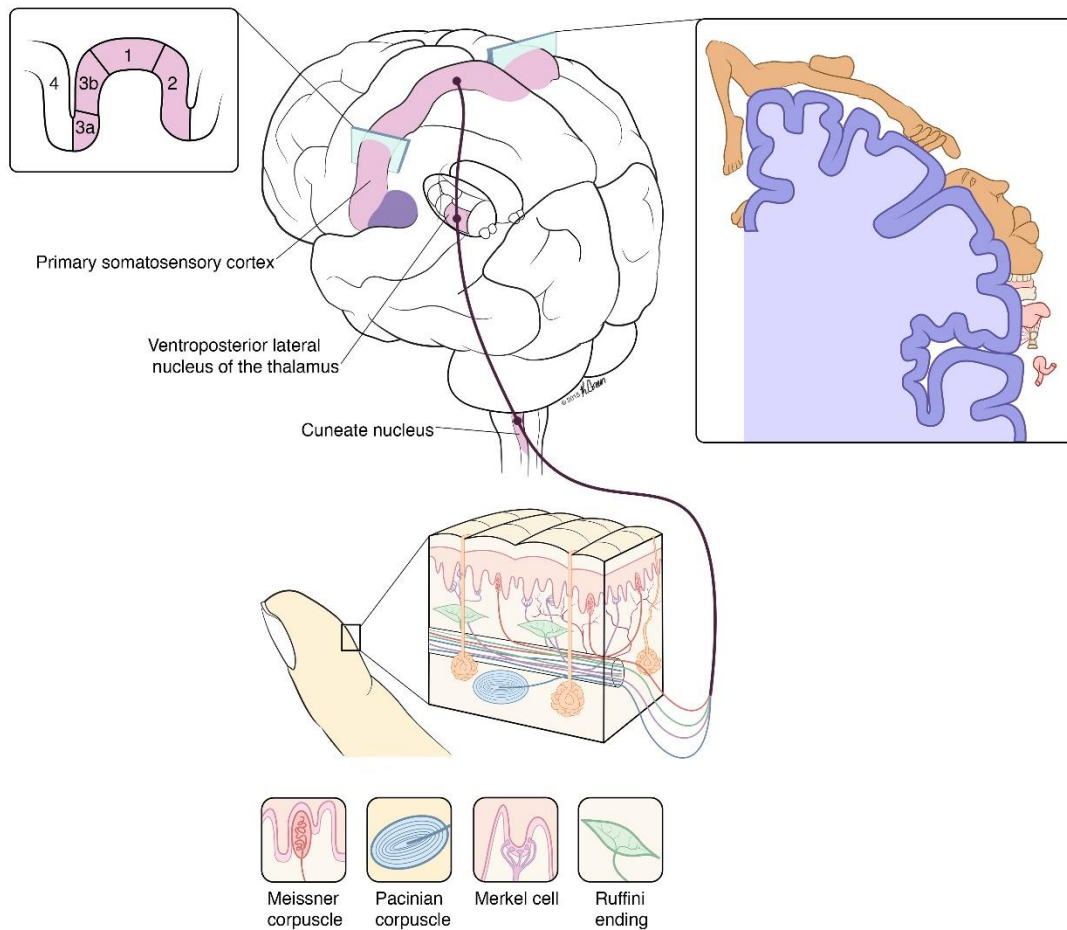


**Figure 1-1.** Medial lemniscal pathway for the sense of touch (illustration by Kenzie Green).

*Meissner corpuscles* are oval in shape, composed of stacks of disc-like lamellae, about 50 x 150  $\mu\text{m}$  in total size, and located in the dermal papillae (Cauna, 1956, Bell et al., 1994, Pare et al., 2001, Nolano et al., 2003). They are innervated by rapidly adapting (RA) afferents, which also have small receptive fields (albeit larger than their SA1 counterparts) and produce transient responses at the onset and offset of skin indentations (Knibestol, 1973). That is, they only respond during dynamic indentations of the skin but not static ones. RA afferents respond best to skin vibrations at intermediate frequencies (peaking in sensitivity around 60 Hz) delivered through a

small punctate probe centered on their RF (Freeman and Johnson, 1982, Muniak et al., 2007). Electrical stimulation of an individual RA afferent elicits a sensation of skin flutter that is localized to a small patch of skin (again matching the afferent's receptive field) (Ochoa and Torebjork, 1983).

*Pacinian corpuscles* have an oval, onion-like appearance, and are typically between 0.5 and 2 mm in length in adults (Pease and Quilliam, 1957, Cauna and Mannan, 1958), and are located in the subcutaneous fat pads of the fingers and palms (Zelena, 1978), among other places. They are innervated by PC afferents, which have large diffuse receptive fields and, like their RA counterparts, produce transient responses at the onset and offset of skin indentations (Johansson, 1978, Vallbo and Johansson, 1984). PC afferents are exquisitely sensitive to skin vibrations, particularly if these are delivered over a wide contact area (Brisben et al., 1999) and peak in sensitivity around 250 Hz, where detection thresholds can be as low as 100 nm. Electrical stimulation of individual PC fibers elicits sensations of skin vibrations that are far more confined than one might expect given the size of their RFs (Ochoa and Torebjork, 1983).

*Ruffini endings* are 1.4-mm long spindle-shaped structures, located deep in the dermis and most densely situated around the nail (Pare et al., 2002, Pare et al., 2003, Birznieks et al., 2009). They are thought to be innervated by slowly adapting type 2 (SA2) fibers, which have large receptive fields and produce sustained responses to sustained skin stretch (Johansson, 1978). Like their PC counterparts, SA2 fibers respond to vibrations over a wide range of frequencies, albeit with lower sensitivity (Gynther et al., 1992). Electrical stimulation of individual SA2 fibers often produces no sensation; when a sensation is produced, it is of pulling of the skin, seemingly deep within the tissue (Ochoa and Torebjork, 1983).

Mechanosensitivity is conferred to the different mechanoreceptors by ion channels in their cell membrane that generate currents in response to mechanical perturbations. There are two mechanisms by which these ion channels might be opened (McCarter et al., 1999, Hu and Lewin, 2006): Mechanosensitive channels in the cell membrane open either directly in response to membrane stretch (Sachs, 2010) or are tethered to fibers in the tissue surrounding the cell membrane, which pull the channels open when this tissue is deformed (Hu et al., 2010). Three ion channel families have been implicated in mammalian mechanotransduction: acid-sensing ion channels (ASIC), transient receptor potential (TRP) channels, and Piezo proteins (Tsunozaki and Bautista, 2009, Coste et al., 2010, Delmas et al., 2011, Coste et al., 2012, Woo et al., 2014, Volkers et al., 2015). While ASICs and TRPs likely mediate visceral and nociceptive mechanosensation (Liedtke and Friedman, 2003, Suzuki et al., 2003, Drew et al., 2004, Nagata et al., 2005, Lu et al., 2009, Kremeyer et al., 2010), Piezo proteins are thought to be primarily responsible for mammalian touch (Delmas et al., 2011, Volkers et al., 2015).

Mechanotransduction is shaped not only by the properties of mechanosensitive ion channels, but also by the mechanical properties of the nerve ending. For example, the Pacinian corpuscle consists of several neatly-arranged concentric lamellae with layers of viscous fluid between each (Pease and Quilliam, 1957). This structure shields the afferent in the center from static deformations while allowing very high-frequency components to pass through easily (Loewenstein and Skalak, 1966). As a result, PC afferents produce a slowly-adapting response to indentations when the Pacinian corpuscle is removed (Mendelson and Lowenstein, 1964, Loewenstein and Mendelson, 1965). Recent evidence suggests that Merkel cells synapse onto SA1 afferents and contain vesicles filled with neuromodulators. Their removal substantially reduces the sustained response of SA1 afferents. Furthermore, isolated Merkel cells produce ion currents in

response to mechanical perturbation (Maksimovic et al., 2014). The role of Merkel cells appears to be to modulate the response of the mechanosensitive SA1 neurite endings. Meissner corpuscles consist of several irregularly-arranged lamellar discs with serrated edges that bend axon terminals of interstitial RA afferents during initial mechanical loading. During sustained loading, a smooth, viscoelastic region in the center of the discs absorbs the stress, allowing the edges of the discs to return to their original positions and, in turn, stop imposing deformation upon the nerve endings. In this way, the characteristic rapidly adapting response of these afferents arises (Takahashi-Iwanaga and Shimoda, 2003).

Mechanoreceptive afferents do not only differ in their response properties, but also in their distribution in the skin. RA and SA1 fibers innervate the glabrous skin of the hand most densely (~140 and 80 units per cm<sup>2</sup> on the fingertip) while PC and SA2 afferents are far less prevalent (~20 and 10 units per cm<sup>2</sup>) (Johansson and Vallbo, 1979). The density of RA and SA1 afferent decreases sharply as one proceeds proximally from the fingertips, whereas that of PC and SA2 afferents remains relatively constant. Note, however, that Pacinian receptors located in the palm of the hand and even in the forearm will respond robustly when the fingertips come into contact with an object (Westling and Johansson, 1987, Delhaye et al., 2012, Manfredi et al., 2012), so large numbers of PC afferents are recruited during interactions with objects, regardless of contact location. Indeed, these receptors are exquisitely sensitive to vibrations that propagate across the skin.

### **Skin mechanics and afferent branching**

Forces applied to the skin's surface propagate through the tissue and produce stresses and strains at the locations of the receptors, which cause the membranes of their neurites to depolarize, ultimately evoking spikes in the associated nerve fibers. Because the stimulus propagates through the tissue before reaching the receptors, these only experience a distorted version of the stimulus:

Certain features in the stimulus are enhanced while others are obscured simply due to skin mechanics (Phillips and Johnson, 1981b, Dandekar et al., 2003, Sripathi et al., 2006). Specifically, external corners and edges in the object are strongly enhanced because these exert more force on the skin's surface than do internal object features. Internal features are further obscured because they are filtered out as the forces exerted on the skin's surface propagate through the tissue because of the presence of adjacent features. From one perspective, skin mechanics are valuable in that they enhance edges and corners, a process that requires specialized neural machinery in the retina (namely lateral inhibition). On the other hand, the sense of touch is poor at conveying complex and fine spatial structure due in part to this mechanical filtering of the skin (Apkarianstielau and Loomis, 1975, Cho et al., 2016). This limitation can be overcome to some extent when the skin moves across the spatial patterns (see section on texture coding).

Because Merkel cells are located in the epidermis, forces applied to the skin's surface do not have to propagate far to reach them. Moreover, various cellular structures tightly anchor Merkel Cells to the epidermis (Munger, 1965, Iggo and Muir, 1969, Halata et al., 2003). As a result, they respond only to local skin deformations and can therefore convey information about skin deformations with a high spatial resolution. Meissner corpuscles are also superficial, being located in the dermal papillae, which are protrusions of the dermis into the epidermis. However, the link between Meissner corpuscles and the epidermis consists of a network of collagen fibers, which is less rigid a coupling than that of Merkel cells (Cauna, 1956, Takahashi-Iwanaga and Shimoda, 2003) and may contribute to the reduced spatial acuity of RA afferents compared to their SA1 counterparts. Pacinian corpuscles are situated deep in the dermis, so forces applied to the skin must propagate long distances to reach them, thereby giving rise to the large and diffuse receptive fields of PC afferents.

The neural image carried by the nerve fibers is further distorted by afferent branching. Indeed, SA1 and RA afferents innervate multiple Merkel cells and Meissner corpuscles, respectively. Individual SA1 afferent and RA fibers may innervate as many as 100 Merkel cells (Johnson, 2001) and 15 to 30 Meissner corpuscles (Johansson, 1978), respectively. How signals from multiple neurite branches are combined to culminate in an afferent spike train remains a topic of debate. According to one view, inspired by work with non-mammals (Adrian and Zotterman, 1926a, b), the afferent response reflects the sum of inputs across all of its neurites. According to the other view, dubbed the "driver" model (Lesniak et al., 2014), spike trains propagate along neurites to an intersection and, from the intersection, will propagate not only orthodromically along the nerve, but also antidromically along the adjoining neurites. Antidromic spike propagation leads to spike collisions along the other neurites, thereby canceling out their contributions to the afferent firing rate. That way, a single neurite "drives" the firing rate of the entire afferent by suppressing the influence of all the other neurites. Anatomical and electrophysiological data from mammals support the driver model (Horch et al., 1974, Lesniak et al., 2014).

Regardless of which mechanisms mediates the integration of signals from the different branches, this branching structure leads to additional spatial filtering of the stimulus in the response. However, the more complex receptive field structures that result from this convergent input may also confer to afferents some preference for certain stimulus features over others. For example, nerve fibers with radially asymmetric receptive fields tend to respond more strongly to edges at some orientations than at others (Pruszynski and Johansson, 2014), which may pave the way for the strong orientation selectivity observed in cortex (see below).

## **Tactile coding in the somatosensory nerve**

Information about objects is multiplexed in the responses of the four cutaneous mechanoreceptive afferents that innervate the glabrous skin of the hand: Some aspects of the responses convey information about shape, others about texture, and yet others about motion. Initially, the different afferent types were thought to play fundamentally different roles in touch (Johnson, 2001). SA1 fibers were thought to mediate tactile shape and texture perception, RA fibers tactile motion perception, PC fibers vibration perception, and SA2 fibers hand proprioception (the sense of the position and movements of the fingers). However, all afferent types are activated during contact with objects and, it turns out, signals from most or all of them convey information about any one object feature (Saal and Bensmaia, 2014). The different types of afferents differ in what features they preferentially respond to: SA1 afferents tend to respond to larger stimulus features (edges, coarse textural features) that are either static or move slowly across the skin; PC afferents are capable of responding to very small stimulus features (less than 1 micron in size) that move rapidly; RA afferents fall somewhere between those two extremes. Because most objects comprise elements whose size vary over orders of magnitude, all fiber types tend to be involved in touch sensations under most circumstances. Nonetheless, different aspects of the afferent responses convey different types of information about an object and the same responses from the same afferents are read out (decoded) in different ways to extract this disparate information.

## **Stimulus magnitude**

Intensity is one of the most basic stimulus dimensions. In vision, it corresponds to brightness; in audition, to loudness; in olfaction, gustation, and touch, it is described using more generic terms: a weak/strong taste, smell, or touch (Bensmaia, 2008). The neural determinants of

tactile intensity were first investigated by Kenneth Johnson, who, along with his mentor Vernon Mountcastle, made the following observation: While the perceived intensity of a sinusoidal vibration applied to the skin grows smoothly as a function of the amplitude of the stimulus, the firing rate of individual mechanoreceptive fibers does not (Figure 1-2A). Instead, the function that relates firing rate of individual fibers to intensity is a piece-wise linear function, punctuated by long plateaus (Talbot et al., 1968a, Johnson, 1974). In contrast, the perceived intensity of a stimulus is a smooth monotonic function of its amplitude. This discrepancy between the responses of individual afferents and the resulting perceptual experience led to the conclusion that the perceived magnitude of a tactile stimulus is determined by the response of a population of afferents. Indeed, if perception were determined by a single afferent, perceptual magnitude would also be constant over large ranges of stimulus amplitude. Similarly, while both the firing rates of mechanoreceptive afferents (Werner and Mountcastle, 1965) and the perceived intensity of skin indentations (Lamotte, 1977) increase linearly with indentation depth, the perceived intensity of indentations depends on the rate of indentation and on the duration of the indentation plateau in ways that cannot be predicted from the responses of any one type of mechanoreceptive afferent (Poulos et al., 1984).

In a psychophysical study (with human participants) paired with a neurophysiological one (with monkeys), using the same set of vibratory stimuli, the perceived intensity of a tactile stimulus was shown to be determined by the response of all afferents that respond to the stimulus (Muniak et al., 2007). While the spike rate of any one population of fibers could not predict how intense a stimulus felt, the total population response predicted with high precision the perceived intensity. Furthermore, spikes from the different populations did not contribute to sensory magnitude equally: SA1 spikes were contribute more to perceived intensity than do RA spikes, which in turn

are weighted more than PC spikes (Bensmaia, 2008). Thus, signals from the various sensory channels are integrated to determine how intense a stimulus will feel.

### **Vibratory frequency**

Skin vibrations evoke sensations with distinct qualities (and mediate primarily by distinct populations of afferents) depending on what range of frequencies they fall in. Skin oscillations ranging in frequency from 1 to 50 Hz evoke a sensation of light flutter, which can be accurately localized and is mediated primarily by RA fibers. As the frequency increases beyond 60 Hz or so, the sensation changes to one of vibratory hum, emanating from deeper tissue and more poorly localized (Talbot et al., 1968a). Human observers can distinguish skin vibrations on the basis of their frequency across both flutter and vibration ranges (Goff, 1967, Franzen and Nordmark, 1975, LaMotte and Mountcastle, 1975, Salinas et al., 2000, Tommerdahl et al., 2005): In the flutter range (5–50Hz), a 10% change in frequency can be perceived about 75% of the time; in the vibration range (>100Hz), a 30% change in frequency is required to achieve this level of discrimination performance. While the ability to discriminate changes in frequency might be in part attributable to the concomitant change in perceived magnitude (Verrillo et al., 1969, Hollins and Roy, 1996, Muniak et al., 2007), changes in vibratory frequency also result in changes in vibrotactile pitch, as evidenced by the fact that tactile frequency discrimination is not substantially impaired when the stimulus amplitude varies unpredictably from stimulus to stimulus (Yau et al., 2009b, Harvey et al., 2013).

A striking feature of afferent responses to sinusoidal vibrations is their entrainment: an afferent tends to produce one spike or burst of spikes confined to a small portion of each stimulus cycle (Figure 1-2B) (Talbot et al., 1968b, Freeman and Johnson, 1982, Mackevicius et al., 2012). This patterning in the spiking response was thought to account for the ability to discern the

vibratory frequency. Indeed, over a range of amplitudes, sinusoidal vibrations evoke a response in afferents but this response is not entrained to the stimulus (LaMotte and Mountcastle, 1975). Over this so-called atonal interval, the vibrations are tangible, but their frequency is indiscernible. While this evidence was circumstantial, it was later confirmed that temporal patterning in afferent responses does convey information about stimulus frequency, not just for sinusoids but also for more complex (and ecological) skin vibrations (Mackevicius et al., 2012). Furthermore, the entrainment of the vibrations to the stimulus shapes the way skin vibrations are perceived and accounts for the perceptual experience of vibrotactile pitch.

In the aforementioned experiments, skin vibrations were generated using vibratory motors, which allows for fine control of the stimulation waveform. These experiments provided insights into how information is encoded in the nerve, and specifically what role spike timing might play. One might ask what ecological role vibrotaction plays. In everyday life, skin vibrations caused by footsteps, as they propagate across the floor, convey information about someone's approach. When we interact with an object indirectly through other objects—like with paper through a writing utensil, with food through an eating utensil, or with the ground through a walking cane—vibrations propagating through the grasped object convey information about the other objects with which it comes into contact (Katz, 1925, Brisben et al., 1999). The transduction and processing of vibrations also plays an important role in the perception of texture, as detailed below.

### **Shape**

When we grasp an object, cutaneous signals convey information about its shape. Cutaneous information about local features of the object at each contact point is integrated with information about the relative position of the contact points—that is, information about the conformation of

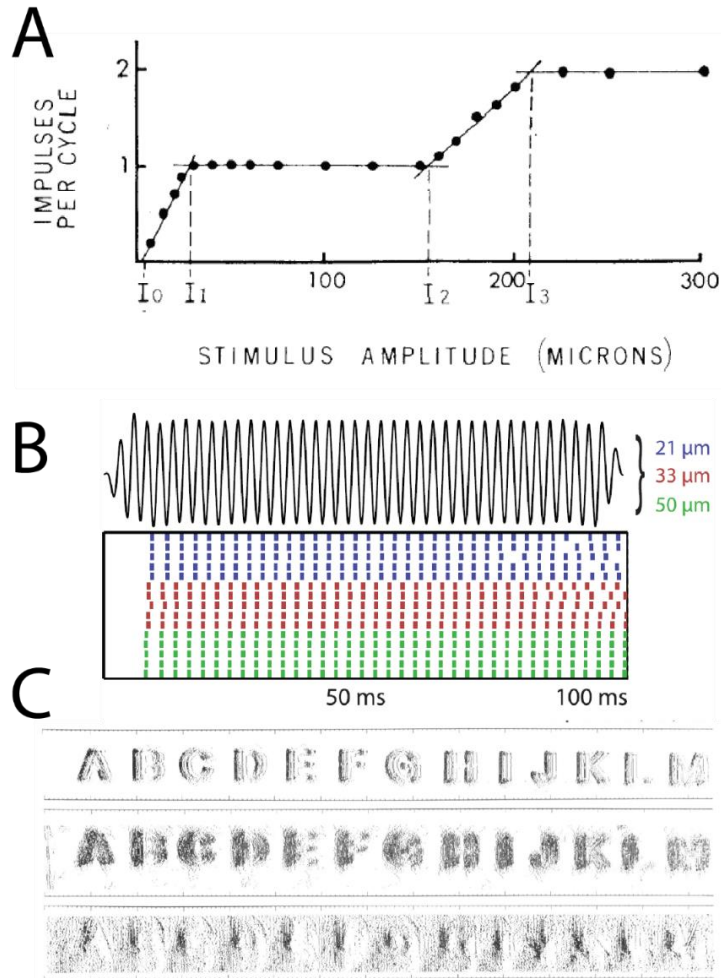


**Figure 1-2.** (A) Firing rate evoked in an RA fiber by 40-Hz skin vibrations of varying amplitudes. The rate increases as a piece-wise linear function of amplitude, interspersed with entrainment plateaus over which the fiber fires an integer number of spikes per stimulus cycle (Johnson, 1974). (B) Responses of a PC fiber to a 400-Hz skin vibration at three amplitudes. The spiking response is highly patterned and repeatable and conveys information about the frequency of the stimulus (Mackevicius et al., 2012). (C) Reconstruction of the spatial pattern of activation evoked in a population of SA1 (top), RA (middle) and PC (bottom) afferents when embossed letters are scanned across the skin. The spatial pattern of activation reflects the spatial configuration of the stimulus (Phillips et al., 1988).

the hand—to achieve a three dimensional image of the object (see below) (Hsiao, 2008). First, we examine how this local feature information is encoded in the responses of mechanoreceptive afferents. When a spatial pattern is indented into or scanned across the skin, its spatial features are reflected in the spatial pattern of activation evoked in SA1 and RA afferents (Figure 1-2C)(Johnson and Lamb, 1981, Phillips et al., 1988, Goodwin et al., 1995, Wheat and Goodwin, 2000, 2001).

SA1 afferents convey the most spatially acute neural image and mediate our ability to discern the smallest tangible features. Tactile spatial acuity is most reliably measured using the grating orientation discrimination task, in which subjects identify the orientation of gratings indented into the skin (with the ridges and grooves parallel or perpendicular to the long axis of the finger). As the ridges and grooves get narrower, it becomes more and more difficult to make out their orientation (Craig and Johnson, 2000). The finest gratings whose orientations can be discerned – with a spatial period of about 2 mm – evoke spatially modulated responses in SA1 but not RA afferents (Phillips and Johnson, 1981a, Bensmaia et al., 2006b). In other words, SA1 fibers signal the presence of a fine grating while RA fibers respond to it as if it were a flat surface. In fact, at the limits of our tactile spatial acuity, RA input seems to interfere with SA1 input: We can better discern small spatial features if RA fibers do not respond (Bensmaia et al., 2006a). Note that this task become trivially easy regardless of groove width if the grating is scanned across the finger (as described below in the section on texture).

However, RA signals do convey information about coarse spatial features. The most compelling evidence for this is provided by the successful use of the optical to tactile converter (Optacon)(Bliss et al., 1970). The Optacon consists of an array of pins that each can be made to vibrate. The idea was to convert the output of a camera scanned across text into patterned activation of the pins so that the letters scanned by the camera would be reproduced on the array. Subjects were able to recognize the letters with reasonable accuracy (Craig, 1980) despite the fact that the Optacon did not activate SA1 afferents at all (Gardner and Palmer, 1989). Thus, while SA1 fibers convey the most acute spatial signal, the spatial image carried by RA fibers can also convey information about the local spatial features of the object. Spatial information stemming from RA

fibers is probably more informative than that from their SA1 counterparts under certain circumstances, for example during dynamic contact with an object.

### **Texture**

We are exquisitely sensitive to surface microstructure, and are able to discern surfaces whose elements differ in size by tens of nanometers and in inter-element spacing by hundreds of nanometers (Skedung et al., 2013). Surface texture morphs slowly into local shape as the elements grow larger and farther apart, but texture extends well into the millimeter range, so texture perception spans about six orders of magnitude in size. This remarkable sensitivity to surface microstructure is made possible by the different mechanoreceptive afferents and their different response properties. Texture perception relies on (at least) two distinct mechanisms. Coarse textural features are encoded in the spatial pattern of activation in SA1 and RA afferents, as are local spatial contours (Figure 1-3A) (Connor et al., 1990, Connor and Johnson, 1992, Blake et al., 1997). At this scale, form and texture overlap. For example, a Braille word has both a form that defines it but also can be described as ‘rough.’ This mechanism for texture perception, however, is inherently limited by innervation density. Combined, SA1 and RA afferents have resolutions on the order of half a millimeter or so. If this mechanism were the only one we used, the range of tangible textures would be much narrower than it is.

Fortunately, the spatial mechanism is complemented by a temporal one: To make out fine textures, we do not simply press our fingers across a surface; we run our fingers across it (Lederman and Klatzky, 1993). Without this lateral movement between skin and surface, we are unable to make out fine surfaced features (Hollins and Risner, 2000). When we run our fingers across a textured surface, small vibrations are produced in the skin. These vibrations are shaped by the texture, the speed at which it is scanned, and geometry of the fingertip skin (Bensmaïa and

Hollins, 2003, Bensmaia and Hollins, 2005, Delhaye et al., 2012, Manfredi et al., 2014). Indeed, the vibrations produced in the skin reflect the spatial layout of surface features, with features whose spatial period matches that of the fingerprint enhanced relative to others. Furthermore, the vibrations dilate or contract systematically (and so their frequency composition translates left and right along the frequency axis) with decreases or increases in scanning speed, respectively. The skin vibrations elicited during texture scanning activate vibrotactile afferents, namely RA and PC afferents (Lamb, 1983, Weber et al., 2013). Texture responses convey information about the stimulus in their temporal patterning, which reflects the temporal structure of the vibrations (Figure 1-3B). In other words, the frequency composition of the skin vibrations is reflected in that of the spiking responses, and these patterns are highly informative about texture identity when decoded with a precision on the order of two to five milliseconds. Furthermore, texture-elicited vibrations propagate across the skin and excite PC afferents throughout the hand and even the forearm. Texture information therefore does not stem solely from the point of contact with the surface but from the entire hand, as evidenced by the fact that subjects can perform a roughness discrimination task even when their fingertip has been numbed with an anesthetic (Libouton et al., 2012). As might be expected, texture-specific spiking patterns also dilate or contract with decreases or increases in scanning speed, respectively (Weber et al., 2013). The temporal mode of texture perception in primates is analogous to the principal mode of texture perception in rodents, who sense texture from deflections produced in their whiskers as they scan them across surfaces (Diamond, 2010).

The spatial and temporal mechanisms are seamlessly integrated to form a holistic percept of texture, shaped by the responses of all activated mechanoreceptive afferents. Texture can be broken down into a number of perceptual dimensions, the most salient of which are

roughness/smoothness, hardness/softness, stickiness/slipperiness, and warmth/coolness (Hollins et al., 1993, Hollins et al., 2000). Of these, the most prominent is roughness, which has received a lot of experimental attention (Hollins and Bensmaia, 2007). The perceived roughness cannot be predicted from the responses of any one population of fibers. Rather, the inhomogeneity in the *spatial* pattern of response in SA1 fibers combined with the inhomogeneity in the *temporal* pattern of response in RA and PC fibers accounts for the perceived roughness of surfaces spanning the range of tangible textures with remarkable accuracy (Weber et al., 2013). This makes sense because uneven surfaces, which are perceived as rougher, produce a spatially inhomogeneous response in SA1 fibers – some SA1 fibers are activated by surface elements impinging upon the RFs while others are not – and responses in RA and PC fibers wax and wane as coarse elements move across their RFs.

Hardness/softness is the subjective continuum associated with the compliance of an object (Harper and Stevens, 1964). Softness perception has been shown to rely primarily on cutaneous cues: eliminating kinesthetic information has no effect on subjects' ability to discriminate softness (Srinivasan and Lamotte, 1995). Indeed, a compliant surface is more liable to conform to the contour of the skin than is a hard one. Accordingly, the compliance of the object may be signaled by the growth of the area over which the skin contacts the object as the contact force increases, as well as by the more distribution of forces exerted by the object on the skin across the contact area. Softness perception has been thought to rely on signals from SA1 fibers (Srinivasan and LaMotte, 1996). First, PC fibers are too sparse and their RFs too large to signal pressure gradients or contact area. Second, the response of RA fibers to a surface indented into the skin is not modulated by the compliance of the surface whereas the response of SA1 fibers is (Srinivasan and LaMotte, 1996). However, the neural code for softness cannot simply be dependent on the strength of the response

evoked in individual SA1 fibers as both the rate at which a surface is indented into the skin and its compliance modulate SA1 firing rates; in contrast, softness perception is independent of the indentation rate. Rather, compliance may be encoded in the spatial pattern of activation across SA1 afferents or perhaps in relative activations of the three populations of afferents.

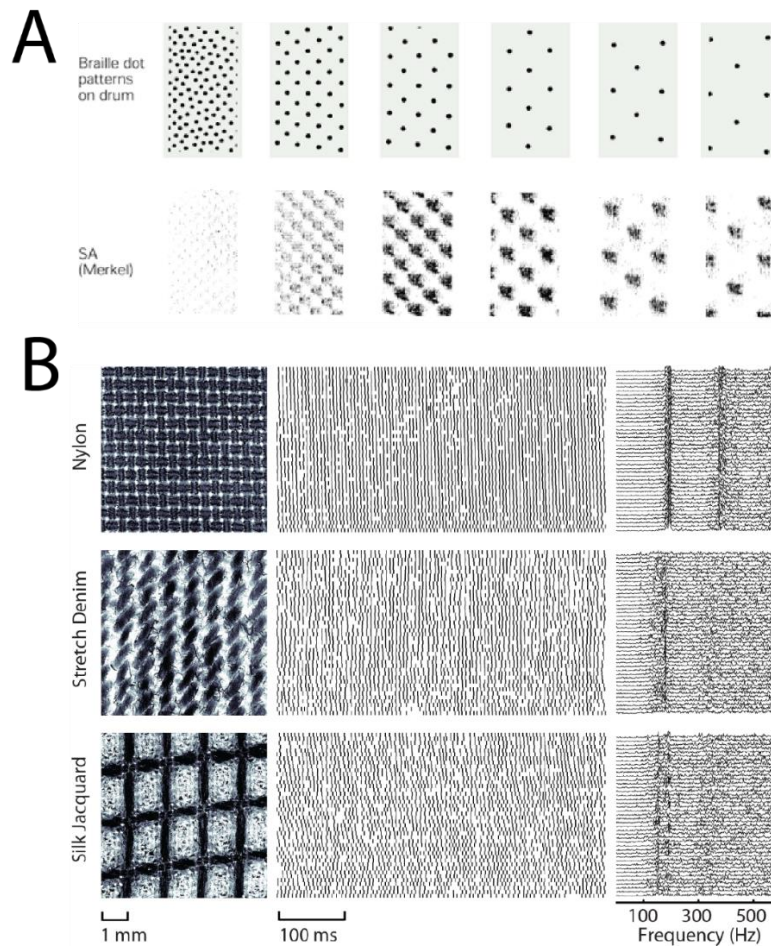


**Figure 1-3.** (A) Reconstruction of the response in a population of SA1 afferents evoked by embossed dot patterns scanned across the skin. The spatial configuration of the dots is reflected in the pattern of activation evoked in the afferents. (B) Response of a PC fiber to three finely textured fabrics. Left: Microscope image of the texture; middle: spiking responses to 40 repeated presentations of the textured surface; right: power spectrum of the neural response. Each texture produces a different but highly repeatable temporal spiking pattern (Weber et al., 2013).

Stickiness/slipperiness is the sensory continuum associated with the friction between skin and surface, i.e. the ratio between the force exerted normal to the surface to that exerted parallel to the plane of the surface (Smith and Scott, 1996). Furthermore, when judging stickiness, subjects

do not substantially vary the normal forces they apply on the surface, but the applied tangential forces tend to vary across surfaces, suggesting that tangential forces are critical in the perception of stickiness (Callier et al., 2015). As slowly adapting type 2 fibers are sensitive to skin stretch (Knibestol, 1975), this population of mechanoreceptive afferent fibers may provide the peripheral signals underlying stickiness perception, although recent evidence suggests that other mechanoreceptive afferents also convey information about tangential forces exerted on the skin (Birznieks et al., 2001).

The warmth or coolness of a surface is another important textural dimension, one that is associated with the thermal conductivity of the material. Metals feel cool because they conduct heat out of the skin whereas plastics feel warm because they do not conduct heat. This sensory information about the thermal conductivity of a surface, which implicates warm and cool fibers in the skin (Ho and Jones, 2006, 2008), is integrated with information about surface microstructure to yield a holistic percept of texture. The perception of texture is thus a canonical example of the interplay of the different modalities, and of the exploitation of their disparate response properties (Saal and Bensmaia, 2014, Pirschel and Kretzberg, 2016).

### **Motion**

The haptic exploration of objects typically involves movement between the hand and the object (Lederman and Klatzky, 1993). As discussed above, if we seek information about texture, we move our fingers across the surface. If we seek information about the shape of an object, we follow its contours with our fingertips. Furthermore, we need to sense how objects move across our skin to dexterously manipulate them. Information about tactile motion is thought to be conveyed by two different mechanisms (Pei and Bensmaia, 2014). One is the sequential activation of mechanoreceptive fibers with neighboring RFs (Gardner and Costanzo, 1980), a mechanism

that is akin to its visual counterpart (involving sequential activation of neighboring photoreceptors). The other is the activation of SA2 fibers, which are sensitive to skin stretch: The skin will tend to be pulled in the direction of the moving stimulus, so these stretch-related signals can convey information about movement direction (Olausson et al., 2000). Afferent firing rates increase monotonically with the speed at which an object moves across the skin, but they are also modulated by texture, so it is not clear how information about speed and texture can be disambiguated from the responses of afferents. In fact, while texture perception is consistent over a wide range of scanning speeds, speed perception is dependent on texture (Depeault et al., 2008). Nonetheless, information about scanning speed is perceptually available (if not veridical) so it remains unknown how this information is extracted from afferent responses. The evidence suggests that motion representations at the periphery involve multiple afferent types (Pei and Bensmaia, 2014).

### **Peripheral signals during object manipulation**

The sense of touch plays a key role in our ability to interact with objects. Indeed, the dexterous manipulation of objects requires the rapid integration of motor commands, sensory cues, and internal predictions. A lack of cutaneous input from the fingertips results in a large compensatory increase in grip force that fails to adapt appropriately to object slips (Augurelle et al., 2003, Nowak et al., 2003). The importance of cutaneous input for object manipulation is underscored by the fact that patients with sensory nerve damage primarily complain of motor deficiencies rather than of the sensory loss itself (Moberg, 1962, Jones and Lederman, 2006).

Information about the forces we exert on an object is critical to our ability to grasp and manipulate it: We apply enough force so that it will not slip from our grasp but not much more than that. Indeed, the safety margin, the amount of force exerted above the minimum necessary to

avoid slip ranges from 10 to 40 %, depending on the individual (Johansson and Westling, 1984, Westling and Johansson, 1984, Augurelle et al., 2003). Mechanoreceptive afferents, particularly SA1 and SA2 fibers, provide precise information not only about the magnitude but also about the direction of forces exerted on the skin (Birznieks et al., 2001, Wheat et al., 2010). Interestingly, SA2 afferents with RFs near the nail are particularly informative as to force direction (Birznieks et al., 2010). The importance of these cutaneous cues to object manipulation is demonstrated in experiments with digital anesthesia: When cutaneous cues are eliminated by anesthetizing the fingertips, subjects exert substantially more force on objects when grasping them (Augurelle et al., 2003).

Most of the classical work on somatosensory processing focuses on perceptual tasks with passively applied stimuli, in which ample time is provided to integrate sensory features at all levels of the somatosensory neuraxis, from periphery to cortex. However, object manipulation involves dynamic, multi-contact interactions. Furthermore, due to delays in the deployment of motor responses that are approximately 100 ms in duration, timely correction for unanticipated sensory signals requires that this information be conveyed within a very short time window (Johansson and Flanagan, 2009). Long motor output delays require the presence of feedforward in addition to feedback signals, implying the presence of an internal model. A broad question therefore emerges from these constraints: how does the somatosensory system manage to do everything it needs to do with so little time to integrate the incoming sensory information?

Much work on peripheral cutaneous signals during object manipulation has focused on recordings of peripheral afferents during an object lifting task (Johansson and Westling, 1984) in which subjects grip a thin rod using the index finger and thumb. Subjects are then instructed to lift the rod, which is attached to a force transducer and a weight. The texture and mass of the

manipulandum can be varied from trial to trial, thereby manipulating the grip and load forces required to perform the task. The task is split into four phases: contact, load, lift, and hold (Figure 1-4). The different types of afferent exhibit distinct response patterns during the task and respond differently during the various phases of the task. The most striking features of the neural signature of this task are the transient bursts of activity tightly coupled with the initiation of the contact and lift phases, which result in large scale deformations of the fingertip and activate afferents terminating all over the fingerpad, not just over the contact area (Bisley et al., 2000, Birznieks et al., 2001). Importantly, the timing of the first spike of these bursts, rather than solely the firing rates of these afferents, appears to be important for determining object properties useful for manipulation, particularly surface curvature (Johansson and Birznieks, 2004, Johansson and Flanagan, 2009, Saal et al., 2009). Arising from and supported by research on the information contained within first-spike timing is a model of how the timing of the responses distributed over the different afferent populations might be used to reliably signal object curvature. In this view, curvature could in principle be decoded by neurons that detect specific patterns of spike coincidence. Presumably, similar mechanisms could be used to extract other features, such as surface friction information vital for determining the amount of grip force needed to support object load (Edin et al., 1992) and the directions of forces applied to the fingertip (Jenmalm et al., 2003), which are useful for detecting object slip. One possibility is that these coincidence detectors exist in the cuneate nucleus in the brain stem, which receives cutaneous information from the hand and input from cortex (Johansson and Flanagan, 2009).

While much information about the object's surface is available upon contact, information about its weight is only made available at the beginning of the lift phase, when the object's weight is supported by the hand. The most striking neural signature at this time is the bursting activity of

PC afferents (Figure 1-4) (Johansson and Edin, 1993). As a subject initiates the load phase, an internal model for the weight of the object is constructed from memory and from information from other sensory modalities (e.g., visual associations between size and weight), which in turn manifests as a corollary discharge signaling the expected time of object lift (Gordon et al., 1993, Jenmalm and Johansson, 1997, Flanagan et al., 2008). The timing of bursting from PC afferents, which signals lift, is then compared with the information from this corollary discharge and a mismatch between the two results in a rapid adjustment of motor output. The notion that weight is computed based on a comparison between an internal model and sensory information is supported by fMRI results wherein bilateral cerebellum, contralateral somatosensory cortex and M1, and ipsilateral posterior parietal cortex are selectively active during mismatches between expected and actual weights (Jenmalm et al., 2006).

### **The touch pathways**

The cuneate and gracile nuclei in the brainstem receive the first synapses from the periphery (Figure 1-1). At first glance, neurons from these nuclei seem to act as simple relays, with responses that reflect a high-fidelity, one-to-one copy of afferent input (Vickery et al., 1994, Gynther et al., 1995). The feedback projections to cuneate nucleus from thalamus (Fyffe et al., 1986) and cortex (Cheema et al., 1983), however, suggests a more complex functional role for the dorsal column nuclei. Indeed, neurons in brainstem nuclei are inhibited by both afferent and cortical input (Andersen et al., 1964, Biedenbach et al., 1971, Marino et al., 2000), and these descending projections are thought to play a role in the movement-gating of cutaneous input (Coquery and Coulmance, 1971, Dyhre-Poulsen, 1975, Rushton et al., 1981, Chapman et al., 1987, Chapman et al., 1988, Chapman, 1994, Post et al., 1994, Wasaka et al., 2012).

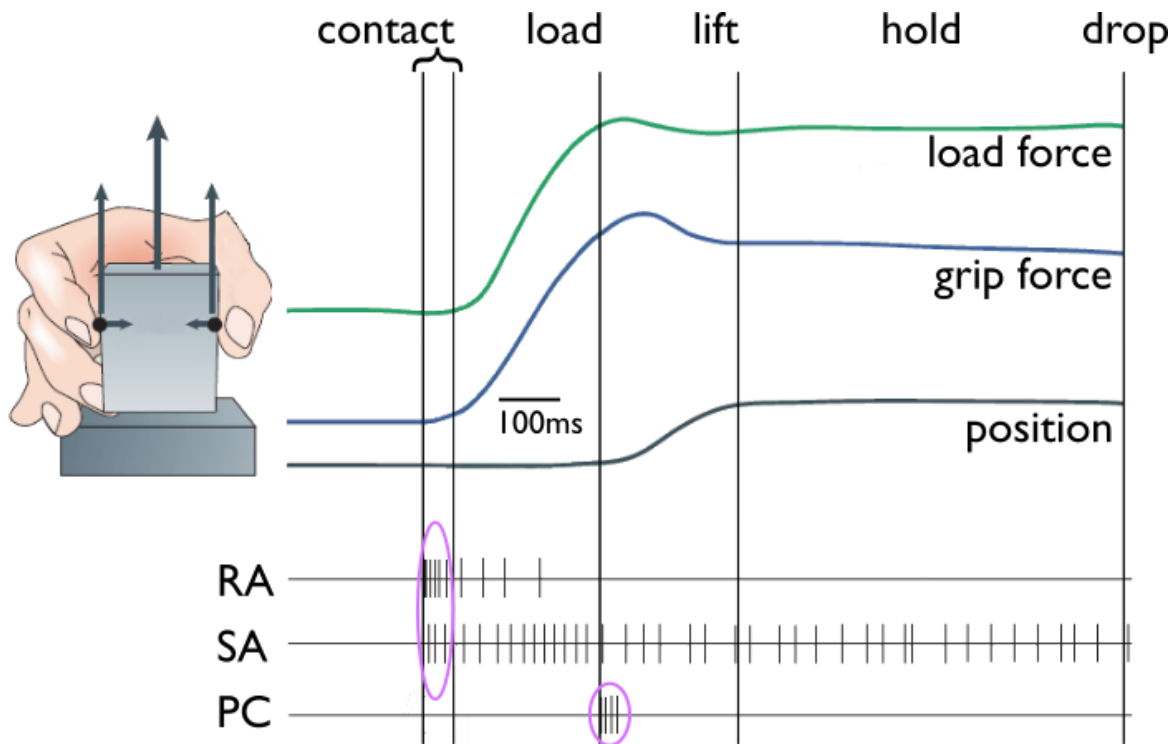


**Figure 1-4.** Typical trial of the object lifting task. Vertical lines denote the boundaries of the task phases. The top two colored traces show the time-varying load force (upward lines in the diagram to the left) and grip force (inward arrows) during the trial. The black trace shows the vertical position of the object as it is lifted off the support surface. The bottom three traces show spike trains of RA, SA, and PC afferents, respectively. Bursts of spikes coinciding with specific task events are circled in magenta. (adapted from Johansson and Flanagan, 2009).

Recent patch clamp studies in cats have revealed that the responses of individual cuneate neurons are dominated by a few primary afferents (4 to 8); as a result, cuneate neurons produce highly repeatable and idiosyncratic responses to tactile stimulation (Bengtsson et al., 2013, Hayward et al., 2014, Jorntell et al., 2014) However, while most of the work investigating the properties of neurons in the dorsal column nuclei has been carried out in a cat model, the neuronal morphology and microcircuitry of this structure and the descending projections it receives differ between primates and cats (Harris et al., 1965, Biedenbach et al., 1971, Molinari et al., 1996). Recent advances in chronic implants are poised to elucidate the organization of these elusive structures in awake, behaving primates (Richardson, 2015, Richardson et al., 2016).

The dorsal column nuclei then send the bulk of their projections to the ventral posterior lateral nucleus of the thalamus (VPL) (Figure 1-1), which has also been traditionally considered to be a simple sensory relay (in humans, the somatosensory nucleus is called Ventral Caudal). At a first approximation, the responses of individual thalamus neurons to tactile stimuli mirror the simple excitatory spatial receptive fields of their afferent input (Bushnell and Duncan, 1987) and are not modulated by attentional state or behavioral goals (in contrast to their counterparts in sensory cortex)(Camarillo et al., 2012, Vazquez et al., 2012). However, counter to this classical view, sensory thalamus exhibits a magnitude and variety of bidirectional interconnectivity with sensory cortex that imply a much more active processing role (Li et al., 2003, Reichova and Sherman, 2004, Van Horn and Sherman, 2004). Moreover, circuitry contained entirely within thalamus acts to modulate thalamic output to cortex. Although the most prominent cell type in thalamus is the relay cell projecting to somatosensory cortex, inhibitory interneurons from roughly twenty percent of neurons in thalamus and are commonly situated between afferents and relay cells in a common three-neuron motif (Penny et al., 1983, Bentivoglio et al., 1991, Arcelli et al., 1997). Inhibitory input from the thalamic reticular nucleus (TRN) also acts to modulate and gate the output of thalamocortical projections (Lee et al., 1994, McAlonan et al., 2008). The implications of this inhibitory thalamic circuitry in stimulus coding are unclear but it confers to thalamus an ability to refine and modulate, rather than merely relay, sensory information to cortex.

In addition to the medial lemniscal pathway for low-threshold discriminative touch, the somatosensory system includes the anterolateral system, which carries information about pain, itch, temperature, and pleasant affective touch (Mendoza and Foundas, 2007, Davidson et al., 2009, McGlone et al., 2014, Rea, 2015). This system receives afferent information from small-diameter C fibers and A $\delta$  fibers that terminate in free nerve endings expressing high-threshold

mechanosensitive (pain), low-threshold mechanosensitive (pleasant affective touch), histamine-sensitive (itch), and exhibit selective heat- and cold-sensitive responses. These afferents form synapses in the dorsal horn of the spinal cord, and these second-order neurons then decussate and ascend the eponymous anterolateral aspect of the spinal cord contralateral to the stimulation site. Emanating from these ascending spinal fibers are multiple axon branches. The spinothalamic pathway is one such branch that sends synaptic connections to third-order neurons in VPL, which in turn project to somatosensory cortex (see below). Other branches of the anterolateral system project to various nuclei in hypothalamus, brainstem, and midbrain responsible for the powerful autonomic and affective responses to painful stimuli.

### **Tactile coding in somatosensory cortex**

Somatosensory cortex can be divided into four modules with differing cytoarchitecture, thalamocortical input, and response properties: Brodmann's areas 3a, 3b, 1 and 2 (Figure 1-1). In fact, area 3 is technically primary somatosensory cortex proper, given the higher density of thalamocortical projections to its layer 4 relative to the rest of so-called S1 (Kaas, 1983). Neurons in area 3a are primarily sensitive to joint movements and seldom exhibit purely cutaneous responses. In contrast, neurons in area 3b and 1 are primarily sensitive to cutaneous stimulation. Note, however, that even cutaneous neurons often respond to joint movements in the absence of object contact (Bensmaia and Tillery, 2014, Kim et al., 2015) but whether or not this movement-related activity contributes to proprioception remains to be elucidated. Neurons in area 2 exhibit both cutaneous and joint-related responses and are thought to be involved in the integration of cutaneous and proprioceptive information necessary for stereognosis (see below).

One of the primary principles governing the organization of somatosensory cortex is somatotopy: Adjacent neurons (along the plane parallel to the cortical surface) respond to adjacent

patches of skin (Figure 1-1) (Pons et al., 1985). As a result, receptive fields progress systematically as one proceeds from the medial to lateral aspects of somatosensory cortex and each module contains a complete map of the body: The lower body is represented near the midline while the head is represented at the lateral extreme of the parietal cortex (Kaas et al., 1979). Furthermore, more cortical volume is devoted to certain body regions than others – a phenomenon dubbed cortical magnification (Sur et al., 1980). Body regions are magnified in proportion to their innervation density and to the functional significance of touch in those regions. As we tend to explore and manipulate objects with our hands and not our backs, the skin of the hand is more densely innervated than is that of the back, and the hand representation in somatosensory cortex is much larger than that of the back, despite the much larger area of the back relative to the hand. For similar reasons, the fingertips are more magnified than is the palm, and large swaths of somatosensory cortex are devoted to the lips as well.

Somatosensory cortical neurons project to the parietal ventral area (PV) and secondary somatosensory cortex (S2), located on the superior border of the lateral sulcus (Disbrow et al., 2003). Very little is known about the RF properties of neurons in PV. S2 neurons have very large RFs, for example covering the entire hand, and often respond to stimulation on both sides of the body (unlike their counterparts in so-called S1). Some evidence suggests that S2 comprises multiple compartments, some exhibiting exclusively cutaneous responses, others both cutaneous and proprioceptive ones.

As discussed above, individual mechanoreceptive afferents convey ambiguous information about a stimulus, which tends then to be distributed across the responses of a large number of fibers. Neurons in primary somatosensory cortex carry more explicit signals about behaviorally relevant stimulus features, such as the orientation of an edge indented into the skin or the motion

of an object across the skin. As has been shown in other sensory modalities and discussed in more detail below, neurons tend to be selective for increasingly complex stimulus features as one ascends the somatosensory neuraxis. Early in the processing hierarchy, neurons have small RFs and are sensitive to simple stimulus features, such as their orientation and direction of motion of local features. Higher up the hierarchy, neurons have larger RFs and are selective for more complex features such as curvature and global motion direction. Furthermore, neuronal responses are increasingly invariant with respect to other stimulus features at higher processing stages; that is, tuning for a given feature is consistent, no matter what the other features of the object are, a phenomenon that has been extensively documented in vision.

### **Vibratory frequency**

As mentioned above, not only does the tactile perception of vibration have an ecological role but the study of the neural encoding of vibration can shed light into how the temporal properties of a stimulus are represented in the somatosensory system. Like their counterparts in the nerve, somatosensory cortical neurons produce entrained responses to skin vibrations; that is, they produce one spike or a burst of spikes within a restricted phase of each stimulus cycle. This entrainment is pervasive for low-frequency stimuli ( $< 50$  Hz)(Mountcastle et al., 1969, Salinas et al., 2000), but is observed for vibrations at up to 800 Hz in a subpopulation of neurons in area 3b (Harvey et al., 2013). For low-frequency stimuli, frequency can be decoded both from the firing rate and from periodicity in the response, as both co-vary with frequency (Salinas et al., 2000, Luna et al., 2005). In contrast, somatosensory cortical firing rates are completely frequency independent at the higher frequencies ( $>100$  Hz), so the only information about the spectral composition of a skin vibration is conveyed in the temporal patterning of the evoked spikes (Harvey et al., 2013).

The frequency-independence of somatosensory cortical firing rates evoked by high-frequency stimuli stands in stark contrast to the strong frequency dependence of PC firing rates, which are primarily responsible for signaling high-frequency vibrations in the nerve. This seeming inconsistency suggests that the PC signals serve to modulate the timing of somatosensory cortical responses without affecting their strength. This phenomenon can be explained if the PC input is integrated over short periods of time and in such a way that it exerts an influence on somatosensory cortical neurons that is excitatory and inhibitory in equal parts (Saal et al., 2015).

### **Shape**

As discussed in detail above, local spatial features of an object, which impinge upon individual fingerpads, are encoded in the spatial pattern of activation in RA and especially SA1 fibers (Figure 1-3A), a representation that is qualitatively analogous to that in the retina. In light of this, it is perhaps not surprising that the representation of shape in somatosensory cortex is qualitatively analogous to its counterpart in primary visual cortex (V1). Indeed, in somatosensory cortex as in V1, a large proportion of neurons (~50%) are tuned for the orientation of an edge indented into or scanned across their RF (Figure 1-5A) (Bensmaia et al., 2008). That is, they respond maximally to an edge at a specific orientation and less so to edges at other orientations. Furthermore, in both sensory cortices, this orientation selectivity is shaped at least in part by the neurons' RF structure: RFs comprise excitatory regions flanked by one or more inhibitory regions (DiCarlo et al., 1998, DiCarlo and Johnson, 2000, 2002). The configuration of the excitatory and inhibitory subfields determines the preferred orientation of the neuron (see inset in Figure 1-5A).

While areas 3b and 1 exhibit comparable orientation selectivity, more complex feature selectivity emerges in area 2, namely selectivity for orientation and curvature (Yau et al., 2013). Neurons in area 2 not only encode the orientation of the stimulus but also its curvature, defined as

a contour with smoothly varying orientation (Figure 1-5B). This curvature tuning is also observed in secondary somatosensory cortex (S2) (Yau et al., 2009c), supporting the notion that feature selectivity gets more complex as one ascends the neuraxis.

Neuronal responses to spatial patterns also become increasingly invariant with respect to stimulus position. Indeed, an orientation selective neuron in area 3b only responds when an edge at its preferred orientation impinges on its small RF. Neurons in area 1 have larger RFs and so are more tolerant to small changes in the position of the edge (Bensmaia et al., 2008). Neurons in S2 can have RFs that cover the entire hand, or even the entire arm (Burton, 1986). Orientation selective neurons in S2 exhibit the same orientation preference over large swaths of their RFs (Figure 1-5C) (Fitzgerald et al., 2006). This positional invariance of the feature tuning draws an analogy to the responses of neurons in high-level visual areas.

### **Motion**

Again, the representation of tactile motion in somatosensory cortex is remarkably analogous to its visual counterpart in V1 (Pack and Bensmaia, 2015a). A subpopulation of somatosensory cortical neurons is tuned for direction of motion. That is, they respond maximally to an edge moving across the skin in a particular direction, respond minimally or not at all to an edge moving in the opposite direction, and produce an intermediate response to edges moving in intermediate directions (Figure 1-6A). For edges, the direction tuning is stronger in areas 1 and 2 than it is in area 3b, as might be expected given their relative positions in the somatosensory hierarchy (Pei et al., 2010). However, the difference is far more pronounced for spatial patterns that consist of edges at several orientations, a difference that can be attributed to the aperture problem.

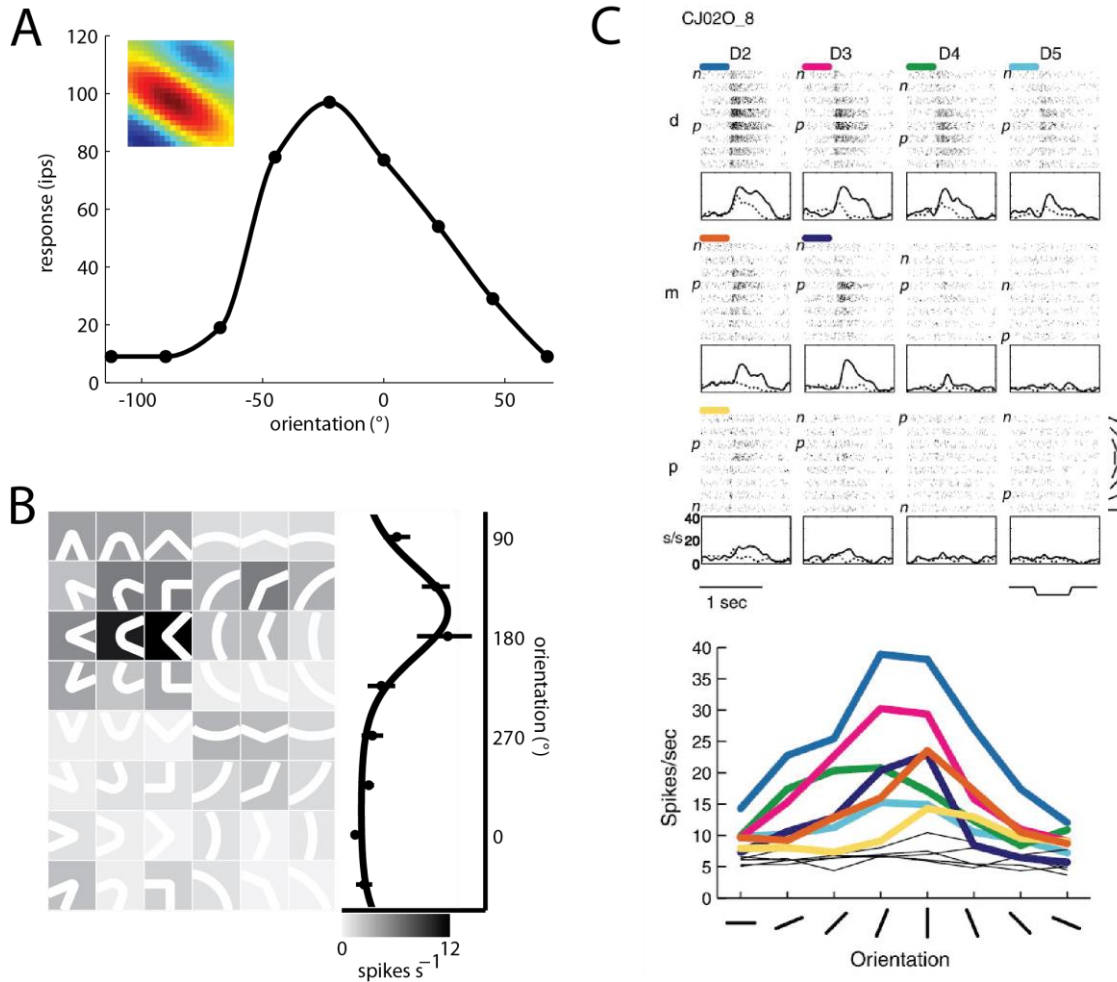


**Figure 1-5.** (A) Orientation tuned neuron in area 3b (inset shows a Gaussian fit to its RF) (adapted from Bensmaia et al., 2008). (B) Curvature and orientation tuned neurons in area 2 (Yau et al., 2013). (C) Orientation-tuned neuron in S2: This neuron's receptive field spans four digits (D2-D5) and multiple pads in each. However, its preferred orientation remains consistent across its RF (approximately aligned with the long axis of the finger) (Fitzgerald et al., 2006).

The aperture problem refers to the geometrical fact that the only information available about the motion of a straight edge is from the component of the motion that is perpendicular to its orientation. That is, if an edge is moving in some direction  $D$  at speed  $S$ , it will seem to be moving in the direction perpendicular to its orientation  $D^*$ , and its perceived speed will decrease as the angle between  $D^*$  and  $D$  increases. To discern the veridical direction of motion of an object, then, requires that information be integrated across different edges at different orientations or that

the motion of terminators – edge endpoints or corners – be observed; indeed, terminators convey unambiguous velocity information. Neurons in area 3b are subject to the aperture problem because they have small RFs and thus typically experience only a single edge at a time. As a result, individually neurons convey ambiguous information about stimulus motion and do not signal the direction of motion of objects comprising multiple edges at different orientations.

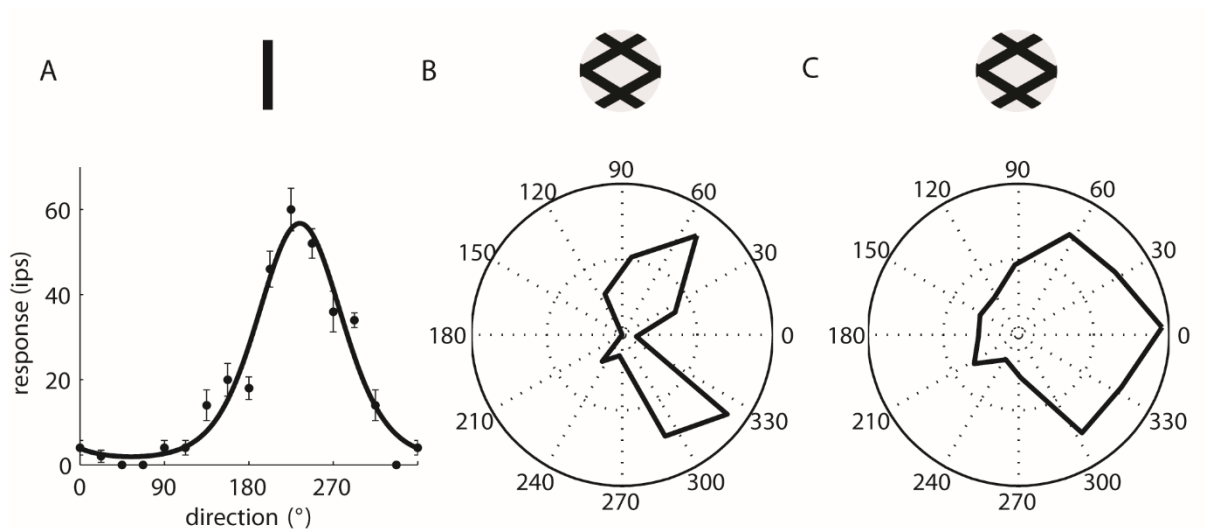


**Figure 1-6.** (A) Direction tuning of a neuron in area 1 to scanned bars (adapted from Pei et al., 2010). (B) Responses of a ‘component’ neuron to plaids scanned in 12 directions. This neuron responds maximally when one of the plaid’s component gratings is moving in its preferred direction. (C) Responses of a ‘pattern’ neuron to plaids. This neuron responds to the plaid’s global direction of motion. Such neurons are only found in area 1. (Pei et al., 2011)

A fruitful paradigm to study motion integration has consisted of probing the perception of motion and its neural basis using plaids, which consist of superimposed gratings. Indeed, the component gratings of the plaid will drive the responses of neurons subject to the aperture problem (Figure 1-6B), but the perceptual experience of the plaid in both vision and touch (Pei et al., 2008) is of the global motion of the plaid, which depends on the velocities of both component gratings.

This implies that a population of neurons somewhere along the neuraxis is able to extract the veridical direction of motion of the stimulus. In vision, this computation is reflected in the responses of so-called “pattern” neurons in medial temporal cortex, which are tuned to the direction of the plaid. In touch, such a population of neurons is found in area 1 (Figure 1-6C) (Pei et al., 2011). When presented with plaids, these neurons respond to the global motion of the stimulus and not the motion of its component gratings. The responses of this population of neurons in area 1 can account for the perceived direction of motion across a wide range of stimulus conditions (Pei et al., 2010, 2011). Pattern neurons are not found in area 3b, again highlighting the hierarchical relationship between areas 3b and 1.

In summary, neurons in area 3b exhibit direction selectivity for edges but “do not see the forest for the trees” when presented with stimuli that consist of multiple contours. In contrast, neurons in area 1 “see the forest, not the trees,” exhibiting consistent direction preference independent of the spatial configuration of the stimulus. These neurons can account for the perceived direction of all tactile motion stimuli, including those moving in an ambiguous direction. In fact, a simple model that describes the output of neurons in area 1 from a simple vector sum of inputs from area 3b accounts for both the neurophysiological and psychophysical data (Pei et al., 2011).

### **Texture**

Little is known about the cortical basis of texture perception, in part because all experiments to date investigating texture representations in cortex used gratings and embossed dot patterns as stimuli. As discussed above, these classes of stimuli engage primarily the spatial mechanism of texture processing and obscure the contribution of the temporal one, which accounts for much of the range of tangible textures. Moreover, because gratings and dot patterns involve

essentially a single parameter (spatial period), they do not provide a rich enough stimulus space to disentangle competing hypotheses about the underlying neural code (Connor et al., 1990).

In experiments with scanned gratings (Darian-Smith et al., 1982, Sinclair and Burton, 1991a, b, Burton and Sinclair, 1994) and embossed dot patterns (Chapman et al., 2002, Bourgeon et al., 2016), the response of the majority of cutaneous neurons in somatosensory cortex were found to be modulated by the spatial period of the stimuli. Furthermore, the responses of a subset of these neurons seems to track the perceived roughness of such textures (Chapman et al., 2002, Bourgeon et al., 2016), consistent with the hypothesis that they are causally implicated in texture perception. As lesions of area 1 result in specific deficits in texture discrimination (Randolph and Semmes, 1974, Semmes et al., 1974, Semmes and Turner, 1977), this area may be part of a pathway specialized for texture processing.

In the somatosensory nerves, coarse and fine textural features are encoded based on spatial and temporal patterns of activation, respectively (as summarized above). The spatial structure of somatosensory cortical neurons – comprising excitatory fields flanked by inhibitory ones (DiCarlo et al., 1998, DiCarlo and Johnson, 2000, 2002) – is well suited to extract information from spatial patterns of afferent activation, and thus to represent coarse textural features. For example, these neurons respond maximally to spatially inhomogeneous stimuli applied to the finger and could thus encode surface roughness, which entails a computation of spatial inhomogeneity (Connor and Johnson, 1992). A subpopulation of somatosensory cortical neurons also responds to complex high-frequency vibrations of the skin of the sort that are produced when fine textures are scanned across the skin (Harvey et al., 2013). While these two properties of somatosensory cortical neurons can in theory mediate the representations of texture in cortex, no systematic experiments have been carried out to investigate the cortical representation of natural textures.

### **Parallels between vision and touch**

Traditionally, touch has been thought of as a spatial sense, drawing remarkable analogies with vision. First, the peripheral image in touch consists of a spatiotemporal pattern of activation across a sensory sheet – the skin –, as is the case with vision and the retina. Second, neurons in somatosensory cortex exhibit orientation and direction tuning, much like their counterparts in V1 (Figure 1-5, Figure 1-6) (Bensmaia et al., 2008, Pack and Bensmaia, 2015b). Furthermore, the receptive field structure of somatosensory cortical and V1 neurons is similar, consisting of excitatory fields flanked by inhibitory ones (DiCarlo et al., 1998, Bensmaia et al., 2008), which can at least in part explain the similar functional properties. Third, higher order representations of both shape and motion are highly analogous in vision and touch, as detailed above (Yau et al., 2009c, Pei et al., 2010, 2011, Yau et al., 2013). Fourth, the tactile perception of shape and motion is similar to its visual counterpart, as evidenced by, for example, similar patterns of errors in letter identification (Phillips et al., 1983) and similar perceptual biases in motion perception (Pei et al., 2008). The similarities in processing make sense as both systems interact with a common environment, with statistical regularities that the two perceptual modalities have evolved to extract (Simoncelli and Olshausen, 2001). Furthermore, visual and tactile representations co-exist when we interact with objects and must therefore be integrated (Lacey and Sathian, 2012), a process that is simpler if the representations are analogous.

### **Parallels between audition and touch**

Although similarities with hearing have not received the extensive experimental treatment as have those with vision, touch and hearing are similar in that both can operate as temporal senses. Indeed, some classes of mechanoreceptive afferents (RA, PC) are exquisitely sensitive to skin vibrations and produce highly repeatable and precise temporal spike patterns, the timing of which

reflects the frequency composition of the skin vibrations (Talbot et al., 1968b, Mackevicius et al., 2012). A subpopulation of somatosensory cortical neurons exhibits sensitivity to high-frequency vibrations and produce responses to skin vibrations characterized by high temporal precision (Harvey et al., 2013). Furthermore, somatosensory cortex is even more sensitive to differences in spike timing than is primary auditory cortex (A1)(Yang and Zador, 2012), a difference that can be attributed to their different positions along their respective neuraxes — somatosensory cortex is three synapses away from primary afferents whereas A1 is five synapses away. Moreover, stimulus information seems to be integrated across frequency bands in similar ways in touch and hearing (Marks, 1979, Makous et al., 1995). These findings together suggest that the somatosensory system is well suited to extract information from environmental oscillations, as is its auditory counterpart.

The temporal mode of touch plays a critical role in texture perception: While coarse textural features are encoded in the spatial pattern of activation in SA1 afferents, the perception of fine features relies on the transduction and processing of skin vibrations that are produced in the skin during texture scanning. Fine features are encoded in the high-precision temporal spiking patterns in RA and PC fibers and these patterns dilate or contract with decreases or increases in scanning speed, respectively (Weber et al., 2013), which amounts to left and right translations of the frequency composition of the neural response along the frequency axis. In contrast, the perception of texture is almost completely independent of scanning speed. Somewhere along the somatosensory neuraxis, then, texture constancy must be extracted from a peripheral image that is highly dependent on scanning speed. This problem is identical to timbre constancy, which also involves translation of a harmonic stack along the frequency axis with changes in fundamental frequency (Yau et al., 2009a). Given that the two problems – texture and timbre constancy – require similar computations, it is likely that they rely on similar neural mechanisms. A key

difference between audition and touch, however, is that the former benefits from a peripheral process akin to Fourier decomposition (in the basilar membrane) whereas the latter does not. However, in both systems, information about the acoustic or tactile stimulus is also encoded in the timing, and it is likely that similar neural mechanisms are involved in extracting this information.

The remarkable analogies between vision, audition, and touch support the notion that the nervous system implements a limited number of strategies – canonical computations – to extract information from the environment, and that these computations span the different sensory modalities (Pack and Bensmaia, 2015b).

### **Affective touch**

The way in which we touch people, for example the speed at which we stroke them, communicates distinct emotions, such as anger, fear, compassion, or love, and the accuracy with which this emotional information is transmitted through touch is comparable to that of vocal and facial expression (Hertenstein et al., 2009). In the somatosensory nerves, pleasant touch is mediated – at least in part – by specialized small-diameter fibers, namely C-tactile afferents, that innervate the hairy skin (Löken et al., 2009). Counterparts to these afferents have yet to be found in glabrous skin. Several regions in cortex are associated with the affective and social aspects of touch. For example, somatosensory cortical activation depends on who does the touching (Gazzola et al., 2012) and some neurons respond to the observation of touch and may support social communication through empathy, a phenomenon dubbed 'mirror-touch synesthesia' (Keysers et al., 2010). The posterior insular cortex is implicated in the experience of pleasant touch and receives projections from C-tactile afferents (Björnsdotter et al., 2009). Affective touch is also represented in orbitofrontal cortex, which is generally associated with affective value (Kringelbach, 2005) and responds weakly to neutral touch (Rolls et al., 2003).

## **The sense of proprioception**

### **Proprioceptive receptors and their associated nerve fibers**

Proprioception is the sense of the location of the body, of its movement, and of the forces that it applies or are applied to it. Proprioception plays a critical role in our ability to plan and execute movements. Without it, we would struggle to perform the simplest activities of daily living (Cole and Sedgwick, 1992, Ghez et al., 1995, Ghez and Sainburg, 1995, Sainburg et al., 1995). Signals about the limb movements originate from receptors embedded in joints, muscles, tendons, and the skin.

*Muscle spindles* are most numerous and sensitive proprioceptors (Prochazka, 1996). Each spindle consists of a bundle of intrafusal muscle fibers running in parallel with extrafusal fibers and contained within a spindle-shaped capsule (Figure 1-7A). Three different fiber types are present in a spindle: nuclear bag 2 and nuclear chain fibers are primarily sensitive to the strain they experience; nuclear bag 1 fibers respond primarily to the rate of change in strain. Primary spindle afferents (Ia) innervate all three types of fibers whereas secondary proprioceptive afferents (II) innervate only the bag 2 and chain fibers. As a result, primary spindle afferents are sensitive to muscle strain and its rate of change whereas secondary spindle afferents are sensitive primarily to the strain (Hulliger, 1984). Muscle spindles are unique somatosensory transduction organs in that their sensitivity can be adjusted by descending input from gamma motor neurons. Action potentials in gamma motor neurons cause contractions of the distal ends of intrafusal fibers, thereby adjusting their baseline tension and thus their mechanical sensitivity to strain. There are two sets of gamma motor neurons: gamma dynamic neurons innervate nuclear bag 1 fibers and modulate primary spindle afferent sensitivity to strain rate; gamma static neurons innervate bag 2 and chain fibers and modulate the sensitivity of both types of spindle afferents (Hulliger, 1984, Prochazka, 1996).

*Golgi Tendon Organs* (GTOs) are located at the musculotendon junction, in series with the contractile portion of the muscle. Each GTO consists of an encapsulated collagenous mesh innervated by several afferents (Figure 1-7B). Signals from GTOs track muscle tension, exhibit little sensitivity to tension rate, and do not adapt to sustained tension levels outside of a transient spike in firing rate at stimulus onset (Gregory and Proske, 1979). GTO afferents signal tension in a quantal manner (Edin and Vallbo, 1990), meaning that their firing rates “step” from one discrete level to another rather than varying smoothly over a continuum. The quantal nature of GTO afferent spiking arises from discrete increases in the number of motor units recruited, with each GTO afferent tracking a subset of motor units (Houk and Henneman, 1967).

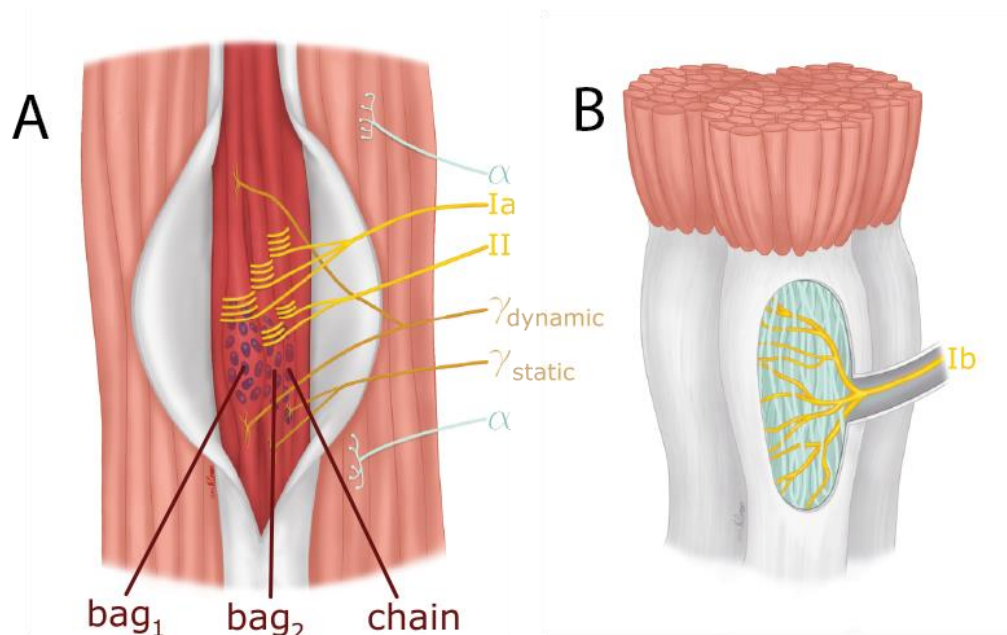


**Figure 1-7.** (A) Muscle Spindle. The spindle capsule contains three types of intrafusal muscle fiber: nuclear bag 1 fibers, which are sensitive to rate of stretch; and nuclear bag 2 and nuclear chain fibers, which are sensitive to static stretch. The  $\gamma$ -dynamic fusimotor neurons selectively innervate bag 1 fibers and adjust sensitivity to the rate of stretch, whereas the  $\gamma$ -static fusimotor neurons selectively modulate the fibers that sense static stretch. Primary (Ia) spindle afferents innervate all three intrafusal fiber types and convey dynamic stretch information. Secondary (II) spindle afferents innervate and convey information from only the intrafusal muscle fibers that sense static stretch. (B) Golgi tendon organ (GTO). The outer tendon is resected to show the GTO (Ib) afferent and the interior collagenous mesh it innervates. A single GTO is situated in series with 10-20 motor units (bundles of muscle fibers, top). GTO afferents convey active muscle force by "counting" the number of recruited motor units (illustrations by Kenzie Green).

*Joint receptors* can be divided into three classes, each of which is analogous to one present in the skin or in muscles. GTOs located in the ligaments signal tension. Ruffini endings and Pacinian corpuscles located in the joint capsule track the level of strain applied to the joint and its dynamics, respectively (Zimny, 1988). These sensory organs are innervated by similar afferent types as those present in the muscle and the skin, but are distinct in their lack of sensitivity to muscle or skin palpation. Afferents that innervate joint receptors tend to only respond when joints are in extreme positions of flexion or extension (Burgess and Clark, 1969, Grigg, 1975).

Proprioceptive afferents follow the same medial lemniscal pathway as their cutaneous counterparts and synapse onto neurons in the external (or accessory) cuneate and gracile nuclei in the brainstem, which in turn project to thalamus and ultimately to cortex. There are other somatosensory pathways of which little is known and that fall outside the scope of the present review.

### **The cortical basis of proprioception**

As is the case with their cutaneous counterparts, proprioceptive afferents send projections to the Dorsal Root Ganglion (DRG) of the spinal cord, where their cell bodies are located. These fibers ultimately synapse onto neurons in the dorsal column nuclei, which in turn project to the ventral posterior lateral (VPL) nucleus of thalamus. In both the dorsal columns and thalamus, proprioceptive and cutaneous signals are segregated: The accessory cuneate receives proprioceptive input whereas the internal cuneate receives cutaneous input; in VPL, cutaneous neurons are located in the central region whereas proprioceptive neurons are located in the outer shell (Kaas, 1983). Little is known about proprioceptive representations in these structures. Note that both touch and proprioception comprise other tracts, which have received far less experimental attention than has the medial lemniscal pathway and that fall outside the scope of this review.

Neurons in thalamus then send projections to two regions of primary somatosensory cortex: Area 3a, located in the bank of the central sulcus, adjacent to motor cortex; and area 2 on the side of somatosensory cortex that borders the intraparietal sulcus. A hierarchical relationship between areas 3a and 2 is often assumed as proprioceptive receptive fields in the latter are larger and respond to more complex conjunctions of features than do those in the former (Sakata et al., 1973, London and Miller, 2013). However, the anatomical evidence for a hierarchical progression from area 3a to area 2 is curiously inconclusive. Although area 2 does receive projections from area 3a, these projections are not as dense as would be expected from other hierarchically coupled cortical areas (Porter, 1991).

Neurons in area 3a exhibit a variety of responses to movements imposed on the limb, as might be expected from the response profiles of proprioceptive afferents. Some neurons respond only to joint movements, others to joint postures, and others produce a phasic response to movement and a tonic one that is posture dependent (Gardner and Costanzo, 1981). One consistent feature of neurons in 3a is that they respond to flexion or extension of a joint but not both.

Area 3a neurons also exhibit sensitivity to forces applied to the limb. When the arm maintains its position against a load, neurons in area 3a will respond with firing rates proportional to the load (Fromm and Evarts, 1982). Just as responses to passive joint movements are unidirectional, so too are load responses of neurons in area 3a. Furthermore, during active movements, neurons in area 3a respond to perturbations that oppose movement in their anti-preferred direction—i.e., they respond to perturbations that apply force in their preferred direction, consistent with the hypothesis that area 3a is implicated in generating an “error” signal useful for adjusting motor output in the presence of unanticipated perturbations.

While the proprioceptive properties of neurons in area 2 have received less experimental attention than have their counterparts in area 3a, area 2 is thought to play an important role in stereognosis, the haptic perception of the three dimensional structure of objects grasped in the hand. First, neurons in area 2 exhibit both cutaneous and proprioceptive responses, a prerequisite for stereognosis. Second, area 2 lesions cause specific deficits in object shape discrimination, while leaving surface texture discrimination relatively spared (Randolph and Semmes, 1974). Third, receptive fields in area 2 are large (Iwamura et al., 1980), often encompassing several digits and therefore well suited to carry representations of whole hand conformations necessary to support stereognosis (see below). In addition to its role in stereognosis, area 2 may also carry an internal model of intended movements, as evidenced by the fact that some neurons in area 2 respond to active movements prior to movement onset (London and Miller, 2013).

### **Phenomenology of proprioception**

Human subjects can detect changes in joint angle of proximal joints of the upper limb better than changes in the angles of distal joints. When sensitivity is measured in terms of the muscle strains, however, joint angular acuity is constant across joints (Hall and McCloskey, 1983), suggesting that spindle and GTO afferents play a key role in the conscious proprioception as these afferents track muscle strains. Furthermore, humans are more sensitive to active movements than they are to passive ones (Gandevia et al., 1992). Presumably, this greater sensitivity for active movements might reflect the convergence of efference copy and sensory input in active movements, which does not occur for passive movements. Finally, some evidence suggests that the responses of cutaneous afferents to skin stretch may influence conscious proprioception. Indeed, when strain is applied to the skin on the dorsal surface of the hand, subjects report illusory movement of the fingers (Edin and Johansson, 1995, Collins and Prochazka, 1996). Although

cutaneous signals follow an anatomical pathway distinct from that followed by their proprioceptive counterparts, these psychophysical results suggest that proprioception involves the integration of cutaneous and proprioceptive signals.

### **Multimodal integration and stereognosis**

The somatosensory system is unique in that it comprises a deformable sensory sheet: As our fingers move, the positions of cutaneous receptors change relative to one another. Thus, to interpret cutaneous signals emanating from each of the fingertips, it is necessary take into account the relative position of the fingers. When we grasp an object, we acquire information about its three dimensional structure, which relies on the integration of cutaneous and proprioceptive information (Berryman et al., 2006, Hsiao, 2008, Yau et al., 2016). As described above, cutaneous signals are first processed in area 3b then project to area 1, which in turn (presumably) sends projections to area 2; area 2 also receives proprioceptive signals, both from area 3a and from thalamus. It should also be noted that limb joint movements activate neurons in areas 3b and 1 in the absence of contact by virtue of the concomitant skin stretch or compression (Costanzo and Gardner, 1981, Gardner and Costanzo, 1981, Chapman and Ageranioti-Belanger, 1991, Nelson et al., 1991, Ageranioti-Belanger and Chapman, 1992, Iwamura et al., 1993, Kalaska, 1994, Krubitzer et al., 2004, Rincon-Gonzalez et al., 2011). Thus, many neurons across somatosensory cortex exhibit both proprioceptive and cutaneous responses. In most multimodal neurons, proprioceptive responses are superimposed on cutaneous ones, so the signals carried by these neurons are ambiguous (Kim et al., 2015). A subpopulation of neurons in somatosensory cortex exhibit more complex, non-linear interactions of the proprioceptive and cutaneous input (Figure 1-8). While multimodal integration in somatosensory cortex has been documented, the resulting representational framework for stereognosis has yet to be discovered. As neurons in area 2 are the

first to receive convergent proprioceptive and cutaneous input, this area is likely implicated in stereognosis. Consistent with this hypothesis, lesions of area 2 produce selective deficits in shape recognition (Randolph and Semmes, 1974).

As discussed above, the somatosensory system is the only modality to comprise a deformable sensory sheet. How cutaneous and proprioceptive information is integrated is one of the great challenges facing sensory neuroscience.

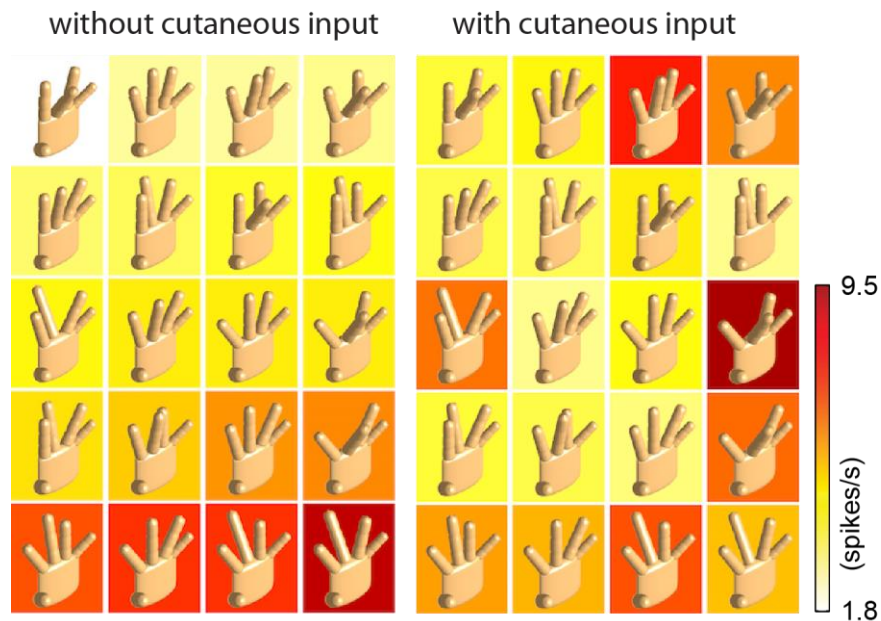


**Figure 1-8.** Neuron in area 2 that exhibits both tactile and proprioceptive responses (courtesy of Sung Soo Kim). This neuron’s activity is modulated simply by moving the digits (left panel). However, responses are further modulated by cutaneous stimulation (right panel). The neuron’s response is a complex function of hand conformation and cutaneous input.

## Conclusions

The sensors underlying the senses of touch and proprioception comprise an elaborate mesh of afferent types conveying information about skin, connective, and muscle tissue stress and strain at various spatial and temporal scales. These afferent types each constitute unique channels of information about objects that are being touched: SAI fibers give local spatial information about

skin deformations useful for detecting edges and coarse features; RA fibers trade spatial acuity for temporal precision and appear to convey clear signals related to object slips; PC fibers operate on spatial scales orders of magnitude larger than either SAI or RA fibers in exchange for the temporal precision to resolve the vibratory consequences of nano-scale spatial features of surfaces scanned across the skin or remote object interaction events such as a grasped object being lifted off a surface; and a variety of proprioceptive afferents, likely in conjunction with SAII afferents, convey information about tissue stretches arising from different configurations and movements of the hand. As one ascends the somatosensory neuraxis, the rule is that information from different afferents is integrated to give rise to filters detecting more and more elaborate features of tactile stimuli, akin to the emergence of more and more elaborate stimulus filters in visual and auditory cortices. Indeed, even information across different afferent types is integrated as early as somatosensory cortex to enable, among other things, a holistic perception of textures spanning eight orders of magnitude. Although this process has received some experimental attention in tactile somatosensory cortex, only basic properties of proprioceptive somatosensory cortical neurons have so far been studied. An understanding of the types of filters and elaborations used in the cortical processing of proprioceptive stimuli is essential to make further progress in understanding the somatosensory hierarchy, especially as both proprioceptive and somatosensory modalities eventually converge in Brodmann's area 2. Moreover, to fully appreciate the roles these senses play during stereognosis, these senses need to be further investigated during grasps and manipulations of multiple objects that require different hand shapes, as opposed to the single object studied in the canonical object manipulation task so far described.

## References

- Adrian ED, Zotterman Y (1926a) The impulses produced by sensory nerve-endings: Part II. The response of a Single End-Organ. *The Journal of physiology* 61:151-171.
- Adrian ED, Zotterman Y (1926b) The impulses produced by sensory nerve endings: Part 3. Impulses set up by Touch and Pressure. *The Journal of physiology* 61:465-483.
- Ageranioti-Belanger SA, Chapman CE (1992) Discharge properties of neurones in the hand area of primary somatosensory cortex in monkeys in relation to the performance of an active tactile discrimination task. II. Area 2 as compared to areas 3b and 1. *Exp Brain Res* 91:207-228.
- Andersen P, Eccles JC, Oshima T, Schmidt RF (1964) Mechanisms of Synaptic Transmission in the Cuneate Nucleus. *Journal of neurophysiology* 27:1096-1116.
- Apkarianstielau P, Loomis JM (1975) Comparison of Tactile and Blurred Visual Form Perception. *Percept Psychophys* 18:362-368.
- Arcelli P, Frassoni C, Regondi MC, De Biasi S, Spreafico R (1997) GABAergic neurons in mammalian thalamus: a marker of thalamic complexity? *Brain research bulletin* 42:27-37.
- Augurelle AS, Smith AM, Lejeune T, Thonnard JL (2003) Importance of cutaneous feedback in maintaining a secure grip during manipulation of hand-held objects. *J Neurophysiol* 89:665-671.
- Bell J, Bolanowski S, Holmes MH (1994) The Structure and Function of Pacinian Corpuscles - a Review. *Prog Neurobiol* 42:79-128.
- Bengtsson F, Brasselet R, Johansson RS, Arleo A, Jorntell H (2013) Integration of Sensory Quanta in Cuneate Nucleus Neurons In Vivo. *PloS one* 8.
- Bensmaia S, Hollins M (2005) Pacinian representations of fine surface texture. *Percept Psychophys* 67:842-854.
- Bensmaia S, Tillery SIH (2014) Tactile Feedback from the Hand. *Human Hand as an Inspiration for Robot Hand Development* 95:143-157.
- Bensmaia SJ (2008) Tactile intensity and population codes. *Behav Brain Res* 190:165-173.
- Bensmaia SJ, Craig JC, Johnson KO (2006a) Temporal factors in tactile spatial acuity: evidence for RA interference in fine spatial processing. *J Neurophysiol* 95:1783-1791.
- Bensmaia SJ, Craig JC, Yoshioka T, Johnson KO (2006b) SA1 and RA afferent responses to static and vibrating gratings. *J Neurophysiol* 95:1771-1782.

- Bensmaia SJ, Denchev PV, Dammann JF, 3rd, Craig JC, Hsiao SS (2008) The representation of stimulus orientation in the early stages of somatosensory processing. *J Neurosci* 28:776-786.
- Bensmaia SJ, Hollins M (2003) The vibrations of texture. *Somatosens Mot Res* 20:33-43.
- Bentivoglio M, Spreafico R, Minciacchi D, Macchi G (1991) GABAergic interneurons and neuropil of the intralaminar thalamus: an immunohistochemical study in the rat and the cat, with notes in the monkey. *Experimental brain research* 87:85-95.
- Berryman LJ, Yau JM, Hsiao SS (2006) Representation of object size in the somatosensory system. *J Neurophysiol* 96:27-39.
- Biedenbach MA, Jabbur SJ, Towe AL (1971) Afferent inhibition in the cuneate nucleus of the rhesus monkey. *Brain research* 27:179-183.
- Birznieks I, Jenmalm P, Goodwin AW, Johansson RS (2001) Encoding of direction of fingertip forces by human tactile afferents. *J Neurosci* 21:8222-8237.
- Birznieks I, Macefield VG, Westling G, Johansson RS (2009) Slowly adapting mechanoreceptors in the borders of the human fingernail encode fingertip forces. *J Neurosci* 29:9370-9379.
- Birznieks I, Wheat HE, Redmond SJ, Salo LM, Lovell NH, Goodwin AW (2010) Encoding of tangential torque in responses of tactile afferent fibres innervating the fingerpad of the monkey. *J Physiol* 588:1057-1072.
- Bisley JW, Goodwin AW, Wheat HE (2000) Slowly adapting type I afferents from the sides and end of the finger respond to stimuli on the center of the fingerpad. *J Neurophysiol* 84:57-64.
- Björnsdotter M, Löken L, Olausson H, Vallbo Å, Wessberg J (2009) Somatotopic organization of gentle touch processing in the posterior insular cortex. *The Journal of Neuroscience* 29:9314-9320.
- Blake DT, Hsiao SS, Johnson KO (1997) Neural coding mechanisms in tactile pattern recognition: the relative contributions of slowly and rapidly adapting mechanoreceptors to perceived roughness. *J Neurosci* 17:7480-7489.
- Bliss JC, Katcher MH, Rogers CH, Shepard RP (1970) Optical-to-tactile image conversion for the blind. *IEEE Trans Man-Machine Sys* MMS-11:58-65.
- Bourgeon S, Depeault A, Meftah EM, Chapman CE (2016) Tactile texture signals in primate primary somatosensory cortex and their relation to subjective roughness intensity. *J Neurophysiol* jn 00303 02015.
- Brisben AJ, Hsiao SS, Johnson KO (1999) Detection of vibration transmitted through an object grasped in the hand. *J Neurophysiol* 81:1548-1558.

- Burgess PR, Clark FJ (1969) Characteristics of knee joint receptors in the cat. *The Journal of physiology* 203:317-335.
- Burton H (1986) Second Somatosensory Cortex and Related Areas. In: *Sensory-Motor Areas and Aspects of Cortical Connectivity*(Jones, E. G. and Peters, A., eds), pp 31-98 Boston, MA: Springer US.
- Burton H, Sinclair RJ (1994) Representation of tactile roughness in thalamus and somatosensory cortex. *Can J Physiol Pharmacol* 72:546-557.
- Bushnell MC, Duncan GH (1987) Mechanical response properties of ventroposterior medial thalamic neurons in the alert monkey. *Experimental brain research* 67:603-614.
- Callier T, Saal HP, Davis-Berg EC, Bensmaia SJ (2015) Kinematics of unconstrained tactile texture exploration. *J Neurophysiol* 113:3013-3020.
- Camarillo L, Luna R, Nacher V, Romo R (2012) Coding perceptual discrimination in the somatosensory thalamus. *Proceedings of the National Academy of Sciences of the United States of America* 109:21093-21098.
- Cauna N (1956) Structure and Origin of the Capsule of Meissner Corpuscle. *Anat Rec* 124:77-93.
- Cauna N, Mannan G (1958) The structure of human digital pacinian corpuscles (corpus cula lamellosa) and its functional significance. *Journal of Anatomy* 92:1-20.
- Chapman CE (1994) Active versus passive touch: factors influencing the transmission of somatosensory signals to primary somatosensory cortex. *Can J Physiol Pharmacol* 72:558-570.
- Chapman CE, Ageranioti-Belanger SA (1991) Discharge properties of neurones in the hand area of primary somatosensory cortex in monkeys in relation to the performance of an active tactile discrimination task. I. Areas 3b and 1. *Exp Brain Res* 87:319-339.
- Chapman CE, Bushnell MC, Miron D, Duncan GH, Lund JP (1987) Sensory perception during movement in man. *Exp Brain Res* 68:516-524.
- Chapman CE, Jiang W, Lamarre Y (1988) Modulation of lemniscal input during conditioned arm movements in the monkey. *Exp Brain Res* 72:316-334.
- Chapman CE, Tremblay F, Jiang W, Belingard L, Meftah el M (2002) Central neural mechanisms contributing to the perception of tactile roughness. *Behav Brain Res* 135:225-233.
- Cheema S, Whitsel BL, Rustioni A (1983) The corticocuneate pathway in the cat: relations among terminal distribution patterns, cytoarchitecture, and single neuron functional properties. *Somatosens Res* 1:169-205.

- Cho Y, Craig JC, Hsiao SS, Bensmaia SJ (2016) Vision is superior to touch in shape perception even with equivalent peripheral input. *J Neurophysiol* 115:92-99.
- Cole JD, Sedgwick EM (1992) The perceptions of force and of movement in a man without large myelinated sensory afferents below the neck. *The Journal of physiology* 449:503-515.
- Collins DF, Prochazka A (1996) Movement illusions evoked by ensemble cutaneous input from the dorsum of the human hand. *The Journal of physiology* 496 ( Pt 3):857-871.
- Connor CE, Hsiao SS, Phillips JR, Johnson KO (1990) Tactile roughness: neural codes that account for psychophysical magnitude estimates. *J Neurosci* 10:3823-3836.
- Connor CE, Johnson KO (1992) Neural coding of tactile texture: comparison of spatial and temporal mechanisms for roughness perception. *J Neurosci* 12:3414-3426.
- Coquery JM, Coulmance M (1971) [Changes in the perception of a somesthetic stimulus during a voluntary movement]. *C R Seances Soc Biol Fil* 165:1946-1951.
- Costanzo RM, Gardner EP (1981) Multiple-joint neurons in somatosensory cortex of awake monkeys. *Brain Res* 214:321-333.
- Coste B, Mathur J, Schmidt M, Earley TJ, Ranade S, Petrus MJ, Dubin AE, Patapoutian A (2010) Piezo1 and Piezo2 are essential components of distinct mechanically activated cation channels. *Science* 330:55-60.
- Coste B, Xiao B, Santos JS, Syeda R, Grandl J, Spencer KS, Kim SE, Schmidt M, Mathur J, Dubin AE, Montal M, Patapoutian A (2012) Piezo proteins are pore-forming subunits of mechanically activated channels. *Nature* 483:176-181.
- Craig JC (1980) Modes of vibrotactile pattern generation. *J Exp Psychol Hum Percept Perform* 6:151-166.
- Craig JC, Johnson KO (2000) The two-point threshold: Not a measure of tactile spatial resolution. *Curr Dir Psychol Sci* 9:29-32.
- Dandekar K, Raju BI, Srinivasan MA (2003) 3-D finite-element models of human and monkey fingertips to investigate the mechanics of tactile sense. *J Biomech Eng* 125:682-691.
- Darian-Smith I, Sugitani M, Heywood J, Karita K, Goodwin A (1982) Touching textured surfaces: cells in somatosensory cortex respond both to finger movement and to surface features. *Science* 218:906-909.
- Davidson S, Zhang X, Khasabov SG, Simone DA, Giesler GJ, Jr. (2009) Relief of itch by scratching: state-dependent inhibition of primate spinothalamic tract neurons. *Nature neuroscience* 12:544-546.

- Delhaye B, Hayward V, Lefevre P, Thonnard JL (2012) Texture-induced vibrations in the forearm during tactile exploration. *Front Behav Neurosci* 6:37.
- Delmas P, Hao J, Rodat-Despoix L (2011) Molecular mechanisms of mechanotransduction in mammalian sensory neurons. *Nature reviews Neuroscience* 12:139-153.
- Depeault A, Meftah el M, Chapman CE (2008) Tactile speed scaling: contributions of time and space. *J Neurophysiol* 99:1422-1434.
- Diamond ME (2010) Texture sensation through the fingertips and the whiskers. *Curr Opin Neurobiol* 20:319-327.
- DiCarlo JJ, Johnson KO (2000) Spatial and temporal structure of receptive fields in primate somatosensory area 3b: effects of stimulus scanning direction and orientation. *J Neurosci* 20:495-510.
- DiCarlo JJ, Johnson KO (2002) Receptive field structure in cortical area 3b of the alert monkey. *Behav Brain Res* 135:167-178.
- DiCarlo JJ, Johnson KO, Hsiao SS (1998) Structure of receptive fields in area 3b of primary somatosensory cortex in the alert monkey. *J Neurosci* 18:2626-2645.
- Drew LJ, Rohrer DK, Price MP, Blaver KE, Cockayne DA, Cesare P, Wood JN (2004) Acid-sensing ion channels ASIC2 and ASIC3 do not contribute to mechanically activated currents in mammalian sensory neurones. *The Journal of physiology* 556:691-710.
- Dyhr-Poulsen P (1975) Increased vibration threshold before movements in human subjects. *Exp Neurol* 47:516-522.
- Edin BB, Johansson N (1995) Skin strain patterns provide kinaesthetic information to the human central nervous system. *The Journal of physiology* 487 ( Pt 1):243-251.
- Edin BB, Vallbo AB (1990) Muscle afferent responses to isometric contractions and relaxations in humans. *Journal of neurophysiology* 63:1307-1313.
- Edin BB, Westling G, Johansson RS (1992) Independent control of human finger-tip forces at individual digits during precision lifting. *The Journal of physiology* 450:547-564.
- Fitzgerald PJ, Lane JW, Thakur PH, Hsiao SS (2006) Receptive field properties of the macaque second somatosensory cortex: representation of orientation on different finger pads. *J Neurosci* 26:6473-6484.
- Flanagan JR, Bittner JP, Johansson RS (2008) Experience can change distinct size-weight priors engaged in lifting objects and judging their weights. *Current biology : CB* 18:1742-1747.
- Franzen O, Nordmark J (1975) Vibrotactile Frequency Discrimination. *Percept Psychophys* 17:480-484.

- Freeman AW, Johnson KO (1982) Cutaneous mechanoreceptors in macaque monkey: temporal discharge patterns evoked by vibration, and a receptor model. *J Physiol* 323:21-41.
- Fromm C, Evarts EV (1982) Pyramidal tract neurons in somatosensory cortex: central and peripheral inputs during voluntary movement. *Brain research* 238:186-191.
- Fyffe RE, Cheema SS, Light AR, Rustioni A (1986) Intracellular staining study of the feline cuneate nucleus. II. Thalamic projecting neurons. *J Neurophysiol* 56:1284-1296.
- Gandevia SC, McCloskey DI, Burke D (1992) Kinaesthetic signals and muscle contraction. *Trends in neurosciences* 15:62-65.
- Gardner EP, Costanzo RM (1980) Neuronal mechanisms underlying direction sensitivity of somatosensory cortical neurons in awake monkeys. *J Neurophysiol* 43:1342-1354.
- Gardner EP, Costanzo RM (1981) Properties of kinesthetic neurons in somatosensory cortex of awake monkeys. *Brain research* 214:301-319.
- Gardner EP, Palmer CI (1989) Simulation of motion on the skin. I. Receptive fields and temporal frequency coding by cutaneous mechanoreceptors of OPTACON pulses delivered to the hand. *J Neurophysiol* 62:1410-1436.
- Gazzola V, Spezio ML, Etzel JA, Castelli F, Adolphs R, Keysers C (2012) Primary somatosensory cortex discriminates affective significance in social touch. *Proceedings of the National Academy of Sciences* 109:E1657-E1666.
- Ghez C, Gordon J, Ghilardi FM, Sainburg R (1995) Contributions of vision and proprioception to accuracy in limb movements. In: *The Cognitive Neurosciences*(Gazzaniga, M. S., ed), pp 549-564 Cambridge, MA: The MIT Press.
- Ghez C, Sainburg R (1995) Proprioceptive control of interjoint coordination. *Can J Physiol Pharmacol* 73:273-284.
- Goff GD (1967) Differential Discrimination of Frequency of Cutaneous Mechanical Vibration. *J Exp Psychol* 74:294-&.
- Goodwin AW, Browning AS, Wheat HE (1995) Representation of curved surfaces in responses of mechanoreceptive afferent fibers innervating the monkey's fingerpad. *J Neurosci* 15:798-810.
- Gordon AM, Westling G, Cole KJ, Johansson RS (1993) Memory representations underlying motor commands used during manipulation of common and novel objects. *Journal of neurophysiology* 69:1789-1796.
- Gregory JE, Proske U (1979) The responses of Golgi tendon organs to stimulation of different combinations of motor units. *The Journal of physiology* 295:251-262.

- Grigg P (1975) Mechanical factors influencing response of joint afferent neurons from cat knee. *J Neurophysiol* 38:1473-1484.
- Gynther BD, Vickery RM, Rowe MJ (1992) Responses of slowly adapting type II afferent fibres in cat hairy skin to vibrotactile stimuli. *J Physiol* 458:151-169.
- Gynther BD, Vickery RM, Rowe MJ (1995) Transmission characteristics for the 1:1 linkage between slowly adapting type II fibers and their cuneate target neurons in cat. *Exp Brain Res* 105:67-75.
- Halata Z, Grim M, Bauman KI (2003) Friedrich Sigmund Merkel and his "Merkel cell", morphology, development, and physiology: review and new results. *The anatomical record Part A, Discoveries in molecular, cellular, and evolutionary biology* 271:225-239.
- Hall LA, McCloskey DI (1983) Detections of movements imposed on finger, elbow and shoulder joints. *The Journal of physiology* 335:519-533.
- Harris F, Jabbur SJ, Morse RW, Towe AL (1965) Influence of Cerebral Cortex on Cuneate Nucleus of Monkey. *Nature* 208:1215-&.
- Harvey MA, Saal HP, Dammann JF, 3rd, Bensmaia SJ (2013) Multiplexing stimulus information through rate and temporal codes in primate somatosensory cortex. *PLoS biology* 11:e1001558.
- Hayward V, Terekhov AV, Wong SC, Geborek P, Bengtsson F, Jorntell H (2014) Spatio-temporal skin strain distributions evoke low variability spike responses in cuneate neurons. *Journal of the Royal Society, Interface / the Royal Society* 11:20131015.
- Hertenstein MJ, Holmes R, McCullough M, Keltner D (2009) The communication of emotion via touch. *Emotion* 9:566.
- Ho HN, Jones LA (2006) Contribution of thermal cues to material discrimination and localization. *Percept Psychophys* 68:118-128.
- Ho HN, Jones LA (2008) Modeling the thermal responses of the skin surface during hand-object interactions. *J Biomech Eng* 130:021005.
- Hollins M, Bensmaia S, Karlof K, Young F (2000) Individual differences in perceptual space for tactile textures: evidence from multidimensional scaling. *Percept Psychophys* 62:1534-1544.
- Hollins M, Bensmaia SJ (2007) The coding of roughness. *Can J Exp Psychol* 61:184-195.
- Hollins M, Faldowski R, Rao S, Young F (1993) Perceptual dimensions of tactile surface texture: a multidimensional scaling analysis. *Percept Psychophys* 54:697-705.

- Hollins M, Risner SR (2000) Evidence for the duplex theory of tactile texture perception. *Percept Psychophys* 62:695-705.
- Hollins M, Roy EA (1996) Perceived intensity of vibrotactile stimuli: the role of mechanoreceptive channels. *Somatosens Mot Res* 13:273-286.
- Horch KW, Whitehorn D, Burgess PR (1974) Impulse generation in type I cutaneous mechanoreceptors. *Journal of neurophysiology* 37:267-281.
- Houk J, Henneman E (1967) Responses of Golgi tendon organs to active contractions of the soleus muscle of the cat. *J Neurophysiol* 30:466-481.
- Hsiao S (2008) Central mechanisms of tactile shape perception. *Curr Opin Neurobiol* 18:418-424.
- Hu J, Chiang LY, Koch M, Lewin GR (2010) Evidence for a protein tether involved in somatic touch. *The EMBO journal* 29:855-867.
- Hu J, Lewin GR (2006) Mechanosensitive currents in the neurites of cultured mouse sensory neurones. *The Journal of physiology* 577:815-828.
- Hulliger M (1984) The mammalian muscle spindle and its central control. *Reviews of physiology, biochemistry and pharmacology* 101:1-110.
- Iggo A, Muir AR (1969) The structure and function of a slowly adapting touch corpuscle in hairy skin. *The Journal of physiology* 200:763-796.
- Iwamura Y, Tanaka M, Hikosaka O (1980) Overlapping representation of fingers in the somatosensory cortex (area 2) of the conscious monkey. *Brain research* 197:516-520.
- Iwamura Y, Tanaka M, Sakamoto M, Hikosaka O (1993) Rostrocaudal gradients in the neuronal receptive field complexity in the finger region of the alert monkey's postcentral gyrus. *Exp Brain Res* 92:360-368.
- Jenmalm P, Birznieks I, Goodwin AW, Johansson RS (2003) Influence of object shape on responses of human tactile afferents under conditions characteristic of manipulation. *The European journal of neuroscience* 18:164-176.
- Jenmalm P, Johansson RS (1997) Visual and somatosensory information about object shape control manipulative fingertip forces. *The Journal of neuroscience : the official journal of the Society for Neuroscience* 17:4486-4499.
- Jenmalm P, Schmitz C, Forssberg H, Ehrsson HH (2006) Lighter or heavier than predicted: neural correlates of corrective mechanisms during erroneously programmed lifts. *The Journal of neuroscience : the official journal of the Society for Neuroscience* 26:9015-9021.
- Johansson RS (1978) Tactile sensibility in the human hand: receptive field characteristics of mechanoreceptive units in the glabrous skin area. *J Physiol* 281:101-125.

- Johansson RS, Birznieks I (2004) First spikes in ensembles of human tactile afferents code complex spatial fingertip events. *Nat Neurosci* 7:170-177.
- Johansson RS, Edin BB (1993) Predictive Feedforward Sensory Control during Grasping and Manipulation in Man. *Biomed Res-Tokyo* 14:95-106.
- Johansson RS, Flanagan JR (2009) Coding and use of tactile signals from the fingertips in object manipulation tasks. *Nature reviews Neuroscience* 10:345-359.
- Johansson RS, Vallbo AB (1979) Tactile sensibility in the human hand: relative and absolute densities of four types of mechanoreceptive units in glabrous skin. *J Physiol* 286:283-300.
- Johansson RS, Westling G (1984) Roles of glabrous skin receptors and sensorimotor memory in automatic control of precision grip when lifting rougher or more slippery objects. *Exp Brain Res* 56:550-564.
- Johnson KO (1974) Reconstruction of population response to a vibratory stimulus in quickly adapting mechanoreceptive afferent fiber population innervating glabrous skin of the monkey. *J Neurophysiol* 37:48-72.
- Johnson KO (2001) The roles and functions of cutaneous mechanoreceptors. *Curr Opin Neurobiol* 11:455-461.
- Johnson KO, Lamb GD (1981) Neural mechanisms of spatial tactile discrimination: neural patterns evoked by braille-like dot patterns in the monkey. *J Physiol* 310:117-144.
- Jones LA, Lederman SJ (2006) *Human Hand Function*. New York: Oxford University Press.
- Jorntell H, Bengtsson F, Geborek P, Spanne A, Terekhov AV, Hayward V (2014) Segregation of Tactile Input Features in Neurons of the Cuneate Nucleus. *Neuron* 83:1444-1452.
- Kaas JH (1983) What, if anything, is SI? Organization of first somatosensory area of cortex. *Physiol Rev* 63:206-231.
- Kaas JH, Nelson RJ, Sur M, Lin CS, Merzenich MM (1979) Multiple representations of the body within the primary somatosensory cortex of primates. *Science* 204:521-523.
- Kalaska JF (1994) Central Neural Mechanisms of Touch and Proprioception. *Can J Physiol Pharmacol* 72:542-545.
- Katz D (1925) *Der Aufbau des Tastwelt*. Leipzig: Johann Ambrosius Barth.
- Keysers C, Kaas JH, Gazzola V (2010) Somatosensation in social perception. *Nature Reviews Neuroscience* 11:417-428.

- Kim SS, Gomez-Ramirez M, Thakur PH, Hsiao SS (2015) Multimodal Interactions between Proprioceptive and Cutaneous Signals in Primary Somatosensory Cortex. *Neuron* 86:555-566.
- Knibestol M (1973) Stimulus-response functions of rapidly adapting mechanoreceptors in human glabrous skin area. *J Physiol* 232:427-452.
- Knibestol M (1975) Stimulus-response functions of slowly adapting mechanoreceptors in the human glabrous skin area. *J Physiol* 245:63-80.
- Kremeyer B, Lopera F, Cox JJ, Momin A, Rugiero F, Marsh S, Woods CG, Jones NG, Paterson KJ, Fricker FR, Villegas A, Acosta N, Pineda-Trujillo NG, Ramirez JD, Zea J, Burley MW, Bedoya G, Bennett DL, Wood JN, Ruiz-Linares A (2010) A gain-of-function mutation in TRPA1 causes familial episodic pain syndrome. *Neuron* 66:671-680.
- Kringelbach ML (2005) The human orbitofrontal cortex: linking reward to hedonic experience. *Nature Reviews Neuroscience* 6:691-702.
- Krubitzer L, Huffman KJ, Disbrow E, Recanzone G (2004) Organization of area 3a in macaque monkeys: contributions to the cortical phenotype. *J Comp Neurol* 471:97-111.
- Lacey S, Sathian K (2012) Representation of Object Form in Vision and Touch. In: *The Neural Bases of Multisensory Processes* (Murray, M. M. and Wallace, M. T., eds) Boca Raton (FL).
- Lamb GD (1983) Tactile Discrimination of Textured Surfaces - Peripheral Neural Coding in the Monkey. *J Physiol-London* 338:567-587.
- Lamotte RH (1977) Psychophysical and neurophysiological studies of tactile sensibility. *Symposium on clothing comfort*.
- LaMotte RH, Mountcastle VB (1975) Capacities of humans and monkeys to discriminate vibratory stimuli of different frequency and amplitude: a correlation between neural events and psychological measurements. *J Neurophysiol* 38:539-559.
- Lederman SJ, Klatzky RL (1993) Extracting object properties through haptic exploration. *Acta Psychol (Amst)* 84:29-40.
- Lee SM, Friedberg MH, Ebner FF (1994) The role of GABA-mediated inhibition in the rat ventral posterior medial thalamus. I. Assessment of receptive field changes following thalamic reticular nucleus lesions. *Journal of neurophysiology* 71:1702-1715.
- Lesniak DR, Marshall KL, Wellnitz SA, Jenkins BA, Baba Y, Rasband MN, Gerling GJ, Lumpkin EA (2014) Computation identifies structural features that govern neuronal firing properties in slowly adapting touch receptors. *eLife* 3:e01488.

- Li J, Guido W, Bickford ME (2003) Two distinct types of corticothalamic EPSPs and their contribution to short-term synaptic plasticity. *Journal of neurophysiology* 90:3429-3440.
- Libouton X, Barbier O, Berger Y, Plaghki L, Thonnard JL (2012) Tactile roughness discrimination of the finger pad relies primarily on vibration sensitive afferents not necessarily located in the hand. *Behav Brain Res* 229:273-279.
- Liedtke W, Friedman JM (2003) Abnormal osmotic regulation in *trpv4*<sup>-/-</sup> mice. *Proceedings of the National Academy of Sciences of the United States of America* 100:13698-13703.
- Loewenstein WR, Altamirano-Orrego R (1958) Generation and propagation of impulses during refractoriness in a Pacinian corpuscle. *Nature* 181:124-125.
- Loewenstein WR, Altamirano-Orrego R (1958) The refractory state of the generator and propagated potentials in a pacinian corpuscle. *The Journal of general physiology* 41:805-824.
- Loewenstein WR, Mendelson M (1965) Components of Receptor Adaptation in a Pacinian Corpuscle. *The Journal of physiology* 177:377-397.
- Loewenstein WR, Skalak R (1966) Mechanical transmission in a Pacinian corpuscle. An analysis and a theory. *The Journal of physiology* 182:346-378.
- Löken LS, Wessberg J, McGlone F, Olausson H (2009) Coding of pleasant touch by unmyelinated afferents in humans. *Nature neuroscience* 12:547-548.
- London BM, Miller LE (2013) Responses of somatosensory area 2 neurons to actively and passively generated limb movements. *Journal of neurophysiology* 109:1505-1513.
- Lu Y, Ma X, Sabharwal R, Snitsarev V, Morgan D, Rahmouni K, Drummond HA, Whiteis CA, Costa V, Price M, Benson C, Welsh MJ, Chapleau MW, Abboud FM (2009) The ion channel ASIC2 is required for baroreceptor and autonomic control of the circulation. *Neuron* 64:885-897.
- Luna R, Hernandez A, Brody CD, Romo R (2005) Neural codes for perceptual discrimination in primary somatosensory cortex. *Nat Neurosci* 8:1210-1219.
- Mackevicius EL, Best MD, Saal HP, Bensmaia SJ (2012) Millisecond precision spike timing shapes tactile perception. *Journal of Neuroscience* 32:15309-15317.
- Makous JC, Friedman RM, Vierck CJ, Jr. (1995) A critical band filter in touch. *J Neurosci* 15:2808-2818.
- Maksimovic S, Nakatani M, Baba Y, Nelson AM, Marshall KL, Wellnitz SA, Firozi P, Woo SH, Ranade S, Patapoutian A, Lumpkin EA (2014) Epidermal Merkel cells are mechanosensory cells that tune mammalian touch receptors. *Nature* 509:617-621.

- Manfredi LR, Baker AT, Elias DO, Dammann JF, 3rd, Zielinski MC, Polashock VS, Bensmaia SJ (2012) The effect of surface wave propagation on neural responses to vibration in primate glabrous skin. *PLoS one* 7:e31203.
- Manfredi LR, Saal HP, Brown KJ, Zielinski MC, Dammann JF, 3rd, Polashock VS, Bensmaia SJ (2014) Natural scenes in tactile texture. *J Neurophysiol* 111:1792-1802.
- Marino J, Canedo A, Aguilar J (2000) Sensorimotor cortical influences on cuneate nucleus rhythmic activity in the anesthetized cat. *Neuroscience* 95:657-673.
- Marks LE (1979) Summation of vibrotactile intensity: an analog to auditory critical bands? *Sens Processes* 3:188-203.
- McAlonan K, Cavanaugh J, Wurtz RH (2008) Guarding the gateway to cortex with attention in visual thalamus. *Nature* 456:391-394.
- McCarter GC, Reichling DB, Levine JD (1999) Mechanical transduction by rat dorsal root ganglion neurons in vitro. *Neuroscience letters* 273:179-182.
- McGlone F, Wessberg J, Olausson H (2014) Discriminative and affective touch: sensing and feeling. *Neuron* 82:737-755.
- Mendelson M, Lowenstein WR (1964) Mechanisms of Receptor Adaptation. *Science* 144:554-555.
- Mendoza JE, Foundas AL (2007) *Clinical neuroanatomy : a neurobehavioral approach*. New York ; London: Springer.
- Moberg E (1962) Criticism and study of methods for examining sensibility in the hand. *Neurology* 12:8-19.
- Molinari HH, Schultze KE, Strominger NL (1996) Gracile, cuneate, and spinal trigeminal projections to inferior olive in rat and monkey. *Journal of Comparative Neurology* 375:467-480.
- Mountcastle VB, Talbot WH, Sakata H, Hyvärinen J (1969) Cortical neuronal mechanisms in flutter-vibration studied in unanesthetized monkeys. Neuronal periodicity and frequency discrimination. *J Neurophysiol* 32:452-484.
- Munger BL (1965) The intraepidermal innervation of the snout skin of the opossum. A light and electron microscope study, with observations on the nature of Merkel's Tastzellen. *The Journal of cell biology* 26:79-97.
- Muniak MA, Ray S, Hsiao SS, Dammann JF, Bensmaia SJ (2007) The neural coding of stimulus intensity: linking the population response of mechanoreceptive afferents with psychophysical behavior. *J Neurosci* 27:11687-11699.

- Nagata K, Duggan A, Kumar G, Garcia-Anoveros J (2005) Nociceptor and hair cell transducer properties of TRPA1, a channel for pain and hearing. *The Journal of neuroscience : the official journal of the Society for Neuroscience* 25:4052-4061.
- Nelson RJ, Li B, Douglas VD (1991) Sensory Response Enhancement and Suppression of Monkey Primary Somatosensory Cortical-Neurons. *Brain Res Bull* 27:751-757.
- Nolano M, Provitera V, Crisci C, Stancanelli A, Wendelschafer-Crabb G, Kennedy WR, Santoro L (2003) Quantification of myelinated endings and mechanoreceptors in human digital skin. *Ann Neurol* 54:197-205.
- Nowak DA, Glasauer S, Hermsdorfer J (2003) Grip force efficiency in long-term deprivation of somatosensory feedback. *Neuroreport* 14:1803-1807.
- Ochoa J, Torebjork E (1983) Sensations evoked by intraneural microstimulation of single mechanoreceptor units innervating the human hand. *J Physiol* 342:633-654.
- Olausson H, Wessberg J, Kakuda N (2000) Tactile directional sensibility: peripheral neural mechanisms in man. *Brain Res* 866:178-187.
- Pack CC, Bensmaia SJ (2015a) Seeing and feeling motion: Canonical computations in motion processing. *PLoS biology*.
- Pack CC, Bensmaia SJ (2015b) Seeing and Feeling Motion: Canonical Computations in Vision and Touch. *PLoS biology* 13.
- Pare M, Behets C, Cornu O (2003) Paucity of presumptive ruffini corpuscles in the index finger pad of humans. *J Comp Neurol* 456:260-266.
- Pare M, Elde R, Mazurkiewicz JE, Smith AM, Rice FL (2001) The Meissner corpuscle revised: a multiafferented mechanoreceptor with nociceptor immunochemical properties. *J Neurosci* 21:7236-7246.
- Pare M, Smith AM, Rice FL (2002) Distribution and terminal arborizations of cutaneous mechanoreceptors in the glabrous finger pads of the monkey. *J Comp Neurol* 445:347-359.
- Pease DC, Quilliam TA (1957) Electron Microscopy of the Pacinian Corpuscle. *Journal of Biophysical and Biochemical Cytology* 3:331-&.
- Pei YC, Bensmaia SJ (2014) The neural basis of tactile motion perception. *J Neurophysiol* 112:3023-3032.
- Pei YC, Hsiao SS, Bensmaia SJ (2008) The tactile integration of local motion cues is analogous to its visual counterpart. *Proc Natl Acad Sci U S A* 105:8130-8135.
- Pei YC, Hsiao SS, Craig JC, Bensmaia SJ (2010) Shape invariant coding of motion direction in somatosensory cortex. *PLoS biology* 8:e1000305.

- Pei YC, Hsiao SS, Craig JC, Bensmaia SJ (2011) Neural mechanisms of tactile motion integration in somatosensory cortex. *Neuron* 69:536-547.
- Penny GR, Fitzpatrick D, Schmechel DE, Diamond IT (1983) Glutamic acid decarboxylase-immunoreactive neurons and horseradish peroxidase-labeled projection neurons in the ventral posterior nucleus of the cat and *Galago senegalensis*. *The Journal of neuroscience : the official journal of the Society for Neuroscience* 3:1868-1887.
- Phillips JR, Johnson KO (1981a) Tactile spatial resolution. II. Neural representation of Bars, edges, and gratings in monkey primary afferents. *J Neurophysiol* 46:1192-1203.
- Phillips JR, Johnson KO (1981b) Tactile spatial resolution. III. A continuum mechanics model of skin predicting mechanoreceptor responses to bars, edges, and gratings. *J Neurophysiol* 46:1204-1225.
- Phillips JR, Johnson KO, Browne HM (1983) A comparison of visual and two modes of tactual letter resolution. *Percept Psychophys* 34:243-249.
- Phillips JR, Johnson KO, Hsiao SS (1988) Spatial pattern representation and transformation in monkey somatosensory cortex. *Proc Natl Acad Sci U S A* 85:1317-1321.
- Pirschel F, Kretzberg J (2016) Multiplexed Population Coding of Stimulus Properties by Leech Mechanosensory Cells. *Journal of Neuroscience* 36:3636-3647.
- Pons TP, Garraghty PE, Cusick CG, Kaas JH (1985) The somatotopic organization of area 2 in macaque monkeys. *J Comp Neurol* 241:445-466.
- Porter LL (1991) Patterns of connectivity in the cat sensory-motor cortex: a light and electron microscope analysis of the projection arising from area 3a. *The Journal of comparative neurology* 312:404-414.
- Post LJ, Zompa IC, Chapman CE (1994) Perception of vibrotactile stimuli during motor activity in human subjects. *Exp Brain Res* 100:107-120.
- Poulos DA, Mei J, Horch KW, Tuckett RP, Wei JY, Cornwall MC, Burgess PR (1984) The neural signal for the intensity of a tactile stimulus. *J Neurosci* 4:2016-2024.
- Prochazka A (1996) Proprioceptive feedback and movement regulation. In: *Handbook of physiology Section 12 Exercise: Regulation and integration of multiple systems*(Rowell, L. and Shepherd, J. T., eds), pp 89-127 New York: American Physiological Society.
- Pruszynski JA, Johansson RS (2014) Edge-orientation processing in first-order tactile neurons. *Nat Neurosci* 17:1404-1409.
- Randolph M, Semmes J (1974) Behavioral consequences of selective subtotal ablations in the postcentral gyrus of *Macaca mulatta*. *Brain research* 70:55-70.

- Rea P (2015) Essential clinical anatomy of the nervous system.
- Reichova I, Sherman SM (2004) Somatosensory corticothalamic projections: distinguishing drivers from modulators. *Journal of neurophysiology* 92:2185-2197.
- Richardson AG, Weigand PK, Sritharan SY, Lucas TH (2016) A chronic neural interface to the macaque dorsal column nuclei. *Journal of neurophysiology* jn 01083 02015.
- Richardson AG, Weigand, P. K., Sritharan, S. Y. & Lucas, T. H. (2015) Somatosensory encoding with cuneate nucleus microstimulation: Effects on downstream cortical activity. 7th International IEEE/EMBS Conference on Neural Engineering (NER) 695–698.
- Rincon-Gonzalez L, Warren JP, Meller DM, Tillery SH (2011) Haptic interaction of touch and proprioception: implications for neuroprosthetics. *IEEE transactions on neural systems and rehabilitation engineering : a publication of the IEEE Engineering in Medicine and Biology Society* 19:490-500.
- Rolls ET, O'Doherty J, Kringelbach ML, Francis S, Bowtell R, McGlone F (2003) Representations of pleasant and painful touch in the human orbitofrontal and cingulate cortices. *Cerebral Cortex* 13:308-317.
- Rushton DN, Rothwell JC, Craggs MD (1981) Gating of somatosensory evoked potentials during different kinds of movement in man. *Brain* 104:465-491.
- Saal HP, Bensmaia SJ (2014) Touch is a team effort: interplay of submodalities in cutaneous sensibility. *Trends in Neurosciences* 37:689-697.
- Saal HP, Harvey MA, Bensmaia SJ (2015) Rate and timing of cortical responses driven by separate sensory channels. *eLife* 4.
- Saal HP, Vijayakumar S, Johansson RS (2009) Information about complex fingertip parameters in individual human tactile afferent neurons. *The Journal of neuroscience : the official journal of the Society for Neuroscience* 29:8022-8031.
- Sachs F (2010) Stretch-activated ion channels: what are they? *Physiology* 25:50-56.
- Sainburg RL, Ghilardi MF, Poizner H, Ghez C (1995) Control of limb dynamics in normal subjects and patients without proprioception. *J Neurophysiol* 73:820-835.
- Sakata H, Takaoka Y, Kawarasaki A, Shibutani H (1973) Somatosensory properties of neurons in the superior parietal cortex (area 5) of the rhesus monkey. *Brain research* 64:85-102.
- Salinas E, Hernandez A, Zainos A, Romo R (2000) Periodicity and firing rate as candidate neural codes for the frequency of vibrotactile stimuli. *J Neurosci* 20:5503-5515.
- Semmes J, Porter L, Randolph MC (1974) Further studies of anterior postcentral lesions in monkeys. *Cortex* 10:55-68.

- Semmes J, Turner B (1977) Effects of Cortical-Lesions of Somatosensory Tasks. *Journal of Investigative Dermatology* 69:181-189.
- Simoncelli EP, Olshausen BA (2001) Natural image statistics and neural representation. *Annu Rev Neurosci* 24:1193-1216.
- Sinclair RJ, Burton H (1991a) Neuronal activity in the primary somatosensory cortex in monkeys (*Macaca mulatta*) during active touch of textured surface gratings: responses to groove width, applied force, and velocity of motion. *J Neurophysiol* 66:153-169.
- Sinclair RJ, Burton H (1991b) Tactile discrimination of gratings: psychophysical and neural correlates in human and monkey. *Somatosens Mot Res* 8:241-248.
- Skedung L, Arvidsson M, Chung JY, Stafford CM, Berglund B, Rutland MW (2013) Feeling small: exploring the tactile perception limits. *Sci Rep* 3:2617.
- Smith AM, Scott SH (1996) Subjective scaling of smooth surface friction. *J Neurophysiol* 75:1957-1962.
- Srinivasan M, LaMotte R (1996) Tactual discrimination of softness: Abilities and mechanisms. . In: *Somesthesia and the Neurobiology of the Somatosensory Cortex*(Franzen, O. and Johansson, R. S., eds), pp 123-135 Basel: Birkhauser.
- Srinivasan MA, Lamotte RH (1995) Tactual Discrimination of Softness. *J Neurophysiol* 73:88-101.
- Sripati AP, Bensmaia SJ, Johnson KO (2006) A continuum mechanical model of mechanoreceptive afferent responses to indented spatial patterns. *J Neurophysiol* 95:3852-3864.
- Sur M, Merzenich MM, Kaas JH (1980) Magnification, receptive-field area, and "hypercolumn" size in areas 3b and 1 of somatosensory cortex in owl monkeys. *Journal of neurophysiology* 44:295-311.
- Suzuki M, Mizuno A, Kodaira K, Imai M (2003) Impaired pressure sensation in mice lacking TRPV4. *The Journal of biological chemistry* 278:22664-22668.
- Takahashi-Iwanaga H, Shimoda H (2003) The three-dimensional microanatomy of Meissner corpuscles in monkey palmar skin. *Journal of neurocytology* 32:363-371.
- Talbot WH, Darian-Smith I, Kornhuber HH, Mountcastle VB (1968a) The sense of flutter-vibration: comparison of the human capacity with response patterns of mechanoreceptive afferents from the monkey hand. *J Neurophysiol* 31:301-334.
- Talbot WH, Darian-Smith I, Kornhuber HH, Mountcastle VB (1968b) The sense of flutter-vibration: comparison of the human capacity with response patterns of mechanoreceptive afferents from the monkey hand. *Journal of Neurophysiology* 31:301-334.

- Tommerdahl M, Hester KD, Felix ER, Hollins M, Favorov OV, Quibrera PM, Whitsel BL (2005) Human vibrotactile frequency discriminative capacity after adaptation to 25 Hz or 200 Hz stimulation. *Brain Res* 1057:1-9.
- Tsunozaki M, Bautista DM (2009) Mammalian somatosensory mechanotransduction. *Current opinion in neurobiology* 19:362-369.
- Vallbo AB, Johansson RS (1984) Properties of cutaneous mechanoreceptors in the human hand related to touch sensation. *Hum Neurobiol* 3:3-14.
- Van Horn SC, Sherman SM (2004) Differences in projection patterns between large and small corticothalamic terminals. *The Journal of comparative neurology* 475:406-415.
- Vazquez Y, Zainos A, Alvarez M, Salinas E, Romo R (2012) Neural coding and perceptual detection in the primate somatosensory thalamus. *Proceedings of the National Academy of Sciences of the United States of America* 109:15006-15011.
- Verrillo RT, Fraioli AJ, Smith RL (1969) Sensation Magnitude of Vibrotactile Stimuli. *Percept Psychophys* 6:366-&.
- Vickery RM, Gynther BD, Rowe MJ (1994) Synaptic transmission between single slowly adapting type I fibres and their cuneate target neurones in cat. *The Journal of physiology* 474:379-392.
- Volkers L, Mechoukhi Y, Coste B (2015) Piezo channels: from structure to function. *Pflugers Archiv : European journal of physiology* 467:95-99.
- Wasaka T, Kida T, Kakigi R (2012) Modulation of somatosensory evoked potentials during force generation and relaxation. *Experimental Brain Research* 219:227-233.
- Weber AI, Saal HP, Lieber JD, Cheng JW, Manfredi LR, Dammann JF, 3rd, Bensmaia SJ (2013) Spatial and temporal codes mediate the tactile perception of natural textures. *Proc Natl Acad Sci U S A* 110:17107-17112.
- Werner G, Mountcastle VB (1965) Neural Activity in Mechanoreceptive Cutaneous Afferents: Stimulus-Response Relations, Weber Functions, and Information Transmission. *J Neurophysiol* 28:359-397.
- Westling G, Johansson RS (1984) Factors influencing the force control during precision grip. *Experimental brain research Experimentelle Hirnforschung Experimentation cerebrale* 53:277-284.
- Westling G, Johansson RS (1987) Responses in glabrous skin mechanoreceptors during precision grip in humans. *Exp Brain Res* 66:128-140.

- Wheat HE, Goodwin AW (2000) Tactile discrimination of gaps by slowly adapting afferents: effects of population parameters and anisotropy in the fingerpad. *J Neurophysiol* 84:1430-1444.
- Wheat HE, Goodwin AW (2001) Tactile discrimination of edge shape: limits on spatial resolution imposed by parameters of the peripheral neural population. *J Neurosci* 21:7751-7763.
- Wheat HE, Salo LM, Goodwin AW (2010) Cutaneous afferents from the monkeys fingers: responses to tangential and normal forces. *J Neurophysiol* 103:950-961.
- Woo SH, Ranade S, Weyer AD, Dubin AE, Baba Y, Qiu Z, Petrus M, Miyamoto T, Reddy K, Lumpkin EA, Stucky CL, Patapoutian A (2014) Piezo2 is required for Merkel-cell mechanotransduction. *Nature* 509:622-626.
- Yang Y, Zador AM (2012) Differences in sensitivity to neural timing among cortical areas. *J Neurosci* 32:15142-15147.
- Yau JM, Connor CE, Hsiao SS (2013) Representation of tactile curvature in macaque somatosensory area 2. *J Neurophysiol* 109:2999-3012.
- Yau JM, Hollins M, Bensmaia SJ (2009a) Textural timbre: The perception of surface microtexture depends in part on multimodal spectral cues. *Communicative & integrative biology* 2:344-346.
- Yau JM, Kim SS, Thakur PH, Bensmaia SJ (2016) Feeling form: the neural basis of haptic shape perception. *J Neurophysiol* 115:631-642.
- Yau JM, Olenczak JB, Dammann JF, Bensmaia SJ (2009b) Temporal frequency channels are linked across audition and touch. *Curr Biol* 19:561-566.
- Yau JM, Pasupathy A, Fitzgerald PJ, Hsiao SS, Connor CE (2009c) Analogous intermediate shape coding in vision and touch. *Proc Natl Acad Sci U S A* 106:16457-16462.
- Zelena J (1978) The development of Pacinian corpuscles. *J Neurocytol* 7:71-91.
- Zimny ML (1988) Mechanoreceptors in articular tissues. *The American journal of anatomy* 182:16-32.

## **CHAPTER 2:**

### **Introduction to shaping behavior and principles of its neural control**

#### **Hand shaping behavior**

##### **Introduction**

To understand neuronal representations of the hand, we must first describe the behaviors it engages in. However, the complexity of the hand defies an obvious, concise description. In this section, we briefly discuss advances in describing hand movements then, focusing on grasp, we enumerate features of grasp that, when combined, enable the manipulation of objects spanning myriad shapes and sizes.

##### **The gamut of hand function**

The complex anatomy of the hand allows it to perform a variety of different functions. Accordingly, one might wish to consider the space in which hand movements reside and determine where grasping – the focus of the present study – falls within this space. To this end, we first examine hand control along two axes: the degree of individuation among digits and the degree to which kinematics or forces are the relevant control parameter.

At one extreme of the first axis, prehensile movements comprise hand behaviors classically considered to require the least individuation across digits. At the other extreme, (non-prehensile) skilled movements such as playing a musical instrument require the most individuation (Jones & Lederman, 2006). Along the second axis, functions are classified generally based on whether or not an object is in contact with the hand. On one side, behaviors involve pre-shaping the hand prior to object contact; on the other side, behaviors involve controlling applied force to maintain grip and prevent slip as the arm acts to lift a grasped object. The focus of this project will be the kinematic control of prehensile movements, in part because an important step in understanding the

neural basis of stereognosis is to understand the proprioceptive representation of prehensile kinematics giving rise to the shape of the hand. Ultimately, the resulting model of proprioceptive coding of hand posture will be fused with the model of tactile coding of object contact to develop a model of stereognosis.

### **Early qualitative characterizations of hand shaping**

Perhaps the earliest attempt of note to characterize the behavior of the grasping hand comes from John Napier beginning in 1956 (Napier, 1956). He studied, in particular, the postures that people adopted when holding various objects and tools in their hands and made qualitative assessments of those grasps. The overarching theme of his line of research was that hand postures adopted for the grasps of different objects appeared to lie on a two-dimensional continuum: Along one dimension were grips of cylinders and hammers of various diameters that involved proximal contact points such as the palm and proximal phalanges, which he dubbed “power grip”; along the other dimension were grips of disks of various sizes that frequently involved contact points at the distal phalanges, which he dubbed “precision grip”. Hand grips could reside on one of infinitesimally spaced points on this continuum, unlike other theories of grip which presumed discrete grip types.

However, Napier’s work focused primarily on the shape of the hand once it had adopted its final position. The movements undertaken by the hand after initial contact and prior to adopting its final posture, in addition to its relationship with the arm during coupled reach-to-grasp movements, remained unexplored. One of the most basic features of hand movement to be teased out was the nature of its typical coordination with reach, as shaping of the hand occurs in tandem during canonical reach-to-grasp movements (M Jeannerod, 1984). Lawrence and Kuypers’ seminal lesion studies of the descending motor tracts in monkeys offered some insight into this

issue (Lawrence & Kuypers, 1968a, 1968b). In particular, the coordinated movements of the digits themselves were more profoundly impaired by the removal of the descending pyramidal tract than were movements of the shoulder and elbow responsible for transporting the hand to the appropriate location. This laid the groundwork in motor systems and motor behavioral research for the notion of separate pathways for the control of reaching and grasping, which paralleled the idea of separate dorsal and ventral streams of information about object location and identity in visual systems neuroscience (Goodale & Milner, 1992; Ungerleider & Haxby, 1994).

### **Simple quantification of hand shaping behavior**

Subsequent research into reach-to-grasp movements sought to quantify the relative time courses and gross kinematic profiles of these presumably separate reach and grasp profiles. The consistent theme that arose from this body of literature was the presence of hand kinematic features that corresponded with the size of a target object and the interaction between hand transport and shaping under normal reach-to-grasp conditions. In particular, the notion of a “maximum hand aperture” arose from observed inflection points in video recordings of reaching and grasping hands (M Jeannerod, 1984). During normal reach-to-grasp, the digits of the hand consistently abduct and extend during the first half of hand transport to create a circle defined by fingertip locations, or “aperture”, roughly 20% larger than required by the size of an object (Marc Jeannerod, 2009). This hand aperture is then reduced with flexions and adductions of the digits through the second half of limb transport, eventually terminating at grasp where object contact is established.

### **Sophisticated quantification of hand shaping behavior: Synergies**

The set of features so far described offer a qualitative, rudimentary picture of the full range of function afforded by the hand. The notions of “power” and “precision” grip, in addition to the decision to treat the aperture of the hand as an important measure, are all based on qualitative

observations. As physiological recording techniques advanced to permit ever more detailed data, extracting meaningful information from these data required a more rigorous quantitative approach.

One such approach, most notably adopted by Emilio Bizzi and colleagues to find ensembles of correlated muscle activity in the legs of the frog (d'Avella, Saltiel, & Bizzi, 2003), was to apply a variant of principal component analysis (PCA) to the time-varying electromyographic (EMG) traces recorded during a variety of behaviors such as leaping and kicking. The resultant weighted vectors of muscle activity (Figure 2-1) were dubbed “muscle synergies”, and surprisingly simple structure could be extracted from this complex array of EMG activity by explaining them in terms of these synergies. Similarly to how Napier had attempted to qualitatively constrain the full range of hand movements to a planar power-precision continuum, a simple three-dimensional continuum inferred systematically using PCA could explain over 60% of the cross-validated variation in the time-varying EMG traces of 13 muscles (d'Avella et al., 2003). In other words, muscle activations often fell into patterns that could be discerned using simple dimensionality reduction algorithms.

Applying this methodology to ever-larger EMG datasets and behaviors of different species, including grasping in primates (Overduin, d'Avella, Roh, & Bizzi, 2008; Weiss & Flanders, 2004), researchers have consistently found simple low-dimensional structure in high dimensional data sets. Similar methods had also been applied to grasping kinematic data of the hand (Santello, Flanders, & Soechting, 1998; Weiss & Flanders, 2004) to find superficially similar low-dimensional structure across mimed grasps of a variety of different objects. A rapidly-emerging quantitative body of literature had come to support a widely held conclusion hitherto only qualitatively surmised—namely, that the control of movement was indeed constrained to a tractably simplified continuum comprising just a handful of dimensions. Thus, an effector as

complex as the hand, which would require many “knobs” to control if every possible hand posture were accessible, was simplified such that only a subset of these postures could be achieved, therefore requiring fewer knobs.

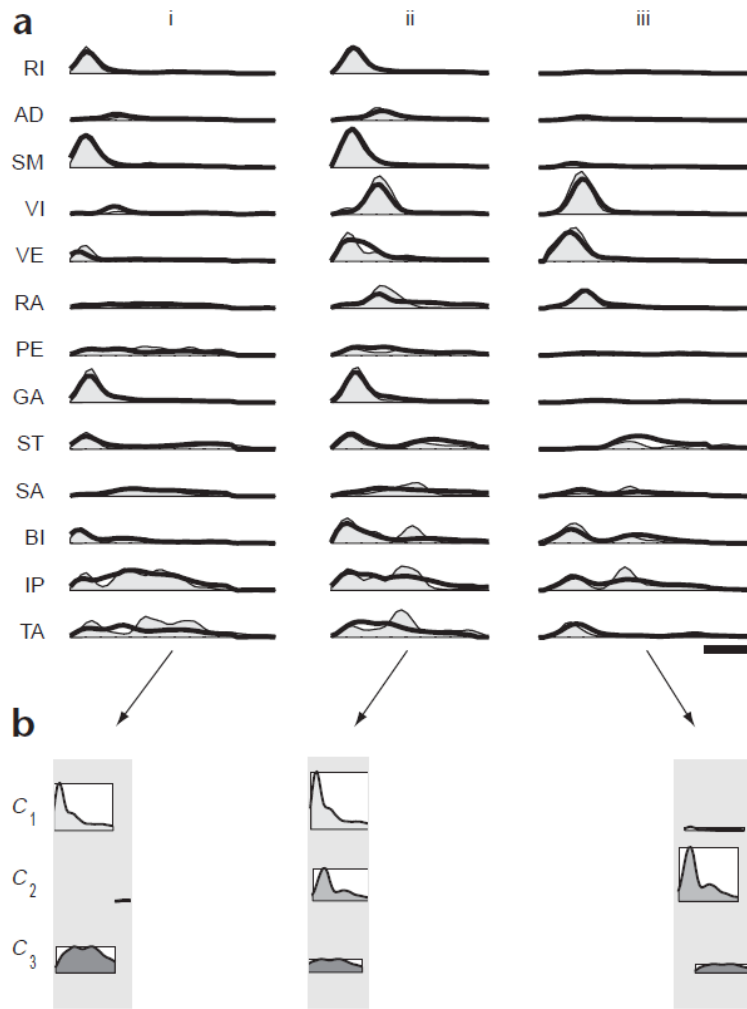


**Figure 2-1.** Rectified low-pass filtered EMG activity (filled gray traces, a) is estimated (black traces, a) using combinations of patterns defined along three muscle synergies (b). A low-dimensional continuum appears at first glance to be a sufficient explanation of muscle activity. Figure from d’Avella, Saltiel, & Bizzi, 2003.

However, a number of limitations and conflicting results are evident in the body of literature on synergies (Tresch & Jarc, 2009). Foremost, behaviors used to assess the presence of synergies can often be very simple, such as two-dimensional planar reaches. When inferring

synergies from a low-dimensional behavior, it becomes difficult to disentangle constraints imposed by the task from putative ones imposed by the neural control system. Moreover, these synergies are inferred using PCA or a similar method which simply aims to explain a threshold amount of variance in the original data. While reasonable, it may not capture the aspects of hand movements that are most useful for discerning different object and grip types. When assessing synergies in terms of their ability to separate among numerous different object grip types rather than raw variance *per se*, the apparent dimensionality and therefore complexity of the multivariate grasp continuum appears to increase (Santello et al., 1998). As such, control of movements may reside on a higher-dimensional continuum than synergy based approaches typically describe.

### **Conclusions**

The hand is a complex effector comprising numerous degrees of freedom. In light of this complexity, researchers have attempted to reduce prehensile behavior to a tractably small set of features such as the power-precision continuum of grip types, hand aperture, and distinct reach and grasp components. These concepts continue to dictate the discussion of hand shaping behavior even as more sophisticated methods have permitted the collection and analysis of increasingly high dimensional data. Indeed, these quantitative methods originally came to the conclusion that the neural control of movement was constrained to a small number of motor primitives, or “synergies”, offering quantitative physiological support for dimensionality reduction as a fundamental strategy of motor control rather than merely an operation of convenience performed by investigators of motor behavior. However, a number of limitations in the study of such synergies cast doubt on just how simplified and low-dimensional the neural control of grasp truly is.

## **The cortical motor control of the arm and hand**

### **The basis of a neural “code” for movement**

Since the work of Sherrington (Sherrington, 1910), the notion of a central motor system defined by an intricate web of divergent outputs onto peripheral effectors has been established. The complexity inherent to such a massively divergent scheme of innervation as far downstream as spinal interneurons, which is likely further exacerbated at the level of motor cortex, has inspired motor cortical neurophysiologists for decades to attempt to collapse this detail into a simple, tractable “code” for movement parameters. Such efforts parallel those seen in attempts to collapse the anatomical complexity of the hand into a low-dimensional continuum of different grip types. They also parallel attempts to explain the neurophysiological consequences of massively convergent inputs onto visual and somatosensory cortical sensory neurons in terms of a simple “code” for particular stimulus features (Pack & Bensmaia, 2015) such as neural coding of object orientation and edge detection. As we will soon see, however, attempts to impose a single overarching “code” on the activity of M1 cortical neurons has proven more elusive than attempts to do so in sensory cortices, leading to no small amount of controversy (Omrani, Kaufman, Hatsopoulos, & Cheney, 2017).

### **Somatotopy as an organizing principle?**

Among the first set of such codes considered to be supported by motor cortex is the notion of a spatial, somatotopic “map” of different parts of the body, wherein the numerous divergent projections of neurons in M1 are presumed to be constrained to some spatially-limited region of the body in a manner predicted by their location in cortex itself. The most famous early attempt to systematically infer a detailed somatotopic map of primary motor cortex (M1) came from Penfield and Boldrey (Penfield & Boldrey, 1937). Their work revealed, through electrical stimulation of

the surface of M1 and the resultant twitches of the body, a coarse somatotopic organization of M1 that paralleled that of cortex posterior to the central sulcus, which he also mapped by electrical stimulation and asking patients the locations of resultant sensations. Subsequent work probing for more detail in this motor somatotopy, however, reveals an idiosyncratic map featuring overlapping representations of the digits (Schieber & Hibbard, 1993) (Figure 2-2A). In contrast, somatosensory cortex remains clearly somatotopic even at this level of detail: A reliable medial-to-lateral progression of cortical neurons with receptive fields (RFs) in digits progressing from 5 to 2 and then the thumb is seen (Pons, Garraghty, Cusick, & Kaas, 1985).



**Figure 2-2.** (A) Mapping the preferred digit of different locations on a patch of motor cortex (shown reconstructed on the left) gives rise to a lack of clear somatotopic separation among the digits (right, different colors represent different preferred digits). Figures from Schieber & Hibbard, 1993. (B) At a more coarsely-grained level of detail, separation of arm and hand representations in M1 appears to follow a general pattern of an arm-coding (Forelimb P) “horseshoe” surrounding a digit-coding (Forelimb D) nucleus. Figure from Park et al., 2001.

One set of attempts to reconcile the idiosyncrasies of the detailed M1 somatotopic map include re-defining the types of somatotopic progressions one might expect to see. For example, whereas somatosensory cortex represents along its own medial-lateral axis portions of the arm and hand progressing from proximal to distal, the M1 representation of the arm and hand appears to radiate from a focal point that represents the fingers to progressively more proximal arm effector

representations in surrounding patches of M1 (Figure 2-2B) (Kwan, MacKay, Murphy, & Wong, 1978; Park, Belhaj-Saf, Gordon, & Cheney, 2001), albeit with a region of considerable overlap in between. Another attempt to reconcile these idiosyncrasies has been to forego the notion of somatotopy altogether: Work by Graziano and colleagues using long-form stimulation trains (Graziano, Aflalo, & Cooke, 2005), as opposed to the extremely brief stimuli typically applied to minimize the spread of current when attempting to determine a precise somatotopic map of M1, seemed to result in reliable spatial segregation of qualitatively different and behaviorally-relevant movement types to form what was dubbed an “ethological action map”. A number of issues with this approach, ranging from the necessarily coarse resolution of such long-form stimulation and the qualitative nature by which movements were clustered, have rendered this a controversial take on the organization of M1.

In summary, a coarse somatotopy in M1 appears to be present. However, at the level of detail needed to understand hand or even arm movements in isolation, M1 somatotopy begins to break down. Attempts to impose structure on the idiosyncrasies of M1 somatotopy at this level of detail are few in number and often contentious.

### **A more detailed code for M1: time-varying limb forces or kinematics?**

In addition to seeking a whole-body map in M1, a vast body of literature has sought more detail: In particular, looking in the time-varying spiking activity of M1 neurons for a correlate with the precise time-varying forces or kinematics generated in the target limb. The vast majority of this literature focuses on muscle activations, forces, and kinematics pertaining of the proximal limb rather than the hand due to its greater experimental tractability. One of the earliest attempts to discover the code in M1 was undertaken by Evarts (Evarts, 1968). In this line of research, Evarts found that the force output at the wrist was most reliably related to M1 spiking activity than were

the wrist kinematics. Applying a constant weight acting against wrist flexion or extension systematically changed firing rate profiles in M1 neurons despite little change in wrist kinematics. However, non-monotonic relationships between force and firing rate and the incidence of some units that appeared to be preferentially responsive to wrist kinematics muddied the waters.

In a subsequent, highly influential study, Georgopoulos and colleagues (Georgopoulos, Kalaska, Caminiti, & Massey, 1982) found cosine-tuned neurons for movement direction in a monkey performing reaching movements constrained to a plane and interpreted this as evidence for the kinematics coding. In subsequent experiments, it was shown that movement direction could be reliably read out from the activity of these neurons (based on a “population vector”)(Georgopoulos, Schwartz, & Kettner, 1986). Later work also found that firing rates appeared to also be monotonically related to movement speed (Moran & Schwartz, 1999) and that the imposition of bias forces, which dissociated movement direction from the forces used to generate them, appeared to have a limited effect on neurons’ preferred directions (Georgopoulos, Ashe, Smyrnis, & Taira, 1992). These experiments differed in important ways from those in the aforementioned force-coding studies: First, reaches involved muscle forces and torques about both the shoulder and elbow joints, not just the wrist; moreover, directional tuning curves involved considerably more averaging, over a large time window, across trials, and even across neurons.

The debate over whether forces or kinematics are represented in M1 continues to this day. The kinematic line of research has received more attention, and as such has been elaborated upon with observations of preferential encoding of limb velocity over limb position in M1 (Paninski, Fellows, Hatsopoulos, & Donoghue, 2004; Wang, Chan, Heldman, & Moran, 2007). However, preferred directions have been known to change direction during the execution of movement, which necessarily challenges the interpretation of M1 kinematic coding in terms of simple cosine-

tuned neurons. Researchers have proposed that this may be evidence of preferential force coding instead (Sergio, Hamel-Pâquet, & Kalaska, 2005), evidence of the encoding of complex kinematic trajectories (Hatsopoulos, Xu, & Amit, 2007), or even evidence that such apparent codes for movement are idiosyncratic consequences of rotational structure that gives rise to M1 activity in the first place (Churchland et al., 2012).

### **Coordinate frames in motor control**

Another line of such research aims to describe the relationship of M1 to muscular force in more detail, in particular recording from EMGs across many forearm muscles giving rise to net forces or movements of the wrist. This line of investigation made use of spike-triggered averaging to identify neurons with “facilitative” or “suppressive” actions on muscles (Cheney, Fetz, & Palmer, 1985; Fetz & Cheney, 1980). A consistent theme in this line of work is that antagonist pairs of flexors and extensors are frequently reciprocally facilitated and suppressed by M1 neurons, with outputs to forearm flexor muscles in particular seeming to be the preferred targets of suppressive outputs from M1.

One may be inclined to wonder whether an “intrinsic” muscle-centered code, where reciprocal agonist-antagonist innervation motifs rather than the net forces or movements they produce, may be a more appropriate coordinate frame in which to conceptualize M1 outputs. Work by Kakei, Hoffman, and Strick (Kakei, Hoffman, & Strick, 1999) aimed to answer the emerging question of whether an intrinsic “muscle” coordinate frame or an extrinsic “Cartesian” coordinate frame was most appropriate to explain M1 spiking activity. They were able to dissociate set correlations between the two coordinate frames and found separate clusters of preferentially intrinsic and preferentially extrinsic neurons are present in M1. Other attempts to dissociate intrinsic and extrinsic coordinate frames have advanced nuanced differences in interpretation

(Morrow, Jordan, & Miller, 2007). Regardless, the common thread is that M1 includes neurons that operate in both extrinsic and intrinsic coordinate frames—it is not, in fact, a monolith with a single uniform code for movement.

### **The hand as potentially a special case of motor control**

Thus far, we have discussed the controversies of motor control as they pertain to the control of reaching and wrist movements. However, some evidence suggests that motor control of grasp and behaviors involving the hand might constitute a special case of motor control, subject to different principles. First, spinal lesions have different effects on monkeys' ability to reach and grasp (Lawrence & Kuypers, 1968a, 1968b). Moreover, anatomical studies have revealed important differences between the caudal and rostral subdivisions of M1 (Rathelot & Strick, 2009). Importantly, the caudal subdivision contains a much larger density of direct cortico-motoneuronal projections, a preponderance of which are sent to extrinsic and intrinsic muscles controlling movements of the digits. In addition, as mentioned above, while M1 is not as clearly somatotopically organized as is somatosensory cortex, the arm and hand representations do seem to be somewhat segregated in M1 (Kwan et al., 1978; Park et al., 2001). Finally, somatosensory feedback seems to play a greater role in grasp than in reaching. In particular, lesions of somatosensory and motor cortices appear at first glance to have similar effects on gross motor behavior, the most notable distinction being the reduction in overall grip strength resultant of M1 inactivation and preferentially abolished coordination among the digits with somatosensory cortical inactivation (Brochier, Boudreau, Paré, & Smith, 1999).

In addition to the anatomical and physiological evidence of a separate representation of arm and hand movements, intuitively the arm and hand support qualitatively different functions. Indeed, while rotations about the shoulder and elbow joints are required to transport the arm to a

target position, movements about the wrist and interphalangeal joints are generally coordinated to shape the hand to an object to establish contact points appropriate for object manipulation. The arm thus places the hand in some location in three dimensional space, whereas the hand must be formed into a specific configuration, two goals that would seem to require markedly different computations.

### **M1 response properties during grasp**

Among the first systematic studies of the motor control of grasp was undertaken by Smith and colleagues in 1975 (Smith, Hepp-Reymond, & Wyss, 1975), who found that during a ramp-and-hold isometric grip force behavior, motor cortical neurons tend to increase their firing rates with respect to the level of force applied, similar to what Evarts noted in the wrist. Subsequent work into precision grip mirrored the progression of wrist- and arm-movement study, in particular expanding into EMG recordings and spike-triggered averaging to work within a more detailed intrinsic coordinate frame. An emergent theme of this line of study is that individual M1 neurons appear to simultaneously facilitate and suppress multiple muscles, although the population of muscles facilitated was surprisingly small, with muscle fields generally comprising roughly 2 muscles that was largely invariant to the number of muscles recorded (Buys, Lemon, Mantel, & Muir, 1986; Mckiernan, Marcario, Karrer, Cheney, & Kar, 1998). This was taken as evidence that M1 control of the hand in particular was well-suited to individual movements of digits by virtue of such apparently small muscle fields. However, it should be noted that the behavioral repertoire of the hand under study was typically fairly simple, either spanning just two grip types—“power” and “precision”, the latter of which only involved the thumb and index finger (Lemon, Mantel, & Muir, 1986)—or involving grasps restricted to the apertures of the wells of a *Klüver board* (Mckiernan et al., 1998).

Research into the neural signatures of these more varied grasping behaviors is a fairly recent development. Varieties of different grasps give rise to a variety of different patterns of EMG activity (Brochier, Spinks, Umilta, & Lemon, 2004) and M1 activity (Umilta, Brochier, Spinks, & Lemon, 2007) specific to each object (Figure 2-3). One may intuit from these results that such variety arises from different preferences for specific small groups of muscles. However, work in another intrinsic coordinate frame, namely in terms of joint angles, seems to find that individual neurons exert control over the movements of far more than two joints. The best explanation of the sort of control exerted by M1 neurons, as assessed during a variety of different grasps, seems to be in terms of combinations of joint movements spanning multiple digits and indeed the entire hand (Saleh, Takahashi, Amit, & Hatsopoulos, 2010; Saleh, Takahashi, & Hatsopoulos, 2012).

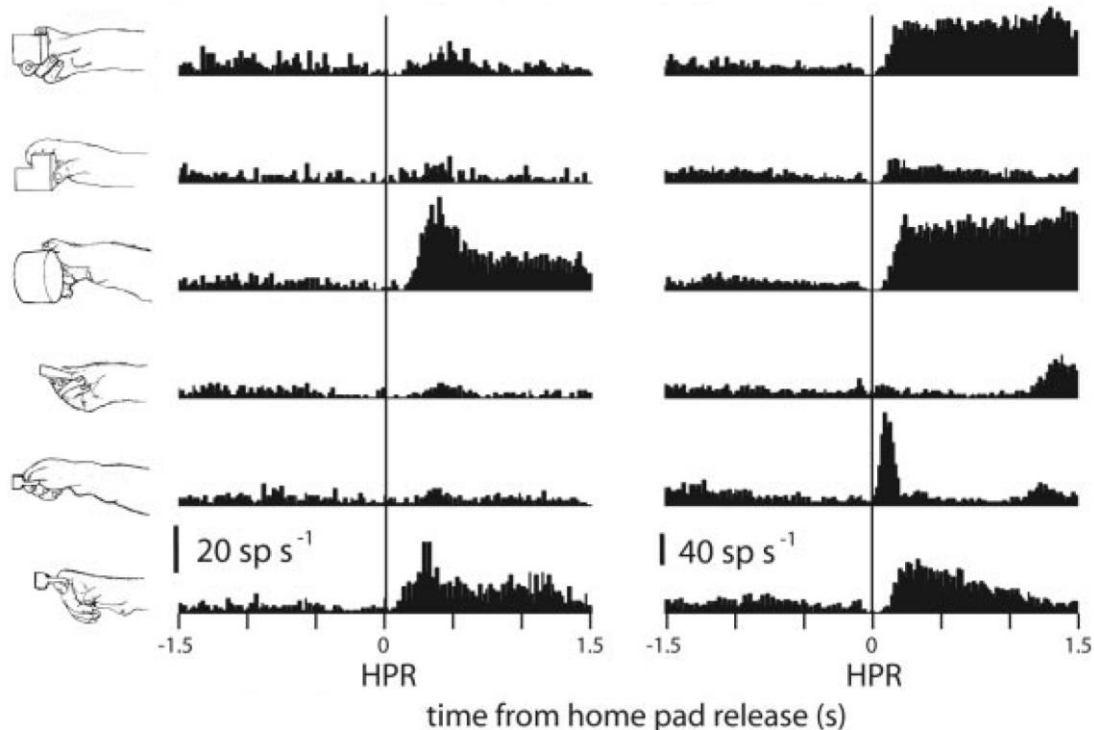


**Figure 2-3.** Firing rates of two different M1 neurons (left and right) during reach-to-grasp of different objects (far left) centered on the onset of the reach, demonstrating just a small sliver of the variety of hand-related responses in M1. Figure from Umilta, Brochier, Spinks, & Lemon, 2007.

## **Synergies to simplify hand control**

Given the complexity of the hand as an effector, some have questioned whether the brain can handle this complexity, suggesting instead that hand movements exist in a lower dimensional space. In particular, “motor primitives” or “muscle synergies” have been put forth as a simplified description of motor behavior in general, including grasping, which should then be reflected in the representation of hand movements in M1. Indeed, stimulation of M1 fails to reveal fractionated representations of digits, instead rise to movements of multiple digits at once. Moreover, the multi-muscle response properties of M1 during grasp could perhaps be reflective of a simpler control scheme defined in terms of just a few multi-muscle synergies.

In support of these ideas, M1 stimulation generates combined activations of muscles that seem constrained to the low-dimensional space inferred from recorded reach-to-grasp behavior (Overduin, d’Avella, Carmena, & Bizzi, 2012). Moreover, time-varying firing rates of ensembles of neurons in cortex appear to be strongly correlated to the synergies of reach-to-grasp movements (Overduin, d’Avella, Roh, Carmena, & Bizzi, 2015).

These studies suffer from limitations that undermine the conclusions, however. The first is the common charge levied against such studies of muscle synergies, namely that the task constrains the complexity of both the movements and the underlying neuronal representation. Another critique is similar to most synergy-based literature, namely that variance explained is a questionable criterion to understand neural constraints. This critique is exacerbated by the presence of two separable behaviors—reach and grasp—which could give rise to a single axis of variance that dwarfs more subtle sources of behavioral variance such as reach direction and grip type. Finally, research into M1 coding of synergies has typically involved the application of smoothing and trial-averaging of neural and kinematic data, which obscures much of the fine structure in the

response and preserves only its coarse structure. With these limitations in mind, questions remain as to whether M1 preferentially encodes synergies. In fact, recent work has suggested that the discharge patterns of M1 cortical neurons are no better explained using synergies of hand movement rather than individual digits (Kirsch, Rivlis, & Schieber, 2014; Mollazadeh, Aggarwal, Thakor, & Schieber, 2014), which are themselves poor predictors of M1 spiking.

### **Conclusions**

How M1 controls the arm and wrist remains elusive. The most consistent feature in the M1 coding literature is that a variety of different kinematic and force parameters can be extracted from patterns of activity in populations of M1 neurons. Single neurons reveal a mosaic of different responses idiosyncratically related to different aspects of muscle activity, movement, and forces, and teasing apart a single “preferred” reference frame defining M1 responses seems impossible. Nonetheless, at least one important feature of M1 responses has been revealed: within a strictly kinematic reference frame, the velocity of the limb is preferentially encoded over the position of the limb. An important element of motor control of the arm and hand, however, is that the control of the two appears to be mediated by physiologically separable mechanisms, probably due to their fundamentally different biomechanical properties (inertial mass, e.g.) and functions (transport vs. object manipulation). It is fair to say that there are more questions than answers when it comes to our understanding of the neural basis for hand movements.

## References

- Brochier, T., Boudreau, M. J., Paré, M., & Smith, A. M. (1999). The effects of muscimol inactivation of small regions of motor and somatosensory cortex on independent finger movements and force control in the precision grip. *Experimental Brain Research*, *128*(1–2), 31–40. Retrieved from <http://www.ncbi.nlm.nih.gov/pubmed/10473737>
- Brochier, T., Spinks, R. L., Umiltà, M. a, & Lemon, R. N. (2004). Patterns of muscle activity underlying object-specific grasp by the macaque monkey. *Journal of Neurophysiology*, *92*(3), 1770–82. <http://doi.org/10.1152/jn.00976.2003>
- Buys, E. J., Lemon, R. N., Mantel, G. W., & Muir, R. B. (1986). Selective facilitation of different hand muscles by single corticospinal neurones in the conscious monkey. *The Journal of Physiology*, *381*(1), 529–549. <http://doi.org/10.1113/jphysiol.1986.sp016342>
- Cheney, P. D., Fetz, E. E., & Palmer, S. S. (1985). Patterns of facilitation and suppression of antagonist forelimb muscles from motor cortex sites in the awake monkey. *Journal of Neurophysiology*, *53*(3), 805–20. <http://doi.org/10.1152/jn.1985.53.3.805>
- Churchland, M. M., Cunningham, J. P., Kaufman, M. T., Foster, J. D., Nuyujukian, P., Ryu, S. I., & Shenoy, K. V. (2012). Neural population dynamics during reaching. *Nature*, *487*(7405), 51–6. <http://doi.org/10.1038/nature11129>
- d'Avella, A., Saltiel, P., & Bizzi, E. (2003). Combinations of muscle synergies in the construction of a natural motor behavior. *Nature Neuroscience*, *6*(3), 300–8. <http://doi.org/10.1038/nn1010>
- Evarts, E. V. (1968). Relation of pyramidal tract activity to force exerted during voluntary movement. *Journal of Neurophysiology*, *31*(1), 14–27. <http://doi.org/10.1152/jn.1968.31.1.14>
- Fetz, E. E., & Cheney, P. D. (1980). Postspike facilitation of forelimb muscle activity by primate corticomotoneuronal cells. *Journal of Neurophysiology*, *44*(4), 751–72. <http://doi.org/10.1152/jn.1980.44.4.751>
- Georgopoulos, A. P., Ashe, J., Smyrnis, N., & Taira, M. (1992). The motor cortex and the coding of force. *Science (New York, N.Y.)*, *256*(5064), 1692–5. <http://doi.org/10.1126/science.256.5064.1692>
- Georgopoulos, A. P., Kalaska, J. F., Caminiti, R., & Massey, J. T. (1982). On the relations between the direction of two-dimensional arm movements and cell discharge in primate motor cortex. *The Journal of Neuroscience : The Official Journal of the Society for Neuroscience*, *2*(11), 1527–37. <http://doi.org/10.1523/JNEUROSCI.02-11-01527.1982>
- Georgopoulos, A. P., Schwartz, A. B., & Kettner, R. E. (1986). Neuronal population coding of movement direction. *Science (New York, N.Y.)*, *233*(4771), 1416–9. <http://doi.org/10.1126/SCIENCE.3749885>

- Goodale, M. A., & Milner, A. D. (1992). Separate visual pathways for perception and action. *Trends in Neurosciences*, *15*(1), 20–25. [http://doi.org/10.1016/0166-2236\(92\)90344-8](http://doi.org/10.1016/0166-2236(92)90344-8)
- Graziano, M. S. A., Aflalo, T. N. S., & Cooke, D. F. (2005). Arm Movements Evoked by Electrical Stimulation in the Motor Cortex of Monkeys. *Journal of Neurophysiology*, *94*(6), 4209–4223. <http://doi.org/10.1152/jn.01303.2004>
- Hatsopoulos, N. G., Xu, Q., & Amit, Y. (2007). Encoding of movement fragments in the motor cortex. *The Journal of Neuroscience : The Official Journal of the Society for Neuroscience*, *27*(19), 5105–14. <http://doi.org/10.1523/JNEUROSCI.3570-06.2007>
- Jeannerod, M. (1984). The timing of natural prehension movements. *Journal of Motor Behavior*, *16*(3), 235–54. Retrieved from <http://www.ncbi.nlm.nih.gov/pubmed/15151851>
- Jeannerod, M. (2009). The study of hand movements during grasping. A historical perspective. In D. A. Nowak & J. Hermsdörfer (Eds.), *Sensorimotor Control of Grasping* (pp. 127–140). Cambridge University Press.
- Jones, L. A., & Lederman, S. J. (2006). *Human hand function*. Oxford University Press.
- Kakei, S., Hoffman, D. S., & Strick, P. L. (1999). Muscle and Movement Representations in the Primary Motor Cortex. *Science*, *285*(5436), 2136–2139. Retrieved from <http://science.sciencemag.org/content/sci/285/5436/2136.full.pdf>
- Kirsch, E., Rivlis, G., & Schieber, M. H. (2014). Primary Motor Cortex Neurons during Individuated Finger and Wrist Movements: Correlation of Spike Firing Rates with the Motion of Individual Digits versus Their Principal Components. *Frontiers in Neurology*, *5*(May), 70. <http://doi.org/10.3389/fneur.2014.00070>
- Kwan, H. C., MacKay, W. A., Murphy, J. T., & Wong, Y. C. (1978). Spatial organization of precentral cortex in awake primates. II. Motor outputs. *Journal of Neurophysiology*, *41*(5), 1120–31. <http://doi.org/10.1152/jn.1978.41.5.1120>
- Lawrence, D. G., & Kuypers, H. G. J. M. (1968a). The functional organization of the motor system in the monkey I. The effects of bilateral pyramidal lesions. *Brain*, *91*, 1–14.
- Lawrence, D. G., & Kuypers, H. G. J. M. (1968b). The functional organization of the motor system in the monkey II. The effects of lesions of the descending brain-stem pathways. *Brain*, *91*(1), 15–36. <http://doi.org/10.1093/brain/91.1.15>
- Lemon, R. N., Mantel, G. W., & Muir, R. B. (1986). Corticospinal facilitation of hand muscles during voluntary movement in the conscious monkey. *The Journal of Physiology*, *381*(1), 497–527. <http://doi.org/10.1113/jphysiol.1986.sp016341>
- Mckiernan, B. J., Marcario, J. K., Karrer, J. H., Cheney, P. D., & Kar, J. H. (1998). *Corticomotoneuronal Postspike Effects in Shoulder, Elbow, Wrist, Digit, and Intrinsic Hand Muscles During a Reach and Prehension Task*. Retrieved from

- Mollazadeh, M., Aggarwal, V., Thakor, N. V., & Schieber, M. H. (2014). Principal components of hand kinematics and neurophysiological signals in motor cortex during reach to grasp movements. *Journal of Neurophysiology*. <http://doi.org/10.1152/jn.00481.2013>
- Moran, D. W., & Schwartz, A. B. (1999). Motor Cortical Representation of Speed and Direction During Reaching. *Journal of Neurophysiology*, *82*(5), 2676–2692. <http://doi.org/10.1152/jn.1999.82.5.2676>
- Morrow, M. M., Jordan, L. R., & Miller, L. E. (2007). Direct Comparison of the Task-Dependent Discharge of M1 in Hand Space and Muscle Space. *J Neurophysiol*, *97*, 1786–1798. <http://doi.org/10.1152/jn.00150.2006>
- Napier, J. R. (1956). The prehensile movements of the human hand. *The Journal of Bone and Joint Surgery. British Volume*, *38-B*(4), 902–913. <http://doi.org/10.1016/B978-1-4160-4389-8.50161-8>
- Omrani, M., Kaufman, M. T., Hatsopoulos, N. G., & Cheney, P. D. (2017). Perspectives on classical controversies about the motor cortex. *Journal of Neurophysiology*, *118*(3), 1828–1848. <http://doi.org/10.1152/jn.00795.2016>
- Overduin, S. A., d'Avella, A., Carmena, J. M., & Bizzi, E. (2012). Microstimulation Activates a Handful of Muscle Synergies. *Neuron*, *76*(6), 1071–1077. <http://doi.org/10.1016/J.NEURON.2012.10.018>
- Overduin, S. A., d'Avella, A., Roh, J., & Bizzi, E. (2008). Modulation of muscle synergy recruitment in primate grasping. *The Journal of Neuroscience : The Official Journal of the Society for Neuroscience*, *28*(4), 880–92. <http://doi.org/10.1523/JNEUROSCI.2869-07.2008>
- Overduin, S. A., d'Avella, A., Roh, J., Carmena, J. M., & Bizzi, E. (2015). Representation of Muscle Synergies in the Primate Brain. *The Journal of Neuroscience : The Official Journal of the Society for Neuroscience*, *35*(37), 12615–24. <http://doi.org/10.1523/JNEUROSCI.4302-14.2015>
- Pack, C. C., & Bensmaia, S. J. (2015). Seeing and Feeling Motion: Canonical Computations in Vision and Touch. *PLoS Biology*. <http://doi.org/10.1371/journal.pbio.1002271>
- Paninski, L., Fellows, M. R., Hatsopoulos, N. G., & Donoghue, J. P. (2004). Spatiotemporal Tuning of Motor Cortical Neurons for Hand Position and Velocity. *J Neurophys*, *91*, 515–532. <http://doi.org/10.1152/jn.00587.2002>
- Park, M. C., Belhaj-Saf, A., Gordon, M., & Cheney, P. D. (2001). Consistent Features in the Forelimb Representation of Primary Motor Cortex in Rhesus Macaques. *J Neurosci*, *21*(8), 2784–2792. Retrieved from <http://www.jneurosci.org/content/jneuro/21/8/2784.full.pdf>
- Penfield, W., & Boldrey, E. (1937). Somatic motor and sensory representation in the cerebral

- cortex of man as studied by electrical stimulation. *Brain*, 60, 389–443.
- Pons, T. P., Garraghty, P. E., Cusick, C. G., & Kaas, J. H. (1985). The somatotopic organization of area 2 in macaque monkeys. *The Journal of Comparative Neurology*, 241(4), 445–466. <http://doi.org/10.1002/cne.902410405>
- Rathelot, J.-A., & Strick, P. L. (2009). Subdivisions of primary motor cortex based on corticomotoneuronal cells. *Proceedings of the National Academy of Sciences of the United States of America*, 106(3), 918–23. <http://doi.org/10.1073/pnas.0808362106>
- Saleh, M., Takahashi, K., Amit, Y., & Hatsopoulos, N. G. (2010). Encoding of coordinated grasp trajectories in primary motor cortex. *The Journal of Neuroscience : The Official Journal of the Society for Neuroscience*, 30(50), 17079–90. <http://doi.org/10.1523/JNEUROSCI.2558-10.2010>
- Saleh, M., Takahashi, K., & Hatsopoulos, N. G. (2012). Encoding of coordinated reach and grasp trajectories in primary motor cortex. *The Journal of Neuroscience : The Official Journal of the Society for Neuroscience*, 32(4), 1220–32. <http://doi.org/10.1523/JNEUROSCI.2438-11.2012>
- Santello, M., Flanders, M., & Soechting, J. F. (1998). Postural hand synergies for tool use. *The Journal of Neuroscience : The Official Journal of the Society for Neuroscience*, 18(23), 10105–15. Retrieved from <http://www.ncbi.nlm.nih.gov/pubmed/9822764>
- Schieber, M. H., & Hibbard, L. S. (1993). How somatotopic is the motor cortex hand area? *Science (New York, N.Y.)*, 261(5120), 489–92. <http://doi.org/10.1126/SCIENCE.8332915>
- Sergio, L. E., Hamel-Pâquet, C., & Kalaska, J. F. (2005). Motor Cortex Neural Correlates of Output Kinematics and Kinetics During Isometric-Force and Arm-Reaching Tasks. *Journal of Neurophysiology*, 94(4), 2353–2378. <http://doi.org/10.1152/jn.00989.2004>
- Sherrington, C. S. (1910). Flexion-reflex of the limb, crossed extension-reflex, and reflex stepping and standing. *The Journal of Physiology*, 40(1–2), 28–121. Retrieved from <http://www.ncbi.nlm.nih.gov/pubmed/16993027>
- Smith, A. M., Hepp-Reymond, M.-C., & Wyss, U. R. (1975). Relation of activity in precentral cortical neurons to force and rate of force change during isometric contractions of finger muscles. *Experimental Brain Research*, 23(3), 315–332. <http://doi.org/10.1007/BF00239743>
- Tresch, M. C., & Jarc, A. (2009). The case for and against muscle synergies. *Current Opinion in Neurobiology*, 19(6), 601–607. <http://doi.org/10.1016/J.CONB.2009.09.002>
- Umiltà, M. A., Brochier, T., Spinks, R. L., & Lemon, R. N. (2007). Simultaneous Recording of Macaque Premotor and Primary Motor Cortex Neuronal Populations Reveals Different Functional Contributions to Visuomotor Grasp. *J Neurophysiol*, 98, 488–501. <http://doi.org/10.1152/jn.01094.2006>

Ungerleider, L. G., & Haxby, J. V. (1994). 'What' and 'where' in the human brain. *Current Opinion in Neurobiology*, 4(2), 157–165. [http://doi.org/10.1016/0959-4388\(94\)90066-3](http://doi.org/10.1016/0959-4388(94)90066-3)

Wang, W., Chan, S. S., Heldman, D. A., & Moran, D. W. (2007). Motor Cortical Representation of Position and Velocity During Reaching. *J Neuro-Physiol*, 97, 4258–4270. <http://doi.org/10.1152/jn.01180.2006>

Weiss, E. J., & Flanders, M. (2004). Muscular and postural synergies of the human hand. *Journal of Neurophysiology*, 92(1), 523–35. <http://doi.org/10.1152/jn.01265.2003>

## **CHAPTER 3:**

### **The structure of hand shaping behavior and its population-level neuronal representation**

#### **Introduction**

Given the surface-level complexity of the hand and its neural representation, we sought to answer the question of whether or not we could find structure in that complexity. Indeed, the number of objects we have monkeys grasp, and consequently the number of grasps they perform, span a gamut of hand shaping behaviors not frequently seen before. As such, simple structure in grasping behavior that has previously been reported may elude the hand in the broader contexts of hand movements that we study here. In particular, we analyze the data to ascertain 1) the degree to which different hand shapes and patterns of neural activity manifest for different objects, 2) the time course over which hand shapes and neural signatures thereof adopt object-specific states, and 3) the complexity—i.e., underlying dimensionality—governing both hand shape and the neural representation thereof. Overall, we find that hand shaping behavior is indeed not as simple as has been previously reported—i.e., time-varying hand kinematics do not merely span a two-dimensional continuum. However, the time evolution of hand shaping and its neural representation mirrors that previously reported. Moreover, the distinctness of grasps on an object-by-object basis reveals that despite their complexity, the kinematics of the hand and the neural representation thereof are indeed structured in a principled manner.

#### **Data are complex yet structured**

To begin to visualize structure in hand-shaping kinematics, we analyze the time-varying angles of the joints of the hand during grasps of different objects (Figure 3-1A-B). Visualizing grasping behavior on a reduced-dimensional continuum, in this case the angles of three particular joints, reveals readily-discernable separation between hand shapes adopted for some objects.

Moreover, this separation among objects can be observed as early as maximum aperture—in other words, well before object contact is made, the shape of the hand has begun to conform to an object-specific state. Nonetheless, we note that some objects tend to “cluster” together on this low-dimensional continuum, which will prompt the use of more principled methods below to identify further object-specific structure in the kinematics.

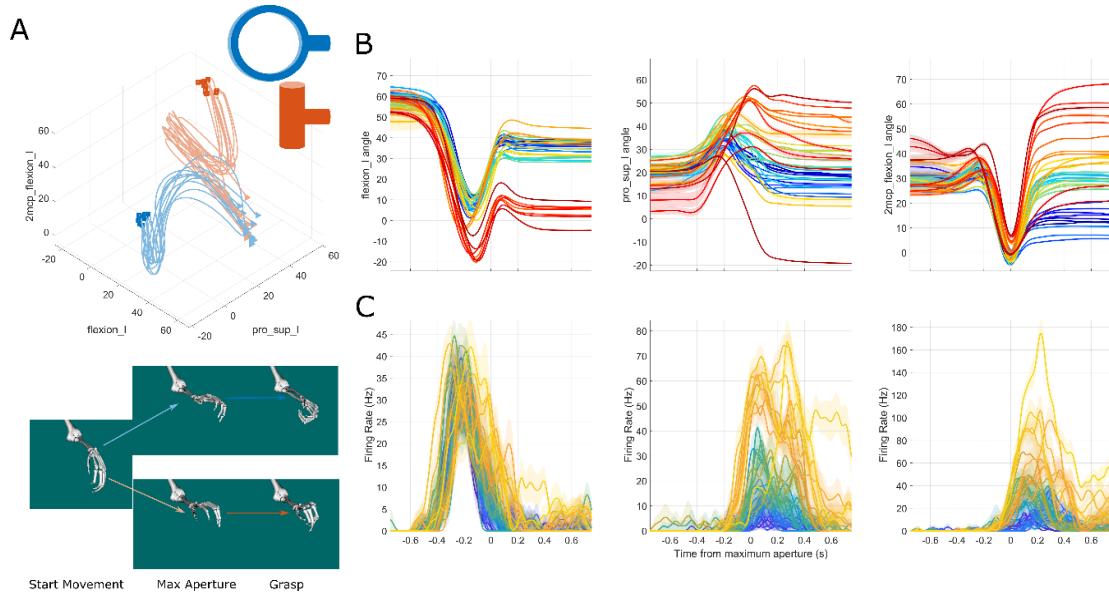


**Figure 3-1.** Different objects give rise to a variety of different kinematics and neural activity. **(A)** A phase plot of three joint angles (flexion\_l being wrist flexion angle, pro\_sup\_l being wrist supination angle, and 2mcp\_flexion\_l being second metacarpal flexion angle) during one monkey’s grasp of two different objects. Each trace represents kinematics during a single grasp trial. Faded triangles (“play” symbols) indicate joint angles 750ms prior to maximum aperture, well before movement began. Dark squares (“stop” symbols) indicate joint angles 750ms after maximum aperture, well after object contact where the hand adopted its final posture. Shown below the phase plot is a series of still frames of the skeletal model of the hand for one presentation of each object, illustrating the progression of the hand’s conformation from a common “start” state to a fully differentiated “grasp” state. **(B)** Separate plots of the same joints against time, this time for *all* objects. Each colored trace gives the mean kinematics for a grasp of a particular object. Shaded regions indicate  $\pm 1$  S.E.M. at each sample time. **(C)** Perievent time histograms (PETHs) for three select M1 and proprioceptive somatosensory cortical neurons for *all* objects. PETHs are constructed by aligning each trial to the time of maximum aperture, calculating the average spike count in each 10ms bin on a per-trial basis, then smoothing the average trace with a centered Gaussian kernel with 35ms width parameter. Each colored trace gives the mean firing rate during grasping of a particular object. Shaded regions indicate  $\pm 1$  S.E.M. at each sample time.

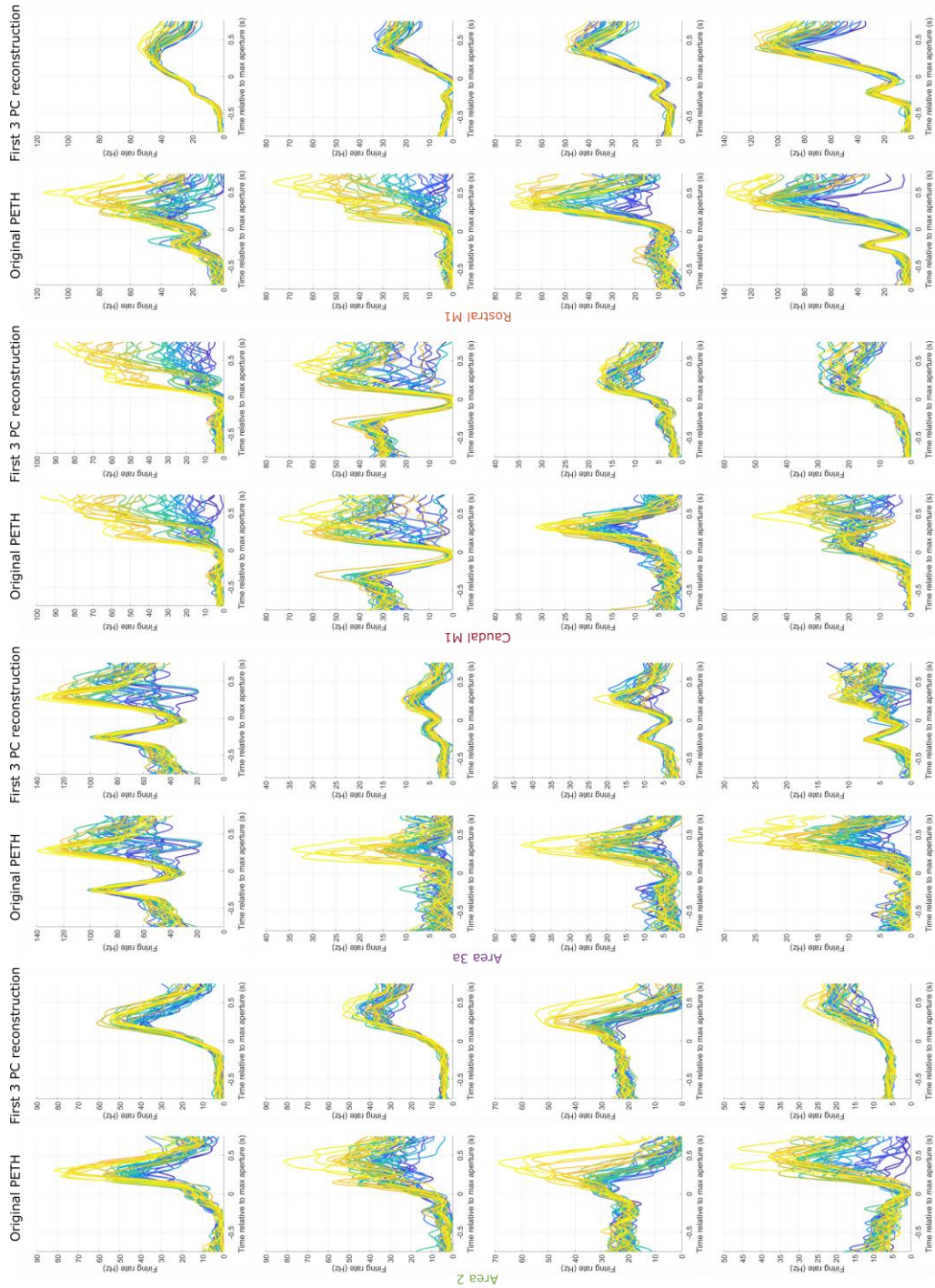


**Figure 3-2.** Sample PETHs and PC reconstructions from neurons across all areas of cortex from which we record. These show the temporal evolution of firing rates with respect to maximum aperture and the separation of firing rate patterns as a function of object identity—and presumably as a function of the corresponding grasp conformation. All PETHs are trial-averaged firing rates of neurons from Monkey 4 in response to different objects, sorted on a neuron-by-neuron basis, computed using similar trial averaging and smoothing procedures as those PETHs in Figure 3-1C. Note that the first 3 PC reconstructions preserve object-dependent variance for a few select neurons, but often fail to capture this structure for a large number of them.

The corresponding time-varying firing rates in sensory and primary motor cortices reveals a similar separation of objects at roughly the time of maximum hand aperture (Figure 3-1C) (Figure 3-2). A number of themes emerge from the peri-event time histograms (PETHs) of these sensorimotor cortical neurons recorded across different monkeys: 1) neuronal responses often show preferentially high firing rates for one set of objects over other sets of objects; 2) response latencies with respect to a kinematic event such as maximum aperture can also vary on an object-by-object basis; and 3) neurons frequently have activity patterns whereby increased or decreased spiking activity relative to baseline is sustained for several hundreds of milliseconds following the initial ramp in firing rate. Collectively, these suggest that these neurons are indeed responding during the task in a manner that varies with different hand shaping trajectories.

### **Control of hand posture is higher-dimensional than previously thought**

Hand postures adopted during grasp are typified by high correlations among joints. Indeed, especially among the fingers, several pairs of joints in our kinematic data are highly correlated (Figure 3-3). To extract potentially meaningful canonical “Eigen-grasps” from these data—c.f. other work (Turk & Pentland, 1991) performing similar dimensionality reduction of face data to obtain “Eigen-faces”—we use principal component analysis (PCA) to find which combinations of joint movements best explain the total variance of whole-hand movements.

When using PCA, we find that roughly 6-9 dimensions are, on average, required to explain 90% of the variance among hand postures adopted during grasp (Figure 3-4A), with 5-8 dimensions appearing to be sufficient to reach this threshold on a monkey-by-monkey basis (Figure 3-5A). This figure is on the same order of magnitude as has previously been reported for comparably diverse hand movements (Ingram, Körding, Howard, & Wolpert, 2008; Marco Santello, Flanders, & Soechting, 1998, 2002; Thakur, Bastian, & Hsiao, 2008). Note that this

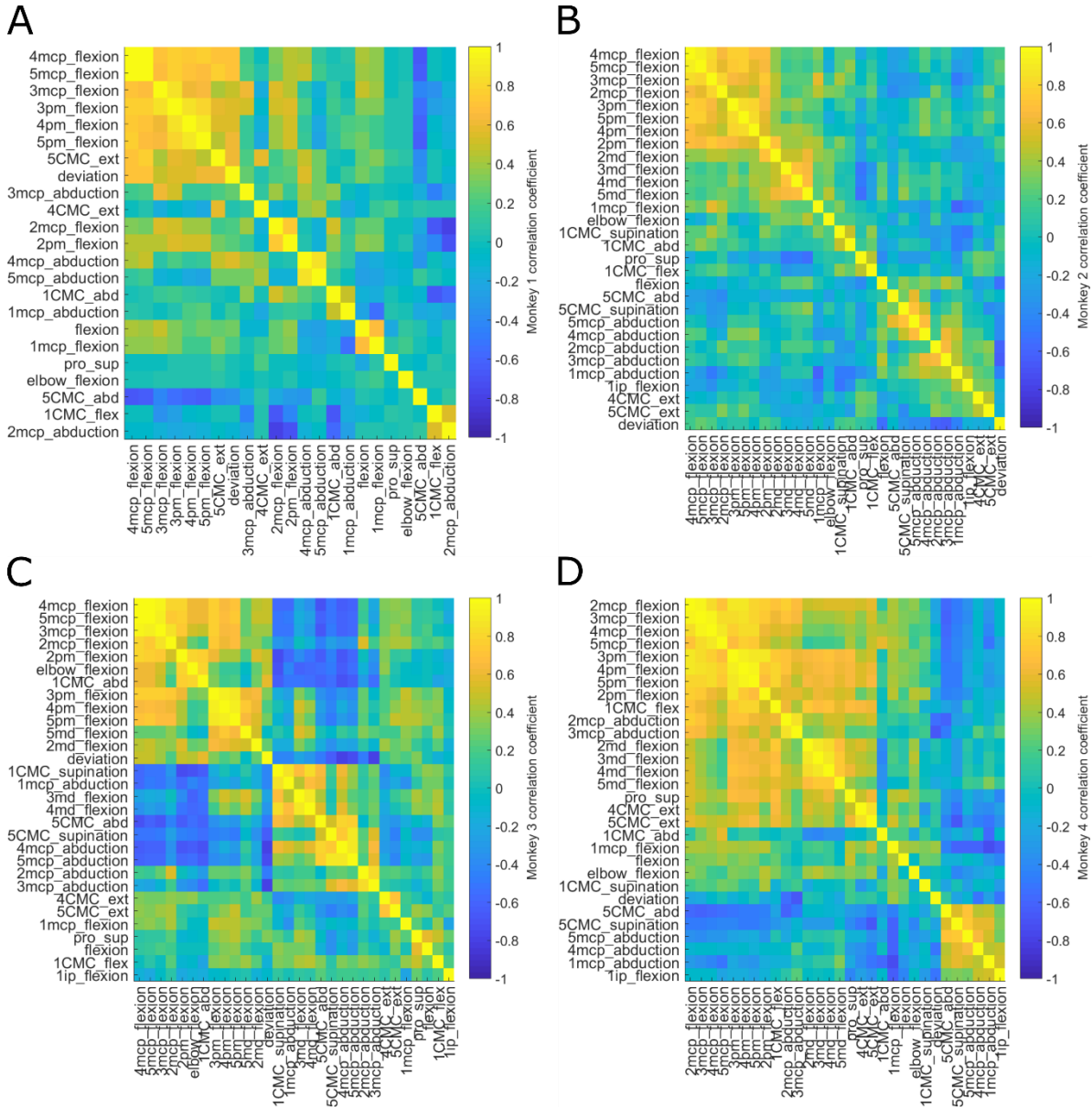


**Figure 3-3.** Kinematic correlation matrices. The absolute values of correlations among joint angular coordinates for (A) Monkey 1, (B) Monkey 2, (C) Monkey 3, and (D) Monkey 4. Correlations are assessed at zero lag, and the order of joints is determined for each monkey with hierarchical clustering so that large groups of highly correlated joints can better be visualized. Joint angular coordinate key: flexion—flexion or extension (“pitch”) of the wrist joint | deviation—ulnar or radial deviation (“yaw”) of the wrist joint | pro\_sup—pronation or supination (“roll”) of the wrist joint | elbow—elbow joint | 1–5—digits 1 through 5, respectively | CMC—carpometacarpal joint | mcp—metacarpophalangeal joint | ip—interphalangeal joint (digit 1 only) | pm—proximal interphalangeal joint | md—distal interphalangeal joint | \_flexion, \_flex, \_ext—flexion or extension (“pitch”) of the joint preceding the underscore | \_abd, \_abduction—abduction or adduction (“yaw”) of the joint preceding the underscore | \_supination—pronation or supination (“roll”) of the joint preceding the underscore.

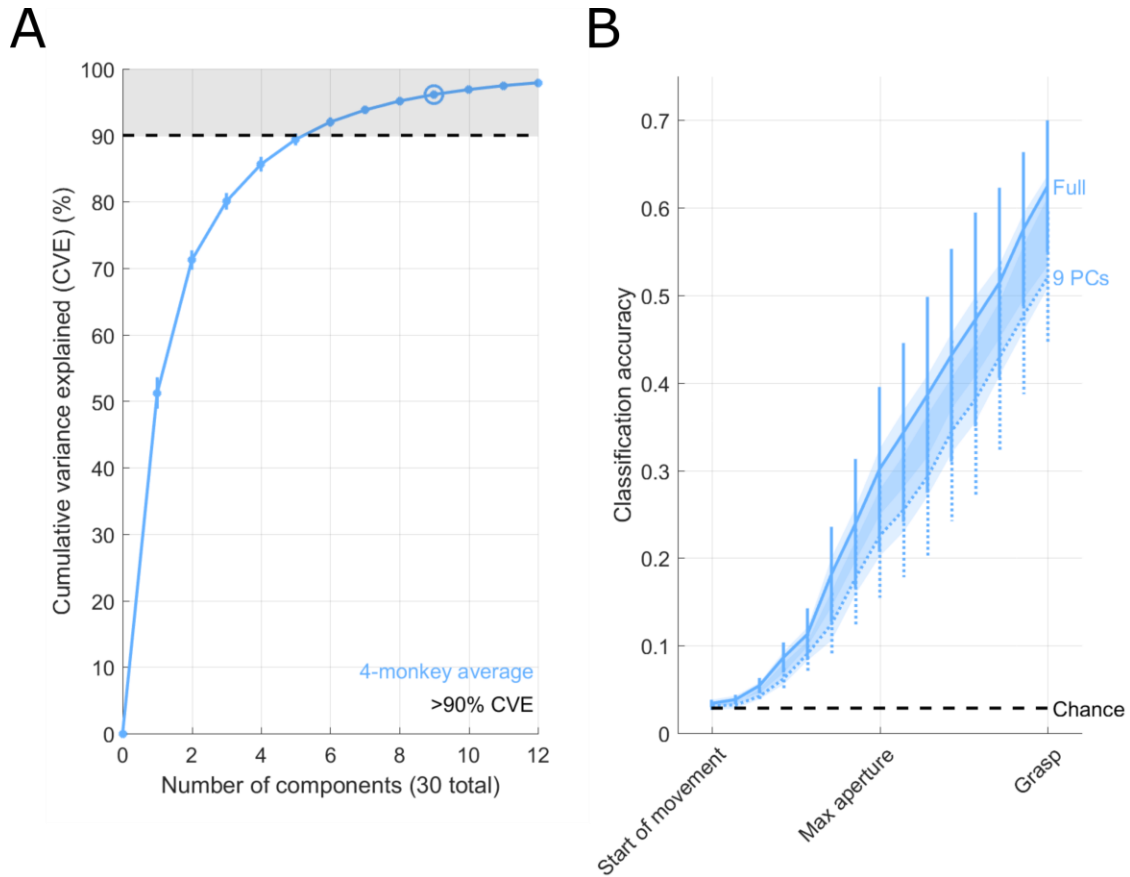


**Figure 3-4.** Analysis of kinematic structure and dimensionality. **(A)** Cumulative scree plot from principal component analysis (PCA) of joint postures, averaged across all four monkeys. The mean CVE first crosses the 90% boundary at 6 principal components (PCs), but more conservatively, the circled point indicates the minimum number of PCs (9) for which the average CVE was *significantly* greater than 90% (one-tailed one-sample t-test,  $T(3) = 7.023$ ,  $p = 2.965e-03$ , significance assessed across all 30 points on the abscissa with the Holm-Bonferroni method of multiple comparisons,  $\text{FWER} < 0.05$ ). The cumulative scree plot is truncated at 12 components but a total of 30 components are present. Vertical lines at each point indicate  $\pm 1$  S.E.M. across monkeys. **(B)** Cross-validated (leave-one-out) accuracy of object classification (multi-class linear discriminant analysis, i.e., LDA) based on joint angular kinematics at different task epochs, averaged across monkeys. Vertical lines at each point indicate  $\pm 1$  S.E.M. across monkeys. Dotted blue lines indicate classifiers using only the first 9 PCs, compared with solid blue lines that show results of classifiers using the full dimensionality of hand kinematics. The shaded regions indicate the mean difference  $\pm 1$  S.E.M. between the two classifiers. As this difference arises from paired data (each monkey has one classifier of each type), its own standard error is indicated with the darkness of the shaded region. The darkest region indicates the mean difference minus 1 S.E.M., and the lightest region indicates +1 S.E.M. When pooling across epochs, the cross-validated full kinematic classifier more accurately determines the object presented from out-of-sample kinematics than the one using only 9 PCs (two-tailed paired-samples t-test,  $T(59) = 9.136$ ,  $p = 6.773e-13$ ).

previous work will often report even lower-dimensional structure by virtue of a different benchmark—e.g., 80% of the variance explained, or seeking an “elbow” in the PCA scree plot.

Moreover, dimensions found using PCA correspond to “Eigen-grasps” that bear qualitative similarity to those found in the aforementioned work (Figure 3-6). The naïve assumption underlying inferences of the dimensionality of the hand using such a 90% cumulative variance criterion is that the majority of the variance in hand movements constitutes motor “signal” under volitional control, with the remaining 10% of variance of hand movements reflecting motor noise not under volitional control.

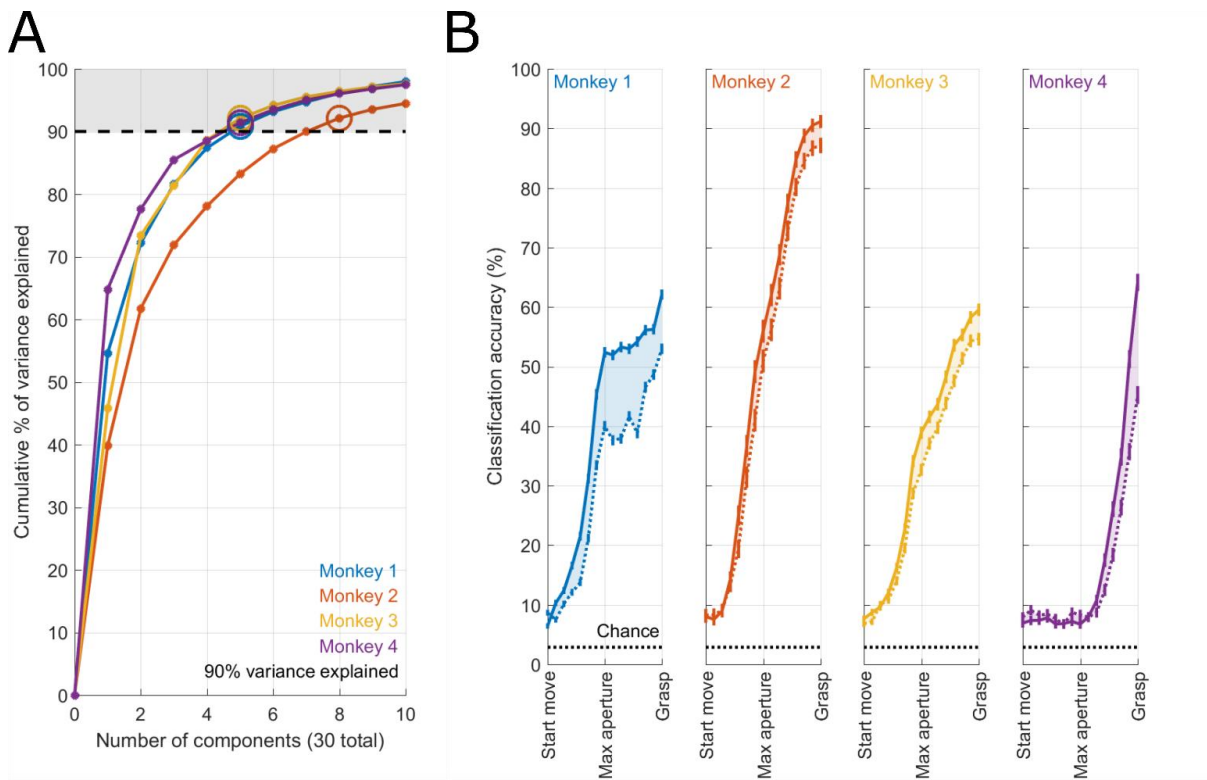


**Figure 3-5.** Analysis of kinematic structure and dimensionality by monkey. **(A)** Cumulative scree plots after applying principal component analysis (PCA) to the joint angular kinematics of each monkey. These scree plots were averaged across monkeys to obtain the plot in Figure 3A. Circles indicate the number of components at which the cumulative scree plot for each monkey exceeds 90% of kinematic variance explained. These traces are averaged to obtain the trace in Figure 3-4A **(B)** Accuracy of kinematic object classification (as in Figure 3B) for each monkey at different task epochs. Again, these accuracies were averaged across monkeys to obtain the mean accuracy curve in Figure 3B. Solid lines indicate full-kinematic accuracy; dashed lines, the accuracy of classifiers using only the first few dimensions to explain at least 90% of kinematic variance—the same number of components as the corresponding circle in (A). Vertical lines at each epoch indicate  $\pm 1$  S.E.M. of classification accuracy. These traces—one from each monkey, each given equal weight—are averaged to obtain the averaged time course of classification accuracy in Figure 3-4B.

We note that for standardized kinematic data, PCA reveals that more dimensions, 10-17, are required on average to explain 90% of the variance (Figure 3-7), which is considerably larger than the aforementioned consensus. Although the fact that PCA is not scale-invariant is well understood, this near-doubling of the number of dimensions suggests that previous attempts to quantify the dimensionality of hand movements may very well have underestimated it. Indeed, traditional PCA methods may merely reflect a vast disparity in the ranges of motion among individual joints of the hand rather than the limited repertoire of co-recruitments of those joints.

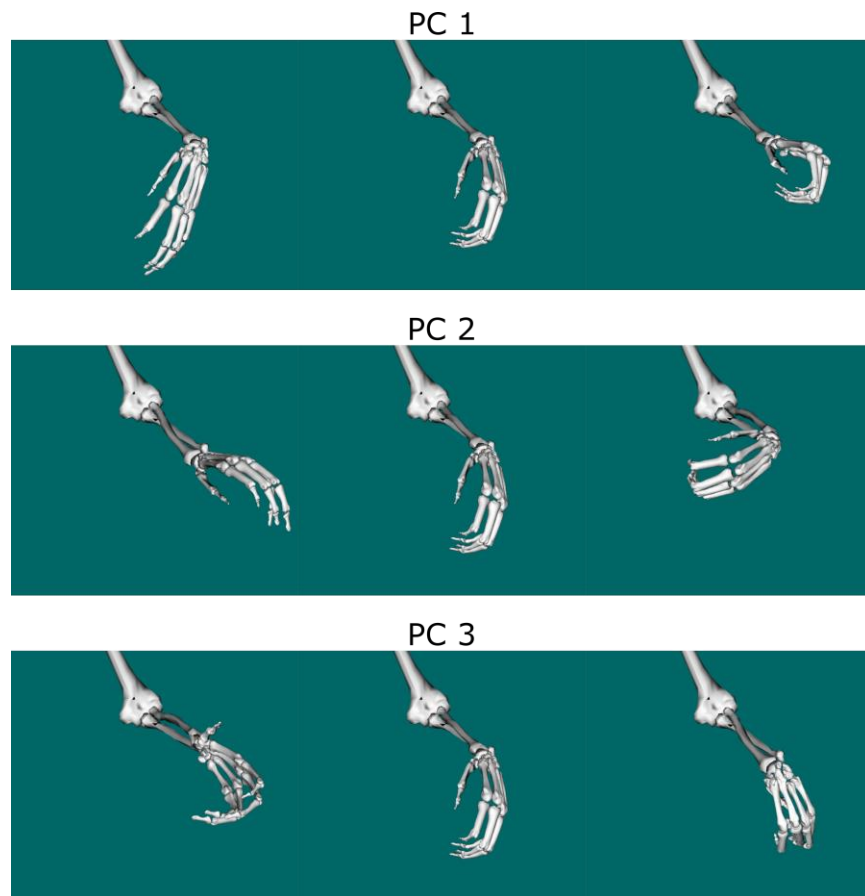


**Figure 3-6.** Visualization of “Eigen-grasps” obtained from principal component analysis (PCA) applied to the joint angular data of Monkey 2. Each row depicts a different Eigen-grasp, with a progression from left to right through that Eigen-grasp’s range of correlated joint angular movements. Although qualitative interpretations of these “Eigen-grasps” could be inferred, we find that such PCs that merely explain the largest fraction of variance fail to capture reliable yet subtle inter-object differences in grasp postures.

We then use patterns of movement spanning multiple joints to obtain a principled estimate of just how separated object-specific grasps are from one another. In particular, we use multi-class linear discriminant analysis (LDA) to classify objects on the basis of the hand shapes adopted

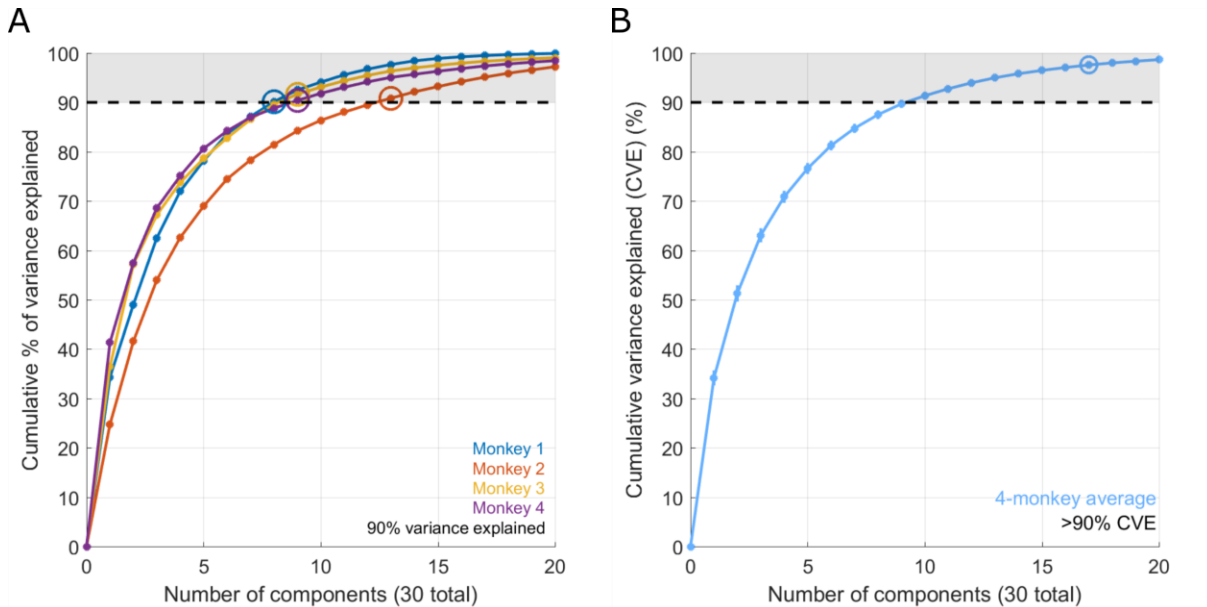


**Figure 3-7.** Cumulative scree plots for PCA run on standardized kinematic data (A) on a monkey-by-monkey basis and (B) averaged across monkeys. Apparent dimensionality increases when assessing kinematic dimensionality using PCA on standardized data, with individual-monkey dimensionalities spanning 8-13 dimensions (A) and monkey-averaged dimensionalities spanning 10-17 components (B). Significance of the second point in (B) is assessed as in Figure 3-4A.

during grasp. Hand postures can be used to correctly identify one of 35 objects with over 60% peak accuracy on average (Figure 3-4B), and with up to 90% accuracy in one monkey (Figure 3-5B). Moreover, classification accuracy ramps gradually to this peak accuracy throughout the trial. Taken together, these results reiterate that the hand gradually conforms to an object-specific posture well prior to contact. However, time-varying classification accuracy using only the first 9 kinematic PCs is significantly lower—roughly 50% peak accuracy on average (Figure 3-4B)—than time-varying classification accuracy using the full kinematics. This seems to indicate that volitional control over the shape of the hand spans more dimensions than naïve interpretations of

PCA and its resultant “Eigen-grasps” would suggest. In particular, the 10% of hand movement variance not explained by the first 9 PCs does not merely reflect motor noise.

### **Neural responses occupy a high-dimensional space**

The correlations among neurons’ firing rates are smaller (Figure 3-8) than are those among different joint angles in the kinematics (c.f. Figure 3-3). Moreover, when using PCA, we find that roughly 50% of all dimensions from which we record in any given sensorimotor area are needed to explain 90% of the variance in those neural responses (Figure 3-9A), compared with as little as 20% of the number of kinematic dimensions needed to reach a similar benchmark. Standardized neural data are even higher-dimensional, with roughly 80% of neural dimensions required to explain 90% of total variance (Figure 3-10). These suggest that neural responses during grasp appear to be even higher-dimensional than grasp kinematics, rather than being constrained to representations of kinematics along just a few axes.

Indeed, this high-dimensional structure of the neural response is seen, for example, in the limited ability of the first few PCs of neural activity to reconstruct PETHs (Figure 3-2). When investigating PETHs filtered by such a compressing auto-encoder, important features distinguishing one object from another in several neurons’ PETHs are not so readily discernable, corroborating other results (Figure 3-9) showing the necessity of including high-order PCs to explain 90% of the neural variance.

To quantify the structure in these high-dimensional population responses, we classify object types based on the neuronal activity recorded from neurons pooled across recording sessions. Neural object classifiers computed for each area reach peak accuracies over 50% (Figure 3-9B), comparable to previously-reported classification accuracy using only M1 data prior to

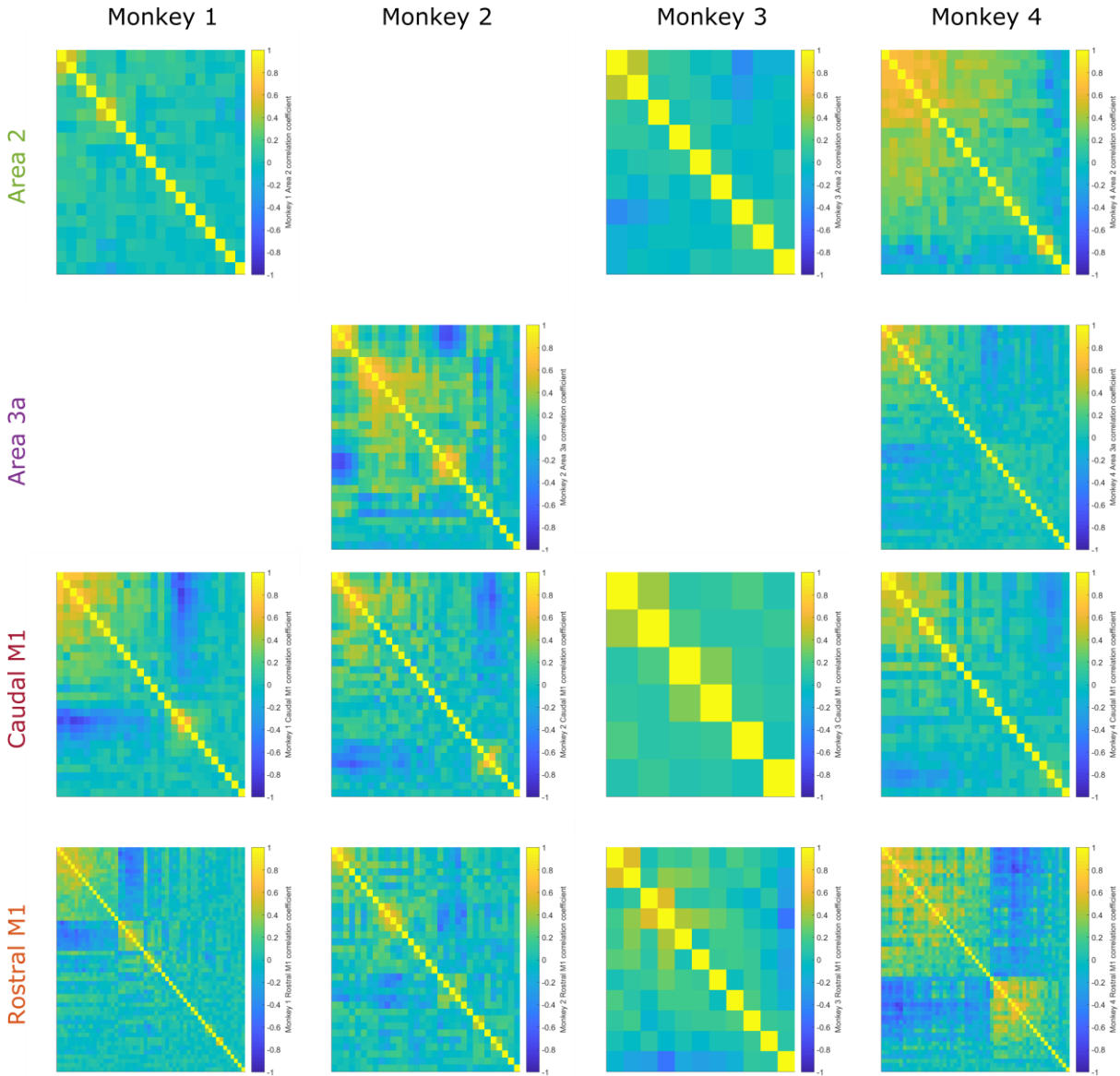


**Figure 3-8.** Neural correlation matrix heatmaps. Rows of heatmaps indicate the cortical area from which neurons were recorded. Columns of heatmaps indicate the monkey from which each correlation matrix was obtained. Correlation matrices are signal correlation matrices; in other words, firing rates are averaged across trials for each object after aligning to object contact, and the correlations of these firing rates extending from 500ms to 10ms prior to contact are represented as the color in each heatmap. Trial averaging was done to permit pooling of neurons across sessions. Only heatmaps with at least 5 neurons are shown.

attempts to cluster objects into similar “grasp types” (Schaffelhofer, Agudelo-Toro, & Scherberger, 2015). Note that the classifiers we use simply compute mean rate over a 500ms bin, a large bin size that we note to be necessary to reach this level of classification accuracy. Neural

classification gradually increases in accuracy throughout the trial, indicating that the neural representation contains object-specific signals prior to object contact, just as the shape of the hand differentiates on an object-by-object basis prior to object contact. Moreover, when extrapolating beyond our sample size, neural classifiers can reach accuracies comparable to kinematic classifiers with as few as 177 neurons (Figure 3-9C). Therefore, neural population responses are high-dimensional and strongly object-dependent, paralleling the object-specific structure of the hand kinematics.

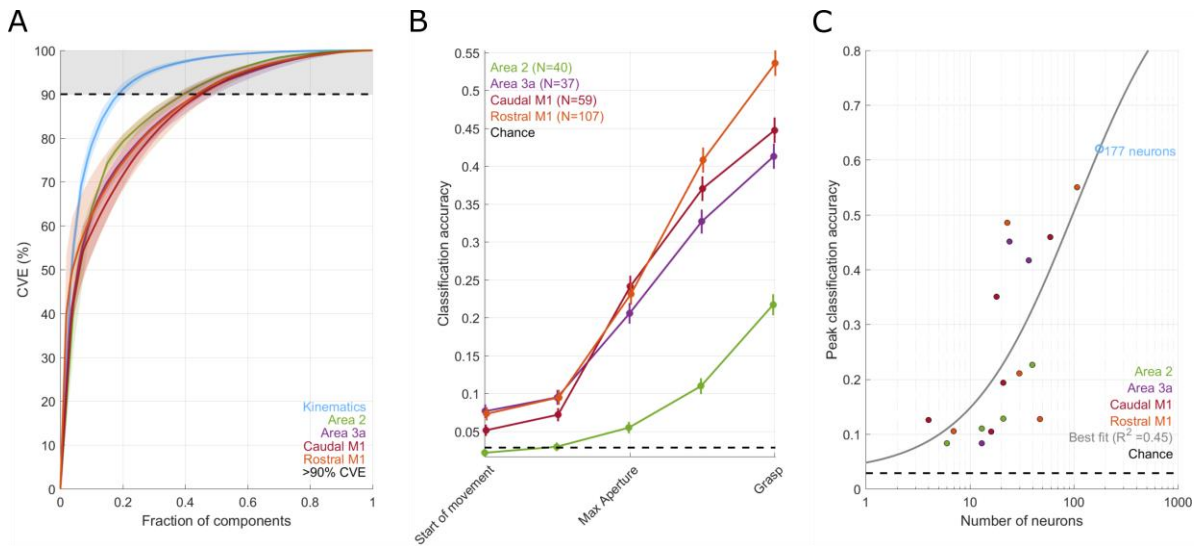


**Figure 3-9.** Analysis of neural structure and dimensionality. **(A)** Cumulative scree plot from PCA of joint postures and neural data, averaged across all four monkeys and plotted in terms of the fraction of the total number of components recorded from any given monkey. We plot in terms of fraction of number of components because population sizes recorded from each area in each monkey vary to give rise to different raw apparent neural dimensionalities that nonetheless align when instead plotted in this manner. We see that only 20% of the kinematic dimensionality is needed for the mean CVE to reach 90%, whereas for the cortical data that fraction jumps up to 40%. Each trace represents the interpolated cumulative scree plot as a function of the fraction of total number of components, averaged across monkeys. Shaded regions surrounding each trace give  $\pm 1$  S.E.M. for each point of each interpolated trace. **(B)** Neural classification accuracy when aligned to different epochs of grasp. Spike counts are taken over a 500ms causal window, and neurons from different sessions recorded from different monkeys are pooled to obtain these classification accuracies. We note that peak cross-validated accuracy reaches roughly 50% in population sizes on the order of 100 neurons. Vertical bars give  $\pm 1$  S.E.M. **(C)** A population of roughly 200 proprioceptive or motor cortical neurons is required to reach mean peak classification accuracy (roughly 60%) of kinematic classifiers, as shown in Figure 3-4B. Single-monkey and pooled-monkey samples from each area are shown as each point on the plot. Logistic regression is fit to these data pooled across cortical areas.

## Discussion & Conclusions

We note that volitional control of the hand spans a higher-dimensional continuum than one would expect at first blush. Indeed, previous results seeking a simplified continuum of hand shaping behavior (M Santello, Flanders, & Soechting, 1998) come to a similar conclusion: Namely, that although a variance-explained criterion obtains an estimate of low-dimensional structure in hand shaping behavior, looking at the dimensions important for discerning different grasps adopted for different objects reveals higher-dimensional structure. We find that the apparent dimensionality of hand kinematics is also extremely sensitive to the ranges of motion of the constituent joints, thereby constituting another mechanism by which previous efforts to quantify the dimensionality of hand shaping may have been underestimated.

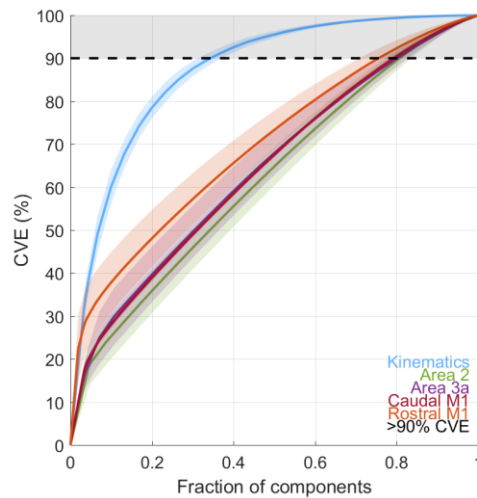


**Figure 3-10.** Standardized cumulative scree plots averaged across 4 monkeys as a function of the fraction of the number of components needed to reach variance explained thresholds. Standardization acts to make neural responses appear even higher-dimensional, with roughly 80% of dimensions being required to explain 90% of the firing rate data.

We also note that the neural signatures of different grasps are also extremely varied. In fact, the apparent dimensionality of population neural data during hand shaping—estimated using a similar variance-explained criterion—exceeds that of the kinematics. This, combined with the

fact that low-variance components of hand shaping have a substantial effect on object classification, supports the notion that volitional control of the hand spans a higher-dimensional space than previously reported. Despite the high-dimensional space in which population neural activity resides, it contains readily-discernable information about object identity—information that we will probe on a neuron-by-neuron basis in the following chapter.

We conclude that the volitional control of hand kinematics is even more complex than it might seem at first, with subtle components of the kinematics being manipulated prior to object contact to give rise to object-specific hand shapes. Methodological concerns arise from prior investigations of the dimensionality of the control over grasp, all of which give rise to chronic underestimation of the dimensionality of hand control. Moreover, we note a variety of different neural responses to the adoption of different object-specific hand postures, which in turn betray a high-dimensional yet highly-informative representation of object-specific information.

## References

- Ingram, J. N., Körding, K. P., Howard, I. S., & Wolpert, D. M. (2008). The statistics of natural hand movements. *Experimental Brain Research*, 188(2), 223–236. <http://doi.org/10.1007/s00221-008-1355-3>
- Santello, M., Flanders, M., & Soechting, J. F. (1998). Postural hand synergies for tool use. *The Journal of Neuroscience : The Official Journal of the Society for Neuroscience*, 18(23), 10105–15. Retrieved from <http://www.ncbi.nlm.nih.gov/pubmed/9822764>
- Santello, M., Flanders, M., & Soechting, J. F. (1998). Postural Hand Synergies for Tool Use. *The Journal of Neuroscience*, 18(23), 10105–10115.
- Santello, M., Flanders, M., & Soechting, J. F. (2002). Patterns of Hand Motion during Grasping and the Influence of Sensory Guidance. *The Journal of Neuroscience*, 22(4), 1426–1435.
- Schaffelhofer, S., Agudelo-Toro, X. A., & Scherberger, X. H. (2015). Decoding a Wide Range of Hand Configurations from Macaque Motor, Premotor, and Parietal Cortices. *Journal of Neuroscience*, 35(3), 1068–1081. <http://doi.org/10.1523/JNEUROSCI.3594-14.2015>
- Thakur, P. H., Bastian, A. J., & Hsiao, S. S. (2008). Multidigit movement synergies of the human hand in an unconstrained haptic exploration task. *The Journal of Neuroscience : The Official Journal of the Society for Neuroscience*, 28(6), 1271–81. <http://doi.org/10.1523/JNEUROSCI.4512-07.2008>
- Turk, M., & Pentland, A. (1991). Eigenfaces for Recognition. *Journal of Cognitive Neuroscience*, 3(1), 71–86. <http://doi.org/10.1162/jocn.1991.3.1.71>

## **CHAPTER 4:**

### **The features of the hand represented in somatosensory and primary motor cortices**

#### **Introduction**

We have thus far found that grasps span a complex, high-dimensional space, as do their neuronal representations. However, we also note that both kinematics and neuronal representations are structured, as evidenced by distinct grasps adopted for different objects and their respective neural signatures. In this chapter, we seek to delve further into the nature of these cortical representations of grasp at the single-neuron level by determining the features of grasps that most consistently and strongly correlate with spiking activity.

In particular, our goal is to quantify the response fields (RFs), or the sets of features of grasp that give rise to spiking responses of proprioceptive cortical neurons. Moreover, we aim to compare and contrast their properties with those of tactile neurons in somatosensory cortex, the latter of which have received more experimental attention. Tactile somatosensory cortical neurons – i.e., neurons in Brodmann’s areas 3b, 1, and 2 with tactile RFs – are known for having RFs that are small, typically comprising only a fraction of a phalanx (Nelson, Sur, Felleman, & Kaas, 1980; M Sur, Merzenich, & Kaas, 1980). Moreover, the vast majority of tactile cells in somatosensory cortex exhibit strong response modulation to transient events such as contact onset and offset (Darian-Smith, Sugitani, Heywood, Karita, & Goodwin, 1982; Pei, Denchev, Hsiao, Craig, & Bensmaia, 2009; Mriganka Sur, Wall, & Kaas, 1984). Sustained responses to sustained skin indentations are weaker and generally accompanied by strong phasic responses during contact transients (onset and offset of contact).

At first pass, proprioceptive responses in somatosensory cortex differ from their tactile counterparts in two important ways. First, a sizeable proportion of proprioceptive cortical neurons

have larger RFs, comprising multiple joints of the arm and hand (Costanzo & Gardner, 1981). Second, a notable proportion of proprioceptive cortical neurons exhibit strictly slowly-adapting response properties. That is, neurons exhibit high-amplitude sustained responses to constant flexion or extension of a given joint; a subset even seeming to track posture with no apparent increased response during movement (Gardner & Costanzo, 1981).

However, these results were qualitative and the stimulation protocols—namely ramp-and-hold and low-frequency sinusoidal movements of isolated single joints or small groups of joints—were very simple relative to the full range of naturalistic hand movements. Our data thus afford us a unique opportunity to rigorously quantify kinematic response properties of hand proprioceptive neurons, including RF size and relative sensitivity to posture and movement. In addition, given the richness of the kinematics as detailed in Chapter 3, these measures are inferred from and thus extend to a larger space of hand kinematics than in previous studies.

Proprioception, in addition to being related to tactile sensation, is also tightly coupled with motor control. The strictly-proprioceptive Brodmann's area 3a sends monosynaptic projections onto neurons in M1 (Huerta & Pons, 1990). In addition, proprioceptive acuity seems most likely to be subserved by muscle spindles (Gandevia, Mccioskey, Burke, Mcc, & Oskey, 1992; Proske & Gandevia, 2012) that respond to length changes of muscles and receive gamma motor input themselves (Prochazka, 2011). Furthermore, proprioceptive—specifically, kinesthetic—acuity appears to be affected by whether or not tension in a relevant muscle is being actively and volitionally maintained (Gandevia et al., 1992). Indeed, the hand pre-shaping behavior studied thus far is volitional, thereby rendering it more directly similar to investigations of M1 response properties during hand shaping (e.g., Umiltà, Brochier, Spinks, & Lemon, 2007) than aforementioned work on proprioceptive cortical responses to passively-generated movements. We

therefore not only compare M1 and somatosensory cortical response properties during volitional hand shaping, we also do so during passive manipulation of the hand—to which M1 neurons are also known to respond (Hatsopoulos & Suminski, 2011)—to investigate the degree to which such response properties are dependent on whether hand kinematics are imposed or generated volitionally.

## **Results**

### **Neural encoding models predict firing rates**

To characterize a neuron's RF, we fit encoding models (Figure 4-1A) to predict each neuron's time-varying firing rates based on kinematic features on a trial-by-trial basis. Specifically, we fit cross-validated generalized linear models (GLMs) to reconstruct as faithfully as possible the spiking activity of each neuron from a linear combination of single-joint postures and movements. We additionally use LASSO regularization to minimize the number of spurious joint angular predictors of spiking activity. Model fits are assessed using a measure called pseudo- $R^2$ , an analogue to the standard coefficient of determination that uses model deviances defined using a Poisson noise model rather than residuals under a Gaussian noise model (see Appendix A: Methods). Example peri-event time histograms (PETHs) for a neuron constructed from both measured and modeled spiking activity for three different objects (Figure 4-1B) illustrate the quality of fit of these models. We find pseudo- $R^2$  values (Figure 4-1C) that are consistent with and often exceed the  $R^2$  values obtained for single-trial predictions of firing rates in proximal limb motor cortex (Table 4-1) (Aflalo & Graziano, 2007). The distribution of pseudo- $R^2$  values we obtain therefore suggests that features of hand kinematics are indeed encoded by these neurons at least as strongly as proximal limb kinematics are encoded by M1.

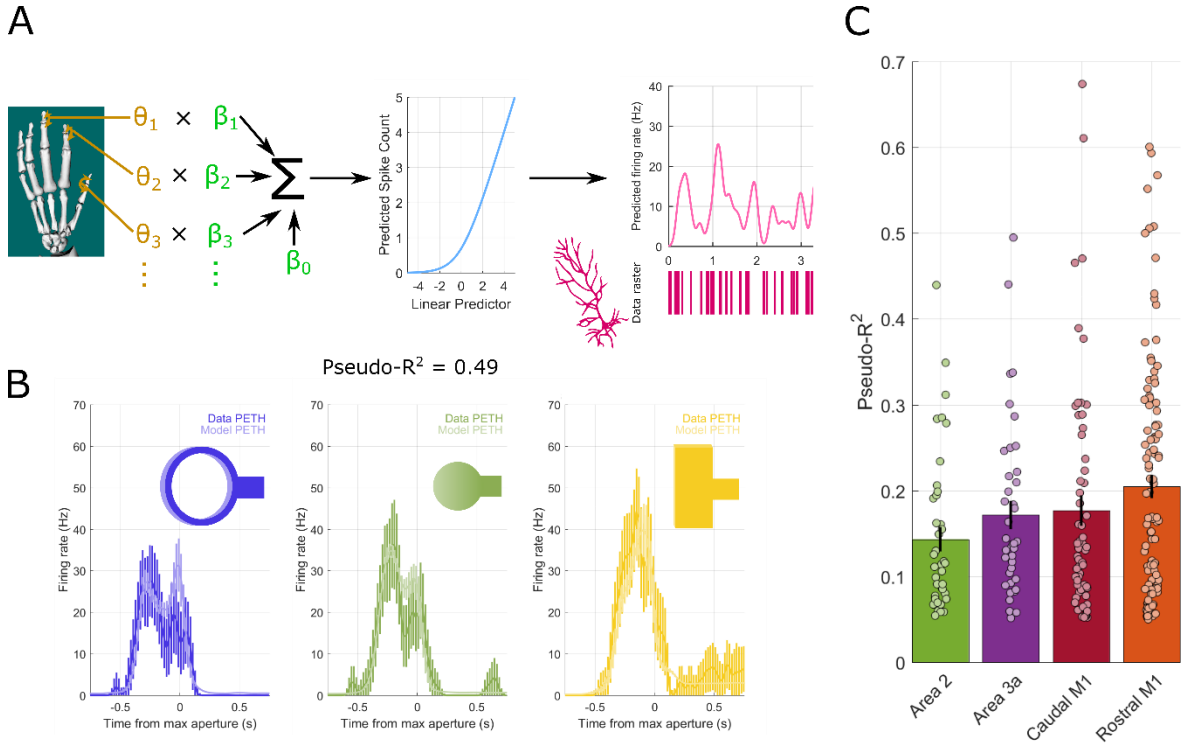


**Figure 4-1.** Generalized linear model (GLM) procedure and performance. **(A)** Flow chart depicting how GLM uses kinematics (left) to create a weighted linear sum that is passed through a soft-plus nonlinearity (middle) to estimate firing rates (right, top) such that they are maximally likely given measured patterns of spiking activity (right, bottom). **(B)** Measured (dark) and predicted (light) peri-event time histograms (PETHs) for three different objects aligned to maximum aperture for an example neuron from area 3a. The pseudo- $R^2$  of the GLM fit to this neuron is 0.49. Vertical bars at each point indicate  $\pm 1$  S.E.M. **(C)** Pseudo- $R^2$  values for each neuron with cross-validated pseudo- $R^2$  greater than or equal to 0.05. Neurons are pooled across sessions and across different monkeys. Bar heights correspond with the mean pseudo- $R^2$  among such neurons in each area. Each point represents the pseudo- $R^2$  of a different neuron. Error bars span  $\pm 1$  standard error of the mean pseudo- $R^2$  of each area. In area 2, the pseudo- $R^2$  values of 41 out of 50 total units (82.0%) are reported, with the remaining 9 units being omitted due to having pseudo- $R^2$  values lower than 0.05; in area 3a, we report 40 of 68 (58.8%); in caudal M1, 59 of 89 (66.3%); and in rostral M1, 107 of 147 (72.8%).

### Neurons encode coordinated combinations of joints spanning the entire hand

First, we find that individual proprioceptive neurons do not exhibit straightforward single-joint response fields (RFs). Instead, we find that neurons encode combinations of multiple joints. To quantify the number of joints tracked by each neuron, we count the number of joints needed to reach or exceed 90% of the squared norm of the multi-joint predictor weight vector (Figure 4-2A).

We find that, on average, roughly eight joints contribute to the spiking activity of each neuron (Figure 4-2B).

**Table 4-1.** Multiple two-sample, equal-variance T-tests for significant differences between goodness-of-fit metrics seen in our hand data versus data from a previous report in proximal limb motor cortical neurons (Aflalo & Graziano, 2007). These proximal limb cortical data were compared with our hand data due to the lack of trial-averaging of the firing rates prior to computing goodness-of-fit. Highlighted cells indicate significant differences (FWER < 0.05, Holm-Bonferroni method). Black squares indicate the lack of enough neurons from our hand dataset to make a comparison ( $N_{\text{hand}} < 5$  with pseudo- $R^2 > 0.05$ ). No mean pseudo- $R^2$  value from any area or monkey in our dataset was significantly smaller than the mean pseudo- $R^2$  seen in the previously reported M1 data to which it was compared. We assume comparability of pseudo- $R^2$  to the traditional coefficient of determination in this analysis. We also only analyze the set of pseudo- $R^2$  or  $R^2$  values in each dataset greater than or equal to 0.05, although this comprised the majority of our hand data (c.f. Figure 4-1) and similarly comprised roughly 65% of the previously reported M1 data.

	Monkey 1	Monkey 2	Monkey 3	Monkey 4
<b>Area 2</b>	p = 5.558 e-01 t(52) = 0.544 E( $\Delta R^2$ ) = 8.995 e-03 N <sub>hand</sub> = 13		p = 3.476 e-01 t(45) = 0.949 E( $\Delta R^2$ ) = 1.714 e-02 N <sub>hand</sub> = 6	p = 1.241 e-03 t(60) = 3.390 E( $\Delta R^2$ ) = 6.327 e-02 N <sub>hand</sub> = 21
<b>Area 3a</b>		p = 4.608 e-06 t(63) = 5.014 E( $\Delta R^2$ ) = 9.890 e-02 N <sub>hand</sub> = 24		p = 2.465 e-01 t(52) = 1.172 E( $\Delta R^2$ ) = 1.696 e-02 N <sub>hand</sub> = 13
<b>Caudal M1</b>	p = 1.068 e-04 t(60) = 4.149 E( $\Delta R^2$ ) = 7.449 e-02 N <sub>hand</sub> = 21	p = 1.840 e-01 t(57) = 1.3448 E( $\Delta R^2$ ) = 1.985 e-02 N <sub>hand</sub> = 18		p = 3.338 e-03 t(55) = 3.068 E( $\Delta R^2$ ) = 7.446 e-02 N <sub>hand</sub> = 16
<b>Rostral M1</b>	p = 9.997 e-01 t(69) = 0.004 E( $\Delta R^2$ ) = 4.642 e-05 N <sub>hand</sub> = 30	p = 1.325 e-02 t(62) = 2.550 E( $\Delta R^2$ ) = 4.703 e-02 N <sub>hand</sub> = 23	p = 4.758 e-06 t(46) = 4.490 E( $\Delta R^2$ ) = 1.461 e-01 N <sub>hand</sub> = 7	p = 3.883 e-13 t(86) = 8.559 E( $\Delta R^2$ ) = 1.860 e-01 N <sub>hand</sub> = 47

We constructed a noisy simulated neural population with single-joint coordinate response fields to assess whether our GLMs yielded multi-joint RFs due to spurious correlations. Indeed, the large correlations among joint angles that we note in Chapter 3 could give rise to such spurious predictors that improve model fits, even if only one among a highly-correlated cluster of joints is truly encoded. A neuron from this population was constructed by first selecting a random joint angular coordinate—the angle or angular velocity of a single axis of rotation of a single joint—to serve as the basis for its time-varying firing rates. Firing rates were simulated by computing

$$v(t) = \log\{1 + \exp[\alpha + \beta x(t)]\}, \quad (4-1)$$

where  $v(t)$  is the firing rate of the simulated neuron at time  $t$ ;  $\alpha$  and  $\beta$  are parameters to be optimized, and  $x(t)$  is the value of the joint angular coordinate that drives the neuron's response at time  $t$ . All simulated neurons were constructed to have a latency of 0 relative to the kinematics

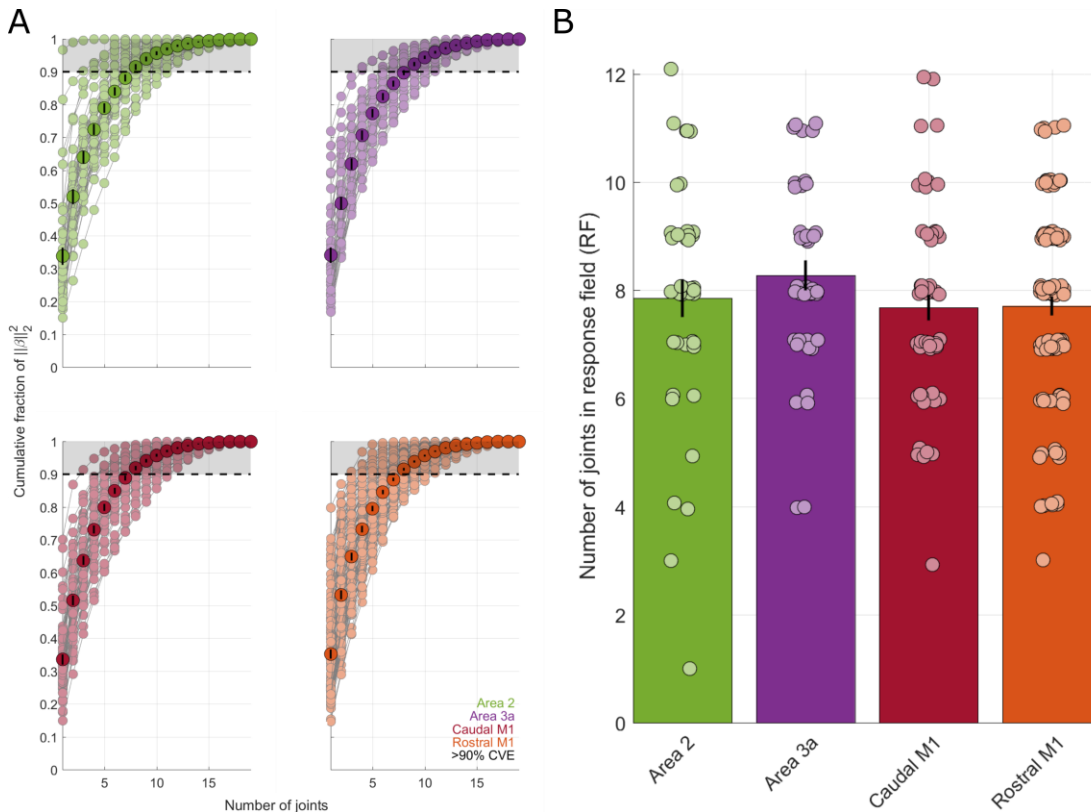


**Figure 4-2.** Neurons track multiple joints distributed over the entire hand. **(A)** To count joints in response fields, we calculate the contribution of each joint to the regression weight vector and count the minimum number of joints required to account for 90% of the regression weight vector's squared norm (gray shaded area). Faded points indicate the cumulative contribution of the best  $N$  joints (abscissa) to the weight vector. Overlaid on these are the average cumulative functions across neurons in each area. **(B)** The average number of joints in a neuron's response field (RF) is roughly eight. There is no difference among areas in terms of the number of joints in the average neuron's RF. Individual points are single neuronal joint counts and can only take integer values; vertical dispersion of these points is artificially inserted to enhance visibility. Error bars in both plots indicate  $\pm 1$  S.E.M.

governing their spiking activity. From these rates, spike counts at each time  $t$  were drawn from a Poisson distribution—MATLAB `poissrnd`—with mean  $v(t)$ .

We then drew a random neuron from which we actually recorded and took note of its overall mean firing rate and peak pseudo- $R^2$ . We then optimize  $\alpha$  and  $\beta$ —MATLAB function `fminunc`—such that the mean rate and pseudo- $R^2$  of the simulated neuron, after simulating its rate-varying Poisson spike counts, were equal to those of the real neuron. In this manner, we attempt to match the firing rates and amount of noise in our simulations to those in our recordings, as those differences could give rise to a different susceptibility of the resulting GLMs to spurious correlations.

We find that our GLMs reliably find the single joint coordinate predictor built into these noisy simulated neurons. In particular, the simulated neurons exhibited clear single-joint coordinate response fields in the vast majority (>70% of  $N = 162$ ) of cases (Figure 4-3). We conclude that the overwhelming number of multi-joint RFs we find in our recorded neural population are unlikely to be the trivial result of our GLMs finding spurious predictors to explain noise in the firing rate data.

Given the size of these multi-joint RFs, on average spanning eight joints, the typical RF must necessarily span multiple digits as A) the wrist and elbow comprise only one joint each, and B) no digit has more than four joints associated with it. Digit 5, for example, is associated with degrees of freedom at its distal interphalangeal joint, proximal interphalangeal joint, metacarpophalangeal joint, and carpo-metacarpal joint. Thus, the large RFs we note in joint-space mirror the multi-digit proprioceptive RFs noted in previous work (Costanzo & Gardner, 1981). However, it is still possible that the multi-digit RFs we observe may be more readily explained in terms of large, multi-articulate muscles such as the common flexor and extensor muscles that insert a tendon into each digit (Schieber, 1995; Serlin & Schieber, 1993).

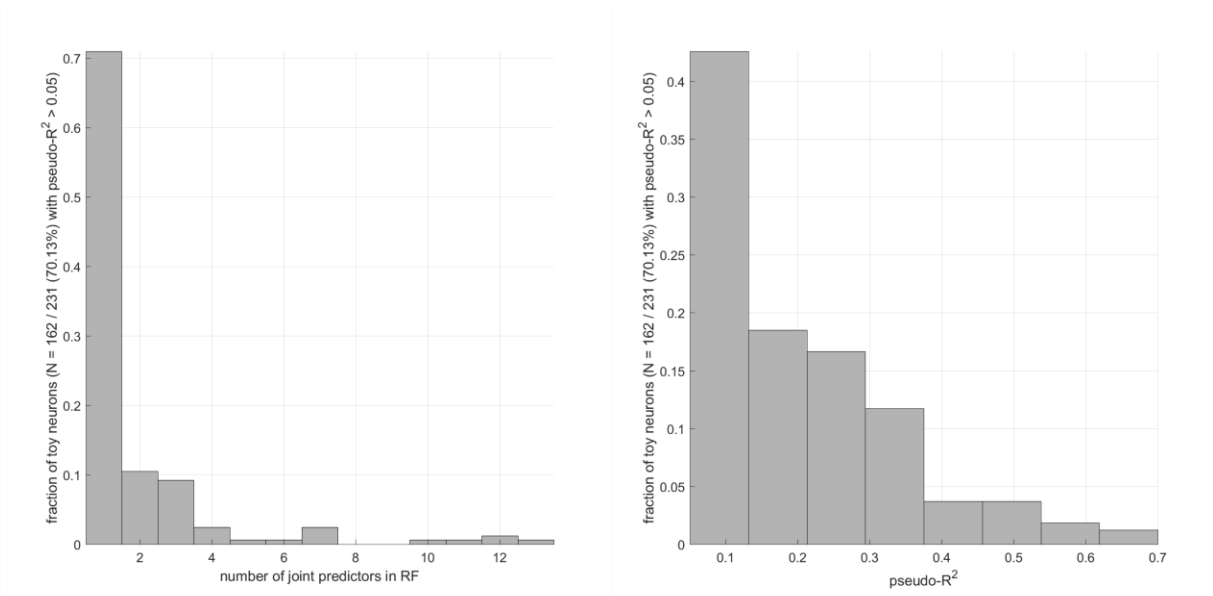


**Figure 4-3.** Simulated neuron populations with single-joint angular coordinate RFs and properties of their GLM fits. *Left.* Histogram of the number of joint predictors contained in the RF inferred via GLM. Note that every simulated neuron responded to just a single joint angular coordinate by design, and that over 70% of these simulated neurons had a GLM RF that recovered this single-predictor RF in spite of inter-joint correlations in the kinematics and noise in the simulated spike counts. *Right.* Distribution of pseudo- $R^2$  values of GLMs fit to these toy neurons, which is similar—by design—to the distribution seen in real cortical neuronal data.

To address this concern, we ran a second set of GLMs that use musculotendon lengths and their derivatives, rather than the angles along joint axes of rotation and their derivatives, as predictors. We count the number of musculotendon complexes included in each RF using similar methods as those used for counting joints, namely by computing the sum of squared standardized regression weights across all predictors – both length and rate of length change – spanning all subunits of each muscle. For example, the flexor digitorum profundus (FDP) has a tendon that inserts onto each digit, each of which is modeled as a separate musculotendon unit in our kinematic model, but whose squared regression weights are added together to obtain a measure of the contribution of the entire FDP musculotendon complex to the RF inferred by GLM. We find that the number of musculotendon complexes in the typical RF counted in this way is equivalent to the

corresponding number of joints (Figure 4-4). This is despite the fact that several muscles span multiple digits and therefore might have yielded GLMs of neural activity with fewer predictors.

### Neurons encode postures of the hand rather than its movements

To assess the degree to which neurons encode hand postures vs. hand movements, we first analyze the pseudo- $R^2$  values for postural and movement encoding models of each neuron. We find that pseudo- $R^2$  values for postural models exceed those for movement-encoding models (Figure 4-5A) (paired-sample T-tests:  $T_{\text{Area 2}(40)} = 5.790$ ,  $p = 9.320 \text{ e-}07$ ;  $T_{\text{Area 3a}(39)} = 8.116$ ,  $p = 6.639 \text{ e-}10$ ;  $T_{\text{Caudal M1}(58)} = 7.037$ ,  $p = 2.542 \text{ e-}09$ ;  $T_{\text{Rostral M1}(106)} = 10.76$ ,  $p = 1.100 \text{ e-}18$ ).

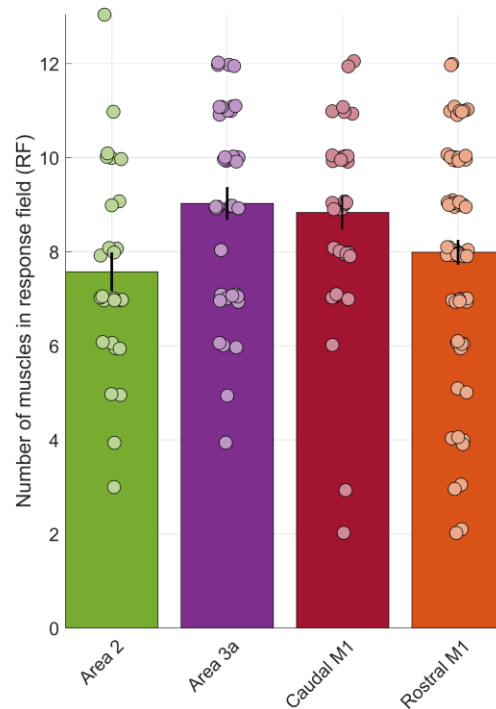


**Figure 4-4.** The number of musculotendon complexes contained in each RF is no fewer than the number of joints in those same RFs (c.f. Figure 4-2B). The same neurons are assessed for musculotendon counts in their RFs using similar methods as described in Figure 4-2A for joint counts. Error bars indicate  $\pm 1$  S.E.M.

Nonetheless, encoding models that included both postures and movements yielded, on average, better fits than did models that included only postures (Figure 4-5B) (paired-sample T-tests:  $T_{\text{Area}}$

$z(40) = 6.581$ ,  $p = 7.225 \text{ e-}08$ ;  $T_{\text{Area 3a}}(39) = 7.875$ ,  $p = 1.393 \text{ e-}09$ ;  $T_{\text{Caudal M1}}(58) = 8.013$ ;  $p = 5.823 \text{ e-}11$ ;  $T_{\text{Rostral M1}}(106) = 11.61$ ,  $p = 1.355 \text{ e-}20$ , suggesting that neurons also carry movement-related signals.

To further quantify the relative contributions of postures and movements, we computed the amount of unique deviance, rather than the total fraction of neural deviance, explained by posture

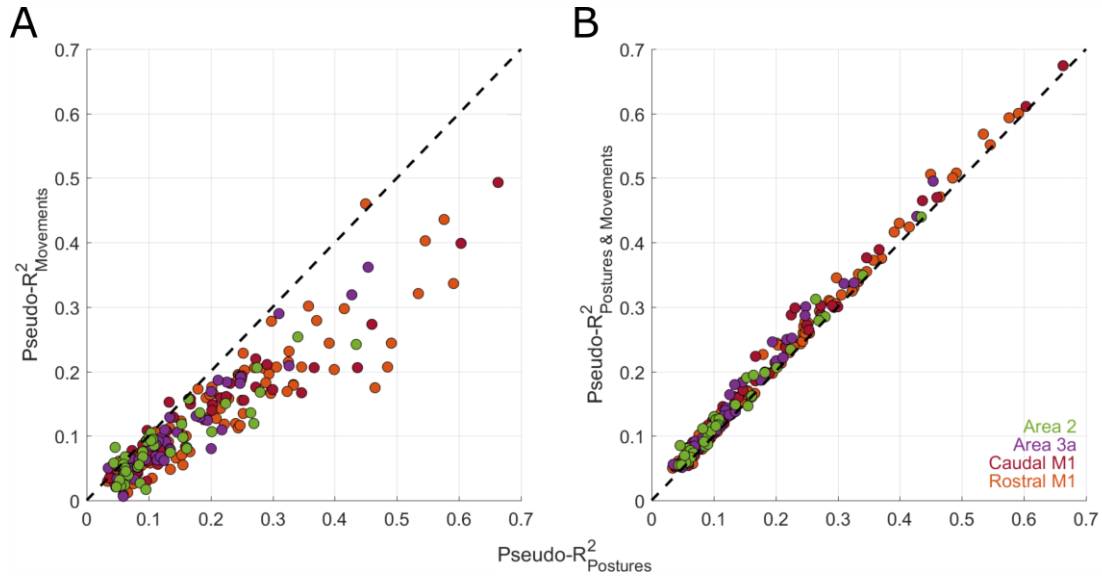


**Figure 4-5.** Results of generalized linear models (GLMs) testing for preferential encoding of joint postures or movements. (A) The distribution of cross-validated pseudo- $R^2$  values computed for GLMs using just joint angles (Postures) as predictors or using just joint angular velocities (Movements) as predictors. Each point represents a single neuron. (B) Same abscissa as (A), but with each point plotted against the pseudo- $R^2$  value obtained using both posture and movement predictors on the ordinate.

and movement models. A measure of such “unique deviance explained” can be obtained by computing partial pseudo- $R^2$  values for each neuron,

$$pR_{X|Y}^2 = \frac{pR_{X,Y}^2 - pR_Y^2}{1 - pR_Y^2}, \quad (4-2)$$

where  $pR_{X|Y}^2$  is the cross-validated partial pseudo- $R^2$  of predictor set  $X$  (postures or movements) after accounting for variance explained by predictor set  $Y$  (movements or postures, respectively);  $pR_{X,Y}^2$  is the cross-validated pseudo- $R^2$  of the GLM that uses both predictor sets to estimate firing

rates; and  $pR_Y^2$  is the cross-validated pseudo- $R^2$  of the GLM that uses only predictor set  $Y$ . This computation is modeled after similar partial coefficient of determination calculations for regression models that assume a Gaussian distribution of residuals. When analyzing these partial pseudo- $R^2$  values (Figure 4-6), we observe that hand postures explain far more unique deviance in the neural data than do movements—i.e., the postural partial pseudo- $R^2$  values are considerably larger than the movement partial pseudo- $R^2$  values (paired-sample T-tests:  $T_{\text{Area 2}}(40) = 5.465$ ,  $p = 2.662 \text{ e-}06$ ;  $T_{\text{Area 3a}}(39) = 7.529$ ,  $p = 4.074 \text{ e-}09$ ;  $T_{\text{Caudal M1}}(58) = 6.056$ ,  $p = 1.101 \text{ e-}07$ ;  $T_{\text{Rostral M1}}(106) = 9.931$ ,  $p = 8.109 \text{ e-}17$ ).

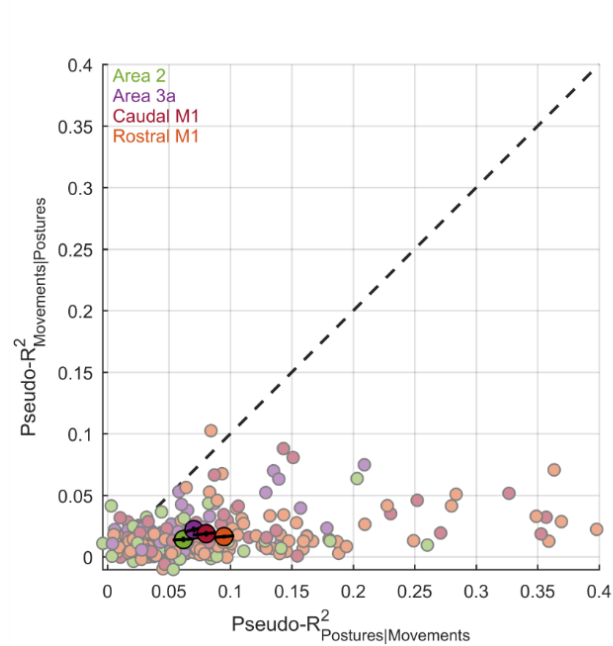


**Figure 4-6.** Partial pseudo- $R^2$  of posture models on the abscissa against movement models on the ordinate. Faded points indicate individual neurons with peak pseudo- $R^2$  (non-partial) of 0.05 of greater. Overlaid fully-saturated points are means over neurons for each area, with error bars indicating  $\pm 1$  S.E.M. along each principal axis of covariance. The vast majority of unique variance in the firing rates of the typical neuron from any of these sensorimotor areas is explained by hand postural information rather than hand joint angular velocity information.

These results from the hand contrast with previously reported results from the proximal limb, where movements are preferentially encoded over positions (Moran & Schwartz, 1999; Paninski, Fellows, Hatsopoulos, & Donoghue, 2004; Reina et al., 2014; Wang, Chan, Heldman, & Moran, 2007). To verify that salience of postures in the neuronal representations of the hand was not an artifact of our analysis, we implemented an identical analysis on analogous data from the proximal limb. Specifically, we applied GLMs to kinematics recorded using a KINARM (Scott, 1999) and neuronal data collected from a UEA in motor cortex as monkeys performed a delayed center-out reaching task (Hatsopoulos, Xu, & Amit, 2007; Kadmon Harpaz, Ungarish, Hatsopoulos, & Flash, 2018; Reimer & Hatsopoulos, 2010). We used cortical responses and associated kinematics starting 1 second before onset of movement and extending 1 second afterwards during reaches to each of eight directions separated by 45 degrees each. We found that the majority of neurons exhibit preferential encoding of movements over positions in the proximal limb (Figure 4-7), consistent with previous reports in the proximal limb but in contrast to our results from the hand. We conclude that the neuronal representations of the proximal and distal limbs are fundamentally different in that the former are dominated by movements whereas the latter are dominated by postures.

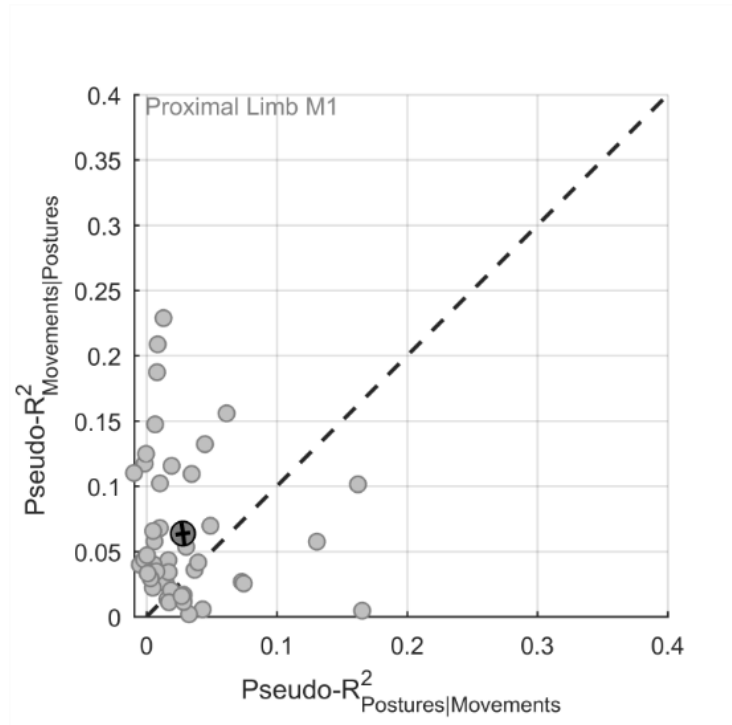


**Figure 4-7.** Partial pseudo- $R^2$  of position and velocity models for GLMs fit to neural data during a center-out reaching task. Conventions are as in Figure 4-6. Note that for the proximal limb, the majority of neurons and, indeed, the mean fall above the diagonal, indicating preferential encoding of velocities over positions. This contrasts with results for hand configurational encoding, where we observe preferential encoding of postures over movements.

### Encoding of passive hand movements

Next, we wished to assess the degree to which neuronal representations were dependent on whether the movements are actively generated or imposed on the (passive) hand. Analysis of these data allowed us to gauge the extent to which the response properties we report might be shaped by motor input or other top-down influences. To this end, we manipulated one monkey's hand (Figure 4-8A) while we recorded the kinematics and neural responses. Since there were not defined trials in these passive measurements, GLMs were fit to data collected throughout the period over which the monkey's hand was manipulated.

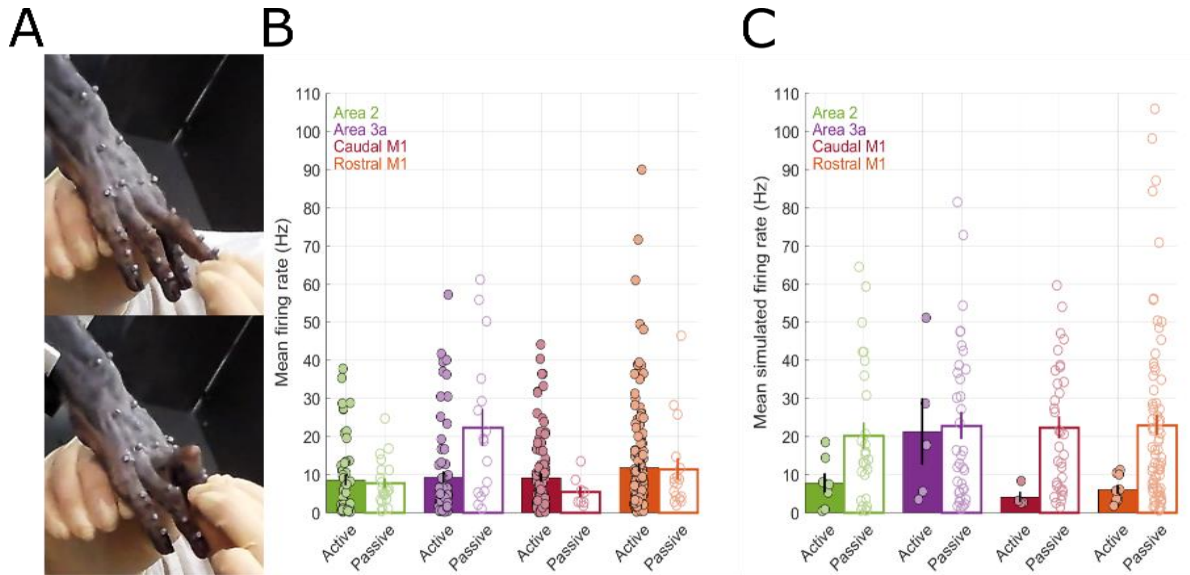


**Figure 4-8.** Mean firing rates of neurons recorded during passive manipulation of the hand compared against those recorded during active, volitional grasp. **(A)** Each digit was passively manipulated by the experimenter. **(B)** Firing rates are generally similar between the two tasks, with the notable exception of area 3a neurons (see text for statistics). **(C)** We simulate firing rates in response to the kinematics from one task—the label on the abscissa—using RFs fit to firing rates and kinematics recorded during the *opposite* task. We note that we should expect firing rates during the passive task to be higher than those during the active grasp task (see text for statistics). Vertical lines centered on the height of each bar indicate  $\pm 1$  S.E.M. Only neurons with pseudo- $R^2 > 0.05$  are considered in (C). Samples from active and passive sessions are not paired, but are rather separate samples.

First, we compare measures of overall neuronal activity across the active and passive conditions—namely, the mean firing rates of neurons. While different neurons are sampled and the kinematics are very different in the two conditions, this analysis might reveal large differences in responsivity during active vs. passive movements. We find that responses in the two conditions are comparable, except in area 3a, where neurons tend to respond more vigorously (Figure 4-8B) in the passive than in the active condition (two-sample two-tailed equal-variances T-test,  $T(82) = 3.351$ ,  $p = 1.219e-03$ ). To assess whether differences in the neuronal responses between the active and passive conditions (or lack thereof) reflect differences in the kinematics, we simulated the responses of neurons recorded in the active condition to the kinematics measured during the passive condition and vice versa (Figure 4-8C). We find that simulated responses in the passive condition are higher than those in the active condition (two-sample two-tailed equal-variances T-

test,  $T(193) = 3.092$ ,  $p = 2.285e-03$ ). We conclude that neurons in area 3a respond comparably in the active and passive conditions, while neurons in the other cortical fields are more responsive during active movements.

Interestingly, however, the encoding properties of neurons—the number of encoded joints and sensitivity to posture vs movement—were comparable across the active and passive conditions (Figure 4-9A, B) as was the overall goodness-of-fit of the GLM models (Figure 4-9C). A possible exception is a modest effect of task type in rostral M1, where the number of joints was modestly larger for imposed movements than for actively generated ones. These analyses suggest that the encoding properties of neurons do not fundamentally change across these two conditions.

## Discussion

### **Proprioceptive neurons in somatosensory cortex have large response fields**

Proprioceptive neurons in somatosensory cortex encode postures and movements distributed over several joints, with a mean of around eight (Figure 4-2B), and these large RFs are observed even during imposed movements of the hand (Figure 4-9A). The size of the response fields of proprioceptive neurons in somatosensory cortex stands in stark contrast to the size of the receptive fields of tactile neurons, particularly in area 3b, which typically include a small patch of skin spanning a fraction of a fingerpad (Nelson et al., 1980; M Sur et al., 1980). While the present work constitutes the first attempt to *quantitatively* characterize proprioceptive response fields in somatosensory cortex, our results are broadly consistent with those from previous qualitative characterizations (Costanzo & Gardner, 1981; Krubitzer, Huffman, Disbrow, & Recanzone, 2004; Pons, Garraghty, Cusick, & Kaas, 1985).

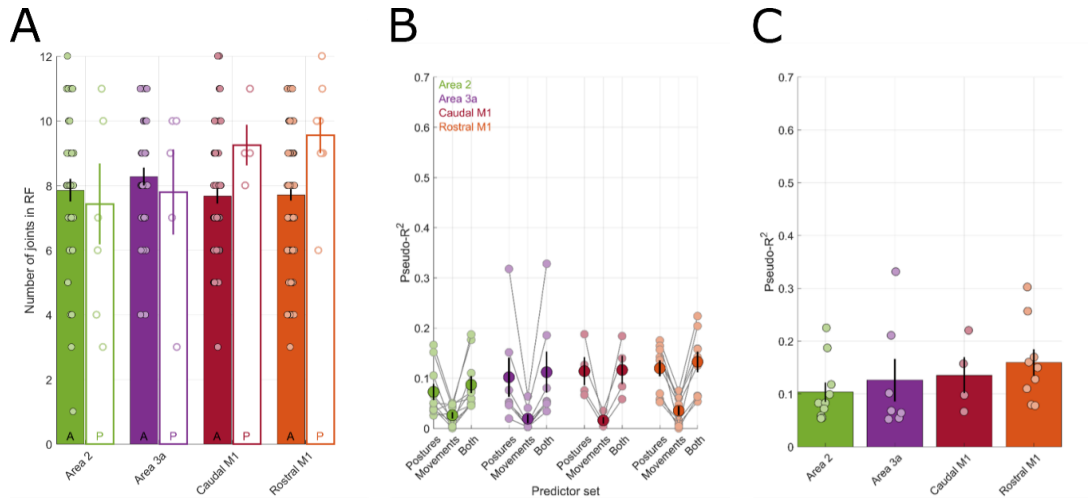


**Figure 4-9.** Properties of GLMs fit to neurons during passive manipulation of the hand. (A) The number of joints tracked by a neuron in each area does not generally change between the active (filled bars and points, labelled “A”) and passive (empty bars and points, labelled “P”) cases (two-sample equal-variance two-tailed T-tests:  $T_{\text{Area 2}}(46) = 0.432$ ,  $p = 6.681 \text{ e-}01$ ;  $T_{\text{Area 3a}}(43) = 0.528$ ,  $p = 6.003 \text{ e-}01$ ;  $T_{\text{Caudal M1}}(61) = -1.699$ ,  $p = 9.441 \text{ e-}02$ ), except in rostral M1 where the number of joints in the typical RF increases during passive movements RF (two-sample equal-variance two-tailed T test:  $T_{\text{Rostral M1}}(114) = -2.927$ ,  $4.137 \text{ e-}03$ ). Each point gives the number of joints in a single neuron’s RF. (B) Pseudo- $R^2$  for posture-only models, movement-only models, and full models. In the passive case, postures are still preferentially encoded over movements of the joints. Not shown are the differences between the partial pseudo- $R^2$  values of postural against movement models, which are no different from those in the active volitional grasp task (two-sample equal-variance two-tailed T-tests:  $T_{\text{Area 2}}(46) = -0.485$ ,  $p = 6.301 \text{ e-}01$ ;  $T_{\text{Area 3a}}(43) = -2.571$ ,  $p = 1.368 \text{ e-}02$ ;  $T_{\text{Caudal M1}}(61) = -0.955$ ,  $p = 3.434 \text{ e-}01$ ;  $T_{\text{Rostral M1}}(114) = -0.279$ ,  $7.806 \text{ e-}01$ ). (C) Pseudo- $R^2$  of GLMs (provided pseudo- $R^2 > 0.05$ ) fit using the kinematics as predictors, which are not significantly different from those seen during active movement (c.f. Figure 4-C) (two-sample equal-variance two-tailed T-tests:  $T_{\text{Area 2}}(46) = 1.092$ ,  $p = 2.804 \text{ e-}01$ ;  $T_{\text{Area 3a}}(43) = 0.631$ ,  $p = 5.313 \text{ e-}01$ ;  $T_{\text{Caudal M1}}(61) = 0.829$ ,  $p = 4.103 \text{ e-}01$ ;  $T_{\text{Rostral M1}}(114) = 1.506$ ,  $p = 1.347 \text{ e-}01$ ). Vertical lines centered on the height of each bar indicate  $\pm 1$  S.E.M. Only neurons with pseudo- $R^2 > 0.05$  are considered. Samples from active and passive sessions are not paired, but are rather separate samples.

The ethological basis of tactile receptive fields and proprioceptive response fields is a matter of speculation. One might conjecture that tactile information – about local spatial features of an object such as edge orientation (Bensmaia, Denchev, Dammann 3rd, Craig, & Hsiao, 2008) and curvature (Yau, Connor, & Hsiao, 2013), for example – is best carried in a representation that preserves local spatial relationships. In contrast, information about the conformation of the hand requires the integration of digit and joint postures spanning the entire hand, thus requiring more distributed response fields. Ultimately, the integration of local shape features at the points of contact between skin and object – carried in tactile representations – must be integrated with

information about the conformation of the hand – carried in proprioceptive representations – to achieve a representation of the three dimensional structure of the object, a process known as stereognosis (Berryman, Yau, & Hsiao, 2006; Hsiao, 2008; Yau, Kim, Thakur, & Bensmaia, 2016).

### **Hand neurons encode postures over movements**

In both somatosensory and motor cortex, neurons encode joint postures of the hand more strongly than they do joint movements. This holds true during both active and passive manipulations of the hand. This contrasts with kinematic encoding of the arm, where both somatosensory cortical neurons (Weber et al., 2011) and motor cortical neurons (Moran & Schwartz, 1999; Paninski et al., 2004; Reina et al., 2014; Wang et al., 2007) preferentially encode joint velocities. This difference between proximal and distal limb representations may reflect differences in the functional roles of these two structures. Indeed, the role of the arm is to place the hand somewhere in three dimensional space, while that of the hand – at least during grasp and object manipulation – is to adopt a conformation that is appropriate to the task. From this perspective, it stands to reason that the control and neural representation of the proximal limb would rely on movement and that of hand conformation would rely on posture.

An alternate explanation for this difference between proximal and distal limb representations arises from the dynamics governing their movements. Indeed, the arm, comprising both the forearm and hand, has more mass than the hand alone so the mechanics of proximal limb movements involve a larger inertial term than those of the digits. Although the specific manner by which a large inertial term may give rise to preferential coding of movement in the nervous system is unclear, it is nonetheless a factor whose influence may need to be accounted for.

### **Response to active vs. imposed hand movements**

The response fields of proprioceptive and motor neurons are similar whether these are computed from responses to active movements or responses to imposed movements of the hand. Indeed, response field size and postural preference are similar for active and passive movements. While this result may not be very surprising for somatosensory neurons, that it applies to M1 is less expected and suggests that the sensory input to M1 is aligned with its output. Note that M1 has previously been shown to be driven by sensory input (Hatsopoulos & Suminski, 2011), so this basic observation is not novel.

Our results suggest, though these experiments were not designed to test this explicitly, that M1 neurons are more active during active movements than passive ones, as expected. Neurons in area 2 also seem to exhibit a preference for active movements, as reflected in higher firing in the active condition. In contrast, somatosensory neurons with response fields on the proximal limb have been shown to alternatively exhibit a preference for either active or passive movement (London & Miller, 2013; Soso & Fetz, 1980). However, the responsiveness of area 2 in the passive condition may reflect increased cutaneous input driven by the experimenter's manipulation of the hand.

In contrast to their counterparts in M1 and area 2, neurons in area 3a do not exhibit a preference of active or passive movement after correcting for differences in kinematics. This finding is consistent with a role of this area as a traditional sensory area, an interpretation that conflicts with a more nebulous role of this area as a “transition zone” area between sensory and motor cortex (E. G. Jones & Porter, 1980). This transition hypothesis is supported by motoneuron-like properties of area 3a neurons, such as spiking activity that precedes movement onset (C

Fromm & Evarts, 1982) and reciprocal connectivity between M1 and area 3a (Huffman & Krubitzer, 2001).

We should note that the sample size of our passively sessions is small and that this data set is confounded by the differences in kinematics and the presence of significant uncontrolled tactile stimulation by the experimenter during hand manipulation. Nonetheless, our results suggest that area 3a neurons are equally responsive to actively generated and imposed movements, as one might expect from a “traditional” sensory area. To test these hypotheses more rigorously will require experiments in which hand kinematics in the active and passive conditions are matched, presumably requiring a robotic exoskeleton—e.g. (Heo, Gu, Lee, Rhee, & Kim, 2012; C. L. Jones, Wang, Morrison, Sarkar, & Kamper, 2014), and cutaneous input is either systematically manipulated and accounted for or eliminated (using local anesthesia, for example).

### **Dependence of postural preference on analytics approach**

A pair of previous studies on kinematic coding in the hand representation has come to a different conclusion regarding the postural preference of motor neurons, finding instead a mixed selectivity with a movement preference (Saleh, Takahashi, Amit, & Hatsopoulos, 2010; Saleh, Takahashi, & Hatsopoulos, 2012). However, three critical differences between the previous study and the present one may account for this seeming discrepancy: 1) the inclusion of regressors at multiple lags; 2) the inclusion of spike history regressors; and 3) the use of a different measure to compare postural vs. movement encoding—namely, counting the number of neurons with a significant weight for each regressor, rather than comparing goodness-of-fit measures. Although the inclusion of multiple regressors at different lags may be important in proximal limb representations in M1 to track changing kinematic preferred directions during hand transport (Hatsopoulos et al., 2007), we find that inclusion of regressors at multiple lags yields only a modest

though statistically significant improvement in goodness of fit (Figure 4-10A). We abandoned multi-lag models due to this modest improvement in fit. Note, however, that a multi-lag model can extract posture from movement (by integrating velocity) and velocity from posture (by differentiating joint angle). These models are thus poorly suited to assess the weighting contributions of posture and movement in the neural responses.

Replicating previous findings (Saleh et al., 2010, 2012), we also find that including spike history regressors significantly improves model fit (Figure 4-10B). However, we find that if we include these terms in the GLM, they tend to dominate their kinematic counterparts. Indeed, kinematics are highly autocorrelated over long time scales (Figure 4-10E), so spike history – reflecting recent kinematics – is an excellent predictor of current neuronal responses. Furthermore, spike history regression weights are more correlated with postural than movement regressors (Figure 4-10C) due to autocorrelations over long time scales for postures than movements (Figure 4-10E), which would preferentially reduce the variance explained by postural regressors relative to that of velocity regressors. Moreover, regression weights for history terms extend hundreds of milliseconds in the past, well outside a reasonable physiological time window (tens of milliseconds) for history-dependent effects (Chen & Fetz, 2005; Pillow et al., 2008; Pillow, Paninski, Uzzell, Simoncelli, & Chichilnisky, 2005), but consistent with the time scale of postural autocorrelations. Including these same spike history terms, in addition to predictors at multiple lags, weakens the postural preference in our neuronal data but does not eliminate it (Figure 4-10D).

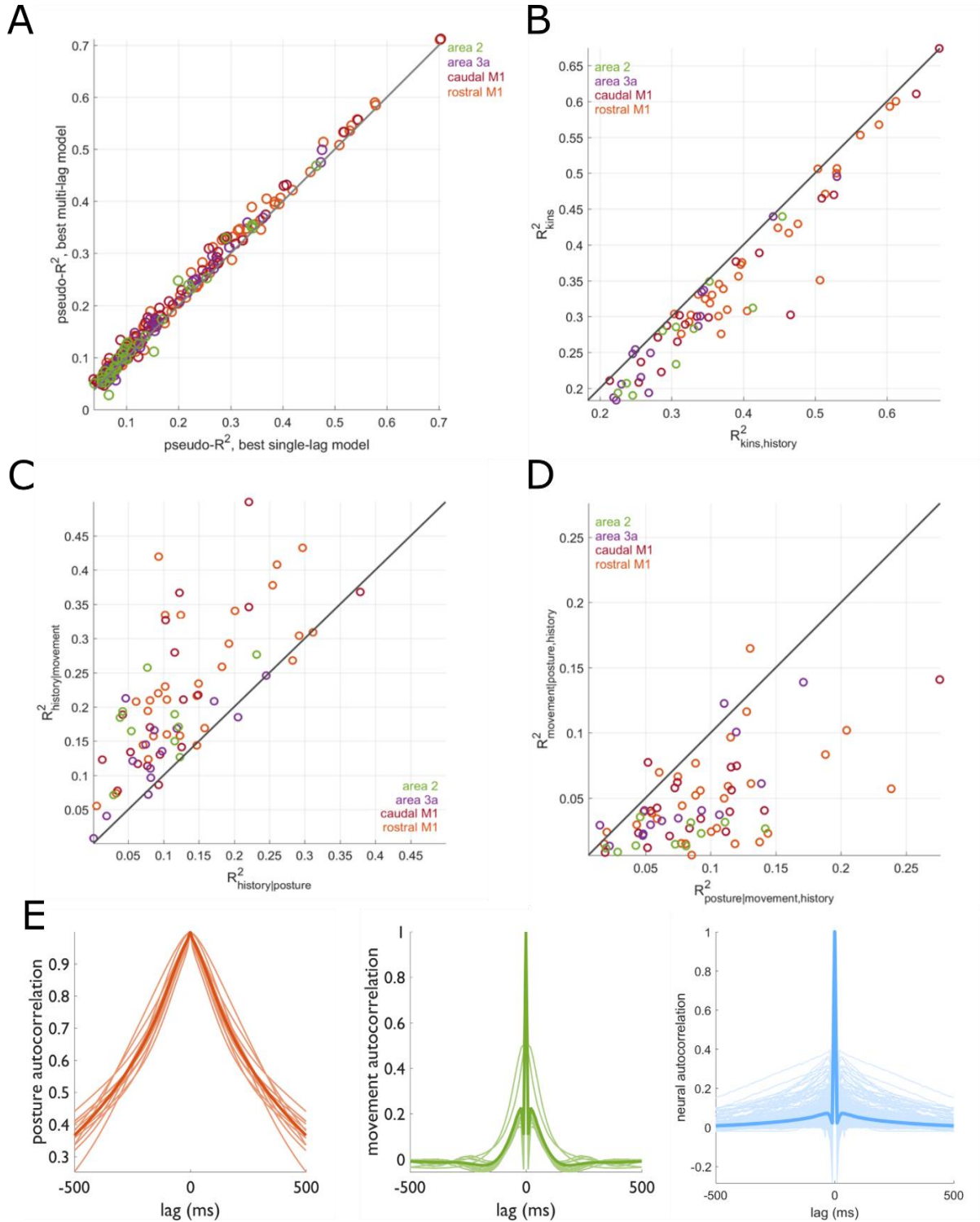


**Figure 4-10.** Reconciliation of this paper’s grasping results with previous reports of grasp encoding (Saleh et al., 2010, 2012).

**Figure 4-10, continued.** (A) Multi-lag models offer only a very slight, albeit significant, improvement over single-lag GLMs in terms of explaining neural activity, as evidenced by most points, or neurons, falling just above the diagonal. (B) History terms offer a significant improvement to single-lag encoding models, as evidenced by most points, or neurons, falling below the diagonal. (C) However, history terms covary more strongly with postures than they do with movements—as evidenced by the majority of points, or neurons, falling above the diagonal—and therefore could preferentially sap predictive power away from postures. (D) Regardless, posture terms are preferentially encoded in terms of partial pseudo- $R^2$  in the majority of neurons—as evidenced by the majority of points falling below the diagonal—even when accounting for history terms. (E) Posture autocorrelations (left) extend farther out temporally than do movement correlations (middle) or (unsmoothed) neural spiking autocorrelations (right) to which GLMs are fit. Underlying firing rates seem to vary on timescales similar to postures, which non-physiological spike history terms extending back as far as 250ms in the past could obscure.

In fact, even when we count neurons with significant weights for each regressor in models that exclude spike history regressors, we still observe a bias toward encoding of postural variables, albeit a slight one (Figure 4-11A). “Significance” in this case is assessed for cross-validated models using the method described earlier and depicted in Figure 4-2A, rather than within-sample p-values as was previously done. We note that this measure of preferential posture- or movement-coding contrasts with the measure by which we normally assess preferential coding: comparisons of pseudo- $R^2$  between models.

However, if we replicate the previous approach in all of its aspects – multi-lag models with spike history regressors and preference measured by neuron count (Figure 4-11B), only then do we obtain movement preference. We conclude that the postural preference we observe in hand sensorimotor representations is robust.

### **Hand representations reflect muscle activations**

Ultimately proprioception relies primarily on signals from afferents that innervate the muscles. M1 and proprioceptive responses might thus be more fruitfully described in terms of muscle activations rather than joint angles and angle velocities. We could not directly test this

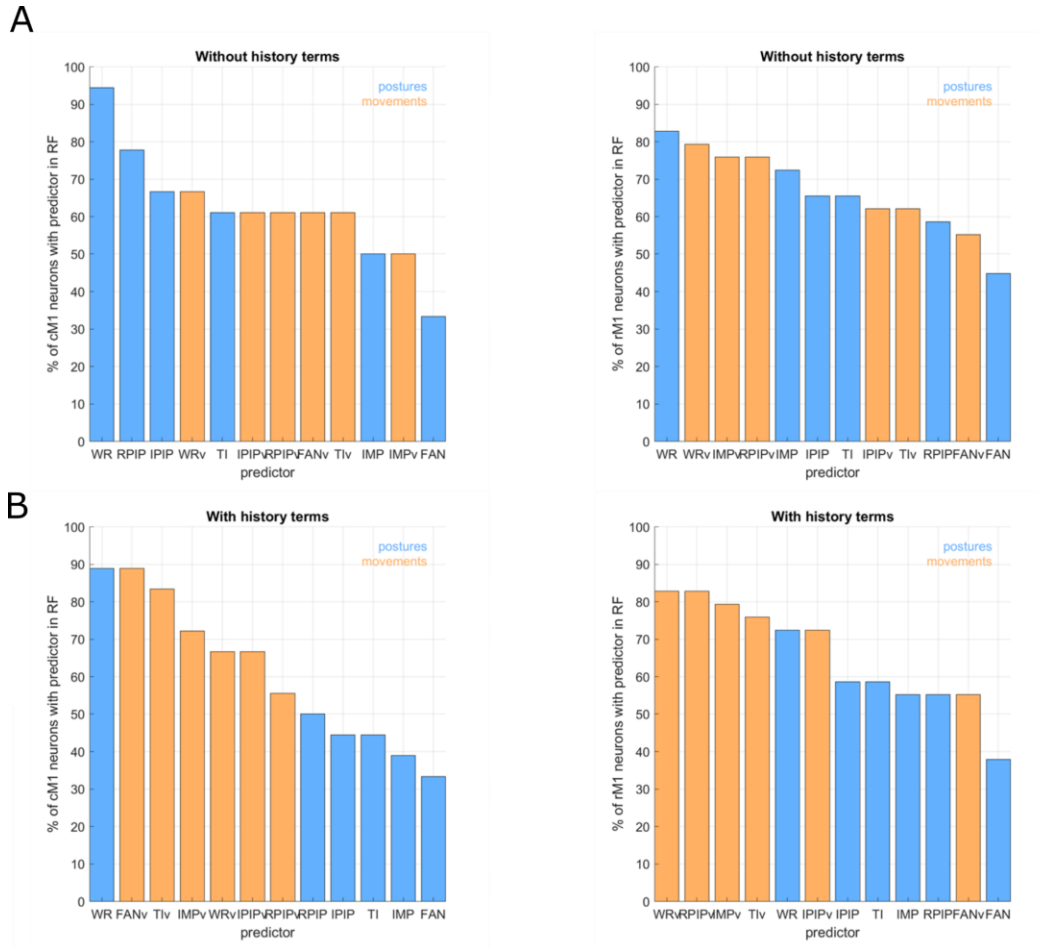


**Figure 4-11.** Continuation of Figure 4-10. **(A)** Counting the number of neurons with each predictor in its RF for multi-lag, no-history models. Joint angular coordinates are converted to the same domain as that used previously (Saleh et al., 2010, 2012) for the purposes of comparison. Postural predictors are the most frequently encoded in both caudal and rostral motor cortices. **(B)** Only when re-incorporating history terms on top of using multi-lag models and counting joints rather than assessing partial pseudo- $R^2$  do we see movement predictors consistently occupying higher-rank slots than posture predictors. Velocity terms appear to have nearly exclusive representation among the top 4 most-encoded joint angular predictors, with wrist posture in caudal M1 being the lone exception.

hypothesis because our animals were not instrumented with electromyographs. As an indirect test of this hypothesis, albeit one that does not account for movement strategies featuring large co-contractions of antagonist muscles, we investigated whether neuronal responses in somatosensory cortex and M1 could be better predicted from time-varying musculotendon lengths, which we could estimate from the kinematics using a musculotendon model of the hand (Figure 4-4). We found that this particular intrinsic reference frame was no more closely associated with cortical

responses than was the kinematic one. Note that we investigate in great detail the suitability of another reference frame – kinematic synergies – in Chapter 5.

### **Contrasting proprioceptive and motor representations of the hand**

In both somatosensory and motor cortices, individual neurons preferentially encode hand postures distributed over multiple joints. Remarkably, neurons in all sensorimotor areas encode hand kinematics over comparable swaths of hand (number of joints) and are indistinguishable in terms of their respective preference for posture vs. movement. One might expect that motor activity leads the movement whereas sensory activity lags it. We found this to be the case in area 2 but not area 3a (Figure 4-12, *right*) (cf. (Christoph Fromm & Evarts, 1982) regarding area 3a). Activity in motor cortex generally led the kinematics, as expected, but even this phenomenon was not reliable. As noted above, however, the long kinematic autocorrelations make our estimates of response latency (lag and lead) very unreliable (Figure 4-12, *left*).

### **Conclusions**

Proprioceptive neurons in somatosensory cortex have large response fields that track multiple joints spanning the entire hand, respond preferentially to multi-joint postures of the hand rather than the movements of those joints, and do so whether movements are actively generated by the animal or imposed by the experimenter. Similar coding properties are observed in M1, including the postural preference, which constitutes a departure from previous reports of M1 coding of proximal limb movements. These differences between hand and proximal limb representations may reflect the fundamentally different roles of the hand and arm.

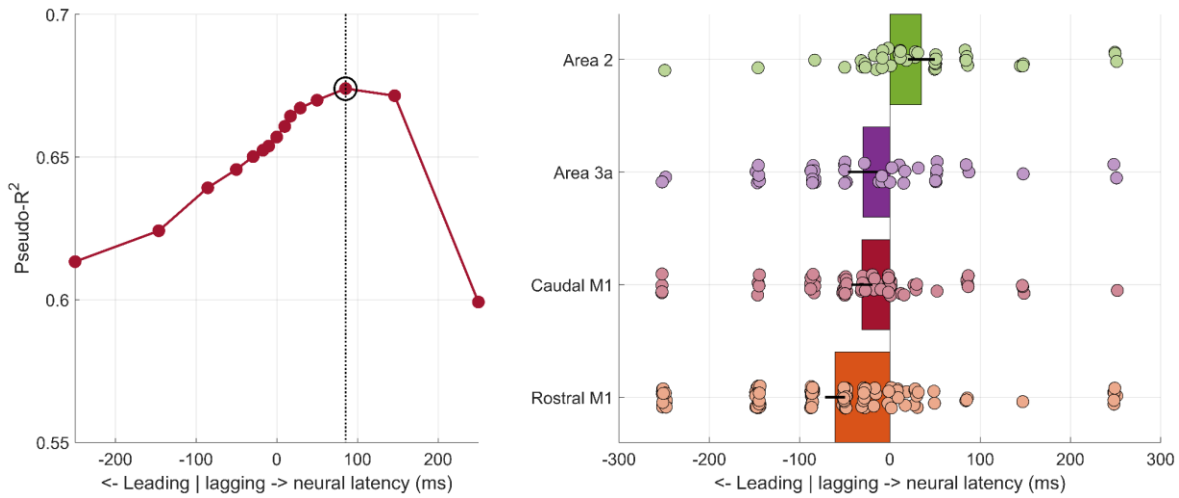


**Figure 4-12.** Optimal neural latencies. *Left.* We fit GLMs fit to multiple different latencies and report for each neuron the latency associated with the largest pseudo- $R^2$  value. Shown is the latency-versus-pseudo- $R^2$  plot for an example neuron from caudal M1. Kinematic autocorrelations rendered estimates of optimal lags hazardous on a neuron-by-neuron basis (see scale of the ordinate). GLMs are used to evaluate latency rather than events such as the start of movement to account for different response fields that could give rise to different apparent latencies via the latter method. *Right.* Estimates of optimal latency for each cortical area after averaging across all neurons with pseudo- $R^2 > 0.05$ . We find that, on average, area 2 neurons significantly lag kinematics (one-sample T-test:  $T(40) = 2.355$ ,  $p = 2.353 \text{ e-}02$ ,  $\bar{\Delta t} = 34.97$  ms), both rostral M1 (one-sample T-test:  $T(106) = -5.417$ ,  $p = 3.816 \text{ e-}07$ ,  $\bar{\Delta t} = -60.73$  ms) and caudal M1 (one-sample T-test:  $T(61) = -2.611$ ,  $p = 1.134 \text{ e-}02$ ,  $\bar{\Delta t} = -30.97$  ms) significantly lead kinematics, and neurons in area 3a neither significantly lead nor lag kinematics on average (one-sample T-test:  $T(41) = -1.835$ ,  $p = 7.373 \text{ e-}02$ ,  $\bar{\Delta t} = -29.87$  ms). Indeed, there is a significant difference among optimal lags across areas (one-way ANOVA:  $F(3,251) = 8.111$ ,  $p = 3.567 \text{ e-}05$ ) that can be attributed to area 2 responses lagging kinematics relative to the other cortical areas (post-hoc Tukey's HSD: all pairwise differences n.s. except those involving area 2,  $p_{\text{area } 3a} = 2.693 \text{ e-}02$ ,  $p_{\text{cM1}} = 1.056 \text{ e-}02$ ,  $p_{\text{rM1}} = 5.030 \text{ e-}02$ , all  $\Delta \Delta t > 0$ ). Significance values of multiple T-tests are assessed here with the Holm-Bonferroni method, with FWER  $< 0.05$  for this family of four comparisons. Slightly different degrees of freedom in these statistical tests relative to the rest of the text are because we compare both joint- and muscle-based models against each other in this figure, whereas we only account for joint-based models in the rest of the text—except where explicitly stated otherwise.

## References

- Aflalo, T. N., & Graziano, M. S. A. (2007). Relationship between unconstrained arm movements and single-neuron firing in the macaque motor cortex. *The Journal of Neuroscience : The Official Journal of the Society for Neuroscience*, 27(11), 2760–80. <http://doi.org/10.1523/JNEUROSCI.3147-06.2007>
- Bensmaia, S. J., Denchev, P. V., Dammann 3rd, J. F., Craig, J. C., & Hsiao, S. S. (2008). The representation of stimulus orientation in the early stages of somatosensory processing. *Journal of Neuroscience*, 28(3), 776–786. <http://doi.org/10.1523/JNEUROSCI.4162-07.2008>
- Berryman, L. J., Yau, J. M., & Hsiao, S. S. (2006). Representation of object size in the somatosensory system. *Journal of Neurophysiology*, 96(1), 27–39. <http://doi.org/10.1152/jn.01190.2005>
- Brochier, T., Spinks, R. L., Umiltà, M. a, & Lemon, R. N. (2004). Patterns of muscle activity underlying object-specific grasp by the macaque monkey. *Journal of Neurophysiology*, 92(3), 1770–82. <http://doi.org/10.1152/jn.00976.2003>
- Chen, D., & Fetz, E. E. (2005). Characteristic Membrane Potential Trajectories in Primate Sensorimotor Cortex Neurons Recorded In Vivo. *Journal of Neurophysiology*, 94(4), 2713–2725. <http://doi.org/10.1152/jn.00024.2005>
- Costanzo, R. M., & Gardner, E. P. (1981). Multiple-joint neurons in somatosensory cortex of awake monkeys. *Brain Research*, 214(2), 321–333. [http://doi.org/10.1016/0006-8993\(81\)91197-5](http://doi.org/10.1016/0006-8993(81)91197-5)
- Darian-Smith, I., Sugitani, M., Heywood, J., Karita, K., & Goodwin, A. (1982). Touching Textured Surfaces: Cells in Somatosensory Cortex Respond Both to Finger Movement and to Surface Features. *Science*. American Association for the Advancement of Science. <http://doi.org/10.2307/1689044>
- Fromm, C., & Evarts, E. V. (1982). *Pyramidal tract neurons in somatosensory cortex: central and peripheral inputs during voluntary movement*. *Brain Research* (Vol. 238). [http://doi.org/10.1016/0006-8993\(82\)90781-8](http://doi.org/10.1016/0006-8993(82)90781-8)
- Fromm, C., & Evarts, E. V. (1982). Pyramidal tract neurons in somatosensory cortex: central and peripheral inputs during voluntary movement. *Brain Research*, 238(1), 186–91. Retrieved from <http://www.ncbi.nlm.nih.gov/pubmed/6805854>
- Gandevia, S. C., Mccioskey, D. I., Burke, D., Mcc, D. I., & Oskey, /. (1992). *Kinaesthetic signals and muscle contradiion*. Retrieved from [https://www.cell.com/trends/neurosciences/pdf/0166-2236\(92\)90028-7.pdf](https://www.cell.com/trends/neurosciences/pdf/0166-2236(92)90028-7.pdf)
- Gardner, E. P., & Costanzo, R. M. (1981). Properties of kinesthetic neurons in somatosensory cortex of awake monkeys. *Brain Research*, 214(2), 301–319. <http://doi.org/10.1016/0006->

- Hatsopoulos, N. G., & Suminski, A. J. (2011). Sensing with the Motor Cortex. *Neuron*, 72(3), 477–487. <http://doi.org/10.1016/J.NEURON.2011.10.020>
- Hatsopoulos, N. G., Xu, Q., & Amit, Y. (2007). Encoding of movement fragments in the motor cortex. *The Journal of Neuroscience : The Official Journal of the Society for Neuroscience*, 27(19), 5105–14. <http://doi.org/10.1523/JNEUROSCI.3570-06.2007>
- Heo, P., Gu, G. M., Lee, S., Rhee, K., & Kim, J. (2012). Current hand exoskeleton technologies for rehabilitation and assistive engineering. *International Journal of Precision Engineering and Manufacturing*, 13(5), 807–824. <http://doi.org/10.1007/s12541-012-0107-2>
- Hsiao, S. (2008). Central mechanisms of tactile shape perception. *Current Opinion in Neurobiology*, 18(4), 418–424. <http://doi.org/10.1016/j.conb.2008.09.001>
- Huerta, M. F., & Pons, T. P. (1990). Primary motor cortex receives input from area 3a in macaques. *Brain Research*, 537, 367–371. Retrieved from [http://ac.els-cdn.com.proxy.uchicago.edu/000689939090388R/1-s2.0-000689939090388R-main.pdf?\\_tid=de6b4b3a-401b-11e7-a42b-00000aab0f02&acdnat=1495587589\\_cb7bebf22699b394368d44fabb3d10c](http://ac.els-cdn.com.proxy.uchicago.edu/000689939090388R/1-s2.0-000689939090388R-main.pdf?_tid=de6b4b3a-401b-11e7-a42b-00000aab0f02&acdnat=1495587589_cb7bebf22699b394368d44fabb3d10c)
- Huffman, K. J., & Krubitzer, L. (2001). Area 3a: topographic organization and cortical connections in marmoset monkeys. *Cerebral Cortex (New York, N.Y. : 1991)*, 11(9), 849–67. Retrieved from <http://www.ncbi.nlm.nih.gov/pubmed/11532890>
- Jones, C. L., Wang, F., Morrison, R., Sarkar, N., & Kamper, D. G. (2014). Design and Development of the Cable Actuated Finger Exoskeleton for Hand Rehabilitation Following Stroke. *IEEE/ASME Transactions on Mechatronics*, 19(1), 131–140. <http://doi.org/10.1109/TMECH.2012.2224359>
- Jones, E. G., & Porter, R. (1980). What is area 3a? *Brain Research Reviews*, 2(1–3), 1–43. [http://doi.org/10.1016/0165-0173\(80\)90002-8](http://doi.org/10.1016/0165-0173(80)90002-8)
- Kadmon Harpaz, N., Ungarish, D., Hatsopoulos, N. G., & Flash, T. (2018). Movement Decomposition in the Primary Motor Cortex. *Cerebral Cortex*. <http://doi.org/10.1093/cercor/bhy060>
- Krubitzer, L., Huffman, K. J., Disbrow, E., & Recanzone, G. (2004). Organization of area 3a in macaque monkeys: contributions to the cortical phenotype. *The Journal of Comparative Neurology*, 471(1), 97–111. <http://doi.org/10.1002/cne.20025>
- London, B. M., & Miller, L. E. (2013). Responses of somatosensory area 2 neurons to actively and passively generated limb movements. *Journal of Neurophysiology*, 109(6), 1505–13. <http://doi.org/10.1152/jn.00372.2012>
- Moran, D. W., & Schwartz, A. B. (1999). Motor Cortical Representation of Speed and Direction

- During Reaching. *Journal of Neurophysiology*, 82(5), 2676–2692.  
<http://doi.org/10.1152/jn.1999.82.5.2676>
- Nelson, R. J., Sur, M., Felleman, D. J., & Kaas, J. H. (1980). Representations of the body surface in postcentral parietal cortex of *Macaca fascicularis*. *The Journal of Comparative Neurology*, 192(4), 611–643. <http://doi.org/10.1002/cne.901920402>
- Paninski, L., Fellows, M. R., Hatsopoulos, N. G., & Donoghue, J. P. (2004). Spatiotemporal Tuning of Motor Cortical Neurons for Hand Position and Velocity. *J Neuroph*, 91, 515–532. <http://doi.org/10.1152/jn.00587.2002>
- Pei, Y.-C., Denchev, P. V., Hsiao, S. S., Craig, J. C., & Bensmaia, S. J. (2009). Convergence of Submodality-Specific Input Onto Neurons in Primary Somatosensory Cortex. *J Neurophysiol*, 102, 1843–1853. <http://doi.org/10.1152/jn.00235.2009>
- Pillow, J. W., Paninski, L., Uzzell, V. J., Simoncelli, E. P., & Chichilnisky, E. J. (2005). Prediction and decoding of retinal ganglion cell responses with a probabilistic spiking model. *The Journal of Neuroscience : The Official Journal of the Society for Neuroscience*, 25(47), 11003–13. <http://doi.org/10.1523/JNEUROSCI.3305-05.2005>
- Pillow, J. W., Shlens, J., Paninski, L., Sher, A., Litke, A. M., Chichilnisky, E. J., & Simoncelli, E. P. (2008). Spatio-temporal correlations and visual signalling in a complete neuronal population. *Nature*, 454(7207), 995–9. <http://doi.org/10.1038/nature07140>
- Pons, T. P., Garraghty, P. E., Cusick, C. G., & Kaas, J. H. (1985). The somatotopic organization of area 2 in macaque monkeys. *The Journal of Comparative Neurology*, 241(4), 445–466. <http://doi.org/10.1002/cne.902410405>
- Prochazka, A. (2011). Proprioceptive Feedback and Movement Regulation. In *Comprehensive Physiology* (pp. 89–127). Hoboken, NJ, USA: John Wiley & Sons, Inc. <http://doi.org/10.1002/cphy.cp120103>
- Proske, U., & Gandevia, S. C. (2012). The Proprioceptive Senses: Their Roles in Signaling Body Shape, Body Position and Movement, and Muscle Force. *Physiological Reviews*, 92(4), 1651–1697. <http://doi.org/10.1152/physrev.00048.2011>
- Reimer, J., & Hatsopoulos, N. G. (2010). Periodicity and evoked responses in motor cortex. *The Journal of Neuroscience : The Official Journal of the Society for Neuroscience*, 30(34), 11506–15. <http://doi.org/10.1523/JNEUROSCI.5947-09.2010>
- Reina, G. A., Moran, D. W., Schwartz, A. B., Snider, J., Lee, D., Harrington, D. L., ... Mcmorland, A. J. C. (2014). On the Relationship Between Joint Angular Velocity and Motor Cortical Discharge During Reaching, 2576–2589.
- Saleh, M., Takahashi, K., Amit, Y., & Hatsopoulos, N. G. (2010). Encoding of coordinated grasp trajectories in primary motor cortex. *The Journal of Neuroscience : The Official Journal of the Society for Neuroscience*, 30(50), 17079–90. <http://doi.org/10.1523/JNEUROSCI.2558->

10.2010

- Saleh, M., Takahashi, K., & Hatsopoulos, N. G. (2012). Encoding of coordinated reach and grasp trajectories in primary motor cortex. *The Journal of Neuroscience : The Official Journal of the Society for Neuroscience*, 32(4), 1220–32. <http://doi.org/10.1523/JNEUROSCI.2438-11.2012>
- Schieber, M. H. (1995). Muscular Production of Individuated Extrinsic Finger Muscles Finger Movements : The Roles of Extrinsic Finger Muscles. *J Neurosci*, 15(1), 284–297.
- Scott, S. H. (1999). Apparatus for measuring and perturbing shoulder and elbow joint positions and torques during reaching. *Journal of Neuroscience Methods*, 89(2), 119–127. [http://doi.org/10.1016/S0165-0270\(99\)00053-9](http://doi.org/10.1016/S0165-0270(99)00053-9)
- Serlin, D. M., & Schieber, M. H. (1993). Morphologic regions of the multitendoned extrinsic finger muscles in the monkey forearm. *Acta Anatomica*, 146(4), 255–66. Retrieved from <http://www.ncbi.nlm.nih.gov/pubmed/8317203>
- Soso, M. J., & Fetz, E. E. (1980). *Responses of Identified Cells in Postcentral Cortex of Awake Monkeys During Comparable Active and Passive Joint Movements*. *Journal of neurophysiology* (Vol. 43). Retrieved from <https://depts.washington.edu/fetzweb/assets/soso-fetz-jnp-1980.pdf>
- Sur, M., Merzenich, M. M., & Kaas, J. H. (1980). Magnification, receptive-field area, and “hypercolumn” size in areas 3b and 1 of somatosensory cortex in owl monkeys. *Journal of Neurophysiology*, 44(2), 295–311. Retrieved from <http://www.ncbi.nlm.nih.gov/pubmed/7411189>
- Sur, M., Wall, J. T., & Kaas, J. H. (1984). *Modular Distribution of Neurons With Slowly Adapting and Rapidly Adapting Responses in Area 3b of Somatosensory Cortex in Monkeys*. *JOURNAL OF NEUROPHYSIOLOGY* (Vol. 51). Retrieved from [https://s3.amazonaws.com/academia.edu.documents/32816692/1984\\_SurWallKaas.pdf?AWSAccessKeyId=AKIAIWOWYYGZ2Y53UL3A&Expires=1535080697&Signature=fAVCH78Zq8%2FJnq%2FAMs3W0aTnhmw%3D&response-content-disposition=inline%3Bfilename%3DModular\\_Distribution\\_of\\_Neurons\\_With\\_Slo.pdf](https://s3.amazonaws.com/academia.edu.documents/32816692/1984_SurWallKaas.pdf?AWSAccessKeyId=AKIAIWOWYYGZ2Y53UL3A&Expires=1535080697&Signature=fAVCH78Zq8%2FJnq%2FAMs3W0aTnhmw%3D&response-content-disposition=inline%3Bfilename%3DModular_Distribution_of_Neurons_With_Slo.pdf)
- Umilta, M. A., Brochier, T., Spinks, R. L., & Lemon, R. N. (2007). Simultaneous Recording of Macaque Premotor and Primary Motor Cortex Neuronal Populations Reveals Different Functional Contributions to Visuomotor Grasp. *J Neurophysiol*, 98, 488–501. <http://doi.org/10.1152/jn.01094.2006>
- Wang, W., Chan, S. S., Heldman, D. A., & Moran, D. W. (2007). Motor Cortical Representation of Position and Velocity During Reaching. *J Neuro-Physiol*, 97, 4258–4270. <http://doi.org/10.1152/jn.01180.2006>
- Weber, D. J., London, B. M., Hokanson, J. a, Ayers, C. a, Gaunt, R. a, Torres, R. R., ... Miller, L. E. (2011). Limb-state information encoded by peripheral and central somatosensory

neurons: implications for an afferent interface. *IEEE Transactions on Neural Systems and Rehabilitation Engineering : A Publication of the IEEE Engineering in Medicine and Biology Society*, 19(5), 501–13. <http://doi.org/10.1109/TNSRE.2011.2163145>

Yau, J. M., Connor, C. E., & Hsiao, S. S. (2013). Representation of tactile curvature in macaque somatosensory area 2. *Journal of Neurophysiology*, 109(12), 2999–3012. <http://doi.org/10.1152/jn.00804.2012>

Yau, J. M., Kim, S. S., Thakur, P. H., & Bensmaia, S. J. (2016). Feeling form: the neural basis of haptic shape perception. *Journal of Neurophysiology*, 115(2), 631–642. <http://doi.org/10.1152/jn.00598.2015>

## **CHAPTER 5:**

### **The case against synergies for hand shaping**

#### **Introduction**

As described in Chapter 4, we found that the response fields of neurons in sensorimotor cortex comprised multiple joints often spanning the entire hand. The principles that might underlie this structure eluded us, however. We reasoned that response fields might reflect hand kinematic synergies. From the strong interpretation of synergies, if these reflect a simplified control system, where each synergy constitutes a “knob” that drives one aspect of hand movements, these knobs should be reflected in the cortical representation of hand movements. Even a weaker interpretation of synergies – that they simply reflect correlated patterns of joint movements – would predict that the correlational structure of the kinematics might be reflected in the brain by virtue of simple Hebbian principles.

To investigate the role that putative postural synergies play in cortical representations of the hand, we 1) revisit the complexity—i.e., dimensionality—of the kinematic and neural data and 2) determine the extent to which low-dimensional representations of kinematic space are preferentially encoded in patterns of neural activity. We find that two critical predictions of the synergy hypothesis fail to materialize: 1) joint angle kinematics that reside outside the low-dimensional manifold are not merely motor noise, but are instead under volitional control; and 2) neuronal responses in sensorimotor cortices are not better explained by a synergy reference frame than they are by kinematics in a joint angular or musculotendon length reference frame.

#### **Complexity of kinematics and sensorimotor cortical responses**

In Chapter 3 we use principal component analysis (PCA) to identify the dimensionality of hand kinematics and the neuronal representations thereof. We find that, while fewer than 10 joint

angular “synergies” quantified in this manner are needed to explain 90% of kinematic variance, kinematic classifiers make use of putative “noise” dimensions outside the 9-dimensional synergy manifold, suggesting that such dimensions are under volitional control and are reliably manipulated to adopt different object-specific grasps. Moreover, we find that the dimensionality of neural population activity exceeds that of the kinematics, which would seem to suggest on the surface that putative hand postural synergies are not preferentially encoded in cortex.

Next, we wished to more explicitly test the synergy hypothesis by applying generalized linear models (GLMs) with synergies as regressors to predict firing rates. Indeed, individual neurons seem to track the states of multiple joints spanning the entire hand simultaneously. If these joint combinations match the computed kinematic synergies, then synergy-based models should be more compact and parsimonious than joint-based ones.

### **Testing preferential encoding of individual synergies**

One possibility is that individual neurons in sensorimotor cortex preferentially encode individual synergies. To test this hypothesis, we implemented GLMs with a single joint or a single synergy as regressor to explain the neuronal firing rates, as has been previously done with M1 responses (Kirsch, Rivlis, & Schieber, 2014; Mollazadeh, Aggarwal, Thakor, & Schieber, 2014). In brief, each of 60 GLMs, with each regressor being the angular position or velocity of one axis of rotation of one joint, is used to estimate the firing rate of each neuron. Note that the joint-based models differ from those implemented in Chapter 4 in that only one regressor is used per model. Similarly, each synergy-based GLM uses regressors comprising the principal component (PC) scores, or their derivatives, from each PC. Principal components are computed for joint angles only then PC scores are differentiated to compute the PC velocities. GLMs are computed at a range of physiologically plausible lags, and the pseudo- $R^2$  of the GLM at the best-fit single lag is selected

for each joint or synergy. We then compare the highest cross-validated pseudo- $R^2$  from joint-based models to that from synergy-based models for each neuron. We find that the fit of the best joint-based GLM is comparable to the fit of the best synergy-based GLM (Figure 5-1). If anything, firing rates are slightly better explained by the best joint than by the best synergy (two-tailed paired-samples T-test,  $T(85) = 2.909$ ,  $p = 4.626e-03$ ).

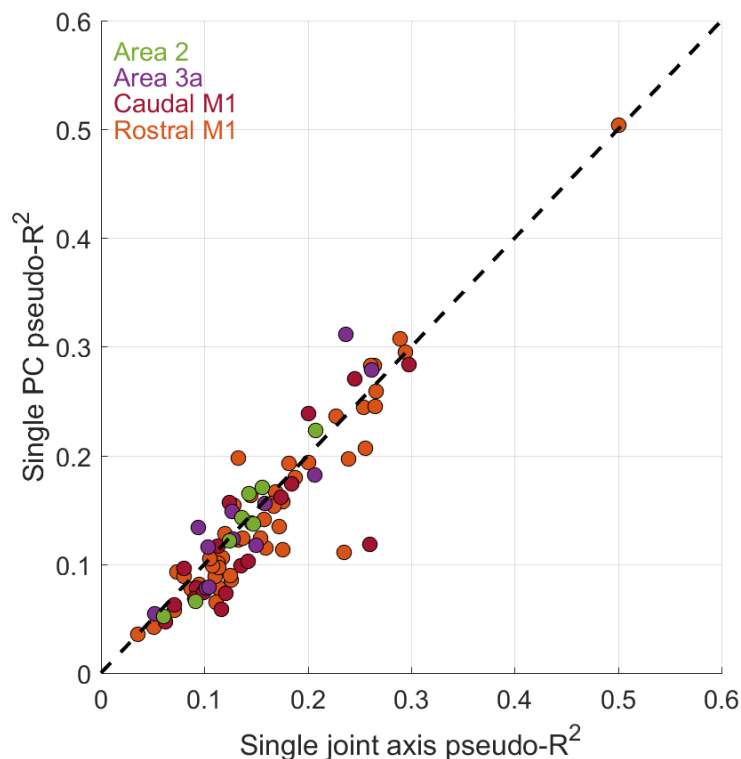


**Figure 5-1.** Comparison of the peak pseudo- $R^2$  of a single joint axis GLM against that of a single principal component (PC) GLM. Peak pseudo- $R^2$  are computed for each model at their own respective optimal lags. The results of GLMs shown here are computed for those neurons with a peak multi-joint pseudo- $R^2$  value of at least 0.20. We note, as has been noted previously in M1 alone for lower-dimensional recordings of individuated finger movements (Kirsch et al., 2014; Mollazadeh et al., 2014), that neurons in sensorimotor cortices with hand response fields (RFs) do not preferentially encode any one PC of hand joint angles over a particular joint angular axis. In fact, the best PC model tends, on average, to be slightly worse-fitting than the best single joint-axis model when pooling results across areas (statistics in text).

Of course, models based on single joints are not as good as those based on multiple joints. However, results from this analysis suggest that at least one interpretation of the synergy

hypothesis does not hold, namely that individual neurons preferentially encode individual synergies.

### **Testing preferential encoding of mixtures of synergies with GLMs**

Another possibility is that the kinematic manifold derived using PCA constitutes a more relevant frame of reference for the neuronal representations of the hand than do individual joint angles and velocities. For example, co-varying joints tend to be grouped together in this rotated space, so to the extent that neurons encode correlated joint angles or movements, PCs will yield more parsimonious models of neuronal responses than do single joints. To test this hypothesis, we fit GLMs as previously described in Chapter 4 and counted the number of joints comprising each neuron's response field (RF). We then repeated the same analysis but using PCs as regressors. We then compared the parsimony afforded by each model: How many significant regressors are needed in joint and in synergy space?

First, we show that the goodness-of-fit of the two models – joint-based and synergy based – was equivalent, as expected since all models had access to all of the variance in the kinematics, albeit in different coordinate frames (Figure 5-2). Second, we found that the required number of PCs was comparable to the required number of joints (Figure 5-3). Roughly 8 PCs, on average, were required to account for the amount of variance explained by 8 joints spanning the entire hand. Moreover, we found that the majority of neurons—190/249 (~76.3%) of neurons across all areas with peak  $R^2 > 0.05$ —had PC-based RFs that included at least one “noise” PC, i.e. a PC beyond the variance cut-off (95% explained). This result, consistent with the kinematic classification results from Chapter 3 wherein low-variance PCs contribute to kinematic-based object classification, suggest that these low-variance PCs are not just noise. These results also suggest

that the kinematic space defined by synergies does not provide a more parsimonious account of the neuronal representation of hand movements and postures than do individual joints.

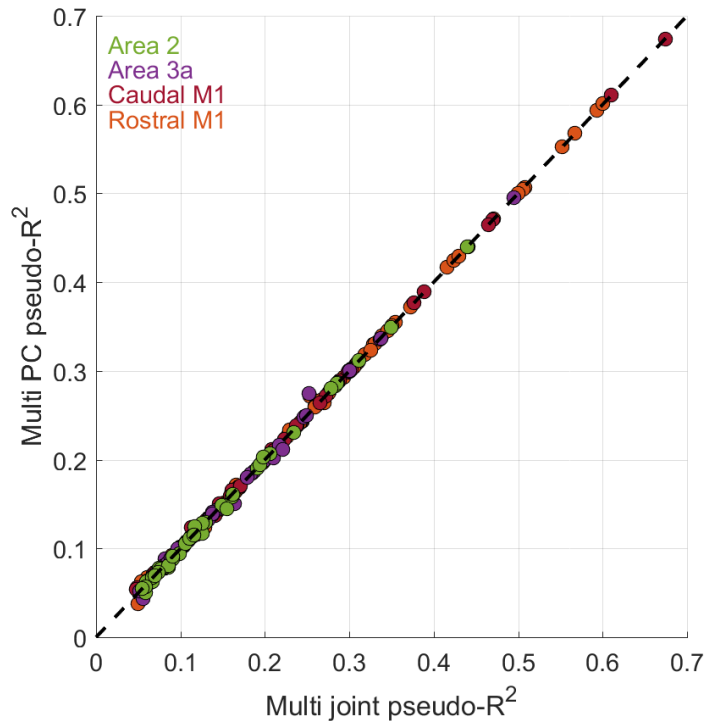


**Figure 5-2.** Pseudo-R<sup>2</sup> of GLMs fit using multiple predictors defined in a joint coordinate frame (abscissa) plotted against those with predictors defined in a principal component (PC) coordinate frame (ordinate). We find that even when regularizing regressions and cross-validating with respect to the LASSO penalty to obtain the best out-of-sample goodness-of-fit, both models fit neural spiking activity similarly well. All models shown have a pseudo-R<sup>2</sup> of at least 0.05.

### Testing synergy encoding in the activity of neuronal ensembles

One might argue that kinematic synergies may not be reflected in the responses of individual neurons but rather in the activity of populations of neurons. Indeed, preferential encoding of synergies has been previously shown at the population level in primary motor cortex (M1) during reach-to-grasp (Overduin, d'Avella, Roh, Carmena, & Bizzi, 2015). In particular, individual PCs of trial-averaged neural activity seemed to track individual PCs of hand kinematics, at least within a highly constrained task paradigm.

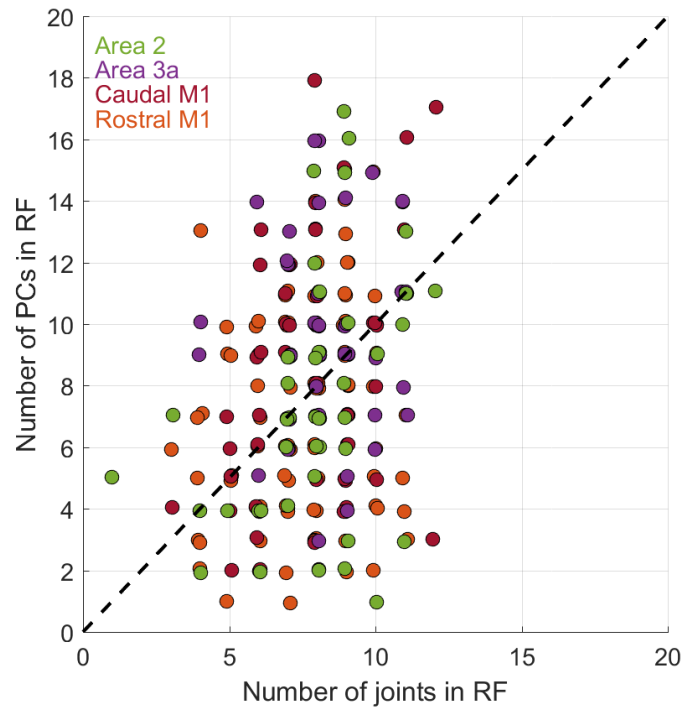


**Figure 5-3.** The number of joints in a neuron’s RF (abscissa) plotted against the number of PCs in that neuron’s RF (ordinate). We find a lack of a significant difference, on average, between the number of PCs or the number of joints needed to explain single neurons’ spiking activity (statistics in text). Moreover, we find that in multi-PC models, the majority of neurons include in their RF at least one low-variance PC generally considered to reside outside of the hand postural synergy manifold (see text). All models shown have a pseudo- $R^2$  of at least 0.05.

To investigate this possibility, we used PCA to obtain principal component scores of trial-averaged firing rates of populations of neurons for each cortical field. We then used PCA to obtain similar scores of trial-averaged kinematics. These two analyses each started with a tensor of size  $T \times N \times O$ , where  $T$  is the number of time bins (50) extending from 500ms to 10ms prior to object contact,  $N$  is the number of neurons or joints recorded from a given monkey, and  $O$  is the number of objects used in the study. We then smoothed neuronal responses with a 35-ms centered Gaussian kernel and averaged kinematics across trials spanning multiple sessions from the same animal, which was not possible with neural data as each session yielded a different sample of neurons. Instead, neural data from different trials were concatenated to obtain a new tensor where the

number of neurons,  $N$ , was equal to the sum of neurons recorded from all sessions. We then rearrange the resultant neural and kinematic tensors such that they were both of size  $(TO) \times N$ , with  $N$  being different for the neural and kinematic matrices, and performed PCA on these reshaped tensors. Each time-varying kinematic PC score and its temporal derivative was then cross-correlated with each neuronal PC score. The peak cross-correlation with kinematic PCs was then compared with the peak cross-correlation with individual joint angular coordinates.

In this case, we take *kinematic* PCs to be kinematic synergies and the *neural* PCs to be “neural ensembles” that describe correlated activity among populations of neurons. Even among these neural ensembles, we found no preferential encoding of kinematic synergies; individual joints were as good predictors of neuronal PC scores as were individual kinematic synergy scores (Figure 5-4) (two-tailed paired-samples T-test,  $T(289) = 0.420$ ,  $p = 6.745e-01$ ). To verify that this result was not an artifact of trial averaging, we recomputed the relationship between synergies and trial-averaged neuronal responses (Figure 5-5) to again find that individual joint regressors were slightly better predictors of spiking activity than were individual synergy regressors (two-tailed paired-samples T-test,  $T(319) = 10.388$ ,  $p = 5.632e-22$ ), replicating results obtained using individual trial responses (Figure 5-1).

We conclude that even a measure of population-level activity in sensorimotor cortices fails to show evidence of preferential encoding of hand postural synergies. Traditional dimensionality reduction applied to the neural data reveals neural dimensions no more correlated with individual synergies than with individual joint angles.

## Discussion

Analysis of the kinematics reveals that components of hand posture outside of the 9-dimensional “synergy” manifold revealed by PCA still convey object specific information. These

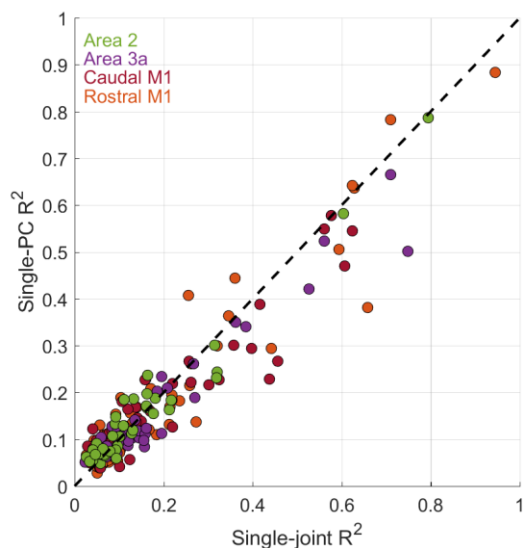


**Figure 5-4.** Trial-averaged “neuronal ensemble”  $R^2$  measures using single joint axes of rotation—both the angles and angular velocities about these axes of rotation—as predictors in a multiple linear regression model (ordinate) plotted against similar models using individual PCs of hand joint movements (ordinate). We note a lack of significant difference in terms of the number of individual joint axes of rotation or kinematic PCs needed to explain neural ensemble activity (statistics in text). All models shown have a maximum pseudo- $R^2$  of at least 0.05.

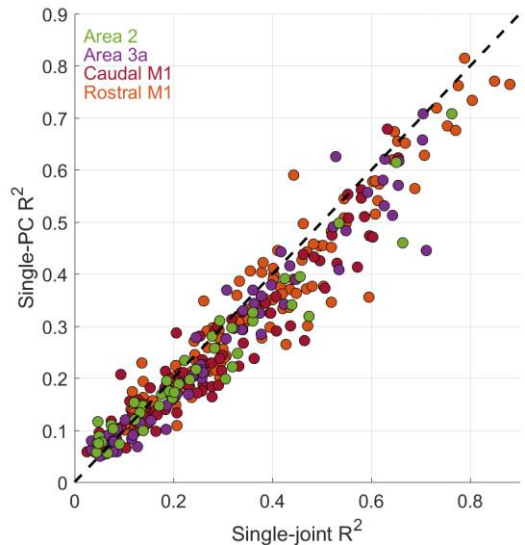


**Figure 5-5.** Trial-averaged single-neuronal firing rate  $R^2$  measures using the same predictors on the ordinate and abscissa as in Figure 5-4. We note that even when averaging across trials, neural activity is no better explained by individual PCs of hand kinematics than by individual joint axes of rotation—in fact, individual joint axes of rotation explain slightly more variance in single-neuronal firing rates than do individual PCs (statistics in text). All models shown have a maximum pseudo- $R^2$  of at least 0.05.

components – traditionally considered to be “noise” – thus seem to be under volitional control and contribute to precise grasping behavior, consistent with previous results, even from studies advocating for a low dimensionality of hand movements (Santello, Flanders, & Soechting, 1998, 2002). This finding contradicts the strong interpretation of the synergy hypothesis, which suggests that these components reflect motor noise rather volitional movement (e.g., McKay & Ting, 2008).

We implemented several tests of the hypothesis that neuronal representations of the hand in sensorimotor cortex reflect postural synergies. First, we found no compelling evidence for preferential encoding of synergies in the responses of *individual* sensorimotor neurons. Indeed, individual synergies were not preferentially encoded over individual joints, and low-variance PCs significantly contributed to the predictions of neuronal responses. Second, using a similar strategy, we found no compelling encoding of synergies in the responses of *populations* of sensorimotor neurons. To the extent that the space of possible kinematics is reduced in control or tracking, this reduced dimensionality is not reflected in neuronal representations of the hand in sensorimotor cortex.

Our conclusions stand in stark contrast with reports of the representation of synergies in M1 (Overduin et al., 2015), but this discrepancy can be accounted for by three key differences. First, in the previous study, the correlation between kinematic synergies and neuronal population responses was observed when data were averaged across trials, but degraded substantially in single-trial analyses. Second, the monkeys performed a small range of movements, which inflated the proportion of variance explained by the first three PCs relative to what we report with a wider variety of hand movements, with such simplified structure likely being further amplified by the aforementioned trial-averaging. Third, the observed correlation was not tested against an alternative hypothesis of neural coding, namely by comparing synergy encoding to single joint or

muscle encoding. Other work on movement representations in M1 (Kirsch et al., 2014; Mollazadeh et al., 2014) also find a lack of preferential encoding of movement synergies, which we extend to somatosensory cortical representations.

Furthermore, the high-dimensional structure in the neuronal representation of the hand that we see in Chapter 3 is consistent with the notion that hand movements exist in a high dimensional space and are not reduced to a more manageable set of synergies—at least to the extent that standard linear methods of dimensionality reduction obtain a suitable estimate of neural dimensionality.

### **Conclusion**

We do not observe preferential encoding of hand postural synergies at either the single-neuron or the neuronal population level. Indeed, a joint-centered reference frame offers just as good and parsimonious an explanation of neural activity as does a synergy-centered reference frame. Moreover, we find that when considering a PC-centered reference frame, low-variance PCs, traditionally considered motor noise by postural synergy models of hand movements, seem to be predictive of the spiking activity of neurons in hand sensorimotor cortices. These findings are consistent with a view that hand movements – and their neuronal representations – occupy a high dimensional space.

## References

- Kirsch, E., Rivlis, G., & Schieber, M. H. (2014). Primary Motor Cortex Neurons during Individuated Finger and Wrist Movements: Correlation of Spike Firing Rates with the Motion of Individual Digits versus Their Principal Components. *Frontiers in Neurology*, 5(May), 70. <http://doi.org/10.3389/fneur.2014.00070>
- McKay, J. L., & Ting, L. H. (2008). Functional muscle synergies constrain force production during postural tasks. *Journal of Biomechanics*, 41(2), 299–306. <http://doi.org/10.1016/J.JBIOMECH.2007.09.012>
- Mollazadeh, M., Aggarwal, V., Thakor, N. V., & Schieber, M. H. (2014). Principal components of hand kinematics and neurophysiological signals in motor cortex during reach to grasp movements. *Journal of Neurophysiology*. <http://doi.org/10.1152/jn.00481.2013>
- Overduin, S. A., d'Avella, A., Roh, J., Carmena, J. M., & Bizzi, E. (2015). Representation of Muscle Synergies in the Primate Brain. *The Journal of Neuroscience : The Official Journal of the Society for Neuroscience*, 35(37), 12615–24. <http://doi.org/10.1523/JNEUROSCI.4302-14.2015>
- Santello, M., Flanders, M., & Soechting, J. F. (1998). Postural Hand Synergies for Tool Use. *The Journal of Neuroscience*, 18(23), 10105–10115.
- Santello, M., Flanders, M., & Soechting, J. F. (2002). Patterns of Hand Motion during Grasping and the Influence of Sensory Guidance. *The Journal of Neuroscience*, 22(4), 1426–1435.

## **CHAPTER 6:**

### **Conclusions**

#### **Summary of results**

The hand is a complex and versatile effector that endows us with a remarkable ability to interact with objects flexibly and effortlessly. Hands also enable amazing dexterity, epitomized by elite musicians. The objective of the present study is to shed light on the neural mechanisms that mediate the dexterity of the hand, focusing on the sensory component responsible for tracking hand movements and postures. To this end, we measure hand kinematics as animals perform a grasping task while we record the responses evoked in sensorimotor cortex. We then seek to assess how the hand kinematics are encoded in the responses of cortical neurons.

First, we find that hand kinematics occupy a higher-dimensional manifold than has been previously reported. Indeed, while a large proportion of variance in the kinematics is contained in a handful of principal components, the remaining variance contains significant information about hand movements and is thus not simply noise, as is sometimes implied.

Second, somatosensory proprioceptive and motor neurons with response fields on the hand preferentially encode posture over movement, in contrast to their counterparts with response fields on the proximal limb. Whether this preference is actively achieved through specialized neural circuits or a consequence of the different inertial properties of the hand relative to the arm is up for debate. However, these differences in response properties may be interpreted as reflecting differences in the function of the hand and arm. The role of the arm is to place the hand somewhere in three dimensional space, the role of the hand is to adopt task appropriate configurations. Proximal limb control may thus be better achieved using a movement-based representation and hand control using a posture-based one.

Third, the response fields of neurons in somatosensory and motor cortex tend to span multiple joints distributed across the hand. Seeking a principle that might underlie the structure of the response fields, we examined whether the correlational structure in joint kinematics might shape these. Specifically, we examined whether kinematic synergies were preferentially encoded in the responses of individual neurons and populations of neurons and found no such relationship existed. Thus, if there is a principle that determines the structure of motor and proprioceptive response fields on the hand, that principle eludes us.

### **Avenues of future research**

#### **Sensorimotor interplay**

One of the interesting and possibly surprising results from the present study is the similarities in the somatosensory and motor cortical representations of the hand. Indeed, in both sensory and motor fields, postures are preferentially encoded over movements and neurons encode multi-digit swaths of hand. Moreover, these properties of motor and proprioceptive representations of the hand are similar whether they are driven by active or passive movements of the hand.

A natural question is whether these similarities arise from functional connections between the two cortical fields. If so, what patterns of connectivity might give rise to such similar-looking representations of hand posture? Prior research has found the presence of sensory-like neurons in primary motor cortex (Hatsopoulos & Suminski, 2011; Lemon, 1981; Lemon, Hanby, & Porter, 1976), which could arise from sensory input originating in somatosensory cortex. Moreover, investigations of proprioceptive sensory areas, both area 3a (Fromm & Evarts, 1982) and area 2 (London & Miller, 2013; Soso & Fetz, 1980), have revealed responses that precede movement onset, which could arise from the flow of information in the other direction, an “efference copy” from motor to sensory cortex. The importance of such an efference copy has been established in a

number of organisms and behaviors (Cullen, 2004), and the likely role of such sensory predictions of motor outputs during object manipulation has also been discussed (Johansson & Flanagan, 2009).

One approach to dissect the signaling between somatosensory and motor cortex is through measures of spike-field coherence between the two areas. Indeed, such measures have been employed in the past to infer patterns of connectivity between somatosensory and motor cortices during orofacial movements (Arce-Mcshane, Hatsopoulos, Lee, Ross, & Sessle, 2014; Arce-McShane, Ross, Takahashi, Sessle, & Hatsopoulos, 2016). Measurements like these in the limb representations may shed light as to the nature of the signals and their roles in motor control.

### **Informing studies of proprioceptive phenomenology**

In addition to the similarity between motor and somatosensory response properties, we note preferential coding of hand postures over movements in proprioceptive somatosensory cortices. In particular, this contrasts with somatosensory cortical responses observed during proximal limb movements, which appear to preferentially encode velocities of the limb (Weber et al., 2011). This differential sensitivity to posture and movement in the respective neural representations of the proximal and distal limb may be reflected in differential perceptual sensitivity to posture and movement for the arm and the hand.

While some previous psychophysical experiments have investigated proprioceptive acuity at the elbow and the digits (Hall & McCloskey, 1983), no attempt was made to disentangle movement from posture perception. In other studies, the perception of posture was separated from that of movement (Cordo, Gurfinkel, & Levik, 2000) by moving the limb so slowly that the movement was not sensed yet a reliably shifted percept of posture was generated. However, this

line of research focused exclusively on the proximal limb and on the separability of posture and movement perception rather than on differential sensitivity.

The present results raise the question of whether we can distinguish arm movements better than arm postures but can distinguish hand postures better than hand movements – as measured by, for example, just noticeable differences. We are currently testing these hypotheses in the laboratory.

### **The dimensionality of hand movements**

We report that hand movements span a higher-dimensional continuum than typically reported. Moreover, to the extent that one could consider hand movements and their neural control “low”-dimensional, proprioceptive and motor cortices do not appear to preferentially represent hand kinematics in terms of “synergies” rather than in terms of joints. We emphasize that we observe this high-dimensional structure during hand movements confined to prehensile movements. One might wonder whether the full range of hand movements – beyond prehensile ones – would be even higher-dimensional.

However, investigations of non-prehensile movements such as typing, piano playing, and sign language finger-spelling (Santello, Baud-Bovy, & Jörntell, 2013) all seem to conclude separate low-dimensional structure in each particular repertoire of hand movements. Such low-dimensional structure has yet to be challenged for these types of movement directly: Little has been done in terms of investigating the degree of overlap of the low-dimensional continua defining each of these behaviors. Furthermore, theories such as optimal feedback control suggest that the low-dimensional structure frequently implied by synergies, rather than reflecting fundamental constraints on the motor system in all contexts, instead reflects highly-task-specific structure in

the movements of the hand (Todorov & Jordan, 2002). Moreover, the effect of combining all such behaviors on the apparent dimensionality of the hand remains to be elucidated.

### **The integration of touch and proprioception**

When we grasp an object, we acquire information about its three dimensional structure based on signals from the hand, a perceptual ability termed stereognosis. Information about the local geometry of the object at each point of contact is conveyed by cutaneous nerve fibers whereas information about the conformation of the hand – and thus the relative positions of those points of contact – is carried by proprioceptive nerve fibers, primarily innervating the muscles and tendons. These two streams of information must be integrated to achieve stereognosis (Hsiao, 2008).

Geometric features of an object have been shown to be encoded in the responses of neurons in the cutaneous fields of somatosensory cortex (Bensmaia, Denchev, Dammann 3rd, Craig, & Hsiao, 2008; Yau, Connor, & Hsiao, 2013). We show that hand conformation is encoded in the responses of the proprioceptive fields, particularly area 3a. Area 2 is the first stage along the medial lemniscal pathway where cutaneous and proprioceptive signals converge (Kaas, 1983) and this convergence gives rise to neurons that exhibit both proprioceptive and tactile responses (Pons, Garraghty, Cusick, & Kaas, 1985). How these two streams of information are combined to achieve stereognosis is unknown. The answers to such questions will require precisely measuring time varying the contact events and time varying hand kinematics while recording the responses evoked in sensorimotor cortex, an endeavor that is currently underway in the laboratory.

### **Decoding hand movements**

So far, we have described how hand kinematics are *encoded* in the responses of individual neurons. One might then wonder how faithfully hand kinematics can be *decoded* from the responses of populations of such neurons.

Most decoders of arm movements exploit the velocity tuning observed in M1 neurons and decode end-point velocity – i.e., the velocity of the hand – from these signals (e.g., Velliste, Perel, Spalding, Whitford, & Schwartz, 2008). Velocity is then integrated to estimate limb position. Given the postural preference of sensorimotor neurons with response fields in the hand, it may be that hand postural decoding may be more successful than velocity decoding. In fact, the few extant decoders of detailed hand posture directly decode the postures of the hand and its joints (e.g., Vargas-Irwin et al., 2010).

The notion of postural versus movement decoding of hand kinematics fits into the broader argument regarding coordinate frames encoded in M1, particularly as they pertain to the utility of such coordinate frames in the control of brain-machine interfaces. In addition to comparing postural against velocity decoding, one would need to validate the generalizability of such kinematic decoders, as a whole, against decoders of hand movements in a muscle-activity coordinate frame. Indeed, such online muscle activity decoders of arm movements have already shown promise as an alternative to kinematic decoders of arm movements (Ethier, Oby, Bauman, & Miller, 2012), in spite of the problem of needing to infer more muscle than kinematic degrees of freedom.

## References

- Arce-Mcshane, F. I., Hatsopoulos, N. G., Lee, J.-C., Ross, C. F., & Sessle, B. J. (2014). Modulation Dynamics in the Orofacial Sensorimotor Cortex during Motor Skill Acquisition. <http://doi.org/10.1523/JNEUROSCI.4367-13.2014>
- Arce-McShane, F. I., Ross, C. F., Takahashi, K., Sessle, B. J., & Hatsopoulos, N. G. (2016). Primary motor and sensory cortical areas communicate via spatiotemporally coordinated networks at multiple frequencies. *Proceedings of the National Academy of Sciences of the United States of America*, *113*(18), 5083–8. <http://doi.org/10.1073/pnas.1600788113>
- Bensmaia, S. J., Denchev, P. V., Dammann 3rd, J. F., Craig, J. C., & Hsiao, S. S. (2008). The representation of stimulus orientation in the early stages of somatosensory processing. *Journal of Neuroscience*, *28*(3), 776–786. <http://doi.org/10.1523/JNEUROSCI.4162-07.2008>
- Cordo, P. J., Gurfinkel, V., & Levik, Y. (2000). Position sense during imperceptibly slow movements. *Experimental Brain Research*, *132*, 1–9.
- Cullen, K. E. (2004). Sensory signals during active versus passive movement. *Current Opinion in Neurobiology*, *14*(6), 698–706. <http://doi.org/10.1016/J.CONB.2004.10.002>
- Ethier, C., Oby, E. R., Bauman, M. J., & Miller, L. E. (2012). Restoration of grasp following paralysis through brain-controlled stimulation of muscles. *Nature*, *485*(7398), 368–371. <http://doi.org/10.1038/nature10987>
- Fromm, C., & Evarts, E. V. (1982). Pyramidal tract neurons in somatosensory cortex: central and peripheral inputs during voluntary movement. *Brain Research*, *238*(1), 186–91. Retrieved from <http://www.ncbi.nlm.nih.gov/pubmed/6805854>
- Hall, L. A., & McCloskey, D. I. (1983). Detections of movements imposed on finger, elbow, and shoulder joints. *J Physiol*, *335*, 519–533.
- Hatsopoulos, N. G., & Suminski, A. J. (2011). Sensing with the Motor Cortex. *Neuron*, *72*(3), 477–487. <http://doi.org/10.1016/J.NEURON.2011.10.020>
- Hsiao, S. (2008). Central mechanisms of tactile shape perception. *Current Opinion in Neurobiology*, *18*(4), 418–424. <http://doi.org/10.1016/j.conb.2008.09.001>
- Johansson, R. S., & Flanagan, J. R. (2009). Coding and use of tactile signals from the fingertips in object manipulation tasks. *Nature Reviews Neuroscience*, *10*(5), 345–359. <http://doi.org/10.1038/nrn2621>
- Jones, C. L., Wang, F., Morrison, R., Sarkar, N., & Kamper, D. G. (2014). Design and Development of the Cable Actuated Finger Exoskeleton for Hand Rehabilitation Following Stroke. *IEEE/ASME Transactions on Mechatronics*, *19*(1), 131–140. <http://doi.org/10.1109/TMECH.2012.2224359>

- Kaas, J. H. (1983). What, if anything, is SI? Organization of first somatosensory area of cortex. *Physiological Reviews*, 63(1), 206–231. <http://doi.org/10.1152/physrev.1983.63.1.206>
- Lemon, R. N. (1981). Functional properties of monkey motor cortex neurones receiving afferent input from the hand and fingers. *The Journal of Physiology*, 311(1), 497–519. <http://doi.org/10.1113/jphysiol.1981.sp013601>
- Lemon, R. N., Hanby, J. A., & Porter, R. (1976). Relationship between the activity of precentral neurones during active and passive movements in conscious monkeys. *Proceedings of the Royal Society of London. Series B, Biological Sciences*, 194(1116), 341–73. <http://doi.org/10.1098/RSPB.1976.0083>
- London, B. M., & Miller, L. E. (2013). Responses of somatosensory area 2 neurons to actively and passively generated limb movements. *Journal of Neurophysiology*, 109(6), 1505–13. <http://doi.org/10.1152/jn.00372.2012>
- Pons, T. P., Garraghty, P. E., Cusick, C. G., & Kaas, J. H. (1985). The somatotopic organization of area 2 in macaque monkeys. *The Journal of Comparative Neurology*, 241(4), 445–466. <http://doi.org/10.1002/cne.902410405>
- Santello, M., Baud-Bovy, G., & Jörntell, H. (2013). Neural bases of hand synergies. *Frontiers in Computational Neuroscience*, 7, 23. <http://doi.org/10.3389/fncom.2013.00023>
- Sergio, L. E., & Kalaska, J. F. (1998). Changes in the Temporal Pattern of Primary Motor Cortex Activity in a Directional Isometric Force Versus Limb Movement Task. *Journal of Neurophysiology*, 80(3), 1577–1583. <http://doi.org/10.1152/jn.1998.80.3.1577>
- Soso, M. J., & Fetz, E. E. (1980). *Responses of Identified Cells in Postcentral Cortex of Awake Monkeys During Comparable Active and Passive Joint Movements*. *Journal of neurophysiology* (Vol. 43). Retrieved from <https://depts.washington.edu/fetzweb/assets/soso-fetz-jnp-1980.pdf>
- Todorov, E., & Jordan, M. I. (2002). Optimal feedback control as a theory of motor coordination. *Nature Neuroscience*, 5(11), 1226–1235. <http://doi.org/10.1038/nn963>
- Vargas-Irwin, C. E., Shakhnarovich, G., Yadollahpour, P., Mislow, J. M. K., Black, M. J., & Donoghue, J. P. (2010). Decoding Complete Reach and Grasp Actions from Local Primary Motor Cortex Populations. *The Journal of Neuroscience*, 30(29), 9659–9669. <http://doi.org/10.1523/JNEUROSCI.5443-09.2010>
- Velliste, M., Perel, S., Spalding, M. C., Whitford, A. S., & Schwartz, A. B. (2008). Cortical control of a prosthetic arm for self-feeding. *Nature*, 453(7198), 1098–101. <http://doi.org/10.1038/nature06996>
- Weber, D. J., London, B. M., Hokanson, J. a, Ayers, C. a, Gaunt, R. a, Torres, R. R., ... Miller, L. E. (2011). Limb-state information encoded by peripheral and central somatosensory neurons: implications for an afferent interface. *IEEE Transactions on Neural Systems and*

*Rehabilitation Engineering : A Publication of the IEEE Engineering in Medicine and Biology Society*, 19(5), 501–13. <http://doi.org/10.1109/TNSRE.2011.2163145>

Yau, J. M., Connor, C. E., & Hsiao, S. S. (2013). Representation of tactile curvature in macaque somatosensory area 2. *Journal of Neurophysiology*, 109(12), 2999–3012. <http://doi.org/10.1152/jn.00804.2012>

## **APPENDIX:**

### **Experimental and analytical materials and methods**

#### **Animals and surgery**

We recorded neural data from four male Rhesus macaques between 6 and 15 years of age and weighing between 8 and 11 kg. All animal procedures were performed in accordance with the rules and regulations of the University of Chicago Animal Care and Use Committee (IACUC). Monkeys received care from a full-time husbandry staff who maintained a 12hr/12hr light/dark cycle, cleaned the animals' living spaces once a week, and gave the animals ample food and enrichment. In addition, a full-time veterinary staff monitored the animals' health. Animals were water-restricted according to a protocol requiring monitoring their weights daily and ensuring an absolute daily minimum water consumption of 10 cc/kg.

Surgical procedures consisted of implantation of a head-fixing post onto the skull, craniotomy, implantation of a sealed recording chamber (monkeys 2-4), and implantation of chronic Utah electrode arrays (UEAs) and floating microelectrode arrays (FMAs) (monkey 1) or of semichronic Microdrive electrode arrays (monkeys 2-4). All procedures were performed under aseptic conditions and under anesthesia induced with ketamine HCl (20 mg/kg, IM) and maintained with isoflurane (10-25 mg/kg per hour, inhaled).

In addition to surgical procedures, monkeys 2-4 also underwent a magnetic resonance (MRI) scan to identify stereotactic coordinates of anatomic landmarks prior to array implantation. MRI scans were conducted using a 3T scanner while monkeys were anesthetized using a similar procedure to that used during surgery.

## **Grasp task**

Four monkeys were trained to grasp thirty-five distinct objects varying in shape, size, and orientation (Figure A-1A). As each monkey performed the task, the time-varying kinematics of the monkey's hand were recorded, as was the neural activity in primary somatosensory and motor cortices using chronically implanted electrode arrays. We used an industrial robot (MELFA RV-1A, Mitsubishi Electric, Tokyo, Japan) to present objects for the monkey to grasp (Figure A-1B). Objects were coupled to the robot with a magnet. On each trial, the monkey was required to grasp the object, hold it for an interval lasting one to three seconds, then maintain grasp of the object as the robotic arm pulled away (Figure A-1C). The animal was rewarded if the object remained in its hand as the robot retracted.

Because we wished to investigate hand movements, we sought to eliminate movements of the proximal arm associated with reaching. However, the use of restraints to hold the arm in place would introduce cutaneous inputs and isometric forces exerted against those restraints, which we would not measure but might affect the neural response. To minimize these confounds, we trained monkeys to volitionally hold their arms stationary while grasping objects. This was achieved by placing a photosensor under each arm (Figure A-1B) and only rewarding the monkeys when they performed the task without moving their arms off the sensors.

## **Kinematic recordings and processing**

Reflective markers were placed at 31 locations straddling the joints of the hand, wrist, forearm, and proximal arm (Figure A-1D). A camera-based motion tracking system (Vantage, VICON, Los Angeles, CA) was used to measure the time-varying three-dimensional coordinates of each of these markers. Ten cameras were used to capture the kinematics of the first monkey at a rate of 250 Hz, whereas fourteen cameras were used to capture the kinematics of the other

monkeys at a rate of 100 Hz. Each marker was then labeled using Nexus software (VICON, Los Angeles, CA).

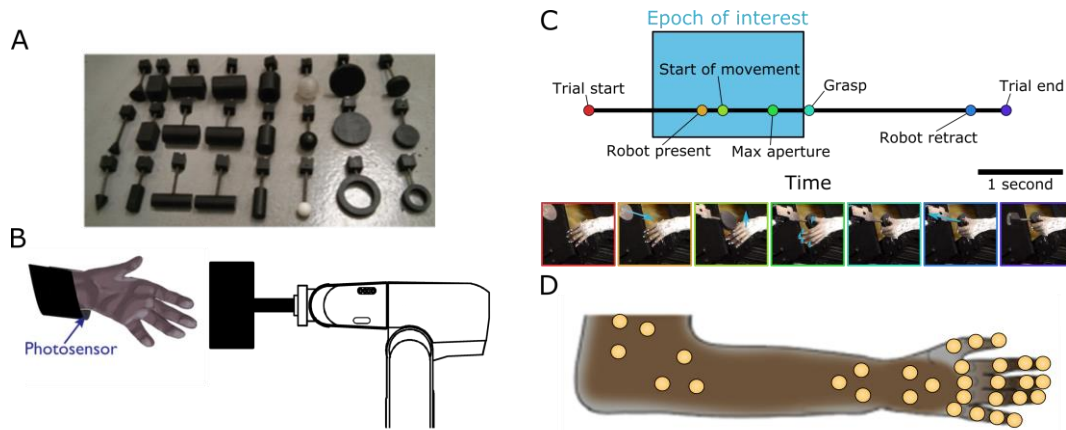


**Figure A-1.** Behavioral task and kinematic recording methods. **(A)** Set of objects varying in shape, size, and orientation to encourage different grasps. **(B)** Presentation of objects to a monkey. An object is magnetically mounted onto a robotic arm. The monkey is seated in a chair with a photosensor placed in its armrest to discourage reaching. A trial begins once an object is mounted to the robot and the monkey’s arm is appropriately positioned to cover the photosensor in its armrest. If at any point during a trial the monkey’s arm is lifted to expose the photosensor to light, the trial is aborted. **(C)** Task timeline. Once the trial starts, the robot positions itself to present the object to the monkey. Once the robot begins to move toward the monkey, the monkey performs a grasp. Each grasp is manually scored off-line for three kinematic events: the start of movement, max aperture, and object contact (i.e., grasp). Neural data from 700ms prior to the start of movement to 10ms prior to grasp comprise the epoch of interest for analysis. After grasp, the monkey then holds the object until the robot retracts. **(D)** Positioning of reflective markers (31 total) on the monkey’s hand for kinematic recording. Triangles are placed just proximal and distal to both the elbow and wrist joints, and markers on the hand are placed at the most distal portions of each metacarpal and phalanx of each digit. Cameras capture the time-varying three-dimensional positions of these markers. With the aid of a musculoskeletal model of the arm and hand, inverse kinematics can be computed to estimate joint angles.

Inverse kinematics were solved using labelled marker kinematics and a musculoskeletal model of the human arm (Anderson & Pandy, 2001; Anderson & Pandy, 1999; de Leva, 1996; S.L. Delp et al., 1990; Dempster & Gaughran, 1967; Holzbaur, Murray, & Delp, 2005; Yamaguchi & Zajac, 1989) ([https://simtk.org/projects/ulb\\_project](https://simtk.org/projects/ulb_project)) implemented in Opensim (Scott L. Delp et al., 2007) ([https://simtk.org/frs/index.php?group\\_id=91](https://simtk.org/frs/index.php?group_id=91)). Individual segments of the model were scaled on a monkey-by-monkey basis using static marker data and Opensim’s built-in scaling function. Segments were scaled such that the distance between any pair of markers in the model—

each of which was bound to a particular segment—matched the distance measured in the static marker data. Inverse kinematics then estimated joint angles of the scaled model such that the distance between its markers and the recorded marker positions were minimized on any given frame of marker video data during grasping movements. We hence obtained estimates of the time-varying joint angles giving rise to the observed marker movements. A total of 22 (Monkey 1) or 30 (Monkeys 2-4) joint angular coordinates, across 13 (Monkey 1) or 19 (Monkeys 2-4) joints, were reconstructed during inverse kinematics. These joint angular coordinates are listed in Table A-1.

Joint angle data were filtered first using a moving median filter (MATLAB `movmedian`) over a centered 83-ms window to remove outliers and sudden jumps in the kinematic data. The output of the moving median filter was then bidirectionally filtered using a 4<sup>th</sup> order low-pass Butterworth filter with a 6 Hz cutoff frequency (MATLAB `filtfilt`). The 4<sup>th</sup> order bidirectional 6Hz cutoff filter has basis in past kinematic data analysis of these hand joint kinematics (Saleh, Takahashi, Amit, & Hatsopoulos, 2010) and also dictated the 83-ms moving median window, which corresponds to the bin duration needed to detect frequency components up to 6Hz given the sampling rate (12 Hz) according to the Nyquist-Shannon sampling theorem. Joint angular velocities were then calculated by differentiating joint angles (MATLAB `diff`).

For each trial, we identified times at which the fingers or wrist began to move (Start), at which the fingers achieved maximum aperture (Max Aperture), and at which the monkey made contact with the object (Grasp). We scored these events manually for each trial.

## Neural recordings

We recorded neural signals from Monkey 1 using Utah electrode arrays (UEAs) (Blackrock Microsystems, Salt Lake City, Utah) placed in the post- and pre-central gyri and from floating

**Table A-1.** Joints and joint angular coordinates reconstructed during inverse kinematics. \* Joint not reconstructed for Monkey 1 kinematics. \*\* Joint angular coordinate not reconstructed for Monkey 1 kinematics.

Joint name	Axis of rotation	Joint name	Axis of rotation
Elbow*	Flexion/Extension (F/E)**	MCP 3	Ab/Ad
Wrist	F/E	PIP 3	F/E
	Deviation	DIP 3*	F/E**
	Supination/Pronation (S/P)	CMC 4	F/E
Carpometacarpal (CMC) 1	F/E	MCP 4	F/E
	Abduction/Adduction (Ab/Ad)		Ab/Ad
	Opposition**	PIP 4	F/E
Metacarpophalangeal (MCP) 1	F/E	DIP 4*	F/E**
	Ab/Ad	CMC 5	F/E
Interphalangeal (IP) 1*	F/E**		Ab/Ad
MCP 2	F/E		MCP 5
	Ab/Ad	F/E	
Proximal interphalangeal (PIP) 2	F/E		Ab/Ad
Distal interphalangeal (DIP) 2*	F/E**	PIP 5	F/E
MCP 3	F/E	DIP 5*	F/E**

microelectrode arrays (FMAs) (MicroProbes, Gaithersburg, MD) placed in the posterior and anterior banks of the central sulcus (Figure A-2A). For the other three monkeys, we recorded neural signals using arrays of depth-adjustable electrodes (SC96, Gray Matter Research, Bozeman,

MT) positioned over the central sulcus (Figure A-2B-E). All the array implants targeted the somatosensory and motor representations of the hand. Spikes were detected as manually-set threshold crossings in voltage traces sampled at 30 kHz then digitally high-pass filtered with a cutoff frequency of 200 Hz. Manual offline spike sorting (Offline Sorter, Plexon, Dallas, TX) was used to identify multiple units in an electrode if more than one was present and to remove non-spike threshold crossings.

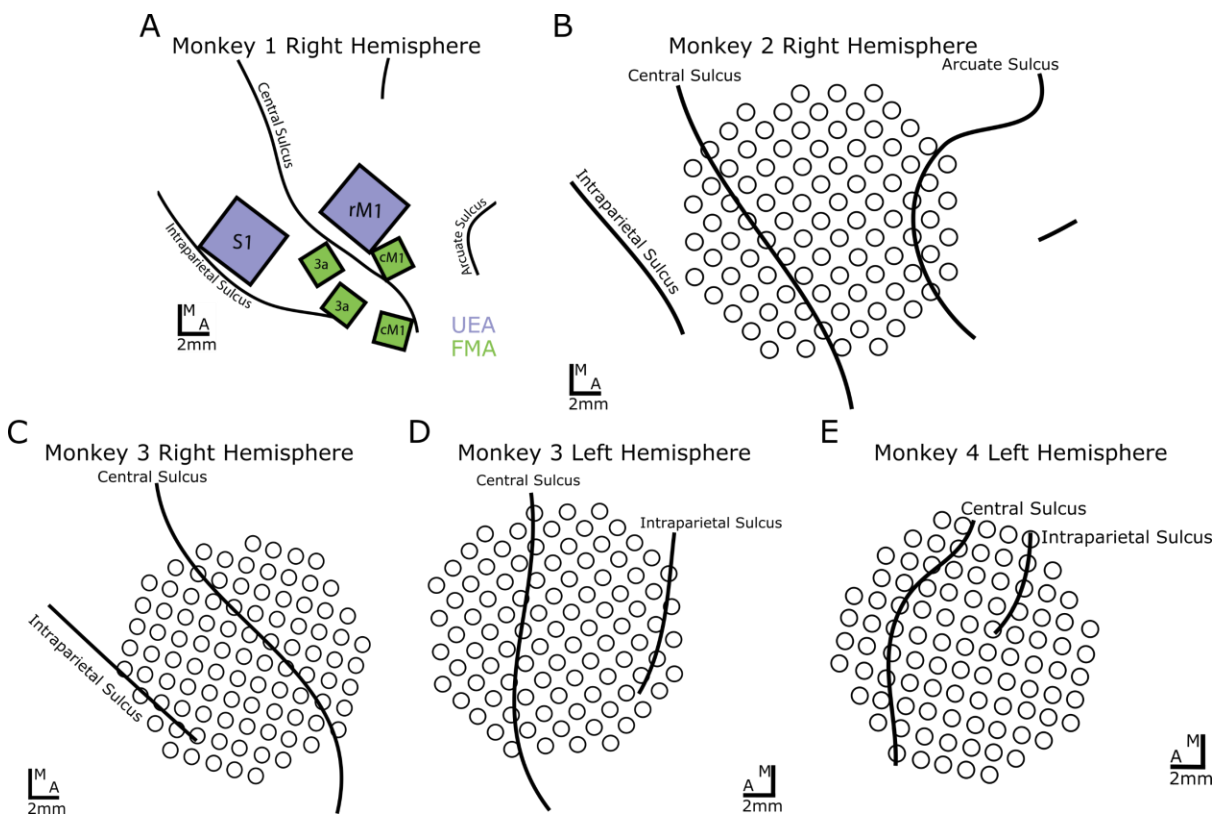


**Figure A-2.** Array placements relative to cortical surface landmarks. **(A)** Monkey 1 was implanted with two Utah electrode arrays (UEAs, Blackrock Microsystems, Salt Lake City, UT) in area 2 and rostral M1 and four floating microelectrode arrays (FMAs, Microprobes, Gaithersburg, MD) in area 3a and caudal M1. **(B-E)** Semichronic SC-96 arrays with individually depth-adjustable electrodes in **(B)** the right hemisphere of monkey 2, **(C)** the right hemisphere of monkey 3, **(D)** the left hemisphere of monkey 3, and **(E)** the left hemisphere of monkey 4.

### **Passive movement sessions**

To compare proprioceptive representation in active and passive touch, we also collected kinematic and neurophysiological data, using the approach described above, while the experimenter passively manipulated Monkey 4's hand. Hand manipulations targeted each individual joint and axis of rotation of the hand as detailed in Table A-1. Only one axis of rotation of one joint was explicitly targeted at any given time, although kinematic recordings were taken such that any joints that also underwent incidental movement—one not explicitly intended by the experimenter or through mechanical linkage with a manipulated joint—would be recorded.

### **Intracortical microstimulation**

A subset of Monkey 4's electrodes were platinum-iridium stimulating electrodes. These electrodes were distributed over the entire extent of the array. We applied intracortical microstimulation (ICMS) through these electrodes and noted any evoked muscle twitches to help determine the anatomical area in which each electrode was situated. Focal stimulation in area 3a, in particular, would be expected to fail to evoke low-threshold muscle twitches by virtue of its lack of monosynaptic projections to spinal motoneurons (Witham, Fisher, Edgley, & Baker, 2016), despite a preponderance of such projections in adjacent caudal M1 also deep in the bank of central sulcus. In a separate set of experiments, ICMS was applied in trains of 20 anodic-leading biphasic pulses delivered at 330 Hz with pulse width and interpulse interval both lasting 200 $\mu$ s and current amplitude ranging from 10-100 $\mu$ A. The presence of a muscle twitch and the identity of the twitching muscle were logged upon consensus of two trained electrophysiologists observing the arm during ICMS.

## **Proximal limb data**

To compare representations of distal vs. proximal limbs in sensorimotor cortex, we also analyzed the kinematics of the proximal limb along with the evoked neural responses as monkeys performed a standard delayed center-out reaching task, previously collected in the laboratory of Professor Nicholas Hatsopoulos (Hatsopoulos, Xu, & Amit, 2007; Kadmon Harpaz, Ungarish, Hatsopoulos, & Flash, 2018; Reimer & Hatsopoulos, 2010) and follow. Briefly, on each trial, the monkey was seated in a planar arm orthosis (KINARM, BKIN Technologies, Kingston, ON, Canada) and began a trial by placing and holding its hand within a radius of the orthosis workspace indicating the “center”. The monkey was then given a cue on a monitor indicating the location toward which to direct a reaching movement. The monkey was trained to wait a full second before a second, “go” cue was presented and the monkey was allowed to move their hand outside the small central radius. The monkey then moved its arm such that its hand—and consequently, the cursor on the screen coupled with its reaching kinematics—was within the cued radius indicating the target location. The monkey was then given a water reward after maintaining its hand in the target region for a few hundred milliseconds. A new trial began when the monkey returned its hand to the center of the workspace.

## **Data Analysis**

### **Dimensionality reduction**

We characterized monkeys’ hand movements using principal components analysis (PCA) on the reconstructed time-varying joint angles. We report  $N$ , the minimum number of components needed to account for 90% of the total variance in these data. Similarly, we also used PCA to characterize population firing rate data taken from 500ms to 10ms prior to grasp wherein the per-event time histograms (PETHs) were concatenated across recording sessions (see section “Pooling

data across sessions”). All dimensionality reduction was performed on non-standardized data, as has been done for other similar dimensionality reduction analyses (Thakur, Bastian, & Hsiao, 2008), which preserves scale information across joints with different ranges of motion and neurons with different ranges of firing rates. However, as other work that investigates dimensionality, particularly of neural data, has done so only after standardizing—i.e., computing the z-scores of—the data prior to computing principal components (Cunningham & Yu, 2014), we include additional figures in the relevant showing the effects of standardization.

### **Temporal alignment**

Classification analysis (see section “Classification algorithm”) required the tracking of object information over time across trials with different durations. To facilitate this comparison, we scored the kinematics for three events: the start of movement (Start), maximum aperture (Max Aperture), and grasp (Grasp) (see section “Kinematic recordings and processing”). Then, to obtain a fine sampling of times across trials, we interpolated nine evenly-spaced pseudo-events between the Start and Max Aperture events and between the Max Aperture and Grasp events. For each event and pseudo-event, after first aligning each trial to that event or pseudo-event, object classification was performed using the vector of instantaneous joint angles—where each vector element is the angle of a given joint—or the vector of spike counts from -500 ms to 0 ms relative to that event—where each vector element is a given neuron’s spike count over that interval.

### **Classification algorithm**

We used multi-class linear discriminant analysis (LDA, MATLAB `fitcdiscr`) with leave-one-out cross-validation to classify the object presented on each trial. For each event, for each cross-validation iteration, we used the  $N \times P$  data matrix  $X$ , where  $N$  is the number of trials—excluding the test trial—and  $P$  is the number of joint angles or neurons being considered, to train

the classifier to predict  $Y$ , the  $N \times 1$  vector of object labels—of which there were 35. Accuracy was then assessed as the fraction of test trials for which the presented object was correctly identified.

### **Pooling data across sessions**

As we were only able to record from 10 to 15 somatosensory cortical neurons per session, it was necessary to pool data across sessions to assess how classification performance scaled with the size of the neuronal population or characterize the dimensionality of sensorimotor neural representations.

Pooling was achieved under the assumption of conditional independence of each neuron. In particular, for each epoch and each session, we first randomly select one trial per object to obtain a test data set matrix of size  $O \times M$ , where  $O$  is the number of objects and  $M$  is the number of neurons recorded during a given session. We then concatenate these single-session trial vectors to generate a virtual test data matrix of size  $O \times P$ , where  $P$  is the number of neurons recorded across all sessions being pooled.

We then compute the mean rates, conditioned on each object, from the remaining training data for each neuron in each of the sessions to be pooled. This results in another matrix of size  $O \times M$ . We then subtract the object-conditioned mean—i.e., the appropriate row of the aforementioned  $O \times M$  matrix—from each row of the  $N \times M$  training neural data matrix for each session, where  $N$  is again the number of trials recorded during a given session that are in the training set. We then concatenate the de-measured  $N \times M$  neural data matrices across sessions to obtain a matrix of size  $N \times P$ . We use this matrix to estimate the  $P \times P$  within-subject covariance matrix,  $W$ . We constrain  $W$  to be a diagonal matrix per the assumption of conditional independence of each neuron.

We then concatenate all sessions'  $O \times M$  mean rate matrices to obtain an  $O \times P$  matrix of mean rates. We then estimate the  $P \times P$  between-object covariance matrix,  $B$ , from this  $O \times P$  matrix. We compute linear discriminant dimensions from the eigenvectors of  $W^{-1}B$  and project the  $O \times P$  test trial matrix onto this eigenvector space. We then classify each trial in this projected test trial matrix on the basis of a minimum Euclidean distance criterion. This procedure is repeated for 25 different cross-validation iterations.

We support our pooling procedure by investigating the similarity of each monkey's object-specific kinematics across different sessions. We note that, whether performing leave-one-out cross-validation or leave-one-session-out cross-validation, classification accuracy remains similar and follows a similar time course, indicating that monkeys performed similar object-specific grasps across sessions (Figure A-3).

To calculate the principal components of neural activity, we aligned all trials to the "grasp" event, computed the peri-event time histogram (PETH) for each neuron on an object-by-object basis, and concatenated those to obtain an estimate of the trial-averaged responses of a larger population of neurons. This resultant matrix was of size  $OT \times P$ , where  $P$  is the number of neurons recorded across all sessions,  $O$  is the number of objects, and  $T$  is the number of grasp-aligned samples over time. Neurons pooled in this manner were pooled across sessions but never across monkeys. We note that performing similar trial averaging on the kinematic data serves to reduce its apparent dimensionality (Figure A-4), meaning that the high neural dimensionality we report in the later chapters represents a lower bound on what could be obtained with large simultaneously recorded populations.

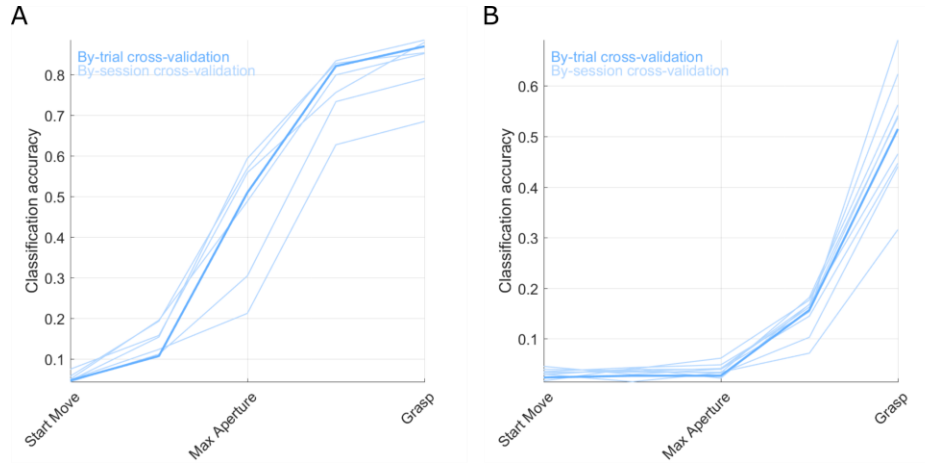


**Figure A-3.** Classification results for two types of cross-validation for **(A)** Monkey 2 and **(B)** Monkey 4, the two monkeys from which enough sessions (6 and 9, respectively) had been recorded to permit generalization in leave-one-session-out cross-validation. Faded traces indicate classification accuracy on one session after training on the other sessions recorded from that monkey. Bold traces indicate classification accuracy when leaving one trial out and training on all other trials pooled across sessions. Leave-one-trial-out cross-validation tends to match the overall accuracy and time course of the leave-one-session-out cross-validated accuracy curves. Kinematics across different sessions are therefore similar enough to minimize the hazard of pooling neural responses across those sessions.

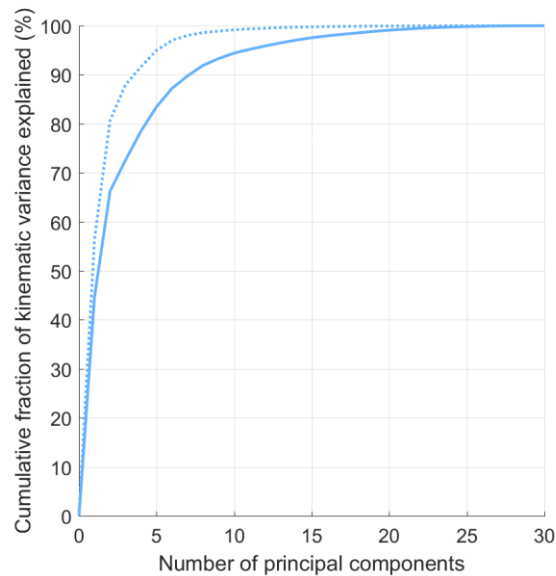


**Figure A-4.** Effect of averaging kinematics over repeated trials of the same object (pooled across sessions) on the apparent dimensionality of Monkey 2's kinematic data. Roughly 8-dimensional at 90% variance explained when not trial-averaged, the kinematics appear to be roughly 4-dimensional when trial-averaged. This indicates that within-trial variability acts to increase the apparent dimensionality of the kinematics, and presumably the neural data as well.

## Generalized linear model

We used a generalized linear model (GLM) to predict the response of each neuron from the hand kinematics. Specifically, we used spike responses starting 700 ms before the start of movement—to capture preparatory activity—to 10 ms prior to object contact—to eliminate cutaneous and kinetic contributions to the response. Kinematics between 1s prior to the start of movement and 290 ms following object contact were considered as predictors at various different lags: For example, a GLM of a motor neuron leading kinematics by 300 ms would predict firing rates using kinematics from 400 ms prior to the start of movement to 290 ms following grasp, and a model of a sensory neuron lagging kinematics by 100 ms would predict firing rates using kinematics from 800 ms prior to the start of movement to 110 ms prior to object contact. In total, 60 predictors were included in the GLM: 30 joint angles and 30 joint angular velocities. Prior to running the GLM, we also standardized the values of the kinematic predictors to remove any scale dependence that regression weights would otherwise exhibit. We use MATLAB code for the nonlinear input model (NIM) (<http://neurotheory.umd.edu/nimcode>) (Mcfarland, Cui, Butts, & Bethge, 2013) to implement GLMs reported in this paper.

The neural data and kinematics were down-sampled to 50 Hz (20 ms bins) prior to running the GLMs. Our implementation of GLM uses a Poisson noise model and an inverse-softplus link function— $X\beta = \log[-1 + \exp(\mu)]$ . Goodness-of-fit was measured using McFadden's pseudo- $R^2$ , which is analogous to the standard coefficient of determination,  $R^2$ , but generalized to account for Poisson noise by using model deviances rather than sums of squared residuals. Pseudo- $R^2$  is computed as follows:

$$Pseudo - R^2 = 1 - \frac{NLL_{model} - NLL_{saturated}}{NLL_{null} - NLL_{saturated}} \quad (A-1)$$

where  $NLL_{model}$  is the negative (poisson) log likelihood of the GLM's predictions of firing rate;  $NLL_{saturated}$  is the negative poisson log likelihood of a perfect model with as many predictors as spike count samples; and  $NLL_{saturated}$  is the negative Poisson log likelihood of a model that assumes the neuron has a constant firing rate. Models were fit only to neurons that spiked at least 100 times in the epoch of interest across all trials in a session to avoid spuriously high correlations resulting from extremely sparse-spiking neurons.

For proximal limb data, we also compared models that incorporated spike history predictors to those that did not. Spike history terms were constructed from neural data filtered with each of a logarithmically-spaced causal raised cosine basis set of smoothing kernels as has been described previously (Pillow et al., 2008; Saleh et al., 2010). A total of seven spike history predictors were added to each model in this manner.

### **Lag analysis**

To identify the optimal lag at which the responses of a given neuron are most closely related to the kinematics, we re-computed the GLM at lags spanning -250 ms—spikes leading the kinematics by 250 ms—to +250 ms—spikes lagging the kinematics by 250 ms (see section “Generalized linear model”). The lag at which the mean cross-validated pseudo- $R^2$  value was highest was taken to be that neuron's optimal response lag and selected for further analysis.

### **Regularization and cross-validation**

One of the objectives of this analysis was to determine which set of joints could account for the responses of a given neuron. To mitigate the risk of overfitting our GLMs and find the minimal set of joints needed to explain neural activity, we used the least absolute shrinkage and selection operator (LASSO), which penalizes the number of predictors in the GLM.

The strength of the LASSO penalty is set by a hyperparameter,  $\lambda$ . We fit  $\lambda$  to maximize the out-of-sample goodness-of-fit (pseudo- $R^2$ ) of firing rate predictions made by the GLM. We employ 60-20-20 cross-validation to fit our LASSO GLMs: In other words, we selected 60% of all samples taken across all trials of a session to train each GLM and obtain regression weights; 20% to act as a validation set to evaluate out-of-sample pseudo- $R^2$  for different values of  $\lambda$ ; and another 20% to estimate the goodness-of-fit of the best model (according to the validation set) on data that were used to fit neither the GLM predictor weights nor the hyperparameter  $\lambda$ .

### Interpreting encoding models

We compute a summary statistic to determine the number of joints in a typical neuron's response field. We also use a t-test to compare neuron-averaged pseudo- $R^2$  values across posture- and movement-based GLMs to determine preferential encoding of one relative to the other. Summary statistics and pseudo- $R^2$  comparisons were computed only for the subset of neurons with a cross-validated pseudo- $R^2$  value of at least 0.05.

Partial pseudo- $R^2$  values were also computed to assess the degree to which postures or movements were preferentially encoded by any given neuron. Partial pseudo- $R^2$  values are analogous to traditional  $R^2$  values obtained from residual regression analyses, which quantify the amount of variance explained by one regression model that is wholly unexplained by another. We calculated partial pseudo- $R^2$  values as follows:

$$pR_{X|Y}^2 = \frac{pR_{X,Y}^2 - pR_Y^2}{1 - pR_Y^2}, \quad (\text{A-2})$$

where  $pR_{X|Y}^2$  is the partial pseudo- $R^2$  of model  $X$  after first removing all deviance explained by model  $Y$ ;  $pR_{X,Y}^2$  is the pseudo- $R^2$  of an encoding model that uses predictors from both model  $X$  and model  $Y$ ; and  $pR_Y^2$  is the pseudo- $R^2$  of an encoding model that only uses predictors from model  $Y$ .

For our purposes,  $X$  could be either a neuron's posture-encoding model ( $pos$ ) or its movement-encoding model ( $mov$ );  $Y$  was then the other of the two models— $mov$  or  $pos$ , respectively. All model ( $pos$ ,  $mov$ , and  $pos,mov$ ) pseudo- $R^2$  values were evaluated at their respective optimal lags.

The number of joints in a neuron's response field is determined as follows. First, because we incorporated different axes of rotation as separate predictors, and because we used both the posture and movement of each joint angle as a separate predictor, we grouped standardized regression weights according to the joints with which they were associated and calculated their respective sum of their squares. Once the sum of squared regression weights was computed for each joint, we determined the minimal set of joints that cumulatively explained 90% of their total sum. We performed similar analyses with synergies—posture and movement as separate predictors—and muscles—lengths, their derivatives, and subunits of larger muscles with different insertions (Reilly & Schieber, 2003; Schieber, 1993) as separate predictors.

In addition, a “co-occurrence matrix” was calculated for each area. The co-occurrence matrix is a symmetric cross-tabulation of pairs of joints that are co-present in the response fields of neurons within that area. Co-occurrence matrices were compared to joint covariance matrices via logistic regression to determine whether or not multi-joint response fields simply reflect natural correlations in the kinematics. Co-occurrence matrix elements for joint pairs from the same digit (e.g., the proximal and distal interphalangeal joints of the index finger) or from different digits (e.g., the distal interphalangeal joints of the index and middle fingers) were compared via two-sample Student's  $t$ -tests (two-tailed, equal variance) to determine whether neurons' response fields were restricted to small localized parts of the hand or were distributed across the entire hand.

## Models of postural synergy encoding

To test whether cortical neurons might preferentially encode postural synergies of the hand (Santello, Flanders, & Soechting, 1998), we used the principal component scores of the joint angular data (see section “Dimensionality reduction”), as well as the derivatives of these scores—i.e., we did not fit a separate PCA model to the velocity data—as predictors in GLMs in lieu of joint angles and angular velocities. We then compared encoding models fit with synergies—i.e., principal components—and joint coordinates using two measures: A) the maximum pseudo- $R^2$  of models constrained to just a single synergy or joint, similar to a previous analysis investigating synergy coding in M1 (Mollazadeh, Aggarwal, Thakor, & Schieber, 2014); and B) the number of synergies or joints in each neuron’s response field (see section “Interpreting encoding models”).

## Simulated neural activity

At several points in the course of this study, we saw fit to simulate neurons that coded for particular features of hand movements to determine what might be expected under the null hypothesis that our recorded neural populations were drawn from a population of such neurons. First, we determined the appropriate RF, whether it be some artificial single-joint, -muscle, or -synergy RF, multi-joint, -muscle, or -synergy RF, or the RF of a real neuron fit to active or passive movement kinematics simulated as though the neuron were actually responding to the opposite experiment’s kinematics. We then projected the target kinematics to which the simulated neuron was to “respond” onto that RF. We then generated firing rates by passing those projected kinematics through a weighted softplus nonlinearity:

$$v(x|\beta, \theta) = \log[1 + \exp(x\beta + \theta)] \quad (\text{A-3})$$

where  $v$  is the one-dimensional vector of firing rates to be generated,  $\beta$  and  $\theta$  are free parameters, and  $x$  is the one-dimensional vector of kinematics projected onto the simulated neuron’s RF. These

rate vectors were then used to generate Poisson random vectors of spike counts. The parameters  $\beta$  and  $\theta$  were ultimately fit to minimize the difference between the noisy simulated neuron's mean firing rate and pseudo- $R^2$  value relative to the source neuron's—with the source neuron being arbitrarily selected from the set of all neurons from which we recorded, subject to the constraint that it had pseudo- $R^2 > 0.05$  and total spike count  $> 100$  in the epoch of interest across all trials. This was done so that a difference in the overall level of activity or noise between simulation and data was not a potential confound when testing for, say, the effects of kinematic correlations in the active and passive cases on GLM-inferred RFs, as one could imagine greater difficulty in fitting GLMs to noisy real data than in fitting such GLMs to comparatively low-noise simulated data.

## References

- Anderson, F. C., & Pandy, M. G. (2001). Dynamic Optimization of Human Walking. *Journal of Biomechanical Engineering*, 123(5), 381. <http://doi.org/10.1115/1.1392310>
- Anderson, F. C., & Pandy, M. G. (1999). A Dynamic Optimization Solution for Vertical Jumping in Three Dimensions. *Computer Methods in Biomechanics and Biomedical Engineering*, 2(3), 201–231. <http://doi.org/10.1080/10255849908907988>
- Cunningham, J. P., & Yu, B. M. (2014). Dimensionality reduction for large-scale neural recordings. *Nature Neuroscience*. <http://doi.org/10.1038/nn.3776>
- de Leva, P. (1996). Adjustments to Zatsiorsky-Seluyanov's segment inertia parameters. *Journal of Biomechanics*, 29(9), 1223–30. Retrieved from <http://www.ncbi.nlm.nih.gov/pubmed/8872282>
- Delp, S. L., Anderson, F. C., Arnold, A. S., Loan, P., Habib, A., John, C. T., ... Thelen, D. G. (2007). OpenSim: Open-Source Software to Create and Analyze Dynamic Simulations of Movement. *IEEE Transactions on Biomedical Engineering*, 54(11), 1940–1950. <http://doi.org/10.1109/TBME.2007.901024>
- Delp, S. L., Loan, J. P., Hoy, M. G., Zajac, F. E., Topp, E. L., & Rosen, J. M. (1990). An interactive graphics-based model of the lower extremity to study orthopaedic surgical procedures. *IEEE Transactions on Biomedical Engineering*, 37(8), 757–767. <http://doi.org/10.1109/10.102791>
- Dempster, W. T., & Gaughran, G. R. L. (1967). Properties of body segments based on size and weight. *American Journal of Anatomy*, 120(1), 33–54. <http://doi.org/10.1002/aja.1001200104>
- Hatsopoulos, N. G., Xu, Q., & Amit, Y. (2007). Encoding of movement fragments in the motor cortex. *The Journal of Neuroscience : The Official Journal of the Society for Neuroscience*, 27(19), 5105–14. <http://doi.org/10.1523/JNEUROSCI.3570-06.2007>
- Holzbour, K. R. S., Murray, W. M., & Delp, S. L. (2005). A Model of the Upper Extremity for Simulating Musculoskeletal Surgery and Analyzing Neuromuscular Control. *Annals of Biomedical Engineering*, 33(6), 829–840. <http://doi.org/10.1007/s10439-005-3320-7>
- Kadmon Harpaz, N., Ungarish, D., Hatsopoulos, N. G., & Flash, T. (2018). Movement Decomposition in the Primary Motor Cortex. *Cerebral Cortex*. <http://doi.org/10.1093/cercor/bhy060>
- Mcfarland, J. M., Cui, Y., Butts, D. A., & Bethge, M. (2013). Inferring Nonlinear Neuronal Computation Based on Physiologically Plausible Inputs. *PLoS Comput Biol*, 9(7). <http://doi.org/10.1371/journal.pcbi.1003143>
- Mollazadeh, M., Aggarwal, V., Thakor, N. V., & Schieber, M. H. (2014). Principal components

- of hand kinematics and neurophysiological signals in motor cortex during reach to grasp movements. *Journal of Neurophysiology*. <http://doi.org/10.1152/jn.00481.2013>
- Pillow, J. W., Shlens, J., Paninski, L., Sher, A., Litke, A. M., Chichilnisky, E. J., & Simoncelli, E. P. (2008). Spatio-temporal correlations and visual signalling in a complete neuronal population. *Nature*, *454*(7207), 995–9. <http://doi.org/10.1038/nature07140>
- Reilly, K. T., & Schieber, M. H. (2003). Incomplete functional subdivision of the human multitendoned finger muscle flexor digitorum profundus: an electromyographic study. *Journal of Neurophysiology*, *90*(4), 2560–70. <http://doi.org/10.1152/jn.00287.2003>
- Reimer, J., & Hatsopoulos, N. G. (2010). Periodicity and evoked responses in motor cortex. *The Journal of Neuroscience : The Official Journal of the Society for Neuroscience*, *30*(34), 11506–15. <http://doi.org/10.1523/JNEUROSCI.5947-09.2010>
- Saleh, M., Takahashi, K., Amit, Y., & Hatsopoulos, N. G. (2010). Encoding of coordinated grasp trajectories in primary motor cortex. *The Journal of Neuroscience : The Official Journal of the Society for Neuroscience*, *30*(50), 17079–90. <http://doi.org/10.1523/JNEUROSCI.2558-10.2010>
- Santello, M., Flanders, M., & Soechting, J. F. (1998). Postural Hand Synergies for Tool Use. *The Journal of Neuroscience*, *18*(23), 10105–10115.
- Schieber, M. (1993). Electromyographic evidence of two functional subdivisions in the rhesus monkey's flexor digitorum profundus. *Experimental Brain Research*, *95*(2), 251–260. <http://doi.org/10.1007/BF00229783>
- Thakur, P. H., Bastian, A. J., & Hsiao, S. S. (2008). Multidigit movement synergies of the human hand in an unconstrained haptic exploration task. *The Journal of Neuroscience : The Official Journal of the Society for Neuroscience*, *28*(6), 1271–81. <http://doi.org/10.1523/JNEUROSCI.4512-07.2008>
- Witham, C. L., Fisher, K. M., Edgley, S. A., & Baker, S. N. (2016). Corticospinal Inputs to Primate Motoneurons Innervating the Forelimb from Two Divisions of Primary Motor Cortex and Area 3a. *The Journal of Neuroscience*, *36*(9), 2605–16. <http://doi.org/10.1523/JNEUROSCI.4055-15.2016>
- Yamaguchi, G. T., & Zajac, F. E. (1989). A planar model of the knee joint to characterize the knee extensor mechanism. *Journal of Biomechanics*, *22*(1), 1–10. Retrieved from <http://www.ncbi.nlm.nih.gov/pubmed/2914967>